Investigating the potential role of mechanistic target of rapamycin complex 1 (mTORC1) in regulating cell fate decisions in *Dictyostelium discoideum*

A thesis submitted to the Board of the Medical Science Division, University of Oxford, in partial fulfilment of the requirements for the degree of Doctor of Philosophy



Yuntao Wang

DPhil candidate in Biochemistry

St. Catherine's College

Department of Biochemistry

Michaelmas Term 2022

Abstract

Understanding the underlying mechanisms of cell fate decisions in response to genetic and environmental factors will help to develop advanced stem cell therapies such as tissue regeneration or replacement of damaged or diseased cells. The social amoebae *Dictyostelium discoideum* is used as a lineage model which has a growth-to-development transition triggered by starvation. When vegetatively growing cells are starved, they aggregate and generate a multicellular organism, which ultimately develops into a fruiting body comprising two major cell types, spores and stalk cells. In mixed aggregates, heterogeneities in genetic background or environmental conditions during growth influence cell fate decisions. Environmental factors such as nutrient history, intracellular calcium (Ca^{2+}) levels and acidic vesicle pH are well-documented to bias cell fate, however, the underlying mechanism remains unclear. Two assays were used to study cell fates in this thesis: chimeric mixing experiments assessing spore formation in multicellular development and monolayer stalk induction assays monitoring the sensitivity to a stalk inducer differentiation inducing factor-1 (DIF-1) in the absence of cell contact.

One potential link between the factors biasing cell fate decisions is the activity of a protein kinase complex known as mechanistic target of rapamycin complex 1 (mTORC1). In mammalian cells, mTORC1 is an important activator of cell growth and proliferation whose activity is dependent on nutrient and energy status and is present on endo-lysosomal acidic compartments when activated. Also, mTORC1 interacts with and regulates Ca^{2+} release from lysosomes through a Ca^{2+} channel protein two-pore channel 2 (TPC2). In *Dictyostelium*, *tpc2*$^{-}$ strains have altered Ca^{2+} signalling, increased acidic vesicle pH and increased mTORC1 activity. Consistent with a role for mTORC1, *tpc2*$^{-}$ cells prefer a stalk cell fate. To investigate whether altering mTORC1 activity can underlie cell fate bias, mTORC1 pathway activity was analysed in cells with different cell fate preferences and high activity correlated with stalk cell fate bias. To determine if this was causal, the consequences of both pharmacological inhibition of mTORC1 and genetic modulation of genes encoding mTORC1 regulators, such as AMP-activated protein kinase (AMPK) and Ras homolog enriched in brain (Rheb), on cell fate were determined. Use of inhibitors suggested that altering mTORC1 pathway activity has a different effect during growth than during development, indicating distinct roles at different stages in cell fate determination.

One mechanism to regulate mTORC1 activity may be through changes in gene expression. The ratio of expression during growth of two genes (*rrgA* and *rigA*) was validated as a marker to predict the cell fate bias prior to development in a range of mutant strains and in different conditions. The expression ratio of these genes is dependent on the presence of specific histone modifications, methylation of histone H3 on lysine 4 and subsequent acetylation, and high *rrgA*/*rigA* ratio correlates with high mTORC1 pathway activity and a stalk cell fate bias.

Overall, this thesis reveals a potential role of mTORC1 pathway activity in regulating cell fate decisions in *Dictyostelium* with wide-spread implications for manipulating this pathway to direct pluripotent stem cells towards defined fates.

Acknowledgements

First of all, I would like to thank my supervisor Prof. Catherine Pears for her generous guidance and support on my project and life during my four-year DPhil degree. I am also grateful to the opportunity of working on an iron project using our model organism with our collaborator, Prof. Hal Drakesmith from the MRC Weatherall Institute of Molecular Medicine (MRC WIMM).

I would like to acknowledge all my colleagues and wonderful friends in the laboratory, such as Huajiang Xiong, Monika Papayova, Julien Brustel, Frederick Richards, Khairul Ramlee, Kelvin Yaprianto, Tomoaki Sobajima who are the best and the smartest people with warm hearts, showing me so many useful techniques and sharing a lot of wonderful tips when I was desperately in need for resolving experiments' mystery. I would not forget the laughter and tears we witnessed for each other, which is significantly related to the results of experiments! Many thanks to Fu-sheng Chang who gave me advice on my work even without overlapping time with me in the department. I am also grateful to the joint lab meetings we had with the Woollard lab, especially Prof. Jonathan Hodgkin who provided insightful comments and suggestions to my work. I also appreciate the people in our lab, Antoine Verslype and others for sharing communal duties together. Also, thanks to my friends from other blocks, Silvia Raineri, Meredith Wouters, Divya Choudhary, Valentine Lagage, Carl Morrow, Yao Meng, Zhihan Bo, Xinyi Feng etc, especially Yuanlin Xu, who accompanied me through my darkest days and always made my days! I am so lucky to be surrounded by devoted friends in my life as well: Tingxi Ma, Peng Tang, Qingniao, Haiyu Chen, Jinyi Zhao, Honglin Chen, Yue Li, Jingnu Xia, Xinyi Xia, Jingjing Sun, especially Chaohui Yang and Mengjia Li who shared the happiest years with me in our undergraduate life and would always be there for me!

Last but not least, this thesis is dedicated to my dearest family, my mum Qiaoling Li and my dad Wenping Wang, who are the best mentors in my life and give me the strongest support to chase my dreams as well as endless encouragement in every aspect of my life. I cherish the unconditional love from them every day. I would also thank my partner Junwen Wang, for being a supportive and loving person throughout these years. Thank you and love you all for making my life and my DPhil journey extraordinary!

Abbreviations

AA	amino acids
AC	adenylyl cyclase
AGC kinase family	protein kinase A, protein kinase G, protein kinase C kinase family
AKT/PKB	protein kinase B
AMP	adenosine 5'-monophosphate
AMPK	AMP-activated protein kinase
ANOVA	analysis of variance
ATP	adenosine 5'-triphosphate
AT1	alveolar type 1
ARF1	ADP-ribosylation factor 1
ArpA	autocrine proliferation repressor protein A
bHLH	basic helix-loop-helix
BHQ	2,5-di(tert-butyl)-1,4-hydroquinone
BODIPY	boron-dipyrromethene
BLAST	basic local alignment search tool
BSR	blasticidin S resistance
bZIP	basic leucine zipper
Ca^{2+}	calcium ion
CaM	calmodulin
CAMKL	Ca^{2+}/calmodulin-activated kinase-like
cAMP	adenosine 3', 5'- cyclic monophosphate
cAR	cAMP receptor
cDNA	complementary DNA
CAX	Ca^{2+}/H^{+} exchanger
Cas9	CRISPR-associated protein 9
CfaD	counting factor-associated protein D
CHO	Chinese hamster ovary
CICR	calcium-induced calcium release
CMF	conditioned medium factor
CPRG	chlorophenol red-β-D-galactopyranoside
CPX	ciclopirox olamine
CRISPR	clustered regularly interspaced short palindromic repeats
CRMP	cysteine repeat modular protein
CT	cycle threshold
CTL	cytotoxic T lymphocyte
CV	contractile vacuole
DAG	diacylglycerol
DATP	damaged-associated transient progenitor
Deptor	DEP-domain containing mTOR-interacting protein
DIF	differentiation inducing factor
DFO	deferoxamine
DMP1	*Dictyostelium* membrane protein 1
DMO	5,5-dimethyl-2,4-oxazolidineolione
DMSO	dimethyl sulfoxide
DTT	dithiothreitol
EDTA	ethylenediamine tetra-acetic acid
EGTA	ethylene glycol tetra-acetic acid

eIF	eukaryotic translation initiation factor
4E-BP1	eIF4E binding protein 1
ESC	embryonic stem cell
EtBr	ethidium bromide
EPI	epiblast
ER	endoplasmic reticulum
FACS	fluorescence-activated cell sorting
FAT	FRAP/ATM/TRRAP domain
FATC	the central FAT domain
FbxA	F-box/WD repeat-containing protein A
Fe^{2+}	ferrous ion
Fe^{3+}	ferric ion
$FeCl_3$	ferric chloride
Fe-S cluster	iron-sulfur cluster
FGF	fibroblast growth factor
FKBP12	12 kDa-FK506-binding protein
FLCN	folliculin
FNIP	folliculin interacting protein
Fpn1	ferroportin 1
FRB	FKBP12-rapamycin-binding domain
FRET	fluorescence resonance energy transfer
G418	geneticin
GABA	γ-aminobutyric acid
GAL	β-galactosidase (β-gal)
GAP	GTPase-activating protein
GCN5	general control non-derepressible 5
gDNA	genomic DNA
GEF	guanine nucleotide exchange factor
GF	growth factor
GLUT	glucose transporter
GDP	guanosine diphosphate
GFP	green fluorescent protein
G protein	guanine nucleotide binding protein
GPCR	G protein-coupled receptor
GTP	guanosine triphosphate
GSH	glutathione
H3	histone 3
H3Ac	histone H3 acetylation
H3K4me3	histone H3 tri-methylation on lysine 4 residue
HAT	histone acetyltransferase module
HEK293	human embryonic kidney 293
HEPES	N-2-hydroxyethyylpiperazine-N'-2-ethanesulphonic acid
HDAC	histone deacetylase
HPLC	high-performance liquid chromatography
ICM	inner cell mass
IFNγ	interferon-gamma
IP_3	inositol 1,4,5-trisphosphate
IP_3R	inositol 1,4,5-trisphosphate receptor
IPLA	inositol 1,4,5-trisphosphate receptor-like protein A
iPSC	induced pluripotent stem cell

IREB1	iron-responsive element-binding protein 1
JNK1	c-Jun N-terminal kinase 1
kDa	kilodaltons
KMT	lysine methyltransferase
Lst8	lethal with sec-13 protein 8
MCLN	mucolipin
MCU	mitochondrial calcium uniporter
MPBD	4-methyl-5-pentylbenzene-1,3 diol
mRNA	messenger RNA
Mt	mitochondria
mTOR	mechanistic target of rapamycin
mTORC1/2	mechanistic target of rapamycin complex 1/2
MW	molecular weight
NAADP	nicotinic acid adenine dinucleotide phosphate
NCKX	Na^+/Ca^{2+}-K^+ exchanger
NCX	Na^+/Ca^{2+} exchanger
NeoR	neomycin resistance
NFS1	nitrogen fixation 1
NMR	nuclear magnetic resonance
Nramp	natural resistance-associated macrophage protein
OE	overexpression
ORF	open reading frame
P2X	ATP-gated P2X receptor cation channel
PAT1	P-type Ca^{2+} ATPase 1
PCR	polymerase chain reaction
PDE	phosphodiesterase
PDK1	phosphoinositide-dependent protein kinase 1
PE	primitive endoderm
PIP_2	phosphatidylinositol 4,5-bisphosphate
PIP_3	phosphatidylinositol 3,4,5-trisphosphate
PI3K	phosphatidylinositol-3’-kinase
PIKK	PI3K-related protein kinase
PKA	protein kinase A
PLC	phospholipase C
PM	plasma membrane
PMCA	plasma membrane Ca^{2+}-ATPase
PRAS40	proline-rich AKT substrate 40 kDa
Protor1/2	protein observed with rictor 1/2
PSF	prestarvation factor
psp	pre-spore
pst	pre-stalk
PTM	post-translational modification
qPCR	quantitative real-time RT-PCR
Rag GTPase	Ras-related GTP binding protein
Raptor	regulatory-associated protein of TOR
RD	reaction-diffusion
rDNA	ribosomal RNA gene
REMI	restriction enzyme-mediated integration
Rheb	Ras homolog enriched in brain
Rictor	rapamycin insensitive companion of mTOR

RNA	ribonucleic acid
ROS	reactive oxygen species
RT	reverse transcription
RTK	receptor tyrosine kinase
RyR	ryanodine receptor
S6K	ribosomal protein S6 kinase
SAGA	Spt-Ada-Gcn5-acetyltransferase
SAHA	suberoylanilide hydroxamic acid
SDF	spore differentiation factor
SDS	sodium dodecyl sulphate
SDS-PAGE	sodium dodecyl sulphate polyacrylamide gel electrophoresis
S.E.M	standard error mean
SESN2	sestrin 2
SERCA	sarco/endoplasmic reticulum Ca^{2+}-ATPase
Sgf29	SAGA-associated factor 29
SGK	serum- and glucocorticoid-induced protein kinase
shRNA	short hairpin RNA
Sin1	stress-activated protein kinase-interacting protein 1
siRNA	small interfering RNA
SLC	solute carrier
SPRY	spore lysis A/ryanodine receptor
SR	sarcoplasmic reticulum
STAT	signal transducer and activator of transcription
TAE	tris-acetate-EDTA
TE	trophectoderm
Tfh	follicular helper T cell
TfR1	transferrin receptor 1 (also known as CD71)
TgrC1	tiger protein C1
Th1	T helper type 1
TIM-3	T cell immunoglobulin and mucin containing protein-3
TM	transmembrane
TPC	two-pore channel
Tris	2-amino-2-(hydroxymethyl-)1,2-propanediol
TRPML	mucolipin (MCLN)
TSA	trichostatin A
TSC1/2	tuberous sclerosis complex 1/2
Vmp1	vacuole membrane protein 1
VPA	valproic acid
TRP	transient receptor potential
TRPP	transient receptor potential polycystin
TTP	tristetraprolin
UTR	untranslated region
UV	ultraviolet radiation
v-ATPase	vacuolar-type H^+-ATPase
VDAC	voltage-dependent anion channel
VGCC	voltage-gated Ca^{2+} channel
VPA	valproic acid
wt	wildtype
YC-Nano 15	yellow cameleon-Nano 15

Contents

Chapter 1: General introduction 1

1.1 Evolution of multicellularity in organisms 1

1.1.1 Development of multicellular organisms 1

1.1.2 Patterning mechanisms in organism development 3

1.2 *Dictyostelium discoideum* as a model organism to study cell fate decisions 6

1.2.1 Developmental life cycle of *Dictyostelium discoideum* 6

1.2.2 *Dictyostelium* as a simple model organism with proteins well conserved throughout eukaryotes 9

1.3 Cell fate decisions in *Dictyostelium discoideum* 11

1.3.1 DIF-1 is a morphogen regulating *Dictyostelium* pre-stalk cell differentiation 11

1.3.2 Genetic differences in mixed aggregates can influence cell fate decisions 15

1.3.3 Cell fate determinants within the same genetic population play roles in cell fate decisions 16

1.3.3.1 Nutrient history in cell growth influences cell fate later in development 18

1.3.3.2 Cell cycle position at the onset of development plays a role in cell fate decisions 18

1.3.3.3 Vesicle pH influences cell fate 22

1.3.3.4 Intracellular Ca^{2+} levels influence cell fate 23

1.4 General aims 27

Chapter 2: Materials and methods 28

2.1 Materials 28

2.2 Methods 32

2.2.1 *Dictyostelium* Cell culture 32

2.2.2 Cell cryopreservation and thawing 32

2.2.3 Electroporation of *Dictyostelium* 33

2.2.4 Genetically modified cell lines 33

2.2.5 Cell development 34

2.2.5.1 Cell development on filter and agar 34

2.2.5.2 Chimeric development to assess spore predisposition 35

2.2.5.3 Monolayer stalk induction assay 35

2.2.6 Imaging 36
2.2.7 General molecular cloning and gene disruption 37
2.2.7.1 Restriction enzyme digestion and ligation 37
2.2.7.2 Transformation of *Escherichia coli* 38
2.2.7.3 Polymerase chain reaction (PCR) 38
2.2.8 Genomic DNA extraction from *Dictyostelium* cells 39
2.2.9 *Dictyostelium* gene disruption by homologous recombination 39
2.2.10 *Dictyostelium* gene disruption by CRISPR-Cas9 strategy 40
2.2.11 Western blot analysis 40
2.2.11.1 Whole cell lysate sample collection 40
2.2.11.2 Western blotting 41
2.2.12 Quantitative real-time RT-PCR (qPCR) 41
2.2.13 Statistics and bioinformatic analysis 42

Chapter 3: Ca^{2+} signalling and cell fate decision 47

3.1 Introduction 47
3.1.1 Ca^{2+} signalling machinery in mammalian and *Dictyostelium* cells 47
3.1.2 IPLA, TPC2 and DMP1 channels in *Dictyostelium* 52
3.1.3 *Dictyostelium* cell fate bias assays used in this thesis 56
3.2 Aims 58
3.3 Results 59
3.3.1 *tpc2*$^-$ cells form fewer spores in chimeric development with AX2 cells 59
3.3.2 Monolayer stalk induction assays confirm stalk cell fate tendency of *tpc2*$^-$ cells 62
3.3.3 *iplA*$^-$ cells show a spore cell fate tendency 64
3.3.4 Investigation of the *dmpA* gene encoding DMP1, a putative Ca^{2+} channel 65
3.3.5 Disruption of *dmpA* gene using both homologous recombination and CRISPR/Cas9 strategies 66
3.3.5.1 Homologous recombination method for constructing *dmpA*$^-$ strain 66
3.3.5.2 CRISPR/Cas9 method for constructing *dmpA*$^-$ strain 71
3.3.6 Characterization of *dmpA*$^-$ cells 77
3.3.6.1 Investigation of the development and growth of *dmpA*$^-$ cells 77
3.3.6.2 Investigation of cell fate decisions in *dmpA*$^-$ strains 79
3.3.7 *tpc2*$^-$ cells still show an effect of glucose growth history on cell fate bias 80
3.3.8 Pre-treatment of *tpc2*$^-$ cells with weak base imidazole reversed the cell fate bias 82

3.3.8.1 Weak bases affect *Dictyostelium* development 82
3.3.8.2 Weak bases alter stalk cell fate decisions in *tpc2*$^{-}$ cells 83
3.4 Discussion 87

Chapter 4: mTORC1 and cell fate decision 93

4.1 Introduction 93
4.1.1 mTORC1 signalling pathway in mammalian cells 93
4.1.1.1 Components in mTOR complexes 93
4.1.1.2 Main downstream effectors of mTORC1 pathway 93
4.1.1.3 Activation of mTORC1 pathway 95
4.1.1.4 Inhibitors of mTOR complexes 98
4.1.2 mTORC1 in cell type differentiation and cell fate regulation 100
4.1.3 mTORC1 signalling in *Dictyostelium* 101
4.1.4 Links between mTORC1 and TPC2 in mammalian models 104
4.1.5 Links between *Dictyostelium* mTORC1 and TPC2 105
4.2 Aims 107
4.3 Results 108
4.3.1 mTORC1 activity is prolonged or higher in cells with a pre-stalk tendency 108
4.3.1.1 Phosphorylation level of 4E-BP1 remains prolonged in developing cells with a glucose-deficient growth history 108
4.3.1.2 Rapamycin-induced development to confirm levels of mTORC1 activity 110
4.3.1.3 Genetic mutants with distinct cell fate bias have prolonged mTORC1 activity in early development 112
4.3.2 Altering mTORC1 activity can influence cell fate decision 113
4.3.2.1 Pharmacological inhibition of mTORC1 via mTOR inhibitors 113
4.3.2.2 Inhibition of mTORC1 using mTOR inhibitors during growth leads to a spore cell fate bias 115
4.3.3 Genetic alteration of mTORC1 activity influences cell fate decisions 118
4.3.3.1 Alteration of mTORC1 activity by manipulating the mTORC1 antagonist AMPK with a genetic mutant strain of AMPK (*ampk*$^{-}$) 118
4.3.3.2 Alteration of mTORC1 activity by manipulating expression of Rheb, an activator of mTORC1 122
4.3.3.2.1 Construction of Rheb overexpressing strains 122
4.3.3.2.2 Verification of Rheb_FLAG overexpressing strains 124

4.3.3.2.3 Characterization of Rheb_FLAG overexpressing strains and construction of mutated Rheb_FLAG_E40K strain 125
4.3.3.2.4 Construction and characterization of a Rheb gene disrupted strain (*rheb*$^{-}$) 134
4.3.3.2.5 Investigation of mTORC1 activity in *rheb*$^{-}$ strain 138
4.3.3.3 Cell fate decisions in genetic mutants involved in the mTORC1 pathway 140
4.3.3.3.1 Loss of AMPK leads to a stalk cell fate tendency 140
4.3.3.3.2 Loss of Rheb in the *rheb*$^{-}$ strain leads to a spore cell fate bias 140
4.3.3.3.3 Overexpressing Rheb in Rheb_FLAG OE strains results in a stalk cell fate tendency 142
4.3.3.3.4 Investigation of whether mTORC1 pathway activity has a predisposition effect in cell fate bias 144
4.3.3.3.5 Leakage of Rheb OE in the dox-on regulatable system in dox-free conditions during growth potentially affects cell fate decisions during development 146
4.3.3.3.6 Developmentally regulated promoters driving Rheb_FLAG expression can be used to study the effect of mTORC1 pathway during development in cell fate decisions 149
4.4 Discussion 150

Chapter 5: Gene expression regulation and cell fate decision 158

5.1 Introduction 158
5.1.1 Gene expression regulating cell type differentiation in development 158
5.1.2 Potential biomarkers for prediction of predisposition of cell fate determination in growing cells 159
5.1.3 Post-translational modifications (PTMs) on histones controlling gene transcription influence cell differentiation 160
5.1.4 *Dictyostelium* methyltransferase Set1 is responsible for H3K4me3 mark 162
5.1.5 Histone variants 165
5.2 Aims 167
5.3 Results 168
5.3.1 Cell fate bias can be predicted by assessing the gene expression ratio of two markers: *rrgA* and *rigA* 168

5.3.2 Cell fates altered by intrinsic genetic factors have distinct *rrgA/rigA* gene expression ratios 172
5.3.3 Genetic predisposition of cells lacking the H3K4 methyltransferase Set1 in cell fate decisions 175
5.3.3.1 *Dictyostelium set1*$^{-}$ cells have an intrinsic stalk cell fate bias 175
5.3.3.2 H3bK4A cells have an intrinsic stalk cell fate bias revealing the importance of the H3K4me3 mark in cell fate decisions 179
5.3.4 Histone acetylation coupled to the H3K4me3 mark affects cell fate decisions 181
5.3.5 Pharmacologically altered histone acetylation via treatment with TSA during growth leads to a cell fate bias 183
5.3.6 Loss of histone H3K4 methylation leads to increased mTORC1 activity during growth and early development 187
5.4 Discussion 189

Chapter 6: Does iron have a role in early development and influence cell fate decisions? 195

6.1 Introduction 195
6.1.1 Iron has essential roles in organisms' growth and development 195
6.1.2 The effects of iron in Dictyostelium 197
6.2 Aims 199
6.3 Results 200
6.3.1 The consequence of altering iron levels during growth and early development 200
6.3.1.1 High concentrations of iron inhibit aggregation 200
6.3.1.2 The effect of iron depletion on *Dictyostelium* cell fate decisions 204
6.3.2 mTORC1 activity in *Dictyostelium* cells with different iron pre-treatment history 206
6.4 Discussion 208

Chapter 7: General discussion and Future work 212

7.1 General summary and discussion 212
7.2 Future experiments 218

References 220

Chapter 1: General introduction

1.1 Evolution of multicellularity in organisms

From the perspective of evolution, development of a eukaryotic organism is a key feature of multicellularity evolved from unicellular eukaryotes at least 1.7 billion years ago (Cooper, 2000). Having undergone several independent multicellular evolutionary events, eukaryotes gain a high level of complexity in organism development and social behaviours (Carroll, 2001), while prokaryotes, such as the filamentous Cyanobacteria, also evolved to have multicellular lives dating back to even earlier times (more than 2 billion years ago) (Lyons and Kolter, 2015). As a new evolutionary "individual", this higher-level multicellular group benefits from cooperation among the lower-level units of individuals, and fitness at a higher level is acquired via conflict mediation (Michod, 1999; Michod and Nedelcu, 2003). Being multicellular during evolution has advantages, such as diluting any harmful mutations within the population for a better chance of survival as a whole organism. The transition from a unicellular to a multicellular organism also allows cells within the body to differentiate into distinct cell types with specialized roles or functions, which is impossible for unicellular organisms to achieve (Michod, 2007).

1.1.1 Development of multicellular organisms

One central interest of studying development of a multicellular organism is to understand mechanisms of cell type determination and pathway choice when multiple cell types are derived from a single cell, or multipotent stem cell. In most cases of development, a sequence of events starts from a single fertilized egg (zygote), following by the formation of blastomere with an increase of cell numbers via asynchronous cell cleavage divisions. Then complexity develops via cell type differentiation, morphogenesis, and pattern formation (Mihajlovic and Bruce, 2017). At early embryonic development stages, molecular and morphological symmetry breaking events are observed (Figure 1.1) and genetic networks controlling gene expression, such as those regulated by Gata6 and Sox17 for primitive endoderm differentiation in mouse embryos, are involved in regulating lineage specification and pattern formation (Chen et al., 2018; Morris et al., 2010; Zernicka-Goetz et al., 2009). Many model organisms such as the nematode worm (*Caenorhabditis elegans*), sea urchin (*Echinoidea*) and the African clawed frog (*Xenopus laevis*) have a clearly visible pre-patterning mediated by asymmetrical

distribution of morphogens in the oocyte or zygote (Chen et al., 2018). In mammalian models such as mouse (*Mus musculus*), blastomeres have less apparent asymmetric dispersal of morphogens but involve more sophisticated and subtle cues e.g. intracellular interactions in typical locations initiating small-scale heterogeneity, which will be reinforced over the next cell divisions to respond to other developmental cues for further pattern formation and cell fate decisions in the descending lineages (Chen et al., 2018), such as primitive endoderm (PE) and epiblast (EPI) which are distributed in a salt-and-pepper manner in the mid-blastocyst (64-cell) stage (Figure 1.2) (Mihajlovic and Bruce, 2017; Schrode et al., 2013).

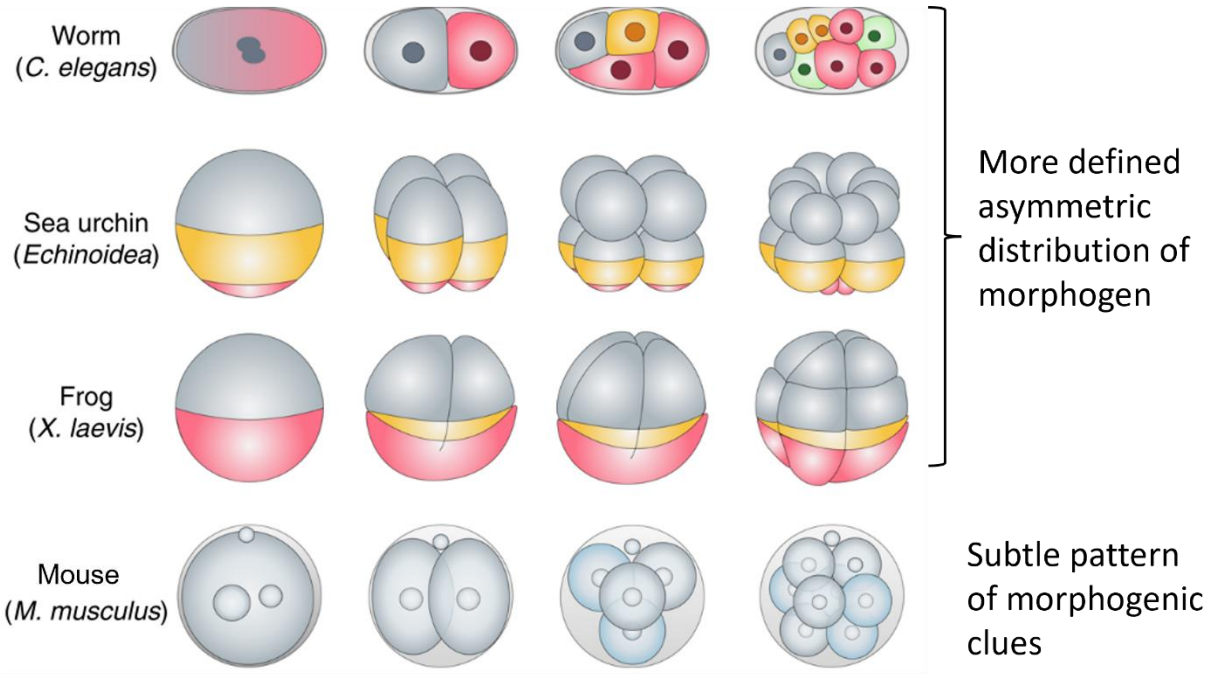


Figure 1.1. Schematic representation of symmetry breaking in early embryonic development in different organisms. In the cases of worm, sea urchin and frog, asymmetrical distributions of pre-patterning morphogens occurring in early embryo development are indicated in different colours, which dictate the cell fate of the blastomeres in later developmental stages. In mouse early embryo development, there is no obvious asymmetric distribution of pre-patterning factors, but some more subtle clues shown in the 4-cell stage shaded in blue are employed for cell fate determination. Adapted from Chen et al. (2018).

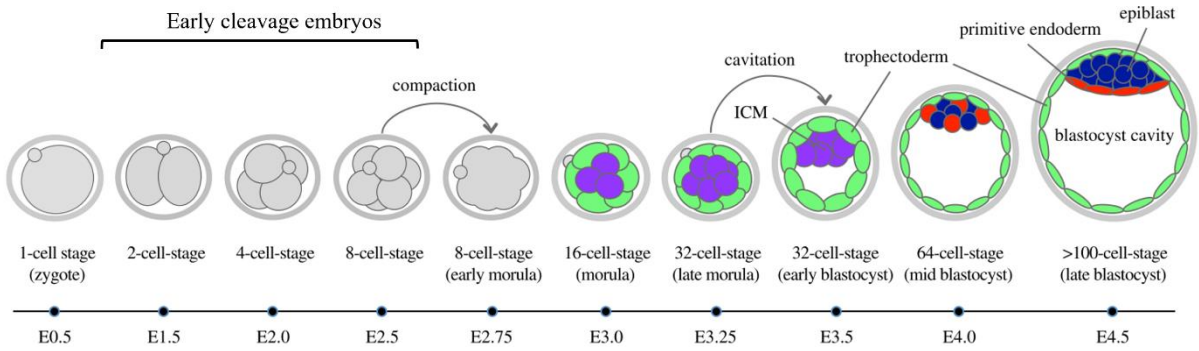


Figure 1.2. Overview of preimplantation mouse embryonic development. A series of developmental events in different embryonic stages happen in a temporal sequence. Early cleavage embryos occur when embryos start to show two cells and they exhibit morphological characteristics identical to the eight-cell stage. The first cell fate decision generates two lineages, the trophectoderm (TE) and the inner cell mass (ICM), followed by the formation of two early blastocyst lineages derived from ICM, primitive endoderm (PE) and epiblast (EPI). Adapted from Mihajlovic and Bruce (2017).

1.1.2 Patterning mechanisms in organism development

One of the key steps in development, pattern formation, plays important roles in gaining complex cell fates and functions in a self-generated multicellular organism during embryogenesis. Pattern formation, by definition, is the process to coordinate uncommitted cells to adopt specific cellular functions in a spatiotemporal order and shape their identities in complex organization (Hadjivasiliou et al., 2016). During this process, genes involved in tissue patterning are induced relying on the responsiveness of cells to morphogens or developmental signals which mediate signalling through transcriptional regulatory networks and designate cell fates (Sagner and Briscoe, 2017). A number of models have been put forward to explain pattern formation. For example, a classic reaction-diffusion (Turing) model was originally proposed in 1952 (Turing, 1990). Depending on dynamic properties e.g. density and diffusion rate, Turing's model describes gradients of one or more morphogens interacting with each other generating distinct types of spatial patterns either depending on positional information or arising autonomously regardless of positional information. Six potentially stable states were analysed from mathematical simulations (Figure 1.3, reviewed by Kondo and Miura (2010)). For instance, case I shows a steady and uniform state when there is no perturbation, while case II complies with morphogen concentration in uniform-phase oscillation such as the systems of circadian rhythms (Ueda, 2007) and heart muscle contraction (Song et al., 2005). Case III

demonstrates the salt-and-pepper pattern formation achieved when cells undergoing differentiation secrete inhibitors to suppress the differentiation of neighbouring cells, and this can be seen in Notch-Delta mediated lateral inhibition in the development of *Drosophila* bristle precursors (Cohen et al., 2010) and the differentiation of epithelial neuroprogenitor cells during embryonic development (Cabrera, 1990). Case IV is an unusual oscillatory state developed from case III which has no typical developmental system as example. Case V demonstrates a scenario of traveling waves which include the spiral patterns originating from the aggregation centre of the social amoeba *Dictyostelium discoideum* during adenosine-3',5'-cyclic phosphate (cAMP) wave propagation in development (Siegert and Weijer, 1995). Case VI forms a Turing pattern that can be seen in oscillating Ca^{2+} waves in frog egg upon sperm entry (Sardet et al., 1998).

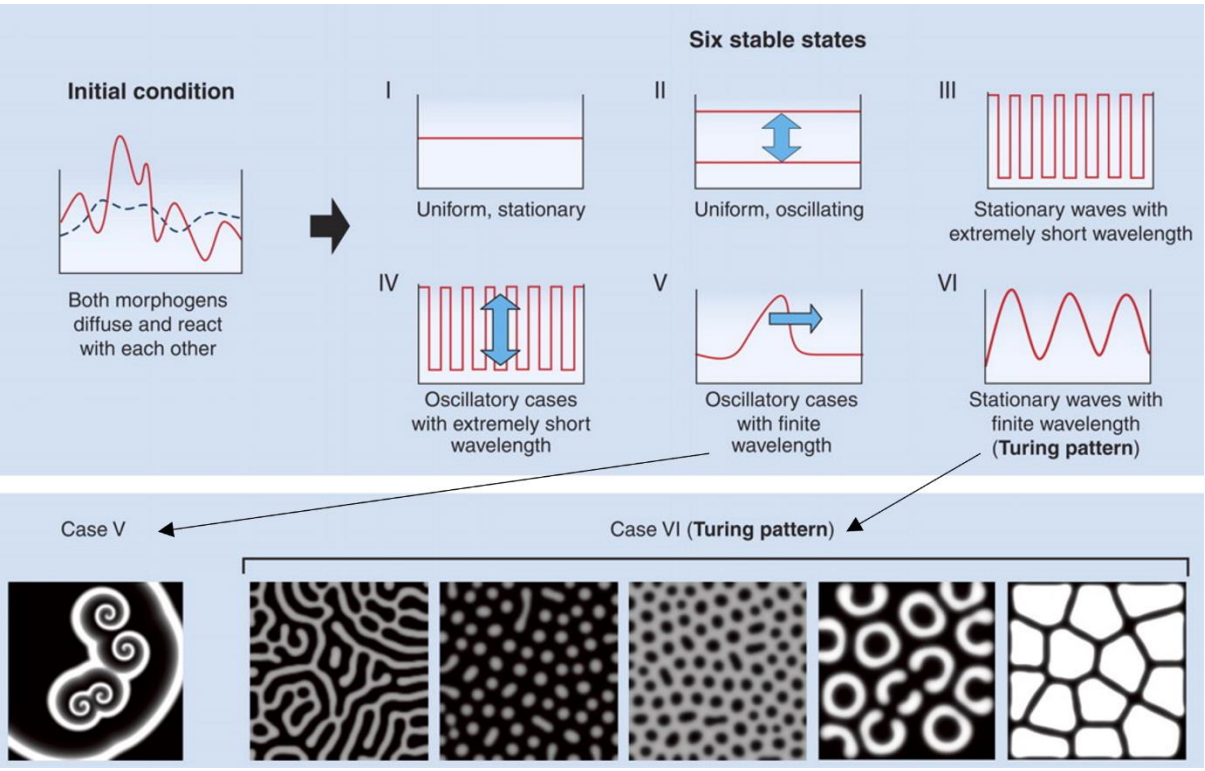


Figure 1.3. Schematic representations of mathematical simulation of Turing's reaction-diffusion (RD) model and patterns formed by the analysis. Upper panel: six steady states generated from the two-factor Turing's RD model. Lower panel: two-dimensional patterns illustrating case V and case VI were generated form the identical equation with slight alteration of parameters. The simulations using Turing's model were analysed with a software available in Kondo and Miura (2010)'s supporting online material. The diagram is adapted from Kondo and Miura (2010).

On a larger scale, there are fewer mechanisms to explain autonomous multicellular spatial patterning other than to morphogen gradients during cell-type differentiation. However, one possibility to achieve that is cells originating from a salt-and-pepper pattern in a differentiating population sort out and physically move to different spaces and develop into coherent tissues in a self-organizing organism (Kay and Thompson, 2009) (Figure 1.4). This dynamic salt-and-pepper patterning has been proposed to be generated during the mound stage of *Dictyostelium* development and is remarkably similar to early mouse blastocyst development which initially has a stochastic and random organization of the progenitors of two distinct cell types, pluripotent EPI and PE. These cells then sort out into the required locations during blastocyst maturation (Morris et al., 2010; Yamanaka et al., 2010). Such stochastic patterning has also been reported in the self-renewal stem cells (Galvin-Burgess et al., 2013; Libby et al., 2019).

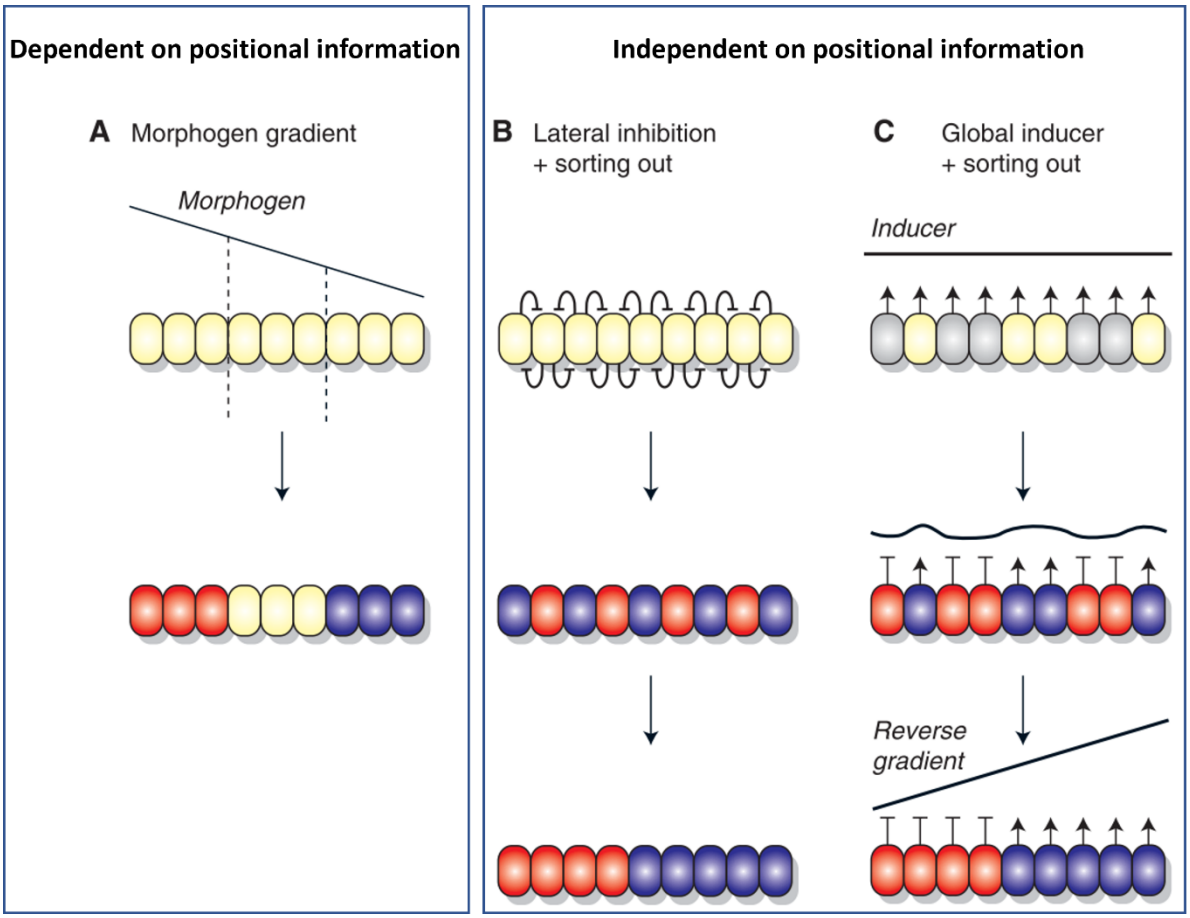


Figure 1.4. Schematic representations of alternative pattern formation mechanisms during development. (A) Patterning restricted to positional information: undifferentiated cells in the population encounter a concentration gradient of morphogen generated via diffusion from a pre-established external source. The cells responding to such a local morphogen gradient differentiate into different cell types indicated in red, yellow, and blue. (B, C) Pattern formation independent on positional information. Different types of cells differentiated in a stochastic and random manner are mixed in the population with a salt-and-pepper distribution in the first place, and then sort out i.e. re-organize themselves to various locations. The initial

differentiation relies on either (B) lateral inhibition which has strict inhibition via local cell-cell interactions, or (C) a global signal or inducer which cells in the population have different sensitivities to, and whose concentration they regulate via negative feedback. A reverse gradient formed by the inducer then occurs after the sorting, and the patterning can continue to react to positional information for the next patterning events. Adapted from Kay and Thompson (2009).

1.2 *Dictyostelium discoideum* as a model organism to study cell fate decisions

The social amoeba *Dictyostelium discoideum* (from now on called *Dictyostelium* in this thesis) is a simple haploid organism belonging to eukaryotes which preys on bacteria and yeast as food sources in the soil (Romeralo et al., 2013). In the laboratory, *Dictyostelium* cells that are able to grow in axenic conditions are actually derivatives of the wildtype strains (such as NC-4) isolated from natural environments, and such so-called axenic or AX strains can be cultured either in shaking suspension or in petri dishes without bacteria and are often used as parental strains for molecular and genetic studies (Sussman and Sussman, 1967; Watts and Ashworth, 1970). These strains have become axenic by increasing the efficiency of macropinocytosis for fluid uptake, for example by mutation of the gene encoding the Neurofibromin NF1 protein which regulates activity of members of the Ras family (Bloomfield et al., 2015).

1.2.1 Developmental life cycle of *Dictyostelium discoideum*

Dictyostelium has an unusual developmental life cycle (Figure 1.5), transiting from a vegetatively growing unicellular stage to a developmental multicellular stage triggered by unfavourable environmental conditions such as nutrient deprivation (Darmon and Klein, 1978; Marin, 1976) and oxidative stress (Bloomfield and Pears, 2003; Kelly et al., 2021) as well as mechanical stress (Hashimura et al., 2022; King et al., 2011). At early onset of development, some cells start to secrete the chemoattractant cAMP (Bonner, 1947, 1970). This extracellular cAMP interacts with cell surface receptors to trigger signalling pathways which mediate important events such as chemotaxis and development as well as secretion of further cAMP (Jin et al., 2008; Konijn et al., 1967). The cells first secreting cAMP become signalling centres which trigger the cAMP signal for chemotactic aggregation as the field of cells generates propagating and periodic cAMP waves (Consalvo et al., 2019; Van Haastert and Devreotes, 2004). *Dictyostelium* cells also secrete a cyclic nucleotide phosphodiesterase (PDE) to degrade the cAMP (Franke and Kessin, 1992), which resembles the regulation of neurotransmitter levels in mammals (Charlie et al., 2006; Steuer Costa et al., 2017). Such localized degradation

of chemoattractant helps to generate waves of cAMP across a field of cells (Karmakar et al., 2021). Cells travel up the overall gradient of cAMP towards the signalling centres where they can adhere to each other which leads to multicellular structure formation. Mound structures start to form at around 12 hrs following starvation. At this stage, cells expressing markers of the two later cell types, pre-stalk and pre-spore genes, are scattered in the population with a salt-and-pepper pattern (Kay and Thompson, 2009). These cells then migrate at different speeds and adhere preferentially to cells of the same types, then sorting out into specific pre-spore (psp) and pre-stalk (pst) regions in the tipped aggregate and optional migrating slug. The pre-stalk region in the slug can be divided into different subtypes of cells by expression of distinct pre-stalk marker genes, for example, pstA cells are found at the most anterior front of slug tip (Jermyn et al., 1989), pstB and pstAB in the central core (Gaskell et al., 1992; Jermyn and Williams, 1991; Sternfeld, 1992) and pstO at the rear of anterior region (Early et al., 1993). On culmination at the end of the 24-hr developmental cycle, fruiting bodies are formed that have a spore head at the top of a supportive vacuolated stalk structure. The final spore and stalk cell types, both derived from an apparently homogenous population of vegetatively growing cells, differentiate in a stable ratio of 80:20 (Bonner, 1967; William and Morrison, 1994). The signalling molecules characterised during development are briefly summarized in Figure 1.6 and are reviewed by Loomis (2014).

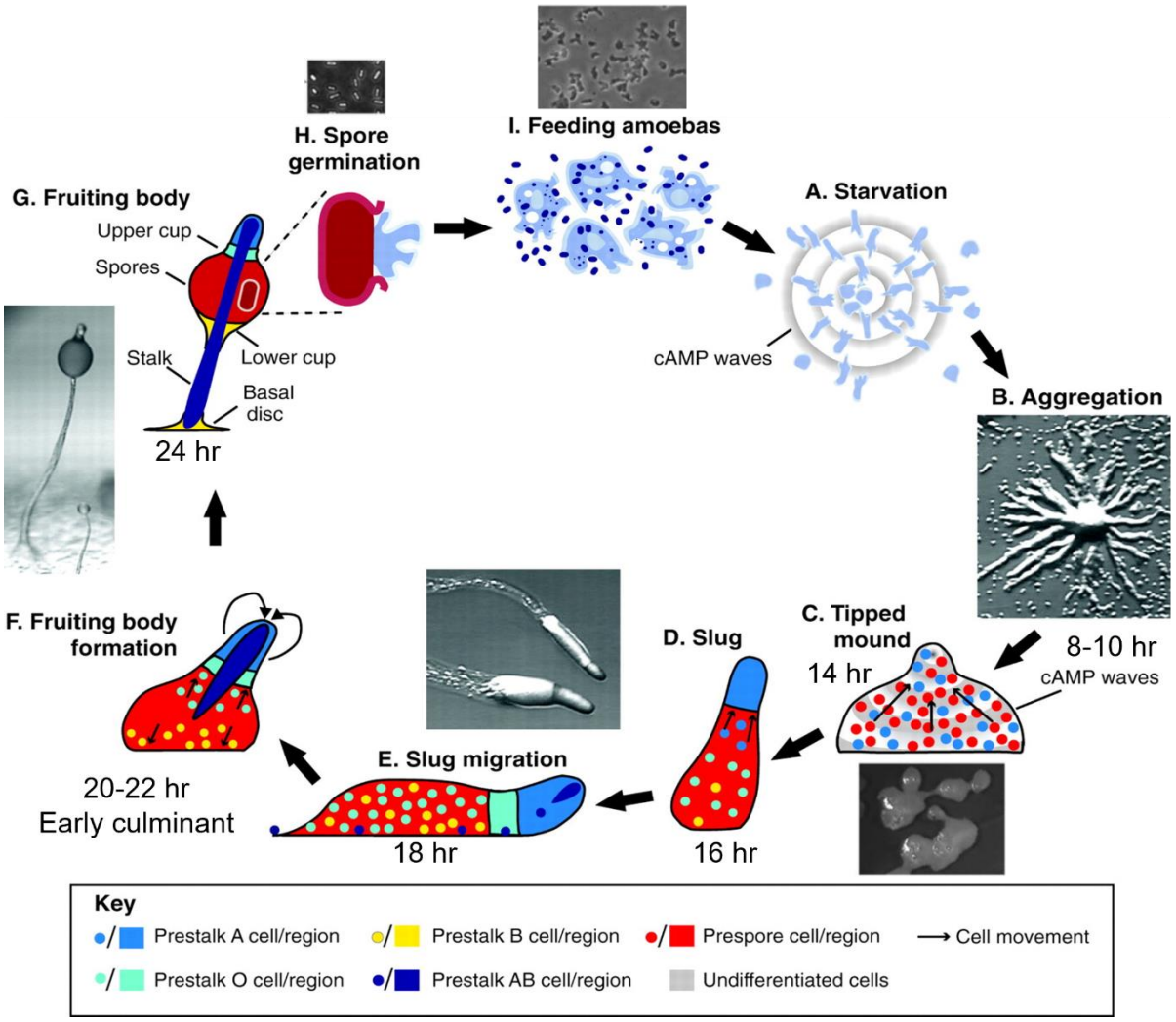


Figure 1.5. Summary of *Dictyostelium* developmental life cycle. Upon nutrient depletion, the developmental program is initiated in the starved cells, secreting cAMP pulses to attract the surrounding cells and leading to cell polarization at around 6 hrs. The chemotactically aggregating cells form streams leading multicellular structures such as mounds at 12-14 hrs and migrating slugs at 16-18 hrs. Cell type differentiation is obvious by slug stage with two main cell fates comprising of pre-spore (psp) cells and pre-stalk (pst) cells, including different clusters of subtypes pstA, pstB, pstO and pstAB, defined by the expression patterns of different pre-stalk genes. These all migrate to particular locations within the culminant structures (20-22 hrs) and self-organize to form fruiting bodies containing viable spores and vacuolated stalk cells at around 24 hrs. When the environment is favourable with rich nutrients again, spores germinate to resume the vegetative stage where the individual cells live unicellularly. Adapted and modified from (Muñoz-Braceras et al., 2013; Schaap, 2007).

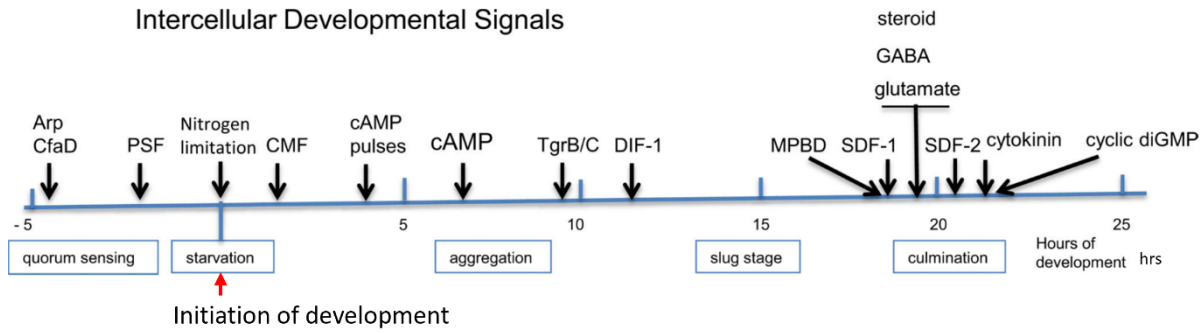


Figure 1.6. Signalling during the time course of *Dictyostelium* development. At different stages of development, transient signals integrate development. In the 5 hrs prior to starvation as the food source is being depleted, vegetative cells still grow and secret proteins functioning as sensors in quorum sensing. For example, proteins such as autocrine proliferation repressor protein A (ArpA) and counting factor-associated protein D (CfaD) as well as prestarvation factor (PSF) are secreted continuously when cell density increases. Following the initiation of development triggered by nitrogen limitation, morphogenesis in response to different signalling molecules occurs over 24 hrs. Conditioned medium factor (CMF) synthesized in growing cells only gets secreted when starvation triggers development. During the first 8 hrs of development, periodic cAMP synthesis and secretion initiate a series of signalling pathways, leading to expression of developmental genes, one of which is tiger protein C1 (TgrC1), a pulse-dependent gene encoding membrane glycoprotein gp150 forming a heterodimer with TgrB1 that regulate cell-cell adhesion and intercellular signalling. TgrC1 also regulates post-aggregative gene expression together with the DNA binding protein GBF. Differentiation inducing factor-1 (DIF-1) is a pre-stalk inducing signal synthesized in pre-spore cells. Later, 4-methyl-5-pentylbenzene-1,3 diol (MPBD) is secreted to induce terminal stalk cell differentiation when cells are preparing to construct fruiting bodies. Spore differentiation factor-1 (SDF-1) is released only just before the culmination stage, and when culmination is nearly complete, cells secrete a steroid to facilitate the release of γ-aminobutyric acid (GABA) which overcomes the inhibitory effect of glutamate preventing the release of SDF-2. At the end of development, cytokinin secreted from fruiting bodies has an inhibitory effect on spore germination, while cyclic-di-GMP inducing pre-stalk gene expression during termination of differentiation has an effect on encapsulation. The timeline is shown above the developmental stages which are indicated in boxes. Adapted from and reviewed by Loomis (2014).

1.2.2 *Dictyostelium* as a simple model organism with proteins well conserved throughout eukaryotes

Dictyostelium cell is a relatively simple system equipped with highly conserved eukaryotic signalling pathways (Loomis, 2014). Many processes implicated in human health are conserved in *Dictyostelium* (Annesley and Fisher, 2009), for example, pathogenic infection responses involving chemotaxis and phagocytosis in *Dictyostelium* are similar to immune responses mediated by neutrophils (Bozzaro and Eichinger, 2011; Manahan et al., 2004; Rosel et al., 2012; Sillo et al., 2008; Van Haastert and Devreotes, 2004), and autophagy is also reported in *Dictyostelium* (Calvo-Garrido et al., 2010; Dominguez-Martin et al., 2017; King et al., 2011; Mesquita et al., 2017). Caspase-independent programmed cell death in higher

eukaryotes can be studied by investigating *Dictyostelium* stalk cell differentiation (Levraud et al., 2003). cAMP signalling is a good example of a conserved signalling pathway. While cAMP signalling commonly controls intracellular physiological events in higher eukaryotes, *Dictyostelium* also produces and uses cAMP to activate downstream targets such as protein kinase A (PKA) which is an essential effector involved in growth-to-development transition and regulation of early developmental gene expression (reviewed by (Schaap, 2011)). On the other hand, while there is no cell surface cAMP receptor identified in mammalian cells (Jackson and Dubey, 2008), in *Dictyostelium*, extracellular cAMP triggers the activation of heterotrimeric guanine nucleotide binding protein (G protein) coupled receptors (GPCR) that relay signals to activate downstream effectors and instruct the transcription machinery to regulate gene expression (Ravnskjaer et al., 2016; Roesler et al., 1988; Saxe et al., 1988). During *Dictyostelium* development, there is no doubt that cAMP plays important roles in cell type differentiation and morphogenesis, promoting pre-spore pathway and directing developmental program (Kay, 1982; Kubohara et al., 2007; Schaap, 2011). The cAMP receptor Car1 (Klein et al., 1988b; Mann and Firtel, 1987), a heterotrimeric GPCR that locates on *Dictyostelium* cell surface, activates a number of downstream signalling pathways including small monomeric G proteins RasG and RasC (Bolourani et al., 2006), and phosphoinositide 3'-kinase (PI3K) (Kolsch et al., 2008) and the AKT/protein kinase B (PKB) (Manahan et al., 2004; Meili et al., 1999b). Ca^{2+} entry from the extracellular environment can also be mediated by GPCR-dependent or independent mechanisms (van Haastert et al., 2007).

Benefiting from its fully sequenced 34 Mb genome, many of the signalling components and pathways in higher eukaryotes are conserved in *Dictyostelium* (Eichinger et al., 2005) and molecular techniques can be used for studying gene and protein function. Even though it diverged before fungi, *Dictyostelium* surprisingly has more human protein homologs than the yeast model *Saccharomyces cerevisiae*, and many of them were found to be involved in cell motility, chemotaxis and phagocytosis, the iconic events in *Dictyostelium* life (Torija et al., 2006b; Williams et al., 2005). The high degree of protein similarity suggests that the genes encoding many of these proteins were lost in yeast, rather than convergent evolution of protein function. From comparative proteome analysis, *Dictyostelium* and humans share 1687 proteins that are absent in *S. cerevisiae* (Muñoz-Braceras et al., 2013), and 24 kinase subfamilies of the metazoan kingdom are found in *Dictyostelium* but not in yeast (Goldberg et al., 2006). For example, a well-conserved vacuole membrane protein 1 (Vmp1) which is reported to be

involved in autophagosome formation during autophagy in mammalian cells (Ropolo et al., 2007; Vaccaro et al., 2008) was identified in *Dictyostelium* but was found to be absent in fungi including *S. cerevisiae* and *S. pombe* (Calvo-Garrido et al., 2010; Calvo-Garrido et al., 2008; Torija et al., 2006a). These and many other examples show that *Dictyostelium* is a valuable model to study human proteins especially if relevant pathways are missing in fungal models.

However, some signalling components are not easily apparent in the *Dictyostelium* genome. For example, some broadly conserved kinases across eukaryotes have been lost in *Dictyostelium* during evolution, such as Ca^{2+}/calmodulin (CaM)-activated kinase-like (CAMKL) subfamilies CHK1 and PASK, ribosomal protein S6 kinase beta-1 (p70 S6K) existing in yeast and plants, and a recognisable protein kinase C (Goldberg et al., 2006). There are also no easily identifiable *Dictyostelium* ryanodine receptors (RyR) which play an important role in eukaryotic Ca^{2+} signalling in muscle cells (Ponting et al., 1997; Tae et al., 2009).

1.3 Cell fate decisions in *Dictyostelium discoideum*

Dictyostelium has been used as a model to study development since the early 1940s (Raper, 1940). Due to its unique unicellular-to-multicellular developmental switch triggered by nutrient depletion and formation of two main cell types, spores and stalk at the end of development, *Dictyostelium* is an ideal model to study cell fate determinants impacting on a 'binary' cell fate system.

1.3.1 DIF-1 is a morphogen regulating *Dictyostelium* pre-stalk cell differentiation

The best characterised morphogen in *Dictyostelium* is the chlorinated hydrocarbon DIF-1, while there are lower abundant DIF forms e.g. DIF-2 and DIF-3 chemically purified and identified (Kay et al., 1999; Masento et al., 1988). In the mound stage of developing *Dictyostelium* cells, DIF-1 (Mw: 307.20) has the ability to institute the basic distinction between pre-stalk and pre-spore cell fates, resulting from its inhibition of pre-spore differentiation and promotion of pre-stalk cell fate (Early et al., 1995; Early and Williams, 1988; Fosnaugh and Loomis, 1991; Kay and Jermyn, 1983; Wang et al., 1986). DIF-1 is a small

signalling molecule traveling across membranes and acts as a global pre-stalk inducer upregulating *ecmA* and *ecmB* pre-stalk gene expression during cell differentiation (Morrison et al., 1994; Saito et al., 2008; William and Morrison, 1994).

The DIF biosynthesis pathway involves multiple steps (Kay, 1998). Within the pathway, hybrid-type polyketide synthetases also known as 'Steely' enzymes are required for producing DIF, for instance, SteelyB (StlB) encoded by *stlB* gene (Austin et al., 2006). Polyketide synthase inhibitors such as cerulenin can inhibit DIF-1 synthesis (Kay, 1998). The polyketide DIF-1 product then undergoes modifications by a flavin-dependent halogenase encoded by the *chlA* gene and the Des-Methyl-DIF-1 methyltransferase encoded by *dmtA* gene, which are involved in DIF-1 biosynthesis processes (Neumann et al., 2010; Thompson and Kay, 2000b). Another Steely enzyme StlA was found to induce spore maturation (Narita et al., 2011) suggesting that there are other related compounds which may act in the spore differentiation pathway. Both *stlB* and *dmtA* mRNAs are enriched in pre-spore population suggesting that pre-spore cells synthesise DIF-1 to induce differentiation of pre-stalk cells. (reviewed by (Loomis, 2014)). There are at least five DIF molecules secreted from developing cells during late aggregation and resolved by high-performance liquid chromatography (HPLC), DIF-1 to 5, and DIF-1, 2 and 3 were identified as chlorinated alkyl phenones, while DIF-4 and 5 are far less characterised with an unknown relationship with DIF-1 (reviewed by (Kay et al., 1999)). Among all these DIFs, DIF-1 is one of the most potent DIFs used in bioassays, and its induction of expression of pre-stalk specific markers includes *drcA* encoding a DIF-dechlorinase for its own degradation and *ecmA* mRNA, both preferentially in pre-stalk cells (Parikh et al., 2010; Velazquez et al., 2011). The DIF-1 concentration is therefore regulated by a negative feedback that has DIF-1, synthesised in pre-spore cells triggering increase of DIF-1 dechlorinase levels in pre-stalk cells for its own breakdown (Insall et al., 1992), which can be illustrated by the general model shown in Figure 1.4C. The dynamics of pre-spore cells making DIF-1 and pre-stalk cells degrading DIF-1 establishes a sharp gradient at the boundary between pre-spore and pre-stalk cells (Loomis, 2014).

A receptor for DIF has not been identified but is thought to be intracellular as DIF molecules are predicted to be membrane permeable, and DIF-1 binding activity was reported in cytoplasm and nucleus (Insall and Kay, 1990). Downstream of DIF-1 signalling, transcription factors

regulating DIF-dependent gene expression have been identified (reviewed by (Fukuzawa, 2011)). For example, a signal transducer and activator of transcription (STAT), STATc which is highly conserved across species from *Dictyostelium* to mammals (Kawata et al., 1997), undergoes DIF-1 dependent tyrosine phosphorylation, dimerization and translocation into nucleus during early development (Araki et al., 1998; Fukuzawa et al., 2001). Also, DIF-1 mediated stalk cell differentiation is greatly dependent on the basic leucine zipper (bZIP) transcription factors DimA and DimB which have homo- and heterodimeric interactions in response to DIF-1 to regulate diverse DIF-1 responses (Huang et al., 2006). Together they control stalk cell formation, as DimB suppresses non-vacuolar cell death and DimA inhibits spore formation (Huang et al., 2006). DIF-1 acts as a direct inducer for pre-stalk *ecmB* gene expression which is expressed in pstB cells. Disruption of the gene encoding DimB which is only enriched in nucleus of pstB cells in slugs leads to depletion of pstB cell differentiation and diminishment of cells within the corresponding tissues, the lower up and basal disc (Yamada et al., 2011). When treated with exogenous DIF-1, a rapid DimB accumulation in nucleus was observed in developing *dmtA*$^-$ cells (which have a loss of DIF-1 production (Thompson and Kay, 2000b)) dissociated from aggregate structures (Zhukovskaya et al., 2006), and this nucleus translocation upon DIF-1 induction is also verified by cells with constitutively expressing DimA and DimB treated with DIF-1 in monolayer setting (Huang et al., 2006). In the presence of exogenous cAMP, DIF-1 mediates DimB to interact with the *ecmA* promoter and therefore regulate *ecmA* expression which is normally expressed in the pre-stalk region at the slug tip (Zhukovskaya et al., 2006). It is worth mentioning that *dmtA*$^-$ cells have defective phenotypes in mid- and late development, such as formation of break up slugs and aberrant fruiting bodies (Thompson and Kay, 2000b). Although these developmental defects in *dmtA*$^-$ cells can be rescued by DIF-1, it was found that only pstO cell differentiation is dependent on DIF-1 in multicellular development and pstA cell type formation is independent on DIF-1 (Thompson and Kay, 2000b). Also, there might be other stalk inducers specific to pstA cell type differentiation rather than DIF-1, such as DIF-6 and DIF-7 polyketides (Serafimidis and Kay, 2005). Overall, DIFs and other developmental cell type inducing signals mediate differentiation of various cell types during multicellular development.

There are also reports that membrane-penetrating DIF-1 diffusing freely into the *Dictyostelium* cells is localized to mitochondria using a fluorescent derivative of DIF-1 (boron-dipyrromethene (BODIPY)-conjugated DIF-1) at the concentration of 5 μM, mediating stalk

cell differentiation via altering mitochondrial activity (Kubohara et al., 2017). However, these concentrations of DIF-1 are an order of magnitude higher than used in biological assays to induce stall cell differentiation. A more well-established potential mechanism of DIF-1 mediating pre-stalk cell differentiation is through induction of elevation of intracellular Ca^{2+} levels. It was reported that the increase in cytosolic Ca^{2+} levels in response to 100 nM DIF-1 upregulates the expression of the *ecmB* pre-stalk gene with kinetics resembling that of the Ca^{2+}-ATPase inhibitor 2,5-di(tert-butyl)-1,4-hydroquinone (BHQ) treatment, and such DIF-1 mediated *ecmB* induction can be inhibited by treatment with Ca^{2+} chelators (Schaap et al., 1996). The DIF-1-induced increase in cytosolic Ca^{2+} levels is dependent on the inositol-1,4,5-trisphosphate receptor (IP_3R)-like A (IPLA) Ca^{2+} channel which is mainly located in the endoplasmic reticulum (ER) Ca^{2+} stores (Traynor and Kay, 2017; Traynor et al., 2000) and required for DIF-induced autophagic cell death (Lam et al., 2008), as 100 nM DIF-1 fails to stimulate an intracellular Ca^{2+} response in *iplA*$^{-}$ cells at vegetative or early development stages (Traynor and Kay, 2017).

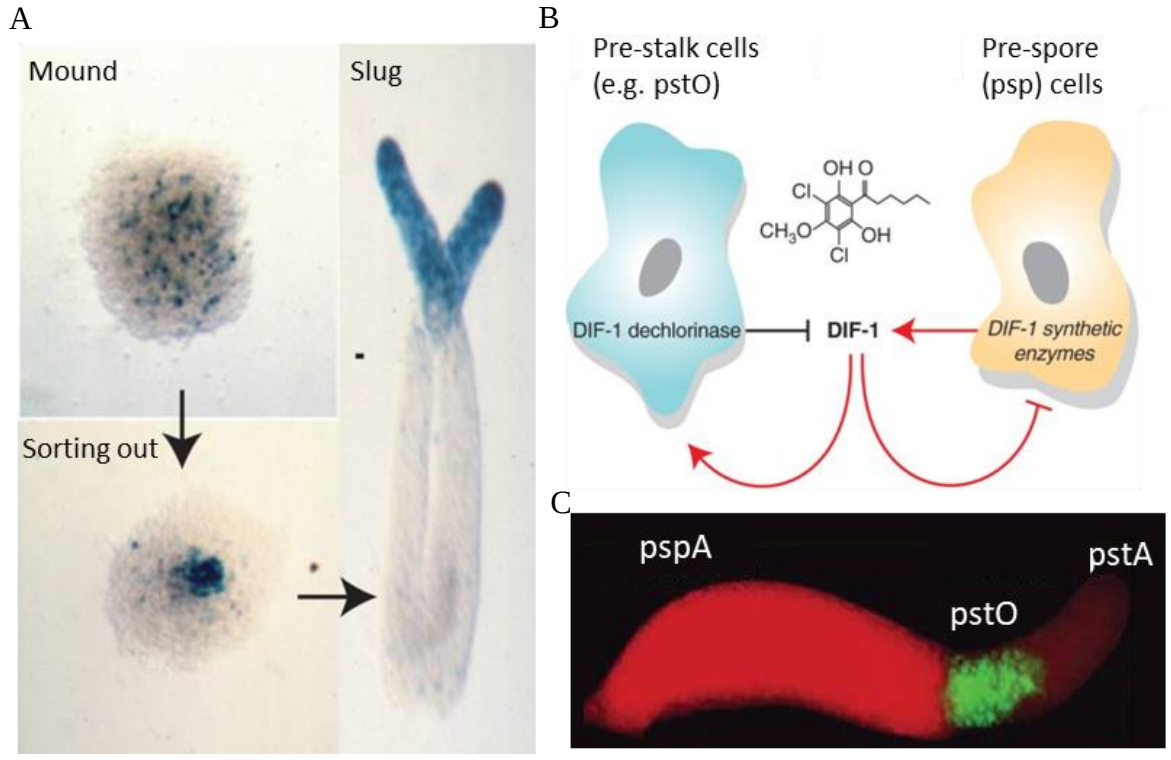


Figure 1.7. DIF-1 roles in patterning during *Dictyostelium* development. (A) At the early mound stage, stalk-and-pepper patterning is observed where the pre-stalk (pst) cells expressing the stalk reporter fusion construct *ecmAO*-lacZ stained in blue colour are intermingled with the unstained pre-spore (psp) cells in a scattered distribution. Next, pst cells migrate into a defined

pre-stalk region at the top of the mound structure which elongates to form the slug structure where pre-stalk cells predominantly localize at the front region. (B) This pattern formation is mediated by the DIF-dependent regulation of pre-stalk cell differentiation (in particular being required for differentiation of pstO cells in multicellular structures). Produced by pre-spore cells, DIF-1 diffuses freely between cells and induces pre-stalk pstO cell differentiation. DIF-1 is degraded by a dechlorinase expressed preferentially in pre-stalk cells and suppresses expression of its own synthetic enzymes as well as inhibiting pre-spore cell differentiation. Therefore, the levels of DIF-1 and the proportion of pstO cells are strictly maintained by these two negative feedback loops. (C) The overall organization of a slug with cell types labelled via *in situ* hybridization. PstO cells labelled green with a probe against the SSM184 cDNA are at the boundary of the pre-stalk and pre-spore region and unlabelled pstA cells are in the most anterior region of the slug (to the right), and the pre-spore cells labelled red using a probe against *pspA*. Image courtesy: Mineko Maeda and Yoko Yamada (Yamada et al., 2005). Adapted from Kay and Thompson (2009).

1.3.2 Genetic differences in mixed aggregates can influence cell fate decisions

In social evolution, a conflict in survival competition points out a potential cheating phenomenon, where some individuals from a different genetic population become 'cheaters' exploiting most of the resources from the 'victim' in a cooperative system without paying a fair share. This can be seen in a spore-forming prokaryotic species *Myxococcus xanthus* with specific mutations to achieve higher sporulation efficiencies distinguishing from the wildtype ancestor (Fiegna et al., 2006; Velicer et al., 1998; Velicer et al., 2000). In *Dictyostelium* development, if there is only one clone of cells developing into fruiting bodies, the sterile stalk cells can still pass their genes onto the next generation and sacrifice themselves to support the others for reproduction (Hamilton, 1964a, b; Li and Purugganan, 2011; Strassmann et al., 2000). However, in mixed aggregates with more than one genetic background, cheating individuals carry various intrinsic genetic factors to allow them to be more capable of survival by producing more spores when developing with other populations who do not possess such survival-benefiting 'cheater' genes. These cheaters with more spore formation in *Dictyostelium* development force the other cells to become dead stalk cells in chimeric development (Khare and Shaulsky, 2010; Li and Purugganan, 2011; Santorelli et al., 2013). Chimeric development using different wild populations was observed and single clones from natural isolates can be cheaters when co-developed with others (Gilbert et al., 2007; Strassmann et al., 2000). Natural variants identified from the wild isolates possess specific genetic variations, such as those encoded by divergent alleles of *tgrB1* and *tgrC1* which are highly polymorphic in natural populations and regulate self-recognition via kin discrimination which favours aggregation with more closely related cells and segregates unrelated cells within mixed populations during

development (Benabentos et al., 2009; Hirose et al., 2011; Ostrowski et al., 2008).

In the laboratory setting, generating pools of genetic mutants containing cheater and victim mutations in *Dictyostelium* allow the study of pathways with different genetic factors influencing cell fate. Isolated from a pool of restriction enzyme-mediated integration (REMI) mutants in the lab, *chtA*$^{-}$ (also called *fbxA*$^{-}$ as the mutation targets a gene encoding a protein with F-box and WD40 repeats) was identified as the first genetic cheater strain, leading to a high level of spore formation when developing with parental cells, but this mutant has defects in spore production when developing on its own, therefore, it is considered as an obligate parasite (Ennis et al., 2003; Ennis et al., 2000; Kupsa and Loomis, 1992; Nelson et al., 2000). Other examples of identified cheater strains include *chtB*$^{-}$ (Santorelli et al., 2013; Santorelli et al., 2008) and *chtC*$^{-}$ (Khare and Shaulsky, 2010; Santorelli et al., 2008). A 'victim' mutant *dimA*$^{-}$ has defects in responding to DIF-1, as *dimA* encodes the bZIP/bRIZ transcription factor required for DIF-1 signalling (Thompson et al., 2004), and the LAS19 clone is an example of a victim mutant isolated from the large-scale genetic screens (Santorelli et al., 2008). To conclude, genetic factors possessed by different populations play roles in determining cell fate tendencies when mixing different populations of cells either isolated from the wild or generated in the laboratory.

1.3.3 Cell fate determinants within the same genetic population play roles in cell fate decisions

Within a seemly homogenous population where cells have an identical genetic background, there are variations between individual cells that cause predisposition to a certain cell fate. Such heterogeneities within cell populations are considered to establish different DIF-1 responsiveness thresholds during early development: the higher the DIF-1 threshold, the lower sensitivity of cells responding to DIF-1, and therefore the less likely these cells are to differentiate into pre-stalk cells (Figure 1.8A). In this DIF-1 threshold model, pre-stalk biased conditions lower the threshold to respond to DIF-1, i.e. cells are more responsive to DIF-1 and then to choose the pre-stalk cell fate, while the pre-spore biased conditions raise this threshold, making cells less sensitive towards DIF-1. One of the molecular bases setting the DIF-1 threshold is through noise-induced oscillations which control the pre-stalk biased gene expression (Figure 1.8B).

Several cell fate determinants from cell growth have been reported to predispose cell fate decisions as sources of non-genetic heterogeneity within an asynchronously dividing population, including the nutrient state, cell cycle position, intracellular pH and intracellular Ca^{2+} levels (see details in the main text and Table 1).

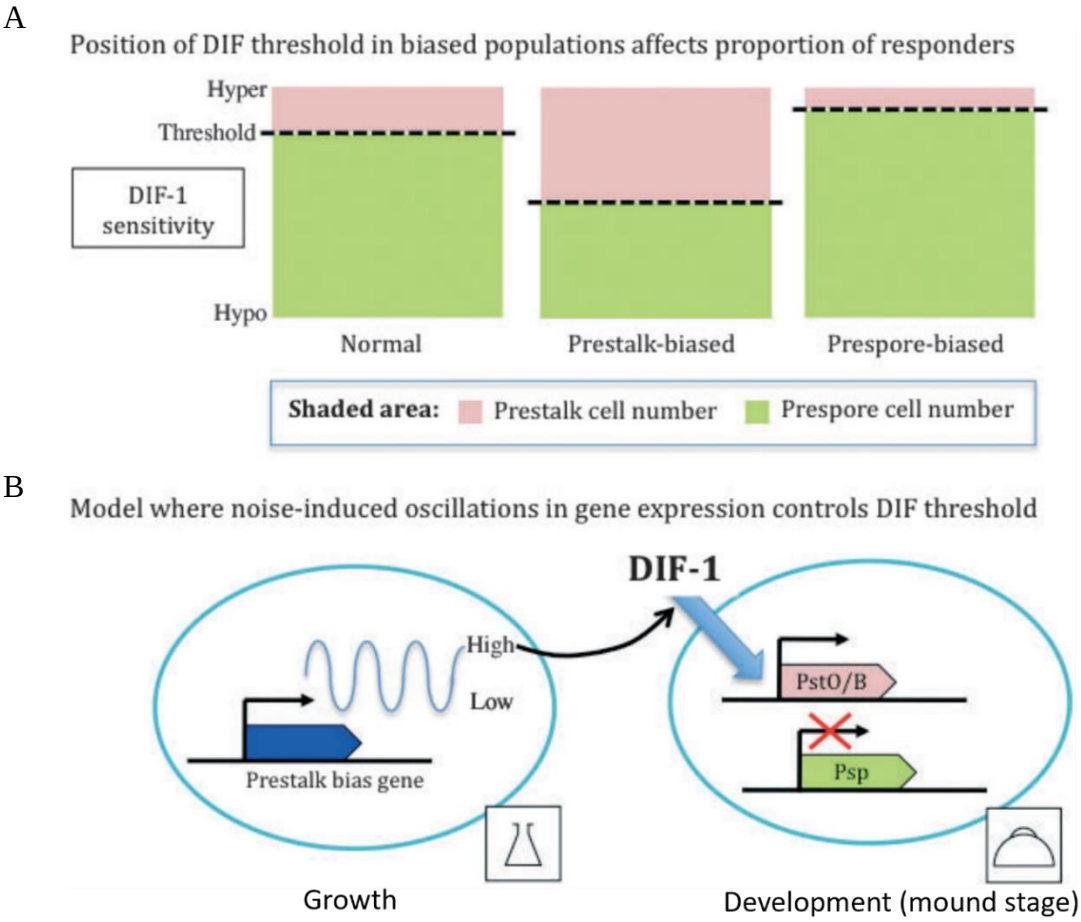


Figure 1.8. Schematic representation of DIF-1 threshold heterogeneity during cell growth influencing cell fate bias in development. (A) The average DIF-1 threshold of a cell population, indicated as a dotted line, differs between normal cells to cells with pre-stalk or pre-spore biases. The thresholds can be changed by growing cells under different conditions which are considered as cell fate determinants, altering the proportions of pre-stalk (shown in pink) and pre-spore (shown in green) cells later in development indicated by the size of the shaded area. (B) The model of noise generated from the expression of a hypothetical pre-stalk bias gene (shown in blue) regulating the DIF-1 response threshold in individual cells. With the upregulated expression of the pre-stalk biased gene, cells during the growth stage are sensitized to DIF-1 (black arrow), allowing the DIF-1 threshold to be lowered for promoting pre-stalk gene expression (shown in pink) and repressing pre-spore gene expression (shown in green) during development e.g. at the mound stage. Adapted from Chattwood and Thompson (2011).

1.3.3.1 Nutrient history in cell growth influences cell fate later in development

Nutrient accessibility is crucial for cell growth and survival. Different sources of nutrients include carbohydrates for energy supply, amino acids and other micronutrients including vitamins (e.g. vitamin A, D and E) and minerals (e.g. sources of calcium, zinc and iron) are key components in synthetic media for laboratory cell culture (Franke and Kessin, 1977; Yao and Asayama, 2017). In *Dictyostelium* axenic growth, HL5 culture medium is commonly used containing yeast extract and peptone as sources of amino acids (Ashworth and Watts, 1970). The presence of amino acids and glucose inhibit cell differentiation through suppressing the activity of adenylate cyclase (AC) that is usually activated early following starvation for cAMP synthesis. However, the inhibitory effects of amino acids and glucose on cell differentiation happen in different times, the former acts at earlier times of starvation and the latter acts subsequently (Darmon and Klein, 1978), indicating different mechanisms involved in responding to starvation of amino acids and glucose.

Alteration of nutrient history during cell growth by incubating vegetatively growing cells in glucose rich (G+) or deficient (G-) culture media is one of the most classic examples to illustrate the predisposition of biased cell fate, and this was first examined experimentally by Leach et al. (1973), developing mixtures of genetically identical cells grown in G+/- media. Cells cultured with G+ medium before development preferentially choose a spore cell fate and those incubated in G- medium choose a stalk cell fate. This result has been verified by others (Blaschke et al., 1986). This bias was shown to correspond to DIF-1 responsiveness by using monolayer assays plating cells at a very low cell density and initiating stalk cell differentiation with buffer supplied with DIF-1, using cells expressing a pre-stalk marker which fuses the lacZ reporter under the control of pre-stalk *ecmAO* promoter. With this method, G- cells have higher sensitivity to DIF-1 and therefore tend to differentiate into pre-stalk cells, consistent with the observations seen in chimeras (Thompson and Kay, 2000a).

1.3.3.2 Cell cycle position at the onset of development plays a role in cell fate decisions

The cell cycle phase of individual growing cells in an asynchronous population is heterogenous and is a good example to show how variations of non-genetic factors affect developmental outcomes. The *Dictyostelium* cell cycle has a really short or even undetectable G1 phase

compared to most other organisms (Weijer et al., 1984b), with a long and variable G2 phase and a shorter S being the main phases, separated by mitosis (M) (reviewed by Weeks and Weijer (1994)). In a growing population, most vegetative cells will be in the G2 phase, while the remainder will be in M or S phase (Muramoto and Chubb, 2008; Zada-Hames and Ashworth, 1978). The variation of cell cycle length contributes to the heterogeneity of cell cycle phases within the whole population of growing cells, priming cells to future developmental fates, for example, longer cell cycle length than the average leads to a relatively stalk cell fate tendency (Gruenheit et al., 2018). The ratio of G2 to M/S phase cells within a population is about 4:1, correlated to the ratios of spore (80%) to stalk (20%) in the fruiting body from development (reviewed by Chattwood and Thompson (2011)). Cells in the S and early G2 phases when starved sort out to the anterior pre-stalk zone of the slug, but late G2-phase cells when starved migrate to the posterior spore region (Araki et al., 1994; McDonald and Durston, 1984; Weijer et al., 1984a). By interfering with the cell cycle using DNA replication inhibitors to lengthen S phase, the M/S-phase population increases and so does the pre-stalk proportion in development, illustrated by the upregulated expression of the pre-stalk markers *cp2* and *ecmA*-lacZ (Gomer and Ammann, 1996), which is in agreement with the experiments starving cells synchronized in S and early G2 phase in monolayer system leading to preferential expression of pre-stalk marker (Gomer and Firtel, 1987). More advancing live-cell imaging techniques using a green fluorescent protein (GFP)-tagged replication factor proliferating cell nuclear antigen (PCNA) to precisely trace S-phase cells for DNA synthesis (Muramoto and Chubb, 2008) support the model initially proposed by Gomer and Ammann (1996) (Figure 1.9).

In an asynchronous population, the development of vegetatively growing *Dictyostelium* cells leads to the formation of 80% spores and 20% stalk cells approximately (reviewed by William and Morrison (1994)), while cell cycle synchronization can alter the proportion of spores and stalk cells in fruiting bodies (Weijer et al., 1984a, b). To generate a population of cells synchronized (or enriched) in the G2 cell cycle phase, cells can either be grown to stationary phase or incubated in a low temperature (e.g. at 10 °C) and after recovering in the fresh growth medium at 22 °C, they are released from G2 phase and go through one or multiple rounds of synchronous division (Maeda, 1986). Cells shortly after release from the G2 arrest during synchronization are enriched in cells in M/S cell cycle phase, and they give rise to around 50% of pre-spore and pre-stalk cells (Weijer et al., 1984a). If developing synchronized cells are

harvested later in G2 phase, the proportion of pre-spore cells increase to 90% and only 10% are pre-stalk cells (Weijer et al., 1984a). Moreover, using *in vitro* monolayer cultures where cells at a low cell density are plated for development and the expression of pre-stalk and pre-spore markers are detected by cell-type specific antibodies, Gomer and Firtel (1987) discovered that when cells are synchronized in S or early G2 phases using the stationary phase release method or a nocodazole block (which blocks cells in M phase), they have a propensity of cells expressing pre-stalk genes and the cells from other phases prefer a pre-spore cell fate. This finding drew a similar conclusion as the *in vivo* experiments that the initial ratio of pre-stalk and pre-spore cells is closely dependent on their cell cycle position. The monolayer experiments also show that this predisposition of cell cycle phase on cell fate decisions in individual vegetative cells is autonomously independent of position in a 3D structure and cell-cell contact (Gomer and Firtel, 1987). An alternative approach looking at multicellular development is in mixing experiments, with asynchronized cells developing together with synchronized cells in either G2 phase or M/S phase: cells synchronized M/S phases predominantly localize in the pre-stalk (anterior) region in the slugs compared to asynchronized portion, while cells from synchronized G2 population become posterior in the slug and have a pre-spore cell fate tendency (Araki et al., 1994; Thompson and Kay, 2000a). This is consistent with the results of monolayer assays assessing DIF-1 sensitivity of cells with pre-stalk reporter *ecmAO*-lacZ in monolayer, which showed cells from different cell cycle phases have different DIF-1 responsiveness. Cold shock-synchronized cells recovered in early S phase are more sensitive to DIF-1 than cells harvested in G2 phase (Thompson and Kay, 2000a). These results support the theory that heterogeneity of cell cycle phases in an asynchronous population has a predisposition effect in clonal differentiation into spore or stalk cell types during development.

Other organisms also have situations in which cell cycle phase regulates development. For example, Notch signalling is cell cycle phase-dependent and is reported to occur only during S phase in *C. elegans* vulva precursor cells, and this is also reported in asymmetric cell division during neurogenesis in *Drosophila melanogaster* (Ambros, 1999). Cell cycle phases influence Ca^{2+} signalling in mammalian cell type differentiation (reviewed by (Machaca, 2010)) and pH regulating cell cycle phase transition as a part of checkpoint mechanism in mammalian cells can also influence stem cell differentiation (Flinck et al., 2018; Liu et al., 2020). In *Dictyostelium*, these two physiological parameters intracellular pH and Ca^{2+} also correlate with cell fate decisions (reviewed by (Chattwood and Thompson, 2011; Jang and Gomer, 2011)).

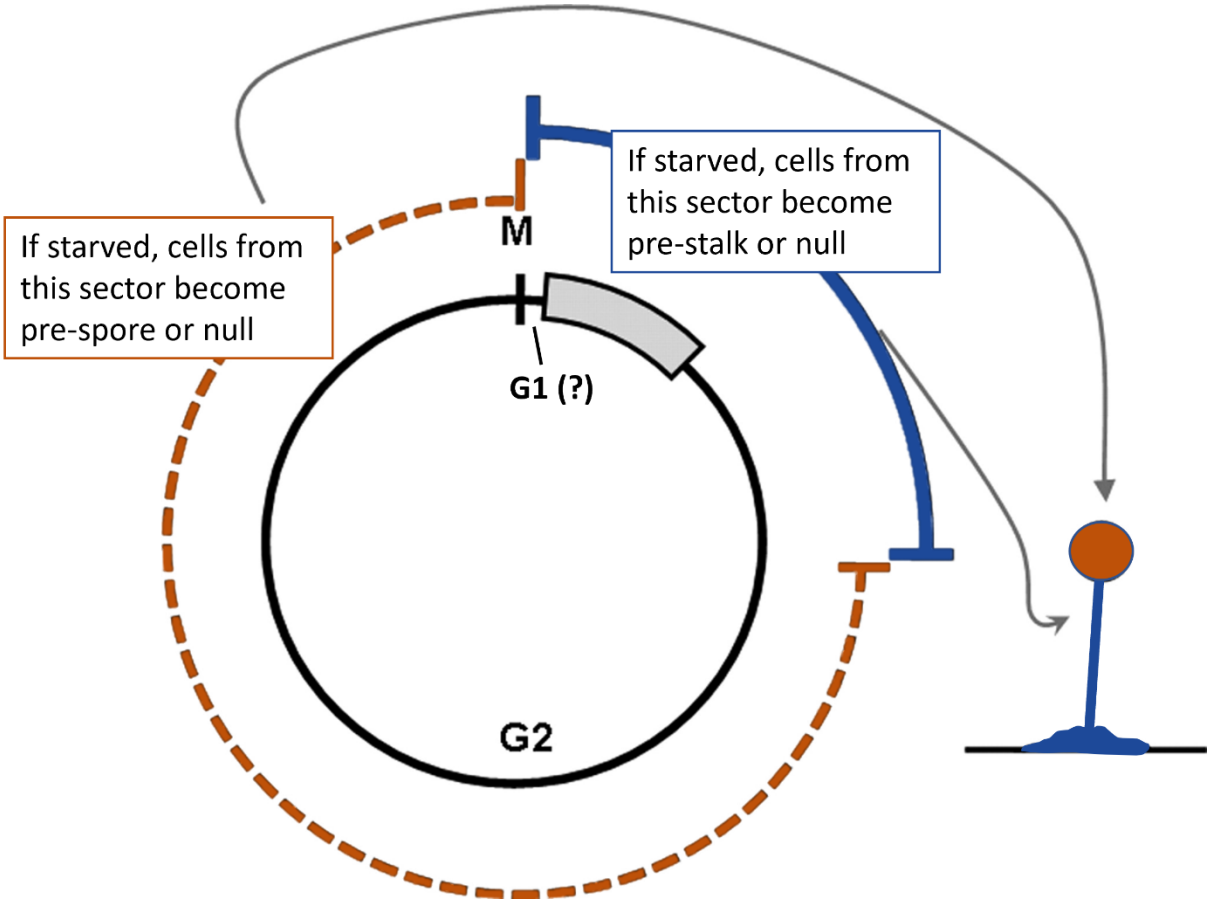


Figure 1.9. Schematic representation of *Dictyostelium* cell cycle-dependent mechanism initiating cell fate decision. The length of cell cycle phases is indicated in an annotated circle. The mitosis stage separating the S phase (shown in the grey box) and the G2 phase, the longest phase in *Dictyostelium* cell cycle, while G1 phase was reported either very short or absent in the cell cycle. This model illustrates the phase of cell cycle at the time of cells being starved regulate the cell type choices from the vegetative growth. In a migrating slug, apart from pre-spore and pre-stalk cell types, there are also null cells which mainly localize in a region between pre-stalk and pre-spore zones and are also intermingled with pre-stalk and pre-spore cells around that region, and these cells are not yet deciding their lineage identities as they are not stained with antibodies against pre-stalk (anti-CP2) and pre-spore (anti-SP70) markers (Gomer et al., 1986; Gomer and Firtel, 1987). When cells are in S and early G2 phase (sector indicated in solid blue line), they tend to be pre-stalk (CP2-positive) or null cells. When cells are in later G2 to M phase (sector shown in dashed red line), they become pre-spore or null cells (Gomer and Ammann, 1996). Adapted from Jang and Gomer (2011).

1.3.3.3 Vesicle pH influences cell fate

pH is an important regulatory factor for development and cell differentiation, such as in human stem cells (Charruyer and Ghadially, 2018; Ulmschneider et al., 2016) and sea urchin eggs (Winkler and Grainger, 1978). In *Dictyostelium*, cell cycle and pH during cell growth link closely to regulation of cell type differentiation (reviewed by (Chattwood and Thompson, 2011)). Intracellular pH oscillates autonomously with cell cycle phases and potentially regulates the mitotic cycle (Aerts et al., 1985). For instance, cells at interphase have a minimum pH of 7.2 which starts to increase at the beginning of protein synthesis and DNA replication and peaks at pH 7.45 during M/S phase (Aerts et al., 1985). The pH oscillation basis during cell cycle progression can be a source of heterogeneity in vesicle pH in growing cells (Chattwood and Thompson, 2011).

Subcellular organelles including endosomes, lysosomes, acidocalcisomes and contractile vacuoles are considered to be 'acidic' compartments due to the existence of vacuolar H^+-ATPases on their membranes creating cross-membrane proton gradients and keeping a low pH level inside the vesicles (reviewed by Gross (2009)). The pH of acidic vesicles, which could vary between cells in the population, is an intrinsic factor proposed to predispose cells to a particular cell fate. The increase of vesicle pH when treating asynchronized vegetative cells with weak base ammonia (NH_4Cl) (Aerts et al., 1985; Davies et al., 1996) is correlated to rapid protein synthesis and DNA replication, but when the DNA replication and protein synthesis of the cell cycle-synchronized cells are blocked by hydroxyurea and cycloheximide respectively, the pH oscillations persists even when the cell cycle is disrupted (Aerts et al., 1985). More importantly, changing the vesicle pH with the weak base ammonia or the weak acid 5,5-dimethyl-2,4-oxazolidineolione (DMO) at the onset of development significantly alters cell fate decisions. For example, when cells are incubated in ammonia treated media (pH 7.8) before development and mix with untreated cells, they tend to form a high pre-spore proportion in the multicellular structure (Aerts et al., 1987).

Although adjusting pH in cells using weak bases such as ammonia and imidazole and weak acids such as acetate were described as altering intracellular pH in *Dictyostelium* cells in early literature (Aerts et al., 1985; Gross et al., 1983). It was shown later that the intracellular targets of weak bases are acidic compartments in *Dictyostelium*. This was confirmed using *in vivo*

nuclear magnetic resonance (NMR) experiments using pH-sensitive ^{31}P-labelled phosphonate probes, showing that the cytosolic pH had no apparent change upon weak base exposure (Davies et al., 1993). Moreover, another NMR experiment and microfluorimetry demonstrated that cytosolic pH is not significantly changed upon DIF-1 treatment, which suggests that the cytosolic pH might not be the main factor to influence cell type differentiation (Inouye, 1988; Kay et al., 1986). Due to the variation of pH measurement, some literature shows the intracellular pH of pre-stalk cells is relatively acidic compared to pre-spore cells (Dominov and Town, 1986; Inouye, 1988) while others argue the difference is trivial (Kay et al., 1986; Ratner, 1986). However, it is certain that pre-stalk and pre-spore cells have differences in the proton exchange ability, as pre-spore cells have four times higher plasma membrane proton pump activity and higher intracellular buffering compacity than the pre-stalk cells (Inouye, 1989).

Changes of vesicle pH during development by weak base and weak acid treatments alter pre-spore and pre-stalk cell fate bias (Aerts, 1988; Dominov and Town, 1986; Gross et al., 1983; Inouye, 1988; Kubohara and Okamoto, 1994). A monolayer assay reports that weak base ammonia inhibits DIF accumulation and suppresses pre-stalk cell type differentiation without affecting the formation of pre-spore cells (Neave et al., 1983). Furthermore, inhibitors of plasma membrane proton pumps reducing vesicle pH can shift the cell fate from pre-spore to pre-stalk tendency (Gross et al., 1988). Genetic mutant strains Hgr5 and Hgr8 that lose acidic endo-lysosomal vesicles have reduced vacuolar H^+-ATPase activity and they are abnormally hypersensitive to the weak base imidazole in development, indicating that weak base-induced alkalinization in acidic compartments affects development (Davies et al., 1996). Weak acid treatment during development in monolayers makes cells become more sensitive to DIF-1 and have increased stalk cell differentiation compared to the untreated control (Kubohara et al., 2007). These results illustrate the role of vesicle pH on cell fate decisions.

1.3.3.4 Intracellular Ca^{2+} levels influence cell fate

The Ca^{2+} signalling toolkit is well-reviewed and can be dated back to early evolutionary roots in protozoa, although less pronounced in prokaryotes (Berridge et al., 2003; Clapham, 2007; Dominguez et al., 2015; Plattner and Verkhratsky, 2013; Shemarova and Nesterov, 2005). The Ca^{2+} signalling machinery orchestrates the development processes in many organisms, including keratinocyte differentiation in mouse epidermal development (Tu and Bikle, 2013)

and larval wing disc development in *Drosophila melanogaster* (Brodskiy et al., 2019). In *Dictyostelium* early development, extracellular cAMP triggers Ca^{2+} influx (Wick et al., 1978) and mobilizes cytosolic Ca^{2+} from intracellular Ca^{2+}-sequestering compartments, dependent on the presence of the IPLA protein, predicted to be a calcium channel on the ER membrane (Flaadt et al., 1993a; Nicholas Europe-Finner and Newell, 1985; Traynor et al., 2000).

Intracellular Ca^{2+} is a crucial morphogenic factor in *Dictyostelium* cell type differentiation during vegetative life and development (reviewed by (Chattwood and Thompson, 2011; Jang and Gomer, 2011)). Intracellular Ca^{2+} levels in pre-aggregation and post-aggregation stages are heterogenous between individual cells in the population (Azhar et al., 1996; Saran et al., 1994). This was observed by fluorescence-activated cell sorting (FACS) using the fluorescent Ca^{2+} probe chlortetracycline (CTC) to detect sequestered Ca^{2+} (Saran et al., 1994) or Ca^{2+}-specific dye indo-1/AM to detect cytosolic Ca^{2+} (Azhar et al., 1996). Vegetative cells with heterogenous Ca^{2+} levels fall into two categories with high or low Ca^{2+}-dependent fluorescence levels, and when starting development, cells with higher fluorescence and therefore with higher Ca^{2+} levels are localized in the pre-stalk anterior region of the slugs, while cells with lower Ca^{2+} levels are observed to be in posterior region with a pre-spore cell fate (Azhar et al., 1996; Saran et al., 1994). At the slug stage, pre-stalk cells have higher levels of resting Ca^{2+} than pre-spore cells (Abe and Maeda, 1989; Baskar et al., 2000). Isolated from slugs, pre-spore cells were able to sequester Ca^{2+} more effectively than pre-stalk cells (Schlatterer et al., 2001).

Moreover, variations in intracellular Ca^{2+} levels during development also alters cell fate decisions. Exposing cells to high Ca^{2+} concentrations during development promotes stalk cell differentiation and inhibits spore cell formation (Maeda, 1970). This is also consistent with the observation that drug-induced intracellular Ca^{2+} increase result in pre-stalk cell differentiation in the slug stage (Baskar et al., 2000). Another way to show intracellular Ca^{2+} levels correlating with the pre-stalk cell fate is through the monolayer system. Using drugs inhibiting Ca^{2+}-ATPases such as thapsigargin or BHQ to increase intracellular Ca^{2+} levels, cells were a hundred times more sensitive to DIF-1 for induction of pre-stalk marker gene expression compared to the untreated control, while chelators such as ethylene glycol tetra-acetic acid (EGTA) reduce cellular Ca^{2+} levels and the responsiveness of cells towards DIF-1 (Baskar et al., 2000; Kubohara et al., 2007; Schaap et al., 1996).

Ca^{2+} is reported to link to the cell cycle and regulates mammalian cell type differentiation (reviewed by (Machaca, 2010)). Similarly, there is a genetic link between intracellular Ca^{2+}, cell cycle and cell fate reported in *Dictyostelium* cells (Chattwood and Thompson, 2011). For example, *ratioA* (*rtoA*) gene expression levels are different in distinct cell cycle phases, with upregulated expression during G2 phase and downregulated levels in M/S phases (Brazill et al., 2000). While *rtoA* expression is normally confined in pre-spore cells during development, the *rtoA*$^{-}$ strain overexpresses pre-stalk markers and has reduced calcium efflux leading to an increase in the number of cells with elevated cytosolic Ca^{2+} levels (Azhar et al., 2001; Brazill et al., 2000; Wood et al., 1996). More strikingly, the *rtoA*$^{-}$ strain has an apparently normal cell cycle but pre-stalk cell differentiation is not coupled to M/S cell cycle phases but originates from random cell cycle phases, indicating that disrupting this link via *rtoA* mutation breaks the cell cycle-dependent cell fate decision program, probably through the dysregulation of Ca^{2+} homeostasis (Wood et al., 1996). Furthermore, acidic vesicles in the endolytic system are often involved in Ca^{2+} sequestration by an ATP-dependent Ca^{2+} transporter which is coupled to the vacuolar H^{+}-ATPase (Milne and Coukell, 1989; Rooney and Gross, 1992b; Xie et al., 1996). Therefore, Ca^{2+} and vesicle pH are closely interrelated, and their interplay might also have regulatory roles on cell fate decisions.

Table 1. Examples of cell fate influencing factors in *Dictyostelium*

Factors influencing intrinsic cell fate bias	Developmental fates		Examples of evidence	References
	Spore	Stalk		
Nutrient history: glucose	G+	G-	GFP-labelled G+ cells localize in the pre-spore (posterior) region in the slug, while GFP-labelled G- cells are located at pre-stalk (anterior) part when developing cells chimerically. G+ cells make more spores when developing with G- cells in mixtures.	(Leach et al., 1973; Thompson and Kay, 2000a)
			G- cells developing in monolayer system are more sensitive to DIF-1 than G+ cells.	
Cell cycle position	mid-late G2 phase; G1 phase	M/S phase to early G2 phase	Cell starved and initiated development at mid-late G2 form aggregates most quickly and sort out into posterior region later.	(Araki et al., 1994; Chen and Kuspa, 2005; Gomer and Firtel, 1987; Gruenheit et al., 2018; Thompson and Kay, 2000a)
			Flow cytometry quantified pre-spore marker *cotB*:GFP expression showing higher percentage of G1 cells differentiated into pre-spore cells. When G1 developing with early G2 cells in chimeras, G1 cells prefer to become pre-spore cell.	
			Synchronized late G2 cells tend to be in pre-spore region in the slug when developing together with asynchronized cells	
			In monolayers, cells from M/S phase when initiating development have higher pre-stalk marker expression and cells from later G2 phase have more pre-spore marker expression.	
Vesicle pH	High vesicle pH	Low vesicle pH	Mutants with defects in vacuolar H^+-ATPases which regulate proton gradients across contractile vacuole membranes prefer pre-spore cell fate.	(Aerts, 1988; Aerts et al., 1987; Davies et al., 1993; Gross, 2009; Gross et al., 1983; Gross et al., 1988; Neave et al., 1983)
			More intracellular acidic compartments localize at pre-stalk region according to neutral red staining experiments and pre-stalk gene expression profile. Altering vesicle pH with weak base or weak acid influences cell type proportioning of pre-spore and pre-stalk cells in development.	
			In monolayer development assays, weak bases e.g. ammonia induces vesicle pH elevation and mediate preferential spore cell formation, while weak acids e.g. propionate allow cells to adopt opposed pre-stalk cell fate.	
Cytosolic Ca^{2+} concentration ($[Ca^{2+}]_i$)	Low $[Ca^{2+}]_i$	High $[Ca^{2+}]_i$	Ca^{2+}-ATPase inhibitor BHQ induces $[Ca^{2+}]_i$ elevation, leading to higher sensitivity towards DIF-1 in monolayer development and increase of pre-stalk gene *ecmB* expression.	(Azhar et al., 1996; Saran et al., 1994; Schaap et al., 1996; Schlatterer et al., 2001)
			Stained with Ca^{2+}-indicator indo-1/AM dye, pre-stalk and pre-spore cells were sorted and monitored by FACS with high and low Ca^{2+} level correspondingly.	
			Intracellular Ca^{2+} levels are heterogenous in vegetative cells, and cells with higher $[Ca^{2+}]_i$ become pre-stalk cells located at anterior region of the slug later in development, while those with lower $[Ca^{2+}]_i$ are in pre-spore posterior area.	

1.4 General aims

Non-genetic heterogeneities among cells respond to different developmental cues including nutrients, cell cycle, pH in subcellular compartment and intracellular Ca^{2+}, driving developmental cell fate decisions from a salt-and-pepper patterning. The main interest of my project is to understand the roles of developmental fate determining factors and potential mechanisms that these factors work through for altering cell fates. This aim comprises several parts as follows:

(1) To determine whether altered Ca^{2+} signalling properties can be dissected using strains defective in Ca^{2+} channels by determining whether these show biased cell fates and whether this bias can be affected by other factors such as nutrient history and vesicle pH.
(2) To study whether mTORC1 pathway activity is a potential cell fate modulator to deconvolute developmental signals for cell type differentiation, and whether it functions as a predisposition or during later development to influence cell fate decisions.
(3) To examine whether gene expression related to cell cycle dynamic regulatory network can be used to predict cell fate and whether histone modifications play a role in determining the gene expression patterns that affect cell fate decisions.

These questions will be addressed using *Dictyostelium* which is a relatively simple lineage tracing model to study the potential mechanisms of cell fate decisions. This will provide information to help understand cell fate decisions in higher eukaryotic model systems such as human stem cells.

Chapter 2. Materials and methods

2.1 Materials

All media and buffers were prepared using double distilled water (milliQ dH_2O).

HL5 (Formedium):

14 g Peptone, 7 g Yeast extract, 13.5 g Glucose, 0.5 g KH_2PO_4, 0.5 g Na_2HPO_4, 0.25 g Dihydrostreptomycin sesquisulphate, 1 mL 1000× vitamin supplement, adjusted pH 6.5, dissolved in milliQ dH_2O to 1L, autoclaved

1000× vitamin supplement:

80 mg Riboflavin, 400 mg B12, 8 mg Biotin, dissolved in milliQ dH_2O to 400 mL, filter sterilised, stored in -20°C

SM agar (Formedium):

10 g Peptone, 10 g Glucose, 1 g Yeast extract, 1.9 g KH_2PO_4, 1.3 g $K_2HPO_4 \cdot 3H_2O$, 0.49 g $MgSO_4$ (anhydrous), 17 g agar, dissolved in milliQ dH_2O to 1L, autoclaved

FM minimal medium (Formedium)

250 mL 4× amino acids, 50 mL 20× vitamins, 20 mL 50× salts (NH_4Cl, $CaCl_2$, $FeCl_3$, $MgCl_2$), 0.1 mL 10,000× trace metals, 10 g glucose, 0.87 g K_2HPO_4, 50 mg dihydrostreptomycin-sulfate, adjusted to 1L, adjusted pH 6.5, autoclaved (developed by Franke and Kessin (1977), recipe on Dictybase: http://dictybase.org/techniques/media/fm-medium.html).

Customized FM minimal medium without iron (Formedium):

19.3 g powdered medium dissolved in 1L milliQ dH_2O, autoclaved.

KK2:

2.59 g KH_2PO_4, 1.04 g K_2HPO_4, dissolved in milliQ dH_2O to 1L, autoclaved

H50 buffer:

20 mM HEPES, 50 mM KCl, 10 mM NaCl, 1 mM $MgSO_4 \cdot 7H_2O$, 5 mM $NaHCO_3$, 1 mM $NaH_2PO_4 \cdot 2H_2O$, adjusted pH 7.0, filter sterilized

HK buffer:

10 mM HEPES, 10 mM KCl, adjusted pH 7.0, filter sterilized

HKC development buffer:

10 mM HEPES, 10 mM KCl, 250 μM $CaCl_2$, adjusted pH 7.0, filter sterilized

LB agar:

10 g Tryptone, 5 g Yeast extract, 10 g NaCl, 20 g agar, adjusted pH 7.0, dissolved in milliQ dH_2O to 1L, autoclaved; (if needed, Ampicillin: 100 μg/mL)

LB broth:

10 g Tryptone, 5 g Yeast extract, 10 g NaCl, dissolved with milliQ dH_2O to 1L, autoclaved; (if needed, Ampicillin: 100 μg/mL)

50× TAE:

242 g Tris-base, 57.1 mL Acetic acid, 100 mL 0.5M EDTA, adjusted pH 8.2, dissolved with milliQ dH_2O to 1L, autoclaved.

Ethidium bromide (EtBr) stained TAE agarose gel (1% w/v):

1 g agarose dissolved in 100 mL 1× TAE (20 mL 50× TAE, diluted with milliQ dH_2O to 1L), 0.5 μg/mL EtBr.

Crude gDNA extraction Lysis buffer:

50 mM KCl, 10 mM Tris-HCl (pH 8.3), 2.5 mM $MgCl_2$, 0.45% NP40, 0.45% tween-20, diluted with milliQ dH_2O to 100 mL. When used, 1 μL of 20 μg/μL proteinase K was supplied per 25 μL lysis buffer.

Stalk medium for monolayer assay:

10 mM MES, 1 mM $CaCl_2$, 20 mM KCl, 1 mM $MgCl_2$, 20 mM NaCl, pH 6.2, with 100 μg/mL PenStrep, filter sterilized

Lysis buffer for monolayer assay:

200 mM HEPES (pH 8.0), 2 mM $MgSO_4$, 4% Triton X-100, with 2mM CPRG (Roche)

10× SDS-PAGE running buffer:

30.3 g Tris-base, 144 g Glycine, 10 g SDS, adjusted pH 8.3, dissolved in milliQ dH_2O to 1L

1× SDS-PAGE running buffer:

100 mL 10× SDS-PAGE running buffer, diluted with milliQ dH_2O to 1L

10× transfer buffer (1L):

30.3 g Tris-base, 144 g Glycine, adjusted pH 8.3, dissolved in 1L milliQ dH_2O

1× transfer buffer (1L):

100 mL 10× transfer buffer, 200 mL methanol, 700 mL milliQ dH_2O

10× Tris Buffered Saline with Tween 20 (TBS) (1L):

24.3 g Tris-base, 80.6 g NaCl, adjusted pH 7.6, dissolved in milliQ dH_2O to 1L

1× TBST:

100 mL 10× TBS, 900 mL milliQ dH_2O, 2 mL Tween-20

2× Laemmli sample buffer:

4% SDS, 20% glycerol, 10% 2-mercaptoethanol, 0.004% bromophenol blue, 0.125 M Tris-HCl, pH approx. 6.8

2.2 Methods

2.2.1 *Dictyostelium* Cell culture

Dictyostelium axenic strain AX2 was used as a parental cell line for all the experiments. *D. discoideum* cells (hereinafter referred to as "cells") were grown on SM agar plates in association with bacteria *Klebsiella aerogenes* (KA) at room temperature (RT) or either in shaking suspension in HL5 with 1% glucose medium (55.5 mM glucose) at 220 rpm, 22°C or in stationary 90 mm petri dishes in 22°C incubators. For cell culture in stationary liquid medium, cells in a confluent 90 mm petri dish would be split around every three days. For cell culture on SM-KA agar, half of KA lawn from a 90 mm SM agar plate was inoculated into 5 mL KK2 and resuspended with vortexing. The homogenized KA suspension was then mixed with *Dictyostelium* cells and 150 µL mixture was spread on 90 mm SM agar plates. Exponential log phase (2~6 × 10^6 cells/mL) cells were used for experiments. Cells in shaking suspension were split to a cell density of 7 × 10^5 cells/mL the day before experiments.

For washing cells for experiments, cells harvested at log phase were spun down using centrifugation at 3000 rpm (1225×g), 3 mins in appropriate temperature: 4°C for electroporation experiments and 22°C for development experiments or cell culture procedures. Then cell pellets were resuspended in appropriate media or buffer such as KK2, followed by centrifugation at 3000 rpm (1225×g), 3 mins again and supernatant was carefully removed by pipetting. Eventually, cells were resuspended in appropriate buffer to the cell density required.

2.2.2 Cell cryopreservation and thawing

To cryopreserve, cells were resuspended from a confluent 90 mm petri dish in 10 mL of HL5 medium and centrifuged at 22°C, 3000 rpm (1225×g), 3 mins. Then cells were washed with HL5 medium once and resuspended in 1.5 mL HL5 medium using vortex and put on ice. Then, 75 µL Dimethyl sulfoxide (DMSO, Sigma) was added to the cell suspension to make 5% DMSO in total and transferred to cryotubes for freezing in sequential steps, eventually stored at -80°C (Fey et al., 2007).

To thaw the frozen culture from -80°C stock, a 90 mm petri dish containing 10 mL fresh HL5 medium was prepared. As soon as a vial of frozen culture (0.5 mL) was defrosted from -80°C to room temperature, the entire content was added into the dish immediately. Once cells settled down, fresh medium was applied to cells by removing the old medium containing DMSO. The dish was kept in 22°C incubator for about a week until revived cells can be observed.

2.2.3 Electroporation of *Dictyostelium*

Exponential log phase cells were collected and washed three times with chilled H50 electroporation buffer, and then resuspended to a density of 5×10^7 cells/mL. In each pre-chilled cuvette with 1 mm electrode gap (Bio-Rad, #1652083), a volume of 100 μL of cells mixed with 4~8 μg of plasmid DNA was added. After 5-min incubation on ice, cells were exposed to two consecutive pulses of 650 V, 25 μF capacitance and 200 Ω resistance with 5-second recovery between pulses (GenePulser Xcell™, Bio-Rad). Immediately, electroporated cells were incubated on ice for 5 mins, transferred to a 90 mm petri dish containing 10 mL fresh HL5 medium and kept at 22°C. Antibiotic selection was applied to electroporated cells the next day.

2.2.4 Genetically modified cell lines

The relevant strains in AX2 background were transfected with plasmid vectors designed to confer selectable markers, such as resistance to neomycin/G418 and blasticidin S. Blasticidin S-resistant (BSR) strains, such as gene disruption strains containing Cre-loxP BSR cassette from pLPBLP vector, were selected for and maintained in HL5 in presence of 10 μg/mL BS (Cambridge Bioscience), whereas G418-resistant strains which encodes neomycin resistance (NeoR) selectable marker, were selected and grown in HL5 containing 10 μg/mL G418 (Invitrogen). Strains which had their BSR cassette removed via Cre-loxP system (such as *tpc2*$^-$ clone TPC22B20) were maintained in HL5 medium.

2.2.5 Cell development

2.2.5.1 Cell development on filter and agar

Cells were developed on nitrocellulose membrane filters, KK2 agar or under buffer. The development buffers such as KK2 or HKC were used in different experimental scenarios.

For filter development, exponentially growing cells were harvested, washed twice at 22°C, 3000 rpm (1225×g), 3 mins and resuspended in KK2 buffer to a density of 5×10^7 cells/mL. Three pieces of 1 cm^2 Whatman filter paper soaked with 100 μL KK2 were fitted into a well of 24-well plate (Greiner) with pre-boiled and dried 3.5 mm nitrocellulose membranes (black filter, pore size 0.45 μm, Millipore Ltd) placed on the top. 2.5×10^6 cells per well were placed on the nitrocellulose membrane in each well to develop in a humidified dark chamber at 22°C and images were captured in appropriate development time points.

For agar development, 500 μL of 1% KK2 agar was dispensed and solidified in each well of a 24-well plate (Greiner) for 2 hrs. Meanwhile, exponentially growing cells were collected and washed twice at 22°C, 3000 rpm (1225×g), 3 mins and resuspended to a density of 5×10^7 cells/mL in KK2 buffer. 7.5×10^5 cells per well were placed on the agar plate, allowing them to develop in the dark chamber at 22°C and images were captured in appropriate development time points.

To test for drug effects on cells developing on agar in the 24-well plate format mentioned above, 25 μL 20× drug solutions were added onto the agar due to intrinsic dilution factor and dried for one hour prior to the plating of cells.

For under-buffer development, exponentially growing cells were collected and washed with KK2 twice at 22°C by centrifuging cells at 3000 rpm (1225×g), 3 mins. The cells were resuspended in developmental buffer to a density of 1.4×10^6 cells/mL and 1 mL of cell suspension was plated in each well of a 12-well plate (Greiner) with the final cell density 4×10^5 cells/cm^2. The cells then were incubated at 22°C and imaged at appropriate times.

2.2.5.2 Chimeric development to assess spore predisposition

Exponential log phase cells were washed in KK2 twice by centrifuging at 3000 rpm (1225×g), 3 mins and resuspended to 5×10^7 cells/mL in KK2. Cells were split into two pools, either to be left unlabelled (vehicle DMSO only) or stained with CellTracker™ Green CMFDA Dye (5-chloromethylfluorescein diacetate, #C2925, Invitrogen) dissolved in DMSO. Labelled pool of cells contained 10 μM CellTracker as the final working concentration, while the unlabelled pool of cells was treated with the equivalent volume of DMSO as the solvent control. Pools of cells were incubated on a roller shaker for 45 mins at 22°C and then washed with KK2 buffer for three times by centrifuging at 3000 rpm (1225×g), 3 mins. After that, pools of cells were resuspended in KK2 to the cell density of 5×10^7 cells/mL. Combinations of labelled or unlabelled cells were mixed in different proportions, and 50 μL of the mixtures were plated onto nitrocellulose membranes in a well of 24-well plates for 24-hr filter development at 22°C (see section 2.2.5.1). By the end of development, all spores from fruiting bodies were harvested and resuspended in 50 μL KK2 buffer, and 30 μL spore suspension was added into coverslips for 30 mins. Coverslips were washed with 70% ethanol followed by 100% methanol accordingly. 2 μL VectaShield® Mounting Medium containing 1.5 μg/mL DAPI was then added to each coverslip with fixed spores which was sealed onto glass microscope slide by clear nail polish.

2.2.5.3 Monolayer stalk induction assay

Early log phase cells with stalk reporter (*ecmB* promoter fused with lacZ) for expressing β-galactosidase (*ecmB*-GAL) were harvested, washed with KK2 and resuspended at 2.32×10^5 cells/mL in stalk medium containing 5 mM cAMP and 50 μM cerulenin. 1.2×10^4 cells in 50 μL were added into each well of a 96-well microplate, incubating for 24 hrs at 22°C. The cells were then washed with KK2 twice by pipetting carefully to remove the buffer in each well. To induce stalk marker expression, 50 μL stalk medium was added lacking cAMP but with various concentrations of DIF-1 (from 0 nM to 100 nM) for individual wells for 24-hr incubation at 22°C. After that, for β-galactosidase expressing cells, lysis buffer with 2 mM CPRG (Roche) was applied to the cells. The 96-well plate then was incubated at 37°C for 2 hrs. β-galactosidase activity was monitored by measuring optical density at 575 nm in microplate reader (BioTek 800TS) (Thompson et al., 2004).

2.2.6 Imaging

Developmental structures of *Dictyostelium* were imaged at the bright field via Leica MZFLIII Fluorescence Stereo Microscope and photographed with Hamamatsu digital camera ORCA-05G or Motic AE21 Inverted Phase microscope with a Coolpix P310 digital camera.

Spore visualization after mixing experiments was performed using Zeiss Olympus IX71 microscope under 100× oil lens with exposure time of 120 ms for DAPI channel, 800 ms for FITC channel and 60 ms for DIC channel.

For imaging cells with endogenous GFP-tagged construct expression, vegetatively growing cells harvest from HL5 growth culture were washed twice in KK2 and resuspended in KK2 at the density of 2×10^5 cells/mL. Next, 1 mL of cell suspension were added into a μ-Dish 35 mm imaging dish (ibidi) and incubated for 15 mins, then 50 μg/mL Blue fluorescent dye Hoechst (Sigma, #33342) was added to the cells for staining nuclei DNA. Zeiss Olympus IX71 microscope was used for imaging the cells (100× oil lens, FITC: 800 ms, Gain: 200; DAPI: 120 ms, Gain: 0).

2.2.7 General molecular cloning and gene disruption

2.2.7.1 Restriction enzyme digestion and ligation

In a standard NEB restriction enzyme digestion reaction, 5 to 10 units of restriction enzyme(s) which correspond to 0.5 to 1 µL of enzyme(s) supplied (NEB) were used to digest 1 µg DNA in compatible NEB buffer, diluted as appropriate, with milliQ dH_2O making the reaction mixture to a final volume of 50 µL. This reaction was incubated in 37°C for one hour and then the sizes of digested products examined on 1% agarose Ethidium bromide (EtBr) gels. For FastDigest (Thermo Scientific) restriction digestion method, 1 µL FastDigest enzyme(s) digested 1 µg DNA in 2 µL universal FastDigest buffer mixing together with milliQ dH_2O to a total volume of 20 µL. After 15 to 30 min-incubation in 37°C incubator, 1% EtBr-stained TAE agarose gel was run (100 V, 30 min) to check the sizes of digested products.

To ligate DNA fragment with sticky ends into a linearized plasmid, the molar ratio of vector DNA to insert DNA was calculated using NEBioCalculator (http://nebiocalculator.neb.com/#!/ligation) based on the differences of their quantities and molecular weights. 1 µL T4 DNA ligase together with 2 µL 10× T4 DNA ligase buffer were used to ligate two DNA fragments in appropriate molar ratio, using milliQ dH_2O to make a 20 µL ligation reaction which was then incubated at 16°C overnight following by heat inactivation at 65°C, 10 mins.

For constructing general homologous recombination gene disruption vectors, the pLPBLP vector (4446 bp) encoding a BSR cassette was used as a backbone. The KpnI and HindIII restriction enzyme sites at the 5' end of the BSR cassette and the NdeI and PstI sites at the 3' end of the cassette were chosen, followed by the standard cloning procedures with restriction digestion and ligation steps (described above) to clone two sections of the coding sequences (5' arm and 3' arm) targeting the gene of interest by homologous recombination.

To construct general CRISPR disruption vectors, an all-in-one CRISPR/Cas9 vector pTM1285 vector (9920 bp) obtained from NBRP Nenkin stock centre (https://nenkin.nbrp.jp/quickSearch/list?keyword=G90426) (Sekine et al., 2018) was used. Pairs of annealed guide RNA oligonucleotides were designed from the target gene sequence.

10 μM individual pairs of these guide RNA oligonucleotides (20 bp) were phosphorylated in the mixture with 1× T4 ligation buffer (containing 1 mM ATP) (NEB, #B0202S) and 5 units of T4 polynucleotide kinase (NEB, # M0201S) in a 10-μL reaction topped up with miliQ water, then they were annealed to each other simultaneously using a thermocycler programme: 37°C for 30 mins, then 95°C for 5 mins, following by cooling to 25°C at 5°C/min. A 20-μL phosphorylation reaction was set up, containing 0.04 μM oligonucleotide duplex which was cloned into the 100 ng pTM1285 entry vector in a digestion-ligation reaction containing 1× FastDigest Buffer (Thermo Scientific, #B64), 1 mM dithiothreitol (DTT) (Invitrogen, #P2325), 1 mM ATP (NEB, #P0756S), 1 μL FastDigest BpiI (Thermo Scientific, #FD1014) and 1 μL T4 DNA ligase (NEB, #M0202S), topped up with MiliQ water. The reaction mixture was incubated in a thermocycler for six cycles of the two steps: 37°C for 5 mins, then 23°C for 5 mins. Eventually the reaction was cooled down to 4°C.

2.2.7.2 Transformation of *Escherichia coli*

For transformation of *Escherichia coli*, plasmids were transformed into competent *E. coli* cells either mach1 or DH5α strains (NEB, #C2987H). 1 μL of purified plasmid extracted by QIAprep® Spin Miniprep Kit (Qiagen, #27106X4) (>200 ng/μL) for retransformation or 10 μL of ligation reaction was added to 100 μL of competent cells on ice for 30 mins. Then, the competent cells were heat shocked in a 42°C water bath for exactly 30 secs, immediately followed by incubation on ice for 5 mins. Cells were then incubated in 900 μL of Lysogeny Broth (LB) for one hour and 100 μL of cells were spread onto a 90 mm LB agar plate with 100 μg/mL ampicillin and incubated overnight at 37 °C.

2.2.7.3 Polymerase chain reaction (PCR)

Standard PCR was performed with MyTaq Red Mix (Bioline) following suggestions from the manufacturer's protocol. The reaction includes MyTaq™ Red Mix (Bioline), 10 μM reverse primer and 10 μM forward primer as well as the template using either bacterial colonies harbouring plasmid DNA after transformation (for colony PCR) or 5 μL genomic DNA (gDNA) extracted from *Dictyostelium* cells. The PCR program was set up with the initialization step at 95°C for 1 min, denaturation step at 95°C for 15 sec, followed by 35 cycles of the annealing step (temperature dependent on targets, 52~58°C) for 2 mins and extension step at 72°C for 30

sec, and the final extension step was set at 72°C for 5 mins. To purify PCR products for further cloning applications, PureLink PCR purification kit (Invitrogen, #K310001) was used following manufacturer's protocol. The primers used for PCR were listed in Table 2.1.

2.2.8 Genomic DNA extraction from *Dictyostelium* cells

For crude genomic DNA (gDNA) extraction used for PCR screening, around 1 million cells were collected from cell culture dishes into a 1.5 mL Eppendorf tube, followed by centrifugation at 3000 rpm (1225×g), 3 min at 22°C. After removing the media, the cell pellet was resuspended in 10 μL KK2 and mix with 10 μL lysis buffer supplemented with 0.8 μg/μL proteinase K. The mixture then was incubated at 95°C for 5 mins to inactivate proteinase K and 5 μL were taken for PCR. For isolating high quality gDNA, Wizard® Genomic DNA Purification Kit (Promega, #A1120) and DNeasy Blood & Tissue Kits (Qiagen, #69504) were used following manufacturer's protocols.

2.2.9 *Dictyostelium* gene disruption by homologous recombination

The gene disruption vector designed for homologous recombination strategy (see section 2.2.7.1) was linearized with KpnI and PstI to liberate the disruption fragments for standard electroporation transfection (see section 2.2.3). The resulting cells were diluted 1 in 10, 100, 1000 and 10000 times with HL5 medium. Each dilution was prepared in 50 mL corresponding to four 96-well plates for each dilution where 100 μL cell solution were plated per well. Cells in 96-well plates were then kept in a 22°C incubator for overnight recovery. The next day 10 μg/mL BS in HL5 medium was applied and selection carried out for at least two weeks until single colonies became visible. Each single colony appeared in a well of a 96-well plate would be resuspended in 100 μL media in the plate and transferred into a well of 24-well plate containing 0.5 mL HL5 with10 μg/mL BS. Cells growing from a single colony of a confluent well from 24-well plates were collected and lysed to extract gDNA for PCR screening. The successful candidates were plated on 150-mm SM agar plates (Greiner) in associated with KA bacteria in total volume of 350 μL (see section 2.2.1) in serial dilutions for isolation of individual clones. The subclones were then transferred to HL5 medium with 10 μg/mL BS.

2.2.10 *Dictyostelium* gene disruption by CRISPR-Cas9 strategy

To introduce gene disruption using CRISPR/Cas9 strategy, two 2-3 μg CRISPR gene disruption vectors (see section 2.2.7.1) were co-transfected into AX2 parental cells in pairs following standard *Dictyostelium* electroporation procedure (Section 2.2.3). The transfected cells were then kept in 90 mm petri dishes in 10 mL HL5 medium in 22°C incubator for overnight recovery. The next day 10 μg/mL G418 in HL5 medium was applied to the cells over three days to select for cells that had taken up the vector and promoting transient expression of the Cas9 protein. The media was then replaced with HL5 with no G418 to enrich for clones without integration of the plasmid. The candidate disruptants then were collected and resuspended in 350 μL KK2 in associated with KA bacteria, followed by serial dilution and plated onto 150-mm SM agar plates (Greiner). Single colonies of independent CRISPR clone started to appear after five days and were isolated by transferred to HL5 medium for further verification and purification for single clones via repeating the serial dilution plating.

2.2.11 Western blot analysis

2.2.11.1 Whole cell lysate sample collection

For collecting cells from vegetative growth, 2×10^6 cells were harvested from shaking suspensions by centrifugation at 3000 rpm (1225×g), 3 min. The cell pellet after removing supernatant was resuspended and lysed in 80 μL pre-warmed 2× sample buffer, following by incubation at 100°C for 6 mins. The samples were stored at -20°C.

For collecting developing cells in shaking suspension, exponentially growing cells were collected and washed with HK buffer twice at 22°C by centrifuging cells at 3000 rpm (1225×g), 3 mins. The cells were resuspended with 5 mL HKC development buffer to a density of 1.4×10^7 cells/mL. 2×10^6 cells were collected from such under-buffer development condition at desired time points and lysed as for the vegetative cell sample collection.

2.2.11.2 Western blotting

Prepared whole cell lysate samples (see section 2.2.11.1) were separated on different percentages of SDS-PAGE gels using standard procedures described in Sambrook et al. (1989), followed by transferring to 0.2 um PVDF membrane (Amersham Hybond, #10600101). The membrane was then blocked with 5% milk-TBST for one hour and then subjected to primary antibodies or the Alexa 680-conjugated streptavidin detection system for methylcrotonyl-CoA carboxylase (MCCC1) as the loading control (Davidson et al., 2013) prepared in 5% milk-TBST for 4°C overnight incubation. After three washes with TBST to remove excessive primary antibody, the membrane was incubated with the relevant secondary antibodies for one hour at RT. Then, the excess secondary antibody was removed by three washes with TBST. SuperSignal™ West Femto Maximum Sensitivity Substrate (Thermo Scientific™, # 34095) was applied to membranes and all blots were imaged for 2-10 mins at room temperature using Odyssey Fc imaging system (LI-COR, Lincoln, NE, USA). To quantify the intensities of bands, Image Studio Lite Ver 5.2 (LI-COR) was used, and intensities of signals were normalized to their loading controls. Then, the values of treated/starved samples in various time points were normalized to the values of untreated/non-starved samples in control groups (0 min) identified as 100%. Primary and secondary antibodies and their dilution are listed in Table 2.2.

2.2.12 Quantitative real-time RT-PCR (qPCR)

For qPCR analysis, total RNA was isolated from *Dictyostelium* cells using the TRIzol® Reagent (Invitrogen, #15596026), from which 10 µg total RNA was purified to remove residual gDNA with TURBO DNA-free™ Kit (Ambion, #AM1907. Then, 2 µg DNase-treated total RNA was reverse transcribed to cDNA using SuperScript™ IV First-Strand Synthesis System (Invitrogen, #18091050). Fast SYBR™ Green Master mix (Applied Biosystems, #4385612) was used following manufacturer's protocol, and each 20-µL reaction containing 20 ng cDNA template and 200 nM of each forward and reverse primers in a well of a MicroAmp™ Fast Optical 96-Well Reaction Plate (Applied Biosystems, #4346907) were performed in StepOnePlus™ Real-Time PCR instrument (Applied Biosystems, #4376600) in fast mode. The program was set as follows: 95°C, 20 sec for initiation; 95°C, 3 sec for denaturation; 60°C, 30 sec for annealing and extension, repeating denaturation and annealing steps for 40 cycles, which is followed by a melting curve analysis (95°C, 15 sec for denaturation first, then starting the analysis from 60°C, 1 min, rising by 0.3°C/sec to 95°C) to test the amplification specificity.

The endogenous control *ig7* gene (*rnlA*, DDB_G0294034) was used for normalization (Vinet et al., 2014). The primers for qPCR are listed in Table 2.1.

2.2.13 Statistics and bioinformatic analysis

For quantification of data, the sample means $\bar{X}$ were used and the number of independent experiments was indicated as n. Sample mean differences were compared using two-tailed student *t*-tests or two-way ANOVA with multiple comparisons in Sidak's method analysed by Prism7 GraphPad and Microsoft Excel. P values and asterisks system define significance level shown below and the asterisks are displayed on relevant figures.

P value	Significance	Asterisks
<0.0001	Extremely significant	****
0.0001 ~ 0.001	Strongly significant	***
0.001 ~ 0.01	Very significant	**
0.01 ~ 0.05	Significant	*
≥0.05	Not significant	ns

For bioinformatics analysis, DNA sequence and amino acid sequence alignments were carried out with Clustal Omega (https://www.ebi.ac.uk/Tools/msa/clustalo/) and BioEdit biological sequence alignment software (downloaded from http://www.mbio.ncsu.edu/bioedit/bioedit.html). NCBI Blast tools (https://blast.ncbi.nlm.nih.gov/Blast.cgi) were used for studying sequence homology among different species and designing PCR primers. Gene and plasmid maps were plotted and annotated using SnapGene (downloaded from https://www.snapgene.com/) and Microsoft PowerPoint. Protein domain analysis was carried out by HMMER (https://www.ebi.ac.uk/Tools/hmmer/search/hmmscan)

or NCBI conserved domain (https://www.ncbi.nlm.nih.gov/Structure/cdd/wrpsb.cgi). Protein modification sites and motifs were predicted by Predictprotein (https://www.predictprotein.org/). For designing sgRNA used in CRISPR/Cas9 gene editing experiments, Crispor (http://crispor.tefor.net/) was used for PAM sequence identification and prediction of sgRNA target specificity.

Table 2.1: Primers and oligonucleotides for cloning and qPCR experiments in this thesis

Name	Purposes	Sequence (5’ to 3’)
KW56_TPC_F	Forward primer of the central TPC coding region	5’-ggtaccaccgctagtccagg
KW57_TPC_R	Reverse primer of the central TPC coding region	5’-gtaaagtactattgatagttgcaggtgg
YW6_ 5_Arm_For_Kpn1	Forward primer with KpnI restriction site for cloning 5’ arm of *dmpA*	5’-aaaaaaggtaccctaaatgtattctatccggtgaatatc
YW7_ 5_Arm_Rev_Hind3	Reverse primer with HindIII restriction site for cloning 5’ arm of *dmpA*	5’-ttttttaagcttttattaataccaccgatatcgcaattg
YW8_ 3_Arm_For_Nde1	Forward primer with NdeI restriction site for cloning 3’ arm of *dmpA*	5’-aaaaaacatatgcaattgcagatggtggaaaacattc
YW9_ 3_Arm_Rev_Pst1	Reverse primer with PstI restriction site for cloning 3’ arm of *dmpA*	5’-ttttttctgcagaggatatagacagcatgtaaaaagaag
YW10_Bsr_F_3R_out	Sequencing primer for *dmpA*$^{-}$ reading from 3’ of BSR to outwards	5’-aaaaaagaagaactcattccactcaaatatac
YW11_Bsr_R_5R_out	Sequencing primer for *dmpA*$^{-}$ reading from 5’ of BSR to outwards	5’-ttttttaatcttctctgtcgctacttctac
YW12_up_5_dmpA_F	PCR screening forward primer of *dmpA* 5’ arm	5’-aaaaaagttccgataaatatggtaatggtac
YW13_Bsr_3_out	PCR screening forward primer of *dmpA* 3’ arm	5’-aaaaaagataaagctgacccgaaagctc
YW14_down_3_dmpA_R	PCR screening reverse primer of *dmpA* 3’ arm	5’-ttttttaataagagtttgaaccaaagagagtag
YW15_Bsr_5_out	PCR screening reverse primer of *dmpA* 5’ arm	5’-ttttttatgctatacgaagttatccgtgg
YW16_Crispr_dmpA_5'_1	Oligonucleotide 1 of vector 1 CRISPR strategy for *dmpA* gene disruption	5’-agcaagacccgttgcatcctacaa
YW17_Crispr_dmpA_3'_1	Oligonucleotide 2 of vector 1 CRISPR strategy for *dmpA* gene disruption	5’-aaacttgtaggatgcaacgggtct
YW18_Crispr_dmpA_5'_2	Oligonucleotide 1 of vector 2 CRISPR strategy for *dmpA* gene disruption	5’-agcaactgaactagttgctttcca
YW19_Crispr_dmpA_3'_2	Oligonucleotide 2 of vector 2 CRISPR strategy for *dmpA* gene disruption	5’-aaactggaaagcaactagttcagt
YW20_Crispr_dmpA_5'_3	Oligonucleotide 1 of vector 3 CRISPR strategy for *dmpA* gene disruption	5’-agcatcttctggcattgtagctgc

YW21_Crispr_dmpA_3'_3	Oligonucleotide 2 of vector 3 CRISPR strategy for *dmpA* gene disruption	5'-aaacgcagctacaatgccagaaga
YW22_dmpA_exon2_For	Forward primer for screening wildtype *dmpA* exon 2	5'-aaaaaaatgtattccaagattgtcaagttg
YW23_dmpA_exon2_Rev	Reverse primer for screening wildtype *dmpA* exon 2	5'-ttttttcagatacgatttgaccttcttc
YW24_ CRISPR_insert_F	CRISPR guide RNA insertion screening; forward primer on Cas9 coding sequence in pTM1285	5'-cgaaaagagagacc
YW25-dmpA_seq_F_crispr	Forward primer on upstream *dmpA* exon 2 for screening *dmpA*$^-$ CRISPR clone	5'-aaaaaagattggggattttcagtaattg
YW26-dmpA_seq_R_crispr	Reverse primer on upstream *dmpA* exon 2 for screening *dmpA*$^-$ CRISPR clone	5'-ttttttcatctgctaaataaatggttcc
YW29_Ig7-[2]-qpcr-Fwd	RT-PCR primer for *ig7* endogenous control	5'-tcgatcagagacgcaagtcg
YW30_Ig7-[2]-qpcr-Rev	RT-PCR reverse primer for *ig7* endogenous control	5'-caccccaacccttggaaact
YW31_RTPCR_dmpA_A_F	RT-PCR forward primer for confirming *dmpA*$^-$ CRISPR combination A deleted region	5'-tgtgtggctcatcagcctattc
YW32_RTPCR_dmpA_A_R	RT-PCR reverse primer for confirming *dmpA*$^-$ CRISPR combination A deleted region	5'-ggatgcaacgggtctattatcg
YW33_RTPCR_dmpA_B_F	RT-PCR forward primer for confirming *dmpA*$^-$ CRISPR combination B deleted region	5'-tattattaggtgatcttgaacgtgttc
YW34_RTPCR_dmpA_B_R	RT-PCR reverse primer for confirming *dmpA*$^-$ CRISPR combination B deleted region	5'-tgattacagaaccaattctaaaaccac
YW37_RTPCR_dmpA_HR_F	RT-PCR forward primer for HR *dmpA*$^-$ strain confirmation in deleted region	5'-tagtagtacaccaggtccaacc
YW38_RTPCR_dmpA_HR_R	RT-PCR reverse primer for HR *dmpA*$^-$ strain confirmation in deleted region	5'-accagatacgatttgaccttcttc
YW39_qPCR_rrgA_F	qPCR forward primer for *rrgA*	5'-gtagaatcaactgcatggaacaag
YW40_qPCR_rrgA_R	qPCR reverse primer for *rrgA*	5'-gttaatatcgtaaacagtagtccaaac
YW53_qPCR_New_rigA_F	qPCR forward primer for *rigA*	5'-atccagagtgtccatcagtag
YW54_qPCR_New_rigA_R	qPCR reverse primer for *rigA*	5'-ccgaaatggtgaccatggtg
YW43_ Rheb_BamHI_F	Forward primer for Rheb with BamHI overhang	5'-aaaggatccatggcaccacaaaaacatagaaagatctg
YW44_ Rheb_R	Reverse primer (short) for Rheb	5'-cattaaaatacaaccttctttttgtggagg

YW45_Rheb_FLAG_stop_SpeI_R	Reverse primer (long) with 1× FLAG tag and stop codon and SpeI overhang for Rheb	5'-tttactagtttacttgtcgtcatcgtctttgtagtccattaaaatacaaccttctttttg tggagg
YW46_GFP_For	Forward primer for GFP coding sequence in fusion construct	5'-aaaaagatggaagcgttcaactagc
YW47_set1_Rev	Reverse primer for *set1* in fusion construct	5'-ttttattgccatttgtataactttcatcc
YW48_Rheb_T23M-01	Mutagenesis primer for T23M in Rheb	5'-tcaacaattatgatgcaatttgttgaaagc
YW49_Rheb_Mutagenesis-01	The end-to-end primer without mutation in Rheb (for T23M)	5'-ttttccaactgctcttgatc
YW50_Rheb_E40K-02	Mutagenesis primer for E40K in Rheb	5'-tccaactattaaaaatacatatcaaaaaataattag
YW51_Rheb_Mutagenesis-02	The end-to-end primer without mutation in Rheb (for E40K)	5'-tggtatgagtctggacaatg
YW55_rheb_CrisprA_oligo1	Oligonucleotide 1 of vector A CRISPR strategy for *rheb* gene disruption	5'-agcacatagaaagatctgtgtaat
YW56_rheb_CrisprA_oligo2	Oligonucleotide 2 of vector A CRISPR strategy for *rheb* gene disruption	5'-aaacattacacagatctttctatg
YW57_rheb_CrisprB_oligo1	Oligonucleotide 1 of vector B CRISPR strategy for *rheb* gene disruption	5'-agcaaacaggtctgagtatggtag
YW58_rheb_CrisprB_oligo2	Oligonucleotide 2 of vector B CRISPR strategy for *rheb* gene disruption	5'-aaacctaccatactcagacctgtt
YW59_snfA-_F	Forward primer for verifying *snfA*$^-$ (*ampk*$^-$ CRISPR strain from Williams lab)	5'-atggagtatgtaaccggtg
YW60_snfA-_R	Reverse primer for verifying *snfA*$^-$ (*ampk*$^-$ CRISPR strain from Williams lab)	5'-agcgtaattgggtgaacc
YW61_rheb_KO_F	Forward primer for screening *rheb*$^-$ CRISPR deletion region	5'-atggcaccacaaaaacatagaaag
YW62_rheb_KO_R	Reverse primer for screening *rheb*$^-$ CRISPR deletion region	5'-cagctcccaatgaacttaagatc
YW65_rheB_FLAG_HindIII_R	For cloning Rheb_FLAG into pKG3013 (ecmBp) and pKG3014 (pspAp) GFP tagged vector	5'-aaaaagcttcttgtcgtcatcgtctttgtagtccattaaaat

Table 2.2. Antibodies used in western blot analyses

Primary Antibodies	Polyclonal or monoclonal	Sources	Dilution	Blocking/dilution agent	Sizes (kDa)	Manufacturer and catalogue number	Corresponding secondary antibodies and dilutions
phospho-4E-BP1 (Thr37/46)	polyclonal	Rabbit	1:1000	5% semi-skimmed milk in TBST	15	Cell Signaling Technology, #2855	Polyclonal goat anti-rabbit Immunoglobulins/HRP (1:10,000) (Dako)
phospho-SGK1 (S422)	monoclonal	Rabbit	1:1000		100	Abcam, #ab55281	
H3K4me3	polyclonal	Rabbit	1:1000		15	homemade	
FLAG	polyclonal	Rabbit	1:2000		Function as a 1-kDa tag	Sigma-Aldrich, # F7425	
actin	monoclonal	Mouse	1:10,000		43	Santa-cruz, #sc-47778	Polyclonal goat anti-mouse Immunoglobulins/HRP (1:10,000) (Dako)
Streptavidin, Alexa Fluor™ 680 conjugate (detecting MCCC1)	-	-	1:1000		80	Invitrogen, #S21378	-

Chapter 3. Ca^{2+} signalling and cell fate decision

3.1 Introduction

3.1.1 Ca^{2+} signalling machinery in mammalian and *Dictyostelium* cells

Ca^{2+} has been proposed to be one factor important for cell fate determination in *Dictyostelium*. Ca^{2+} ion as a mobilizing secondary messenger is used ubiquitously in eukaryotic cells with versatile and important roles in regulating biological and physiological activities (Berridge et al., 2000), such as muscle contraction (Hill-Eubanks et al., 2011), neuronal electricity activity and metabolism (Berridge, 1998; Ivannikov et al., 2013) as well as mammalian reproduction and embryonic development (Miao and Williams, 2012; Stewart and Davis, 2019). The Ca^{2+} signalling toolkit is well-reviewed and the machinery of Ca^{2+} release can be dated back to early evolutionary routes in protozoa, although they are less pronounced in prokaryotes (Berridge et al., 2003; Clapham, 2007; Dominguez et al., 2015; Plattner and Verkhratsky, 2013; Shemarova and Nesterov, 2005). Moreover, Ca^{2+} signalling machineries orchestrate the development processes in many organisms, such as keratinocyte differentiation during mouse epidermal development (Tu and Bikle, 2013), larval wing disc development in *Drosophila melanogaster* (Brodskiy et al., 2019) and behavioural decision-making in olfactory neurons of *Caenorhabditis elegans* (Tanimoto et al., 2017). Disrupting Ca^{2+} homeostasis via pharmacological substances, for example, colchicine-mediated intracellular Ca^{2+} increase in mammalian or cancer cell models affect cardiac electricity activity and induce cytotoxicity (Lu et al., 2016; Sun et al., 2019). Pathologically, dysregulation of Ca^{2+} signalling leading to high basal level of $[Ca^{2+}]_i$ at resting status, deteriorates cognition in Alzheimer's Disease mouse models (Berridge, 2014).

In eukaryotic cells, cytosolic Ca^{2+} concentrations are kept extremely low at around 100 nM compared to extracellular Ca^{2+} levels (1-2 mM). This level is strictly regulated by Ca^{2+} channels and transporters e.g. pumps and exchangers on the plasma membrane (PM) or membranes of two classes of subcellular Ca^{2+}-storing organelles: neutral stores such as the ER (or sarcoplasmic reticulum (SR) in muscle cells) (Bagur and Hajnoczky, 2017; Laude and Simpson, 2009) or acidic stores such as lysosomes (Figure 3.1A). Many of these components

are highly conserved between *Dictyostelium* and mammalian cells (Figure 3.1B, Table 3.1). including Ca^{2+} pumps such as a plasma membrane Ca^{2+}-ATPase (PMCA) and a SR/ER Ca^{2+}-ATPase (SERCA) as well as PAT1 found in the contractile vacuole (Moniakis et al., 1995; Moniakis et al., 1999). Ca^{2+} exchangers such as Na^+/Ca^{2+} exchanger (NCX), Na^+/Ca^{2+}-K^+ exchanger (NCKX) and Ca^{2+}/H^+ exchanger (CAX) also exist in *Dictyostelium*. Together these maintain a physiologically low cytosolic Ca^{2+} level when unstimulated in animal cells (reviewed in (Clapham, 2007; Gross, 2009)), and *Dictyostelium* cells has a slightly lower intracellular Ca^{2+} level around 50 nM at resting stage but still comparable to other eukaryotic cell types (Abe et al., 1988). Signalling pathways trigger a transient rise in this low cytosolic Ca^{2+} level. *Dictyostelium* cells have a GPCR-dependent Ca^{2+} influx mechanism triggered by extracellular ligands cAMP and folate (Klein et al., 1988a; Pan et al., 2016; van Haastert et al., 2007) and can produce inositol-1,4,5-trisphosphate (IP_3) by a conventional phospholipase C (PLC) route or an unconventional mechanism via synthesis from other inositol phosphates which then mediates Ca^{2+} release from intracellular Ca^{2+} stores (Europe-Finner and Newell, 1986; Flaadt et al., 1993b; Van Dijken et al., 1995). The transient Ca^{2+} release into cytosol is through different intracellular Ca^{2+} channels, e.g. voltage-gated and ligand-gated Ca^{2+} channels. Well-conserved examples of channels localized on intracellular Ca^{2+} stores in *Dictyostelium* include an IP_3 receptor-like channel (IPLA) in the ER (Lusche et al., 2012; Traynor et al., 2000) and two lysosomal targeted channels: a transient receptor potential (TRP) channel mucolipin (also known as TRPML) conserved with human TRPML1 and a two-pore channel 2 (TPC2) homologous to human TPC2 (Lima et al., 2012; Wilczynska et al., 2005). Ca^{2+}-induced Ca^{2+} release (CICR) is mainly mediated by IP_3R on SR/ER in mammalian cells and can be triggered by influx of Ca^{2+} from outside the cells or from other organelles such as lysosomes (Morgan et al., 2013), showing the interplay between Ca^{2+}-storing organelles (Bagur and Hajnoczky, 2017), and this phenomenon can also be found in *Dictyostelium* (Malchow et al., 2008).

In *Dictyostelium*, a cytosolic $[Ca^{2+}]_i$ increase has also been reported to be induced by DIF-1 and an increase of cytosolic Ca^{2+} levels correlates with pre-stalk gene expression and pre-stalk cell differentiation (Azhar et al., 1997; Schaap et al., 1996; Verkerke-van Wijk et al., 1998). It was reported that DIF-1 localizes to mitochondria (Mt) and mediates mitochondrial Ca^{2+} release, which might be a potential pathway to cause the increase of cytosolic Ca^{2+} level and thus induce stalk cell fate (Kubohara et al., 2017). However, use of a genetically encoded fluorescence resonance energy transfer (FRET)-based Ca^{2+} sensor YC2.60 with yellow and

cameleon fluorophores (Horikawa et al., 2010) has shown that the DIF-1 dependent cytosolic Ca^{2+} increase is lost in *iplA*$^{-}$ cells (Traynor and Kay, 2017), demonstrating an essential role for the ER in this response.

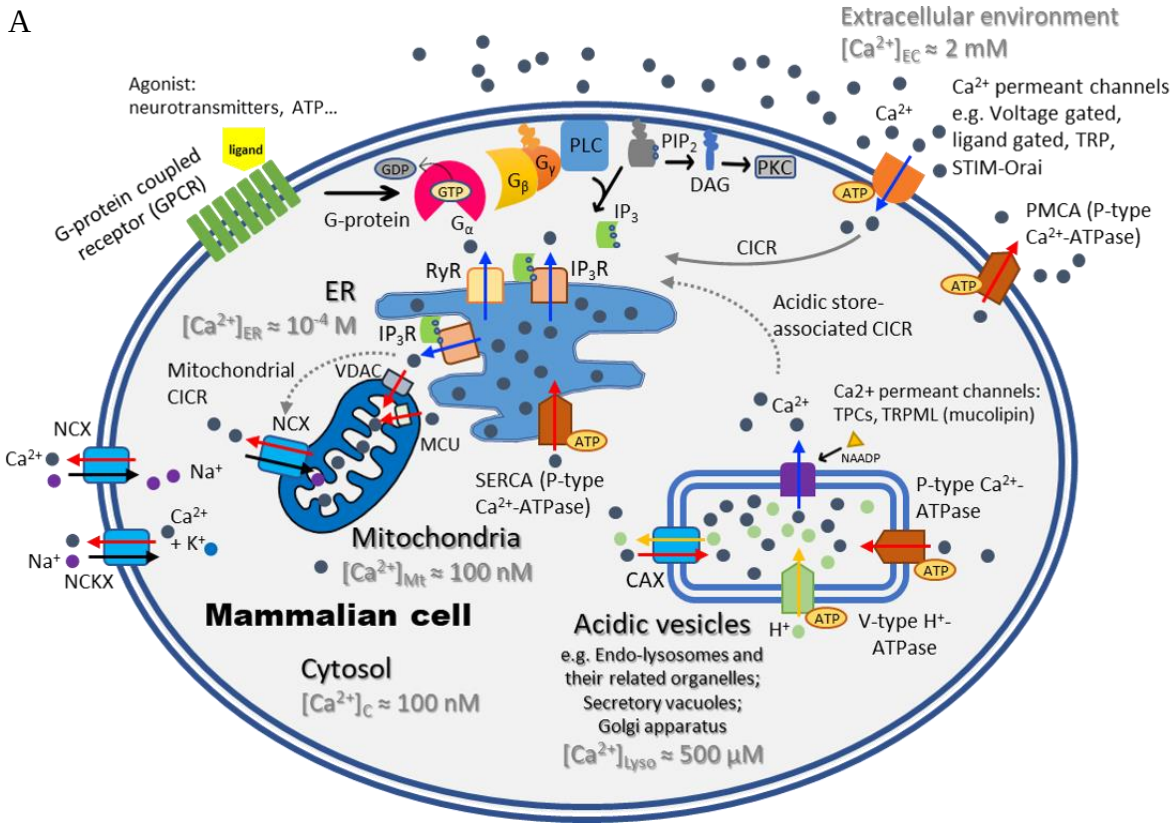


Figure 3.1. Summary of Ca^{2+} signalling and components maintaining Ca^{2+} homeostasis in (A) mammalian cells and (B) *Dictyostelium* cells. (A) On the PM, GPCRs activated by agonists from environment stimulate signalling transduction by producing secondary messengers such as IP_3 and diacylglycerol (DAG) generated from the hydrolysis of phosphatidylinositol 4,5-bisphosphate (PIP_2) by PLC. IP_3 diffuses in the cells to trigger downstream Ca^{2+} channels, ER-targeted IP_3Rs.Plasma membrane Ca^{2+} channels can also allow entry from extracellular environment e.g. nicotinic acetylcholine receptors can be opened by neurotransmitters in the central nervous system. Voltage-gated channels opened by the change in action potential at depolarized membranes and TRP channels responding to temperature or osmotic stresses contribute to Ca^{2+} influx and increased $[Ca^{2+}]_i$. ER and SR in muscle cells are the main neutral Ca^{2+} stores equipped with Ca^{2+} channels Ryanodine receptors (RyR) and IP_3R which are crucial mediators of CICR. SERCA and PMCA are examples of P-type Ca^{2+} pumps energised by ATP, transporting cytosolic Ca^{2+} against concentration gradients into internal Ca^{2+} stores e.g. ER or across PM for Ca^{2+} efflux. The other main Ca^{2+} stores are acidic organelles, and the best examples are endosomes, lysosomes and their related vesicles. The acidic pH environments in these organelles are created by V-type H^{+}-ATPases which use ATP to transport protons into the acidic Ca^{2+} stores. CAX exchangers then move Ca^{2+} into the acidic store in exchange for protons. TPCs gated by NAADP and TRPML stimulated by stresses are the main channels regulating the release of lysosomal Ca^{2+}. Ca^{2+} channels in Mt include VDAC and MCU taking up Ca^{2+} in the cytosol released from ER stores.

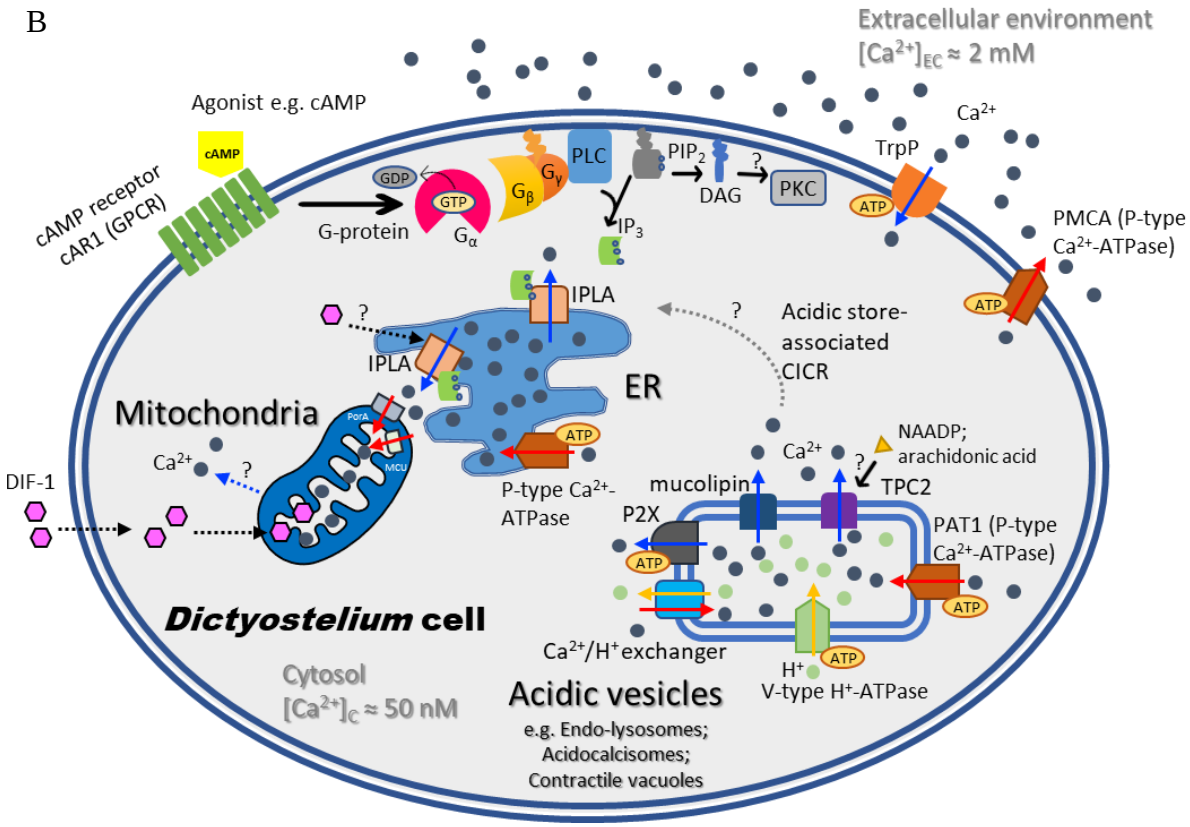


Figure 3.1. Summary of Ca^{2+} signalling and components maintaining Ca^{2+} homeostasis in (A) mammalian cells and (B) *Dictyostelium* cells. (B) *Dictyostelium* cells have evolutionarily conserved Ca^{2+} signalling components. Activation of cAMP receptor (cAR1) upon cAMP signal at cell surface tiggers downstream signalling pathways via secondary mobilizing messengers IP_3 and DAG, the former stimulating IPLA on neutral Ca^{2+} stores and the latter might have a role in stimulating protein p21-activated kinase D (PakD) with diacylglycerol binding domain conserved to PKC (Friedberg and Rivero, 2010; Garcia et al., 2014). TrpP channels similar to mammalian TRPP2 are gated by ATP and cellular stresses to facilitate Ca^{2+} influx into *Dictyostelium* cells. Membrane-penetrable DIF-1 that causes $[Ca^{2+}]_C$ increase dependent on IPLA (Traynor and Kay, 2017). Red arrows: Ca^{2+} movement that decreases $[Ca^{2+}]_C$; blue arrows: Ca^{2+} movement that increases $[Ca^{2+}]_C$; yellow arrows: proton movements in or out of the Ca^{2+}-storing organelles. Dashed lines and question marks: still elusive mechanisms. The abbreviation and citations are in the main text. The diagrams are adapted and updated from (Chang, 2016).

Table 3.1. Examples of *Dictyostelium* Ca^{2+} channels/transporters

Ca^{2+} channels/transporters	Gene ID on Dictybase	Homologues in other eukaryotes (general)	Locations in cells	Activators	References
IPLA	DDB_G0292564	IP_3R	cytoplasmic vesicular membranes/ER (major); PM (minor)	IP_3, Ca^{2+}, cAMP, folate, DIF-1, GABA, L-glutamate	(Flaadt et al., 1993b; Lam et al., 2008; Lusche et al., 2012; Schaloske et al., 2005; Traynor and Kay, 2017; Traynor et al., 2000)
SPRY domain-containing protein (dual specificity kinase spore lysis A/ryanodine receptor)	DDB_G0272202	RyR	cytoplasmic vesicular membranes	Ca^{2+}, cyclic ADP ribose, ATP, FKBP12	(Ponting et al., 1997; Tae et al., 2009)
TrpP (PKD2)	DDB_G0272999	TRPP2	PM, early endolytic compartments	ATP, ADP	(Lima et al., 2014; Traynor and Kay, 2017)
MscS (mechanosensitive channel)	DDB_G0277253	MscS	PM	mechanical stimuli	
P_2XA/E	DDB_G0272004	$P_2X2/4$	Contractile vacuoles	ATP	(Baines et al., 2013; Fountain et al., 2007; Ludlow et al., 2009; Ludlow et al., 2008)
MCLN	DDB_G0291275	TRPML	Vacuolar membranes of acidic vesicles e.g. endosomes, lysosomes	Ca^{2+}	(Lima et al., 2012)
TPC2	DDB_G0289105	TPC2		NAADP, AA	(Chang, 2016; Chang et al., 2020)
PzoA	DDB_G0282801	Piezo 2	PM	mechanical stimuli	(Hashimura et al., 2022; Srivastava et al., 2020)
DMP1	DDB_G0275065	-	Cellular membranes	-	This thesis and (Khosla et al., 2006; Thompson et al., 2007)
MCU	DDB_G0286429	MCU	Mitochondria	Ca^{2+}	(Yuan et al., 2020)
PorA	DDB_G0271848	VDAC	Mitochondria	Voltage stimuli	(Forte et al., 1987; Heidorn-Czarna et al., 2021)
PAT1	DDB_G0277861	PMCA	Contractile vacuoles, PM	ATP	(Moniakis et al., 1995; Moniakis et al., 1999)
CAX1	DDB_G0279301	CAX	Vacuolar membranes of acidic vesicles, PM	ATP	(Rooney and Gross, 1992a; Shigaki et al., 2006)

3.1.2 IPLA, TPC2 and DMP1 channels in *Dictyostelium*

The *iplA* gene is the only gene encoding a protein with significant homology to the IP_3 receptor (IP_3R) protein in *Dictyostelium* (Traynor et al., 2000). There are no genes predicted to encode RyRs but the *Dictyostelium* genome encodes proteins with a spore lysis A/ryanodine receptor (SPRY) domain highly conserved with other RyR isoforms (Ponting et al., 1997; Stajdohar et al., 2017; Tae et al., 2009). IPLA has a similar topology of six-transmembrane domains to other eukaryotic IP_3Rs (Traynor et al., 2000) and is located on a cytoplasmic vesicular membrane in *Dictyostelium* cells (Lusche et al., 2012). By inference from other IP_3Rs, IPLA was expected to function as a Ca^{2+} channel on internal Ca^{2+} stores regulating capacitative Ca^{2+} uptake through PM (Lusche et al., 2012; Shanley et al., 2006; Traynor et al., 2000). cAMP-induced Ca^{2+} release depends on IPLA (Traynor et al., 2000; Wilczynska et al., 2005), while the polycystin-type TrpP mediating Ca^{2+} entry via ATP hydrolysis is independent of IPLA (Traynor and Kay, 2017). The *iplA*$^-$ strain has chemoattractant-triggered receptor-mediated Ca^{2+} entry defects (Schaloske et al., 2005; Shanley et al., 2006; Traynor et al., 2000), and Lusche et al. (2012) also reported that *iplA*$^-$ cells have aberrant chemotaxis responding to a spatial Ca^{2+} gradient, suggesting IPLA plays roles in pathways of Ca^{2+} chemotaxis. IPLA is also involved in autophagic cell death pathways regulated by Ca^{2+} fluxes (Lam et al., 2008).

Dictyostelium TPC2 is predicted to be an endocytic Ca^{2+} channel (Lima et al., 2012; Wilczynska et al., 2005). With two sets of six transmembrane (TM) domains linked by two EF-hand motifs, *Dictyostelium* TPC2, encoded by the only *tpc* gene (*tpc2*) in *Dictyostelium* shares 29% identity with human TPC2 (Chang et al., 2020). TPC2 has been found to be not required for mechanical stress-mediated rheotaxis (Lima et al., 2014). In our lab, Chang et al. (2020) has found that *tpc2*$^-$ cells have increased acidic vesicle pH, and the strain is more sensitive to weak base inhibition of aggregation. Also, developing *tpc2*$^-$ cells show a delay in aggregation with slightly aberrant and delayed cAMP-mediated Ca^{2+} signalling waves and a lower basal level of cytosolic Ca^{2+} which is consistent with *Dictyostelium* TPC2 being a Ca^{2+} channel (Chang et al., 2020).

Apart from those Ca^{2+} channel orthologues already identified in *Dictyostelium*, there may be other putative Ca^{2+} channels expressed that might reveal useful information about their role and function using *Dictyostelium* as a model. One example of such is a potential TRP-like Ca^{2+}

channel, *Dictyostelium* Membrane Protein 1 (DMP1) encoded by the *dmpA* gene (DDB_G0275056). DMP1 has conserved transmembrane (TM) domains (Khosla et al., 2006) which are also similarly found in some Ca^{2+} channel related proteins from other species, such as a SPRAY protein in *Neurospora crassa* (Bok et al., 2001) (Figure 3.2). There are conserved inter-TM motifs and cysteine-rich multipass TM domains between DMP1 and cysteine repeat modular proteins in the malaria parasite *Plasmodium falciparum* (pfCRMP1/2) which is involved in host-parasite interactions in malaria parasite life cycle (Real et al., 2021; Thompson et al., 2007). Khosla et al. (2006) reported that strains in which the gene encoding DMP1 has been disrupted have developmental defects, such as aberrant fruiting body formation, abnormal sorus colour, reduced sporulation and delayed development. It was also found that disruption of the *dmpA* gene can rescue the aggregation defects in a Ras-GTPase protein RasC disrupted (*rasC*$^{-}$) background (Khosla et al., 2006). Upon cAMP-mediated activation of its receptor, RasC is a key regulatory protein for activating the adenyl cyclase (AC) and AKT/PKB effector pathways and plays essential roles in cAMP relay and aggregation in early development (Lim et al., 2001; Wessels et al., 2004). Ras signalling has been confirmed to regulate *Dictyostelium* cell fate bias, for example, constitutively active RasG and RasD proteins with G12T mutations and overexpression of RasD play a role in pre-stalk cell differentiation (Chattwood et al., 2013; Jaffer et al., 2001; Louis et al., 1997; Reymond et al., 1986). Hence, with the potential regulatory role of Ras proteins in cell fate bias and Ca^{2+} signalling, DMP1 is an interesting candidate that might link Ca^{2+} to Ras signalling pathways and cell fate.

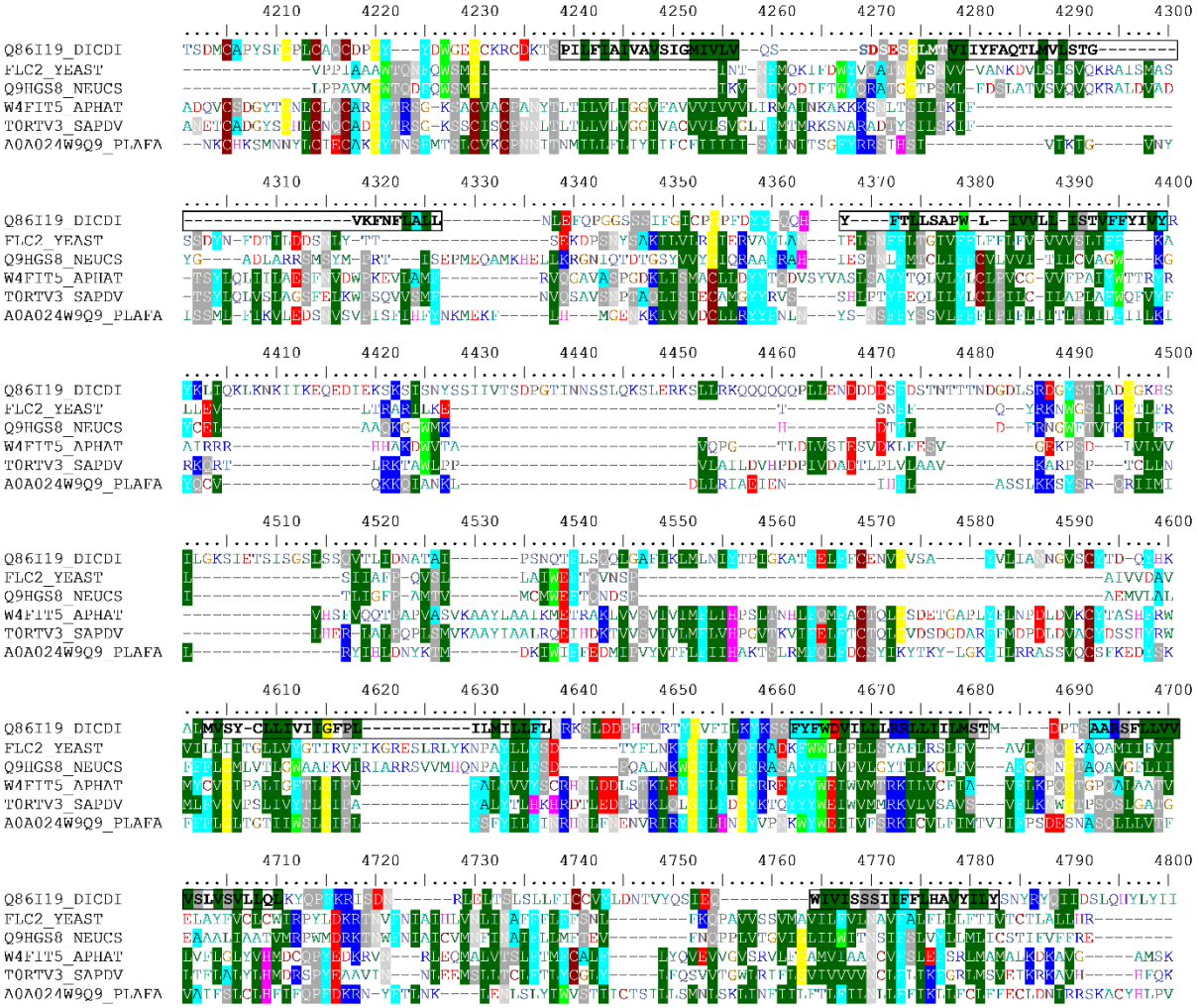


Figure 3.2. Amino acid sequence alignment of the putative *Dictyostelium* Ca^{2+} channel protein DMP1 with Ca^{2+} signalling related proteins from other species. *Dictyostelium* DMP1 encoded by *dmpA* gene (Uniprot ID: Q86I19) is predicted to have seven TM domains (bold, within squared boxes) according to the UniProtKB/Swiss-Prot database. Sequences from fungal proteins, FLC2 from yeasts (Uniprot ID: P39719) and SPRAY from *N. crassa* (Uniprot ID: Q9HGS8, which is a TM protein that regulates the distribution of Ca^{2+} via calcineurin (Bok et al., 2001)), as well as proteins from oomycetes (Uniprot ID: W4FIT5 from *Aphanomyces astaci* and Uniprot ID: T0RTV3 from *Saprolegnia diclena*) and CRMP1 (Uniprot ID: A0A024W9Q9) from *Plasmodium falciparum* were analysed. Oomycete proteins are predicted to be TRP ion channels by SMART (6.7e-13) (J. Thompson, pers. comm., unpublished). The Alignment was performed using Clustal Omega tool and the representation were coloured based on the sequence identities and similarities (shade threshold: 60%) using BioEdit software.

To study the relationship between intracellular Ca^{2+} levels and cell fate bias, modulation of genes encoding components of Ca^{2+} sequestration and signalling can be used. Although Ca^{2+} has been linked to cell fate in *Dictyostelium*, it is currently unclear whether it is cytosolic Ca^{2+} levels, store Ca^{2+} levels or Ca^{2+} released from subcellular compartments in response to a particular signal that affects cell fate decisions. *Dictyostelium* Ca^{2+} channel mutant strains,

therefore, are useful to alter endogenous Ca^{2+} signalling for studying effects of intracellular Ca^{2+} on cell fate decisions. For instance, the average basal levels of $[Ca^{2+}]_c$ in *tpc2*$^-$ and *iplA*$^-$ are significantly lower than that from AX2 cells, so the first two strains can be used to probe the role of basal cytosolic Ca^{2+} levels as well as release from neutral and acidic stores. Since intracellular Ca^{2+} and vesicle pH are considered to influence cell fate decisions (see Chapter 1 section 1.3.3.3 and 1.3.3.4), TPC2 is Ca^{2+} channel that potentially links these cell fate-determining factors and therefore was investigated further in this chapter. The putative Ca^{2+} channel mutants *tpc2*$^-$, *iplA*$^-$ and *dmpA*$^-$ used in this thesis are listed in Table 3.2.

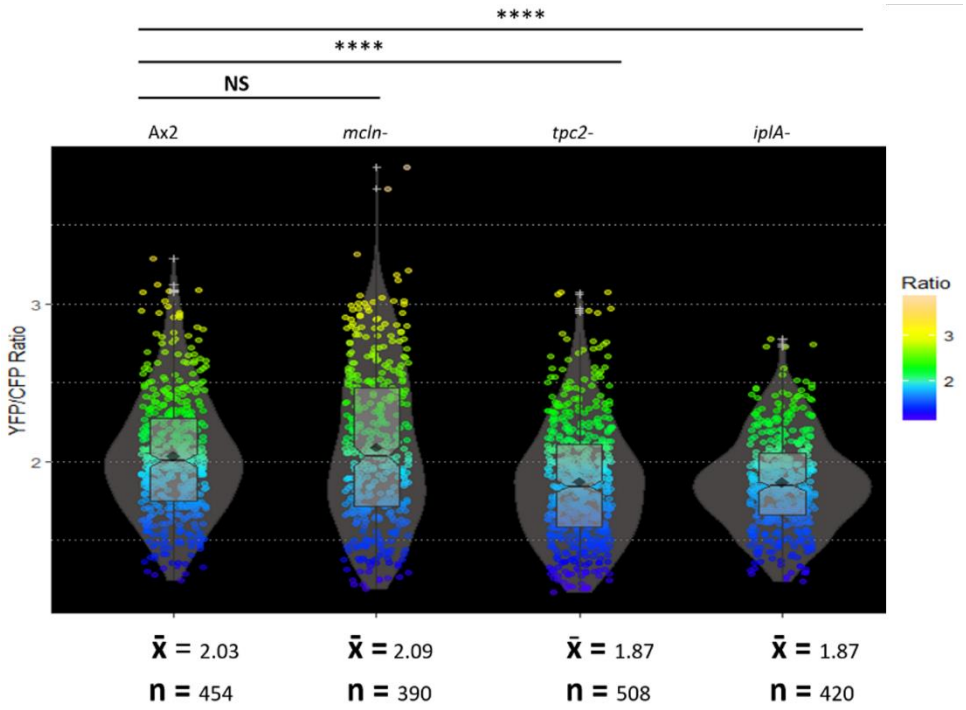


Figure 3.3. Basal $[Ca^{2+}]_c$ levels in AX2 and mutant cell lines with disrupted putative Ca^{2+} channels. Using a FRET-based ultrasensitive Ca^{2+} indicator YC-Nano 15 transfected into cells, the observed emission of YFP/CFP ratios indicating intracellular Ca^{2+} levels can be analysed (Horikawa et al., 2010). Cells in vegetative growth were washed in HKC development buffer with low Ca^{2+} level and plated in imaging dish for 15 mins. The ratios of YFP/CFP in individual vegetative cells indicating the levels of $[Ca^{2+}]_c$ were detected from the imaging process excited at 438 nm wavelength by a widefield fluorescence inverted microscope (DeltaVision Elite), and the emissions of YFP and CFP were captured at 548 nm and 475 nm wavelengths, respectively. The dots of $[Ca^{2+}]_c$ in single cells were plotted in the violin plot overlaid with the notched box-and-whisker plot illustrate the distribution and significance between each strain. The outliers are shown as cross markers and the mean values were illustrated as diamonds. The significance of the differences between mutants and AX2 were analysed using the Wilcoxon rank-sum test (NS: non-significant; ****: $P < 0.0001$). Basal $[Ca^{2+}]_c$ level for *tpc2*$^-$ is 1.87 ± 0.38, which is similar to the level seen in *iplA*$^-$ (1.86 ± 0.30), and both lower than the level in AX2 (2.03 ± 0.38), while mucolipin disrupted strain *mcln*$^-$ has similar $[Ca^{2+}]_c$ level (2.09 ± 0.50) compared to AX2. The diagram was adapted from unpublished data from Chang (2016).

Table 3.2. *Dictyostelium* Ca^{2+} channel null strains in AX2 background used in this thesis

Subcellular locations	Ca^{2+} channels	Gene disrupted strains	Sources of the strains
Acidic stores (e.g. endo-lysosomes)	TPC2	*tpc2*$^{-}$	Constructed by Fu-sheng Chang (Chang, 2016; Chang et al., 2020)
Neutral stores (e.g. ER) and PM	IPLA	*iplA*$^{-}$	
Predicted to be in cellular membranes	DMP1	*dmpA*$^{-}$	Constructed in this thesis

3.1.3 *Dictyostelium* cell fate bias assays used in this thesis

Two cell fate assays, chimeric mixing experiments and monolayer stalk induction assays have been used in this thesis to evaluate cell fate tendencies in different environmental conditions and mutant strains. The experimental design of mixing cells with different backgrounds for chimeric development was firstly proposed by Leach et al. (1973). Mixing experiments then became a common method to assess spore cell fate tendency in multicellular development. Thompson and Kay (2000a) used green fluorescent protein (GFP)-labelled cells to track vegetative cells with different predispositions during growth, e.g. with or without glucose presence (G+/-) and investigated the GFP localization in a slug or quantified GFP spores as a percentage of total spore formation. In this thesis, the chimeric mixing experiments were based on the method reported in Thompson and Kay (2000)'s work but conducted with a different labelling approach using CellTracker live-cell fluorescent dye to visualize green spores at the end of the development.

Around the 1970s and 1980s, prototypes of monolayer assays using cell cultures at low cell densities were used to study cell differentiation and possible morphogens or signalling molecules involving in cell type formation such as a stalk inducer, DIF-1 and cAMP was found to promote spore cell differentiation and suppress stalk cell differentiation (Berks and Kay, 1988; Bonner, 1970; Dominov and Town, 1986; Kay, 1982, 1987; Kay and Jermyn, 1983; Town et al., 1976). Monolayer assays monitoring stalk cell differentiation were more commonly used to study cell fate as DIF-1 responsiveness of pre-stalk marker gene induction has been shown to correlate with cell fate preference in a dose-dependent manner (Thompson and Kay, 2000a). Although there are monolayer assays to induce spore formation in the presence of cAMP (Gross et al., 1983; Kay, 1982), none of those have been reported to be cAMP dose-dependent to potentially monitor preferences. The DIF inducible pre-stalk genes,

ecmA (Dd63) and *ecmB* (Dd50) encode extracellular matrix proteins that predominantly form slime sheath and stalk tube (Jermyn et al., 1987; Kopachik et al., 1983; William and Morrison, 1994; Williams et al., 1987), and they have distinct expression patterns during development maximized at either slug formation or culmination (Jermyn et al., 1987; Morrison et al., 1994). Pre-stalk gene *ecmB* expression can be mediated by accumulation of the bZIP transcription factor DimB which is translocated to the *ecmB* promoter upon DIF-1 induction (Yamada et al., 2011; Zhukovskaya et al., 2006). DIF can also inhibit pre-spore gene expression and suppress spore cell differentiation via cytosolic Ca^{2+} increase-mediated inhibition of aggregative and pre-spore gene expression (Early and Williams, 1988; Kay and Jermyn, 1983; Verkerke-van Wijk et al., 1998; Wang et al., 1986). Pre-stalk gene reporter constructs were made producing β-galactosidase (β-gal) fusion constructs under the control of the promoter sequences of both *ecmA* and *ecmB* (*ecmA*-GAL and *ecmB*-GAL) (Jermyn and Williams, 1991), and *ecmAO*-GAL (Early et al., 1993) was used in the monolayer stalk induction assay reported by Thompson and Kay (2000a), where high DIF-1 sensitivity was interpreted as stalk cell fate bias. This monolayer stalk induction assay using DIF-1 is ideal for quantification by measuring the β-galactosidase activity indicating the stalk cell differentiation.

Thus, these two chosen assays complement each other as one monitors spore formation and the other stalk cell differentiation, and both are quantifiable. One is in multicellular development and so is responding to all endogenous signals, however the monolayer assay is useful for treatment of cells with pharmacological reagents as well as comparing strains.

3.2 Aims

This chapter studies the correlation between cell fate decision making and the interplay of fate determining factors in *Dictyostelium*. This can provide better understanding of individual cells processing differentiation cues in a self-organized organism, in terms of altering cell fate bias.

The aims of this chapter are:

(1) To investigate the role of intracellular Ca^{2+} channels in cell fate decisions using strains with genetic disruption of genes encoding putative Ca^{2+} channels TPC2, IPLA.
(2) To generate strains with disruption of the *dmpA* gene comparing two methods: traditional homologous recombination (Faix et al., 2004) and a more recent CRISPR/Cas9 genome editing system (Muramoto et al., 2019) and investigate any role in cell fate decisions.
(3) To investigate whether the cell fate bias observed in *tpc2*$^{-}$ cells is due to alteration of acidic vesicle pH.

3.3 Results

3.3.1 *tpc2*$^{-}$ cells form fewer spores in chimeric development with AX2 cells

Chang et al. (2020) reported that *tpc2*$^{-}$ cells had a lower basal cytosolic Ca^{2+} level during growth. Preliminary data generated by a project student in the lab suggested that these cells may have a stalk fate bias (E. Warren, pers. comm). Chimeric mixing experiments were performed to study cell fate tendency in multicellular development by assessing spore formation. The workflow of these experiments is explained in Figure 3.4A. Vegetative cells in HL5 shaking suspension were incubated over 2 days until growing to log phase. The exponentially growing cells then were harvested and either labelled with CellTracker fluorescent dye (L) or incubated/unlabelled with DMSO vehicle control (UL). These populations were then mixed and developed in different input percentages: 10%L/90%UL, 50%L/50%UL and 90%L/10%UL. After development, the proportion of green spores in harvested fruiting bodies was counted as a quantitative measurement of spore cell fate bias. Positive controls of mixing experiments were performed to confirm the labelling process using AX2 wildtype and *tpc2*$^{-}$ cells (clone: TPC22B20) growing in normal glucose sufficient HL5 medium (Figure 3.4B). By performing homogenous mixing experiments with both populations, i.e, labelled AX2 cells mixed with unlabelled AX2 cells, and the same control experiments for the mutant *tpc2*$^{-}$ cells, the input ratio of fluorescent cells labelled before development corresponded well to the output ratio of fluorescent spores after development, for example, when 10% AX2 cells were labelled and mixed with 90% unlabelled AX2 cells, the output of green spores is 10.7% ± 0.3% (Mean ± standard error mean (S.E.M)). However, when including 90% labelled cells fewer than 90% green spores were detected in both strains. Therefore, it is important to carry out complementary experiments with labelling of both populations to detect biases at this percentage, and other mixing ratios were performed to verify the results. Overall, the control mixing experiments verified that the fluorescent label remained stably during development, did not interfere with spore differentiation and unlabelled spores did not autofluorescence.

The cell fate bias of *tpc2*$^{-}$ cells was tested by mixing experiments with parental AX2 cells (Figure 3.4C), revealing a stalk cell fate tendency in *tpc2*$^{-}$ cells. For example, when 10% AX2 labelled cells were mixed with 90% *tpc2*$^{-}$ unlabelled cells, a more than two-fold increase in

green spores was observed compared to the 10% input (25.3% ± 1.8%). Conversely, when 10% *tpc2*$^{-}$ labelled cells mixed with 90% AX2 unlabelled cells, fewer green spores formed than the input ratio (9.4% ± 0.3%). This same trend was observed in all mixing ratios. The *tpc2*$^{-}$ strain was also verified and housekeeping gene *ig7* (or *rnlA*, DDB_G0294034) which encodes mitochondrial large ribosomal RNA was included as a PCR positive control (Figure 3.4D). In summary, chimeric mixing experiments can be used to assess spore cell fate tendency, and *tpc2*$^{-}$ cells have a stalk cell bias in chimeric development with AX2.

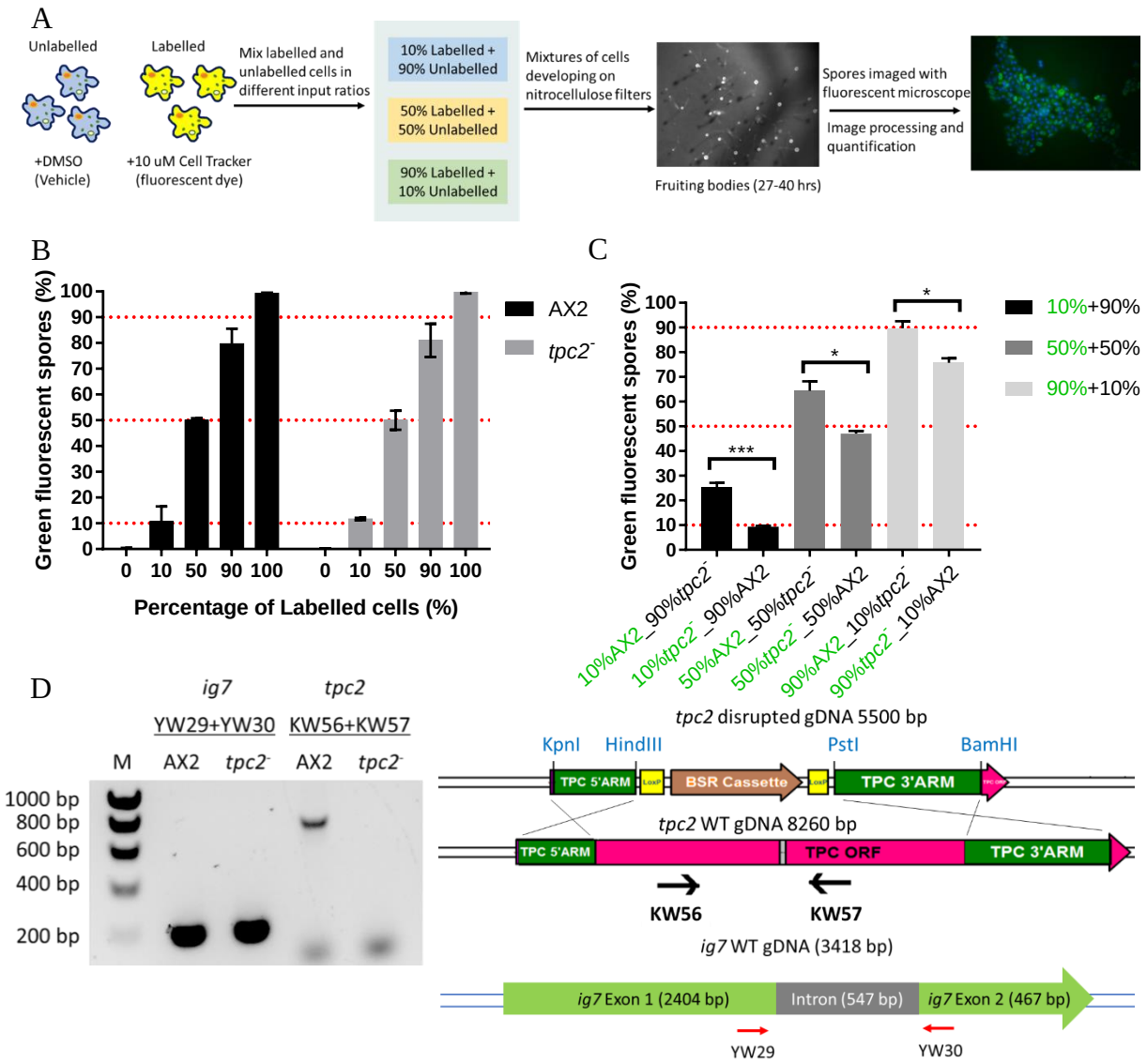


Figure 3.4. Chimeric mixing experiments to monitor spore cell fate bias in *tpc2*⁻ cells. (A) Schematic work flow of mixing experiments to quantify spore cell numbers and reveal fate bias. Cells incubated in static petri dishes at 22°C were seeded at the density of 2×10^5 cells/mL in normal HL5 medium and grown for 48 hrs to exponential growth phase at 22°C in a shaking incubator (220 rpm). Exponentially growing cells were collected and washed in KK2 buffer twice by centrifugation at 3000 rpm, 22°C for three minutes, and resuspended in KK2 to 5×10^7 cells/mL, and the incubated with 10 µM fluorescent CellTracker™ Green CMFDA Dye (Life technologies) (L) or with DMSO vehicle control (UL) for 45 mins on a roller at room temperature. After washing with KK2 three times, labelled and unlabelled cells were proportionally mixed in 10/90, 50/50 or 90/10 ratios. In a well of 24-well plate, 50 µL of the mixture of cells at 5×10^7 cells/mL in KK2 was plated on nitrocellulose filters at 22°C in a dark room for around 40 hrs. Spores were harvested and fixed on coverslips mounted with DAPI-containing VECTASHIELD mounting medium for imaging by fluorescent microscopy. The number of green spores (CellTracker labelled) and the total number of spores (blue nuclei stained with DAPI) were quantified using imageJ software. (B) Control experiments for the potential effect of cell labelling in mixing experiments. AX2 and *tpc2*⁻ cells growing exponentially in HL5 medium (containing 1% glucose) were labelled or unlabelled as described above. Labelled and unlabelled cells from the same strain were mixed and developed in different proportions and spores counted as above. N = 3. Mean ± S.E.M.

(C) *tpc2*$^{-}$ cells (clone: TPC22B20) were mixed with AX2 cells in chimeric mixing experiments and analysed as described in (A). The labelled portions are highlighted in green. N = 3. Mean ± S.E.M. Student *t*-test (two-tailed): *: P < 0.05; **: P < 0.01; ***: P < 0.001. (D) Verification of *tpc2*$^{-}$ strain (clone: TPC22B20). Left panel: RNA was extracted from exponentially growing cells (*tpc2*$^{-}$ and AX2) and the resulting cDNA analysed by PCR using primer sets amplifying a region of exon 1 of the *tpc2* gene deleted in the null strain (KW56+KW57) and a endogenous control *ig7* (YW29+YW30). PCR products were analysed on a 1% ethidium bromide (EtBr) agarose gel. Expected cDNA PCR product sizes were 190 bp for *ig7* and 775 bp for central region of the *tpc2* gene. Right panel: Schematic representations of *tpc2* and *ig7* gene in gDNA. Upper right panel: *tpc2* gene and the homologous recombination strategy for constructing *tpc2*$^{-}$ mutant cell line. The relative location of the primer set KW56+KW57 is shown in the diagram. Adapted from Chang (2016). Lower right panel: brief map of *ig7* gene encoding mitochondrial large rRNA subunit (*rnlA*, DDB_G0294034) used as a control for testing the quality of DNA used in PCR experiments. Using YW29+YW30 primer set for PCR, expected gDNA PCR product size is 737 bp and cDNA product is 190 bp.

3.3.2 Monolayer stalk induction assays confirm stalk cell fate tendency of *tpc2*$^{-}$ cells

The monolayer stalk induction assays performed in this thesis used the method described in Thompson and Kay (2000). Figure 3.5A illustrates the workflow of the assay. All cells used in monolayer assays were transfected with an *ecmB*-GAL stalk reporter construct (*ecmB*-GAL) and maintained in selective G418 (Jermyn and Williams, 1991) before monolayer stalk induction assays. A low cell density of cells plated in each well of 96-well plate ensured that cells remained without cell-cell interactions and thus would not form multicellular developmental structures under monolayer conditions. In the first 24-hr incubation, cAMP was added to enable cells to become responsive to exogenous DIF-1, while cerulenin was added was to inhibit endogenous DIF-1 biosynthesis (Kay, 1998). Various concentrations of DIF-1 subsequently replaced cAMP to induce stalk marker gene expression for the next 24-hr incubation. Cells then were lysed, releasing β-gal expressed from the *ecmB*-GAL gene and the expression level quantified following addition of chlorophenol red-β-D-galactopyranoside (CPRG) substrate. Hence, the DIF-1 sensitivity in cells was analysed by assessing stalk marker expression levels. Monolayer stalk induction assays were performed to test whether *tpc2*$^{-}$ null strain has altered cell fate tendency via monitoring its DIF-1 sensitivity compared to AX2. Higher level of stalk marker expression induced by low DIF-1 concentrations indicated high DIF-1 sensitivity in *tpc2*$^{-}$ cells comparing to AX2 (Figure 3.5B). For example, in *tpc2*$^{-}$ cells, *ecmB*-GAL expression upon 10 nM DIF-1 induction (47.5% ± 9.4%) is three times more than that detected in AX2 cells (14.0% ± 1.3%). This was consistent with the observation of the phenotype of reduced spore formation in chimeric mixing experiments when developing with

AX2. This stalk bias shown in monolayer *tpc2*$^{-}$ development was consistent with the results using another clone of *tpc2*$^{-}$ cells carried out by a previous project student (E. Warren, pers. comm.). It should be noted that *tpc2*$^{-}$ has a lower basal level of cytosolic Ca^{2+} (Chang, 2016) (Figure 3.3), and yet it prefers stalk cell fate, which does not agree with the reports of higher intracellular Ca^{2+} levels correlating with stalk cell differentiation (Azhar et al., 1996) (also see Chapter 1 section 1.3.3.4).

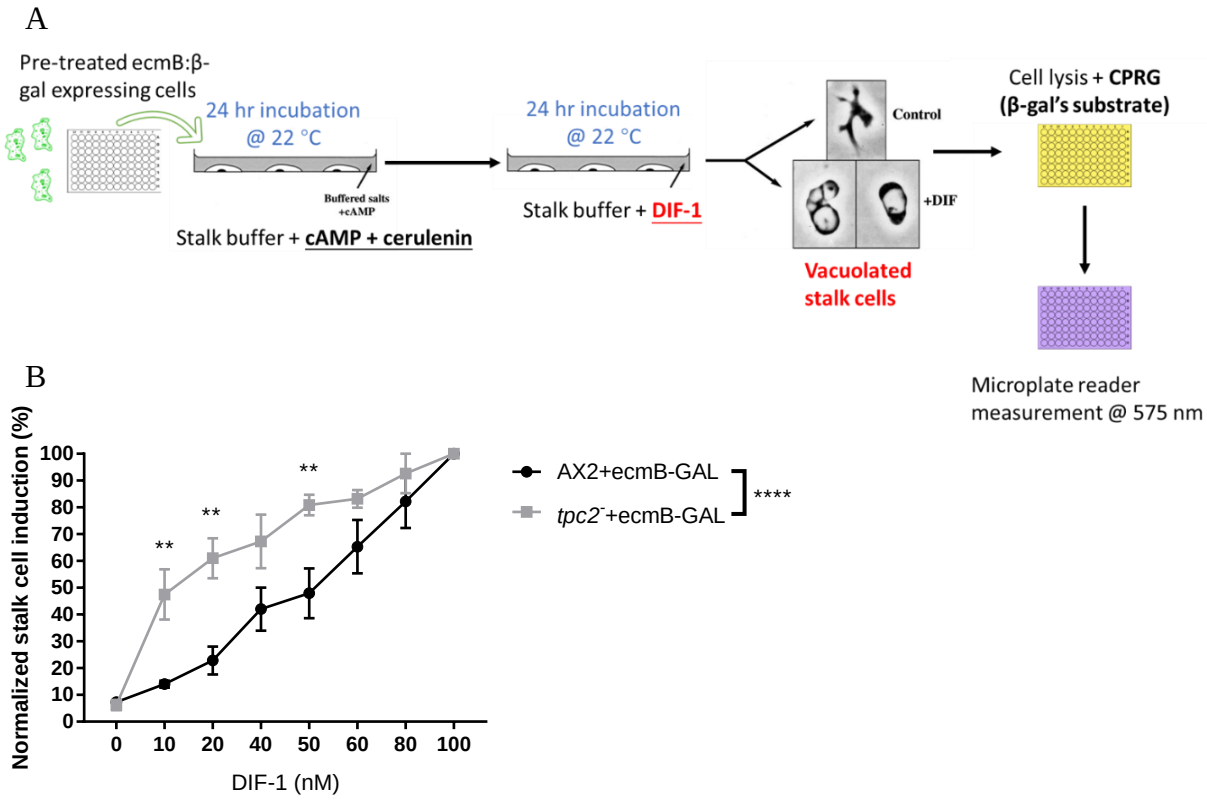


Figure 3.5. Monolayer stalk induction assays for monitoring DIF-1 sensitivity in developing cells. (A) Schematic work flow of monolayer DIF-1 assay to assess stalk cell fate tendency. Cell morphology photos were adapted from Kay et al. (1999). Cells transfected with DIF-inducible stalk cell marker construct (*ecmB*-GAL) were harvested when exponentially growing and were washed in KK2 twice. Then, the cells were resuspended at a density of 2.32×10^5 cells/ mL in stalk buffer with 5 mM cAMP and 50 µM cerulenin and 50 µL suspension (11600 cells) was plated in each well of a 96-well plate, incubated at 22°C for 24 hrs. Various DIF-1 concentrations then replaced cAMP to induce stalk marker expression for another 24 hrs at 22°C. Lysis buffer with 2 mM CPRG was applied to the cells and the plate was incubated at 37°C for 60 mins. β-galactosidase enzymatic activity in response to DIF-1 was quantified by a microplate reader by endpoint absorbance measurement at 575 nm. (B) Monolayer stalk induction assay of AX2 and *tpc2*$^{-}$ cells (N = 3) expressing *ecmB*-GAL stalk marker were performed. The expression levels were normalized to the 100 nM DIF-1 treated groups defined as 100%. Mean ± S.E.M. Two-way ANOVA: **: $P < 0.01$; ***: $P < 0.001$; ****: $P < 0.0001$.

3.3.3 *iplA*$^{-}$ cells show a spore cell fate tendency

To further investigate the role of Ca^{2+} in regulating cell fate decisions, a strain with disruption of the *iplA* gene encoding a Ca^{2+} channel resembling IP_3R in mammalian cells on the neutral Ca^{2+} stores was used. A gene disruption vector pTD5 for making *iplA*$^{-}$ null strain with homologous recombination method was constructed by Traynor et al. (2000). This construct was used to disrupt the *iplA* gene in AX2 cells in our lab (Chang, 2016). Previous lab data shows that *iplA*$^{-}$ strain has a lower basal cytosolic Ca^{2+} level in growth (Wilcoxon rank-sum test, mean ± standard deviation (SD), 1.9 ± 0.3), similar to *tpc2*$^{-}$ (1.9 ± 0.4) (Figure 3.3, unpublished data from Chang (2016)). One of the transformant clones of *iplA*$^{-}$ generated from his work was verified by PCR on gDNA (clone: iplAI2D) and used in the experiments in this thesis (Figure 3.6A).

The *iplA*$^{-}$ strain was used in mixing experiments and monolayer stalk induction assays to explore whether this Ca^{2+} channel mutant would have a cell fate bias. Surprisingly, mixing experiments showed that *iplA*$^{-}$ cells preferred to form spores compared to AX2 cells in all mixing ratios (Figure 3.6B). For example, when 10% labelled cells were mixed with 90% unlabelled cells, AX2 formed 9.7% ± 0.1% spores, while *iplA*$^{-}$ formed 13.9% ± 1.2% spores. With 50%L/50%UL input ratio, only 45.6% ± 4.5% spores were formed from AX2 formed but *iplA*$^{-}$ formed more spores than the initial input (60.4% ± 1.4%). Therefore, the overall phenotype of *iplA*$^{-}$ in mixing experiments indicates a spore cell fate bias. In the monolayer stalk cell assay, a slight reduction of stalk marker expression in *iplA*$^{-}$ cells relative to AX2 cells was observed at lower DIF-1 concentrations (less than 20 nM) consistent with a prespore bias (Figure 3.6C). This indicates that the disruption of IPLA presumed to result in interruption of Ca^{2+} signalling from neutral Ca^{2+} stores, which imposes a spore cell fate decision. Since cells with higher intracellular Ca^{2+} level have been reported to the choose a pre-stalk cell fate, and lower Ca^{2+} level in cells promoted a pre-spore cell fate (Azhar et al., 1996), the observation of lower basal cytosolic Ca^{2+} level in *iplA*$^{-}$ (Chang, 2016) (Figure 3.3) correlates to its spore cell fate preference.

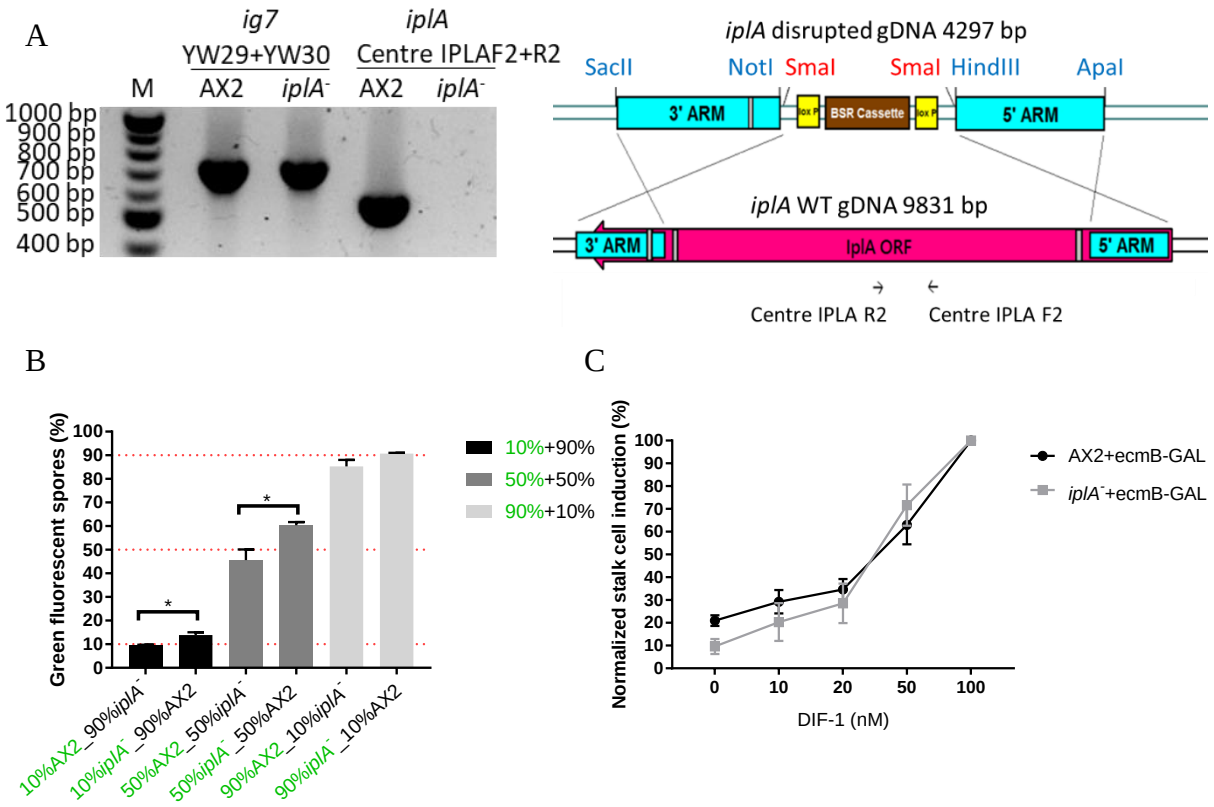


Figure 3.6. Effect of disruption of the *iplA* gene on cell fate decision. (A) gDNA verification of *iplA*$^-$ strain (clone: iplAI2D) was performed by PCR using primer sets Centre IPLAF2+Centre IPLAR2 which amplifies the region disrupted in the null cells and control *ig7* (YW29+YW30). Left panel: 1% agarose gel stained by EtBr was used to visualize the PCR results. Expected gDNA PCR product sizes are 737 bp for *ig7* and 565 bp for *iplA*. Right panel: A schematic representaion of *iplA* gene map and homologous recombination strategy for disrupting *iplA*. The primers Centre IPLAF2 and Centre IPLAR2 are shown in the diagram for screening the deleted region in *iplA*$^-$ clones. Apated from Chang (2016). (B) Development of chimaeras of AX2 and *iplA*$^-$ cells. Labelled portions within the mixing ratios are indicated in green. Mixing experiments were performed as described in the legend to Figure 3.4A. N = 3. Mean ± S.E.M. Student *t*-test (two-tailed): *: P < 0.05. (C) Monolayer stalk induction assay of AX2 and *iplA*$^-$ cells expressing the stalk marker *ecmB*-GAL were carried out as described in the legend to Figure 3.5A. N = 3 .Mean ± S.E.M.

3.3.4 Investigation of the *dmpA* gene encoding DMP1, a putative Ca^{2+} channel

DMP1, encoded by gene *dmpA* (5199 bp, DDB_G0275065), is a putative Ca^{2+} TRP ion channel (Figure 3.2, J. Thompson pers. comm.). An online bioinformatics tool (predictprotein.org) for predicting subcellular localization and gene ontology (GO) terms (Table 3.3), predicted that DMP1 is located on the plasma membrane (GO term ID: GO:0005886, LocTree3 prediction confidence: 54). Transmembrane helix distribution also predicted that DMP1 is a membrane-targeted protein (Figure 3.7). In order to investigate any role for DMP1 in cell fate decisions, *dmpA*$^-$ strains were constructed by both a traditional homologous recombination strategy and

the more recently established CRISPR/Cas9 gene editing technology. This was to introduce the CRISPR/Cas9 editing system to our lab and compare these two methods of making gene disruption strains in *Dictyostelium*.

Table 3.3. Gene Ontology Prediction for *dmpA* encoded protein

Category of Ontologies	GO ID	GO Term	Reliability (%)
Biological Process Ontology	GO:0007186	G protein-coupled receptor signalling pathway	43
	GO:0007214	gamma-aminobutyric acid signalling pathway	43
Cellular Component Ontology	GO:0016021	integral component of membrane	44
	GO:0016020	membrane	44
Molecular Function Ontology	GO:0004965	G protein-coupled GABA receptor activity	43

Prediction results using goPredSim method were adapted from Predictprotein online tool

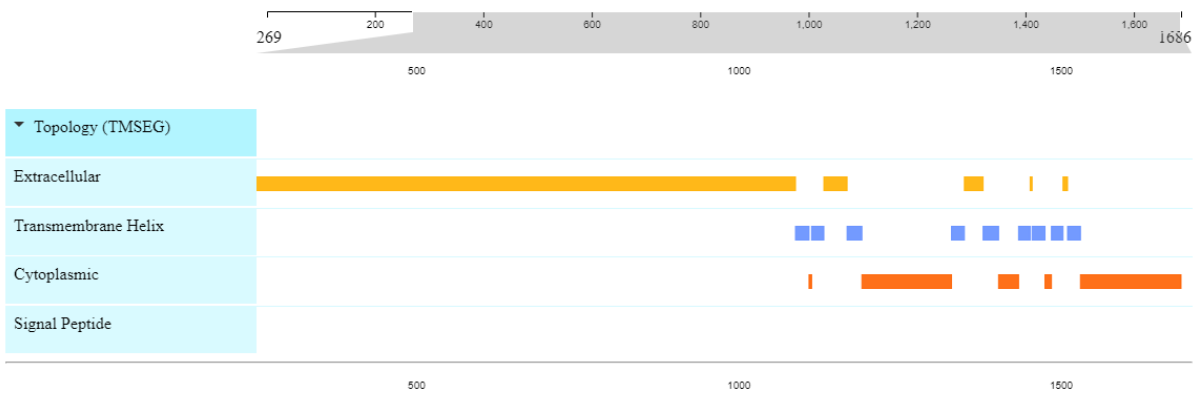


Figure 3.7. Transmembrane Helices Prediction for DMP1. This was performed using TMSEG method from predictprotein.org online bioinformatics server.

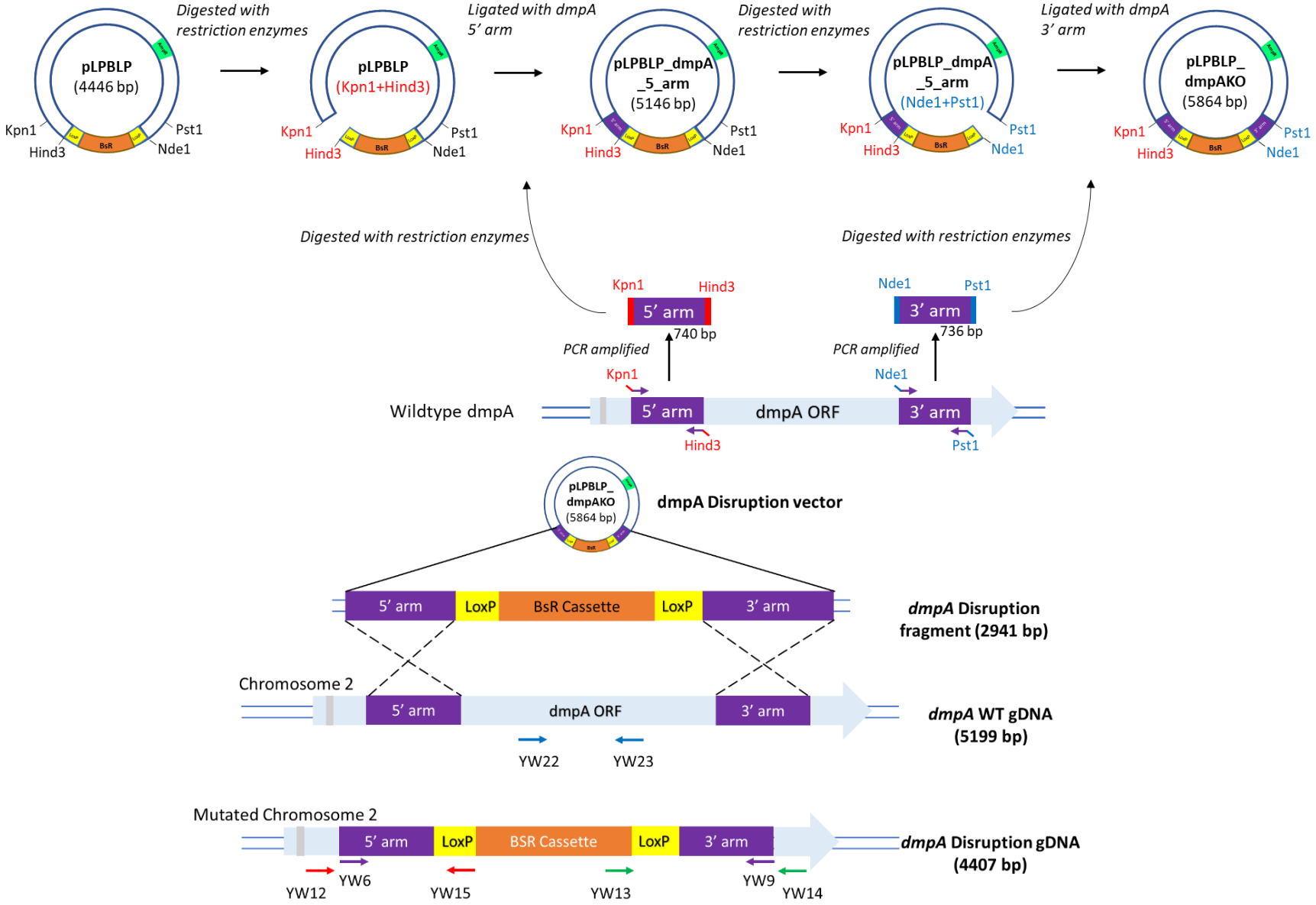
3.3.5 Disruption of *dmpA* gene using both homologous recombination and CRISPR/Cas9 strategies

3.3.5.1 Homologous recombination method for constructing *dmpA*$^-$ strain

In the homologous recombination (HR) strategy (Figure 3.8A), the vector pLPBLP was chosen which contains a Blasticidin S resistance (BSR) cassette which can be recycled using the Cre-loxP system to enable the future generation of strains containing multiple gene disruptions (Faix et al., 2004). Two gDNA sequences from the 5' and 3' ends of the *dmpA* gene were designed to be 5' and 3' arms for the disruption vector to introduce a large deletion of the second exon (2270 bp) replaced with a BSR cassette (1478 bp) (Figure 3.8A). This strategy would also cause a frameshift mutation, producing a truncated and non-functional protein as

this deleted region includes three potential TM domains (Figure 3.8A and Figure 3.9). These two arms were amplified by PCR using primers YW6 and YW7 with KpnI and HindIII restriction sites for 5' arm cloning and YW8 and YW9 with NdeI and PstI restriction sites for 3' arm cloning. They were subsequently cloned into pLPBLP vector digested with the same restriction enzymes, and each step was confirmed by either sequencing or restriction digests (Figure 3.8B). The final construct pLPBLP_dmpAKO was transfected into AX2 cells via electroporation, and serial dilutions of the transfected cells in 96-well plates were selected under 10 μg/mL BS and single colonies were transferred to 24-well plate for analysing *dmpA* gene disruption. gDNA of *dmpA*$^{-}$ candidate clones was extracted and verified by PCR using different primers designed to identify those with gene disruption (Figure 3.8C). Through PCR screening, two independent clones out of 115 candidates were identified: dmpAII76 and dmpAI31. Further purification using a serial dilution method was used to isolate single clones for each of these candidates to ensure the clones were free from parental contamination.

A


pLPBLP
(4446 bp)
Kpn1
Hind3
BsR
Pst1
Nde1
Digested with restriction enzymes
pLPBLP
(Kpn1+Hind3)
Ligated with dmpA 5′ arm
pLPBLP_dmpA_5_arm
(5146 bp)
Digested with restriction enzymes
pLPBLP_dmpA_5_arm
(Nde1+Pst1)
Ligated with dmpA 3′ arm
pLPBLP_dmpAKO
(5864 bp)
Digested with restriction enzymes
Digested with restriction enzymes
5′ arm
740 bp
3′ arm
736 bp
PCR amplified
PCR amplified
Wildtype dmpA
dmpA ORF
dmpA Disruption vector
LoxP
BsR Cassette
3′ arm
dmpA Disruption fragment (2941 bp)
Chromosome 2
dmpA ORF
dmpA WT gDNA (5199 bp)
YW22
YW23
Mutated Chromosome 2
BSR Cassette
dmpA Disruption gDNA (4407 bp)
YW12
YW6
YW15
YW13
YW9
YW14

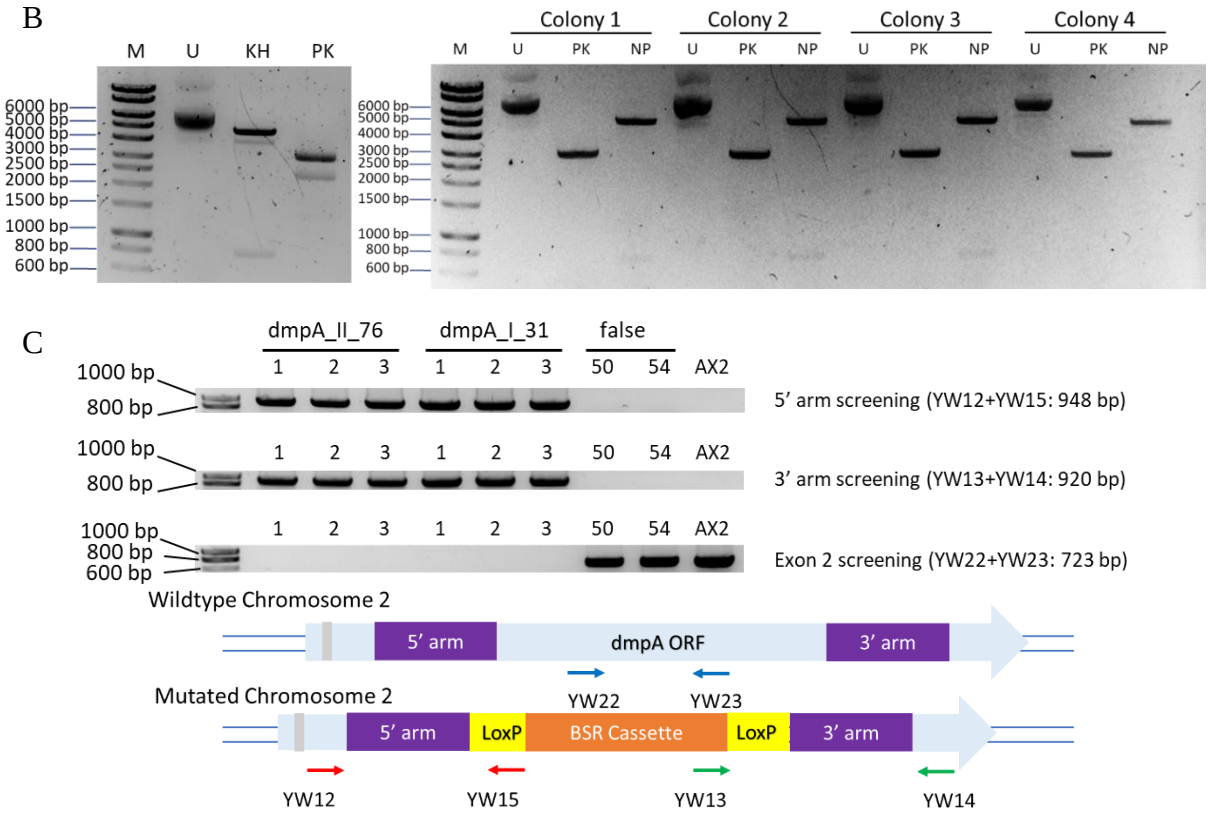


Figure 3.8. Homologous recombination (HR) strategy for constructing a *dmpA* gene disruption strain. (A) Schematic representation of HR method for disrupting the *dmpA* gene. pLPBLP (4446 bp) is a gene disruption vector backbone containing a BSR cassette flanked by loxP sites. The 5' arm (740 bp) and 3' arm (736 bp) of *dmpA* PCR products were amplified with primers with overhangs compatible with different sets of restriction enzymes: KpnI + HindIII for 5' arm and NdeI + PstI for 3' arm. The final construct pLPBLP_dmpAKO (5864 bp) was confirmed by sequencing and then transfected into AX2 cells by electroporation to disrupt wildtype *dmpA* open reading frame (ORF). Transformants were then plated in 96-well plates in serial dilutions in BSR selection for screening to identify *dmpA*$^{-}$ candidates. (B) Left panel: Restriction digest of an intermediate vector containing the 5' arm of *dmpA* in pLPBLP_dmpA_5_arm (colony #1 as an example). U: undigested pLPBLP_dmpA_5_arm vector (5146 bp), KH: KpnI+HindIII double digest (4406 bp and 740 bp) (fainter band around 4 kb is the undigested supercoiled vector, PK: PstI+KpnI double digest (2905 bp and 2241 bp). Right panel: Restriction control digest of final construct pLPBLP_dmpAKO with BSR cassette flanked by *dmpA* 5' and 3' arm inserted (four colonies as examples). U: undigested pLPBLP_dmpAKO (5864 bp), PK: PstI+KpnI double digest (2905 bp and 2959 bp, close to each other and are not resolved), NP: NdeI+PstI double digest (5128 bp and 736 bp). (C) Upper panel: Single clones purified from *dmpA* deletion candidates screened from pLPBLP_dmpAKO transformants dmpAII76 and dmpAI31 were picked and gDNA was tested with different PCR primers: YW12+YW15 for insertion of the *dmpA* 5' arm (948 bp) and YW13+YW14 for correct insertion of the *dmpA* 3' arm (920 bp). YW22+YW23 were used to ensure that the centre region of the *dmpA* gene in exon 2 (723 bp) was not present in the disrupted clones. Transformants that contained random insertion of the vector but did not have the gene disruption (dmpA_50 and 54) were experimental controls for the PCR screening, while AX2 acted as a control for the absence of BSR cassette and the presence of wildtype *dmpA* gene sequence. Lower panel: Schematic representation of PCR primers used for screening independent clones of *dmpA* HR knockout cell line. Both (B) and (C) were examined on 1% EtBr agarose gels with marker (M) HyperLadder 1kb (Bioline).

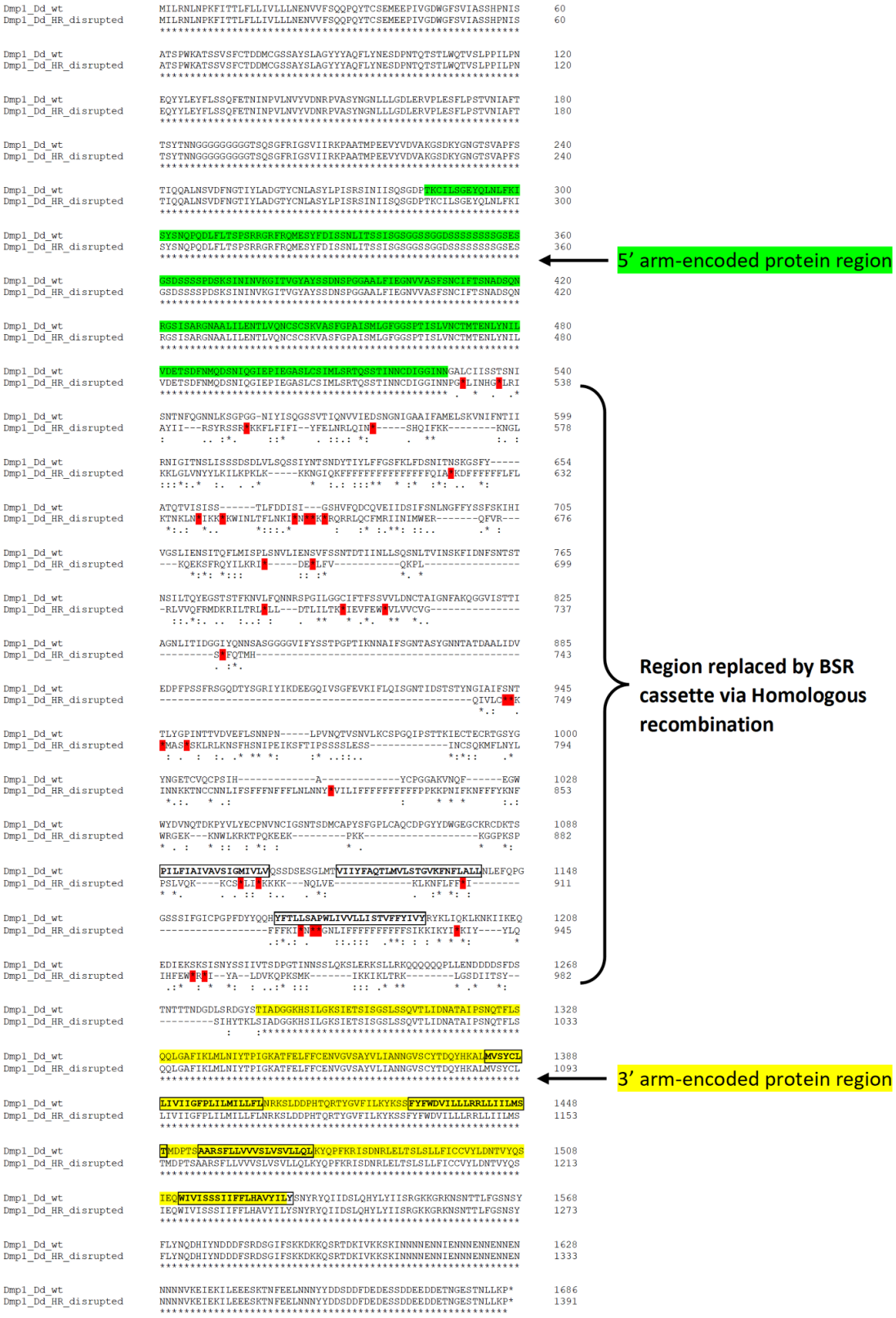


Figure 3.9. Alignment of amino acid sequences of wildtype and HR gene disrupted DMP1. In the wildtype DMP1 sequence (UniProt: Q86I19), regions highlighted in green and yellow show the amino acids encoded by 5’ arm and 3’ arm, and the middle region is the disrupted region replaced with BSR cassette from pLPBLP. The predicted TM domains are in black square boxes. In the mutated DMP1 sequence, premature stop codons are highlighted with red. An online sequence alignment tool Clustal Omega was used.

3.3.5.2 CRISPR/Cas9 method for constructing *dmpA*$^-$ strain

To compare methods of generating genetically disrupted strains, an alternative CRISPR/Cas9 gene disruption strategy was also used to make *dmpA*$^-$ cell lines (Figure 3.10A). An all-in-one CRISPR/Cas9 expression vector pTM1285 (Sekine et al., 2018) was used (Left panel, Figure 12B). A protocol adapted from the Williams Lab (Royal Holloway, University of London) was followed. Using an online program Crispor developed by Concordet and Haeussler (2018) to predict guide RNAs, three sets of single-guide RNA (sgRNA) sequences (20 bp) were selected, as they were predicted not to have off-target effects. They are also in close proximity to the 5' end of the *dmpA* gene, where sequences 1, 2 and 3 are 579 bp, 330 and 771 bp downstream of the ATG start codon respectively. For each sgRNA, a pair of complimentary oligonucleotides were designed having different 4 bp-overhangs (AAAC or AGCA) on the top or bottom strand to facilitate cloning into the BpiI restrictions site in a correct direction in the vector. For construction of three different *dmpA* disruption vectors, each pair of sgRNA was cloned into pTM1285 and verified by PCR using a forward primer YW24 designed from the C-terminal GFP-tagged Cas9 coding sequence and one of the oligonucleotides in the guide RNA as the reverse primer, generating a 500-bp PCR fragment (Figure 3.10B).

Following successful cloning of all three constructs, the vectors were co-transfected in three combinations into AX2 cells three times (Figure 3.10C). The transformants on the following day underwent three-day incubation in HL5 containing 10 μg /mL G418 to allow transient expression of CRISPR/Cas9 disruption vector. Then, serial dilutions were plated onto SM agar with bacteria *Klebsiella aerogenes* and incubated for about five days until single translucent plaques appeared. The leading edge from these single plaques representing a single colony were transferred to liquid culture in 24-well plates for further PCR screening of gDNA to identify potential gene disruptants. From PCR screening, four clones out of 50 isolated from serial dilution plates had large deletions verified in gDNA (Figure 3.10D) and cDNA (Figure 3.10F), using the primers verified on AX2 gDNA templates beforehand (Figure 3.10E). In total, 6 colonies from these four large deletion clones were picked and sent for sequencing. It was confirmed that all six independent clones had deletions introducing frameshifts (Figure 3.11A), leading to multiple premature stop codons (Figure 3.11B). This indicates that these frameshift mutations would lead to the formation of truncated, presumably non-functional proteins with the coding sequence of TM domains also disrupted.

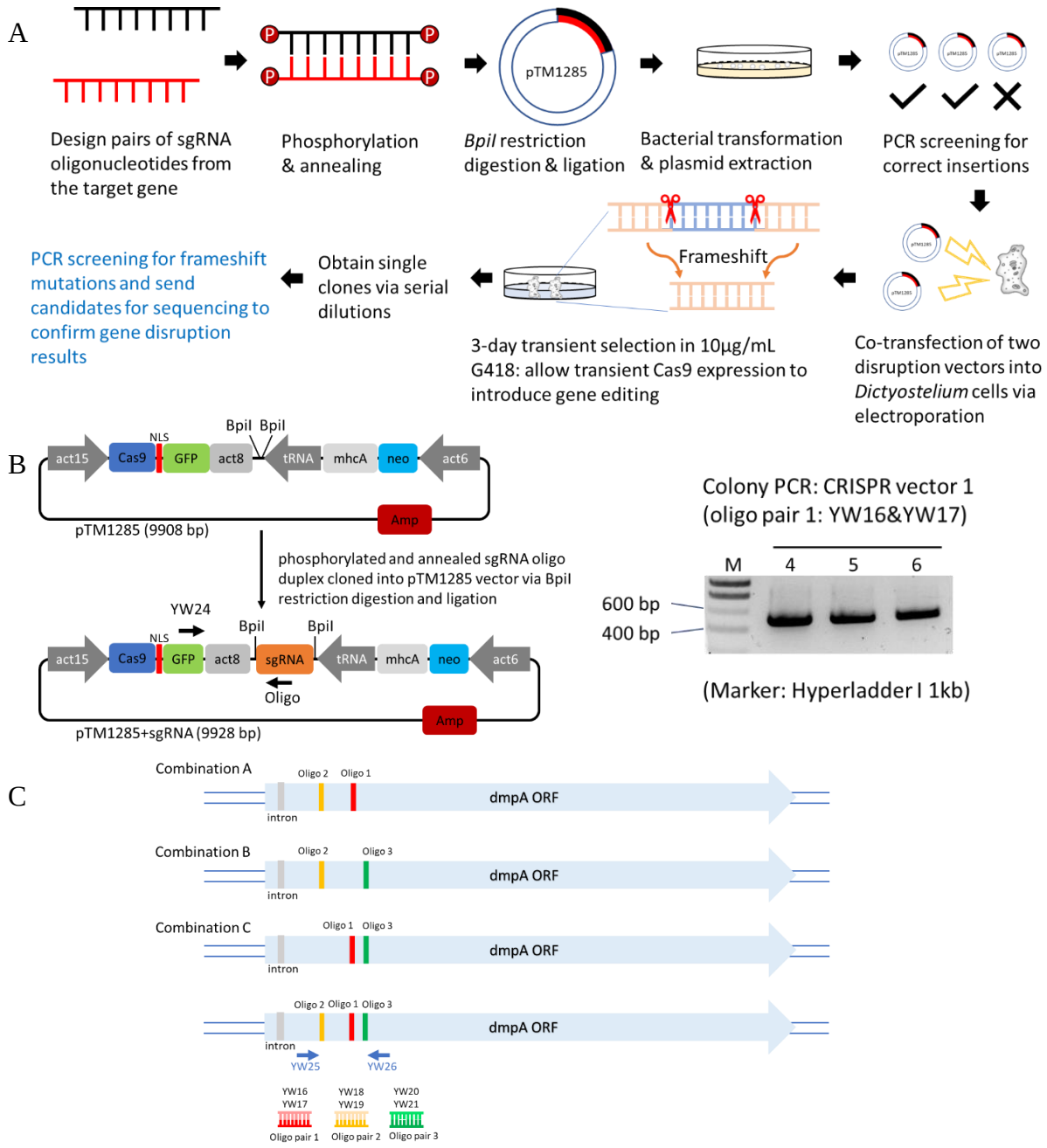


Figure 3.10. CRISPR/Cas9 strategy for *dmpA* disruption. (A) Schematic representation of CRISPR/Cas9 gene disruption workflow. (B) Left panel: cloning of sgRNA oligos (20 bp) in pairs which have different overhangs (top strand: AGCA; bottom strand: AAAC) into all-in-one CRISPR/Cas9 expression vector pTM1285 (9908 bp) (adapted from Sekine et al. (2018)). Primers for screening the successful insert into pTM1285 were YW24 forward primer in GFP at the C terminus of Cas9 and the oligo with reverse direction in the sgRNA duplex at the bottom strand as the reverse primer. Right panel: Example of colony PCR screening for *dmpA* CRISPR disruption vector 1 (colony #4, 5 and 6). Forward primer YW24 (upstream of sgRNA) and reverse primer YW16 (oligo in reverse direction) were used to perform PCR experiments, generating a 500-bp band, visualised on 1% EtBr agarose gel. (C) Schematic representation of relative positions of three pairs of sgRNA oligos used in co-transfection. Combination A contained oligo pair 1 (YW16+YW17) and oligo pair 2 (YW18+YW19). Combination B had oligo pair 2 and oligo pair 3 (YW20+YW21). Combination C involved oligo pair 1 and oligo pair 3.

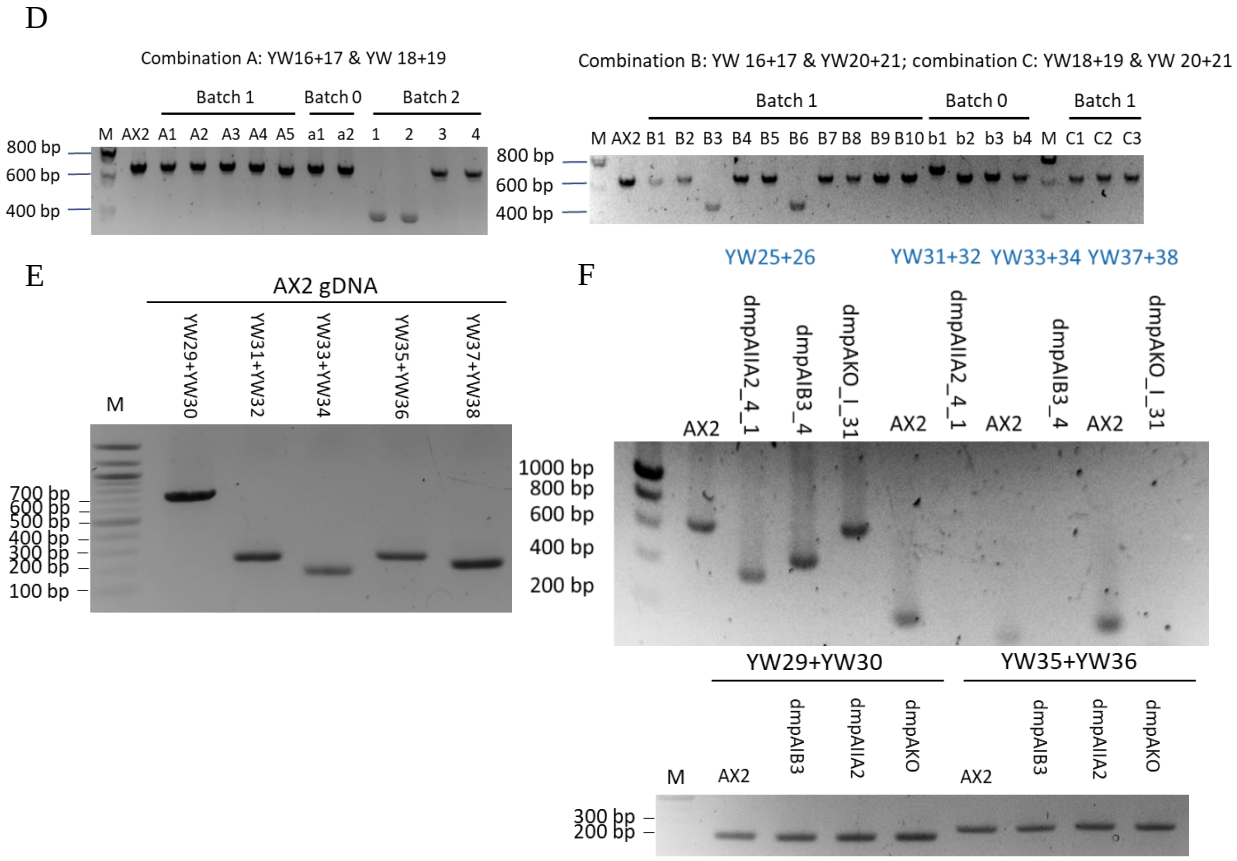


Figure 3.10. CRISPR/Cas9 strategy for *dmpA* disruption. (continued) (D) Examples of PCR screening of *dmpA*$^{-}$ CRISPR candidates with different combinations of disruption vectors co-transfection. YW25 and YW26 primers were designed flanking the expected *dmpA* CRISPR disrupted regions, producing a 643-bp band from PCR with wildtype gDNA. In combination A (left panel), the second batch of transfection contained two independent clones (dmpAIIA1 and dmpAIIA2) with large deletion, producing a shorter band (374 bp) in PCR with YW25+YW26 primer set. Combination B (right panel) also had two independent clones (dmpAIB3 and dmpAIB6) with large deletion in the first batch of transfection, generating a 457-bp fragment in PCR screening with YW25+YW26 primers. Combination C did not have large deletion mutant sequence. (E) PCR experiments for testing primers using wildtype AX2 gDNA templates. YW29+YW30 produce a 737 bp-band of endogenous control *ig7*. YW31+YW32 amplify the deleted region with combination A (YW16+YW17 and YW18+YW19) in *dmpA* and give a wildtype band of 224 bp. YW33+YW34 amplified the deleted region with combination B (YW18+YW19 and YW20+YW21) in *dmpA* and a wildtype band of 153 bp. YW35 and YW36 designed 1486 bp and 1694 bp downstream of ATG start codon of *dmpA* gene (also within the 5' arm homologous region in the HR gene disruption strategy) were used to amplify a wildtype 235 bp band downstream of the deleted region. YW37+YW38 were primers for verifying the deleted region in *dmpA*$^{-}$ HR strains and the wildtype band was 196 bp. These results were analysed on 1% EtBr agarose gel with the marker (M) Quick-load 100 bp DNA ladder (NEB). (F) RT-PCR experiments for verifying *dmpA*$^{-}$ strains. Upper panel: cDNA verification of AX2, single clones of CRISPR strain dmpAIIA2_4_1 and dmpAIB3_4 as well as a single clone of HR strain dmpAKO_I_31 via RT-PCR. YW25+YW26 primers flanking *dmpA* CRISPR-disrupted region produced a wildtype band of 653 bp (seen in AX2 and dmpAKO_I_31) and bands of 374 bp for dmpAIIA2

and 457 bp for dmpAIB3. YW31+YW32 amplifying the deleted region in combination A (YW16+YW17 and YW18+YW19) give a 224 bp-wildtype band. YW33+YW34 amplified the deleted region with combination B (YW18+YW19 and YW20+YW21) to produce a 153 bp-wildtype band. YW37 + YW38 which generated a 196-bp wildtype band were primers for verifying the deleted region in *dmpA*$^{-}$ HR strains. These results were analysed on 1% EtBr agarose gel with the marker (M) HyperLadder 1kb (Bioline). Lower panel: examples of positive control RT-PCR experiments to verify cDNA quality of *dmpA*$^{-}$ clones from CRISPR (dmpAIB3 and dmpAIIA2) and HR (dmpAKO) gene disruption strategies. For each sample, total RNAs were extracted with Trizol method from growing cells and cDNAs were synthesized by RT-PCR (Invitrogen, SuperScript IV RT Kit, #18090010). An endogenous control *ig7* amplified with YW29+YW30 to produce a 190 bp band, and the downstream sequence of CRISPR disrupted region amplified with YW35+YW36 generate a 235 bp band. The marker (M) is Quick-load 100 bp DNA ladder (NEB) examined on 1% EtBr agarose gel.

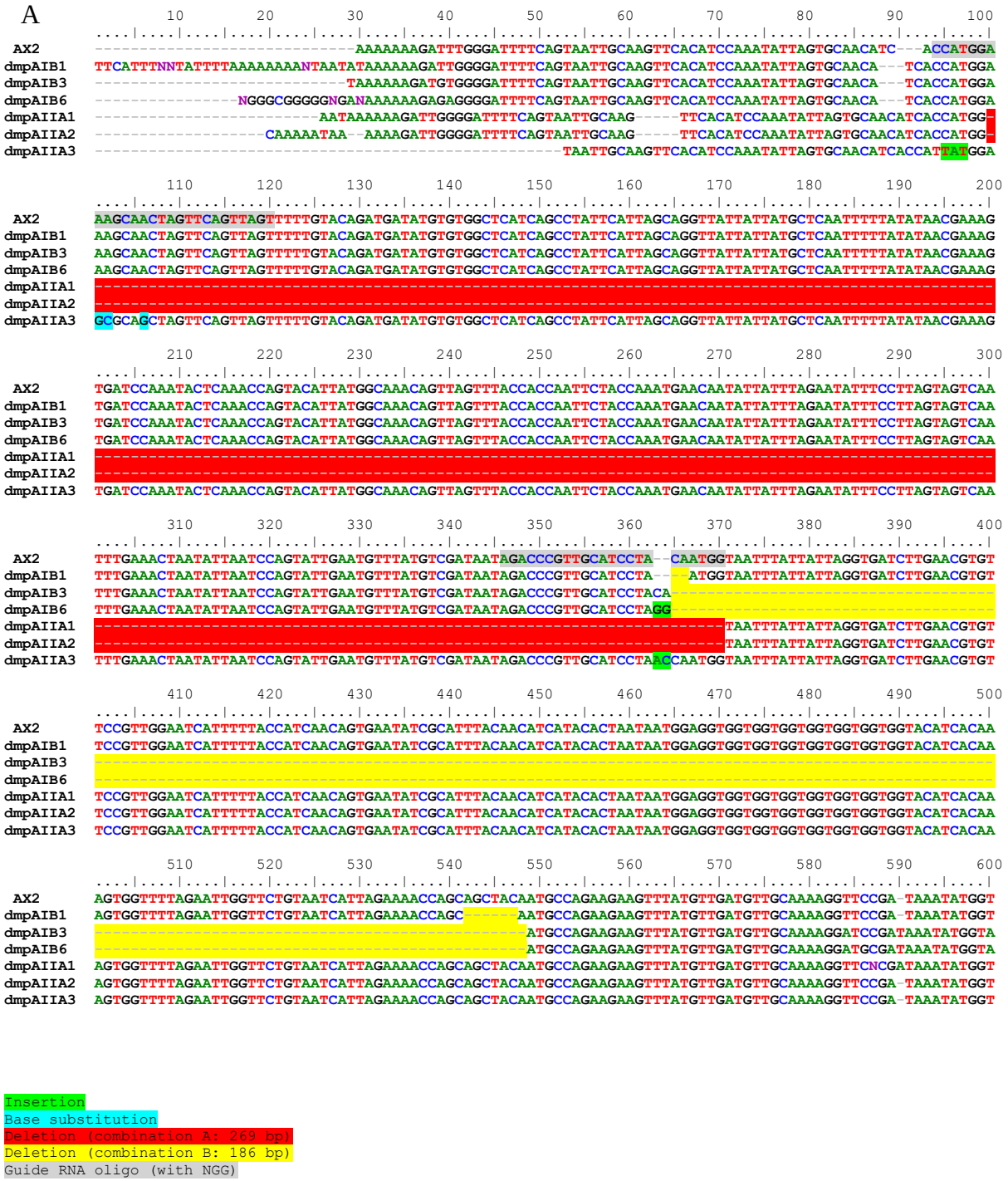


Figure 3.11. Alignments of DNA and amino acid sequences of *dmpA*$^{-}$ gene disruption strains constructed using the CRISPR/Cas9 strategy. Clustal Omega (1.2.4) multiple sequence alignments were performed and BioEdit software was used to annotate sequences. (A) Sequencing results of the *dmpA* gene in AX2 and six *dmpA*$^{-}$ CRISPR strains with frameshift mutations. The mutations are highlighted in different colours: red and yellow representing the large deletion in combination A (269 bp) and B (196 bp) respectively; insertions are highlighted in green and base substitutions in blue. The grey-shaded sequences showed the location of sgRNA oligos (with NGG) for targeting the *dmpA* gene.

B

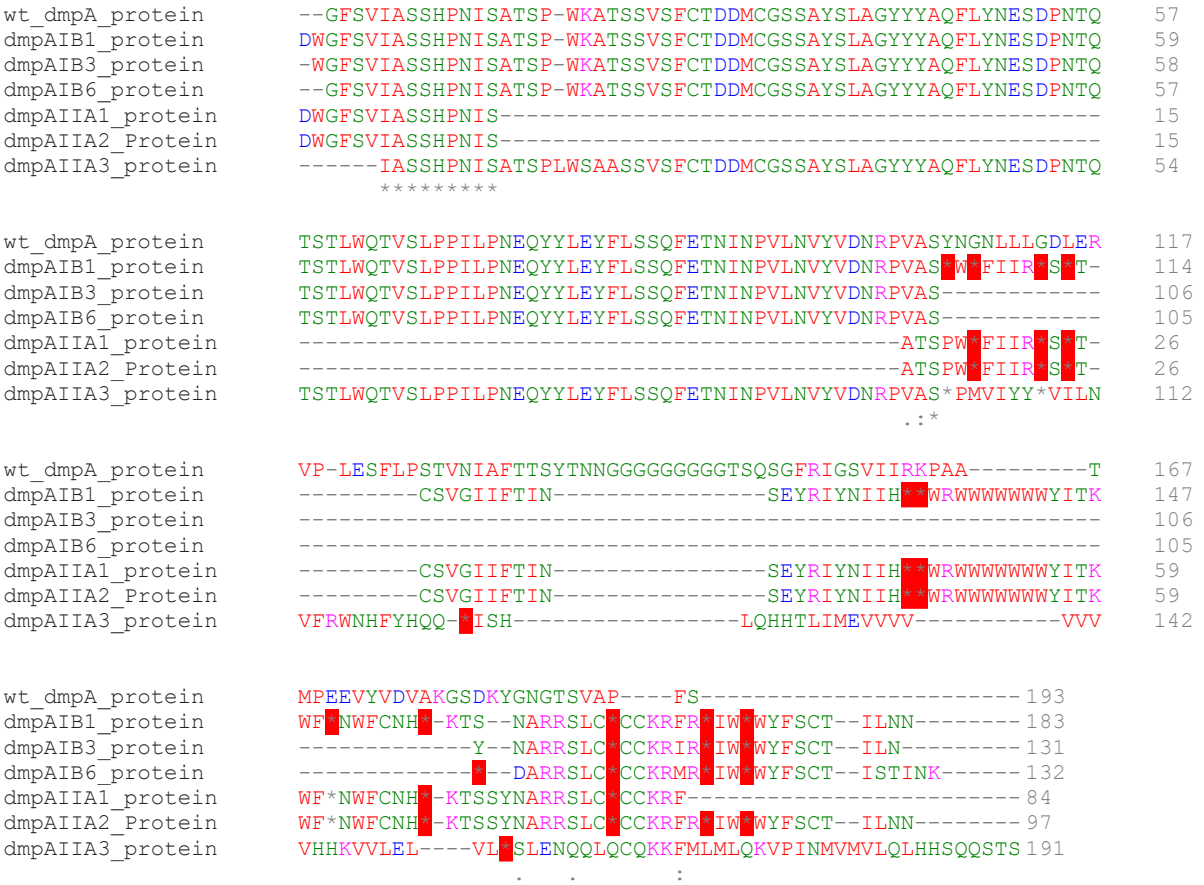


Figure 3.11. Alignments of DNA and amino acid sequences of *dmpA*$^{-}$ gene disruption strains constructed using the CRISPR/Cas9 strategy. (continued) (B) Amino acid sequence alignments of DMP1 in wildtype AX2 and the six *dmpA*$^{-}$ CRISPR strains. The premature stop codons in the amino acid sequences are highlighted in red.

In conclusion, both the HR gene disruption method and CRISPR/Cas9 system were successfully performed to construct *dmpA*$^{-}$ strains. Compared to the traditional HR method, the CRISPR/Cas9 gene disruption strategy was more efficient and time-saving for generating mutations in cells. Hence, the CRISPR/Cas9 method was introduced into our lab and is preferable for future gene disruption. However, it is still important to verify the phenotypes of the cells generated by both methods are consistent.

3.3.6 Characterization of *dmpA*$^{-}$ cells

3.3.6.1 Investigation of the development and growth of *dmpA*$^{-}$ cells

Growth and development of *dmpA*$^{-}$ strains constructed by both the HR and CRISPR gene disruption methods were characterized before performing cell fate assays. To compare the development of *dmpA*$^{-}$ strains constructed with different strategies, *dmpA*$^{-}$ clones generated by HR (dmpAKO_I_31 and dmpAKO_II_76_3) and CRISPR (dmpAIB3_4_1 and dmpAIIA2_4_1) methods were developed on nitrocellulose. Their developmental structures and timing had no phenotypic difference from the wildtype, and they all form fruiting bodies around 24 hrs on nitrocellulose filters similar to parental AX2 cells (Figure 3.12A). In an under-buffer aggregation assay, the *dmpA*$^{-}$ CRISPR clones were also similar to AX2 in development timing and phenotypes (Figure 3.12B). During vegetative growth, two different CRISPR-generated *dmpA*$^{-}$ clones had a similar growth rate during exponential growth compared to parental AX2 cells but an extended growth phase before entering the stationary stage at a higher cell density (Figure 3.12C), similar to that seen in *tpc2*$^{-}$ cells which probably have some defects in quorum sensing mechanism (Chang et al., 2020). Thus, the *dmpA*$^{-}$ strains constructed from HR and CRISPR methods have the same phenotypes in development, and extended growth phase prior to stationary phase was observed in *dmpA*$^{-}$ CRISPR strains.

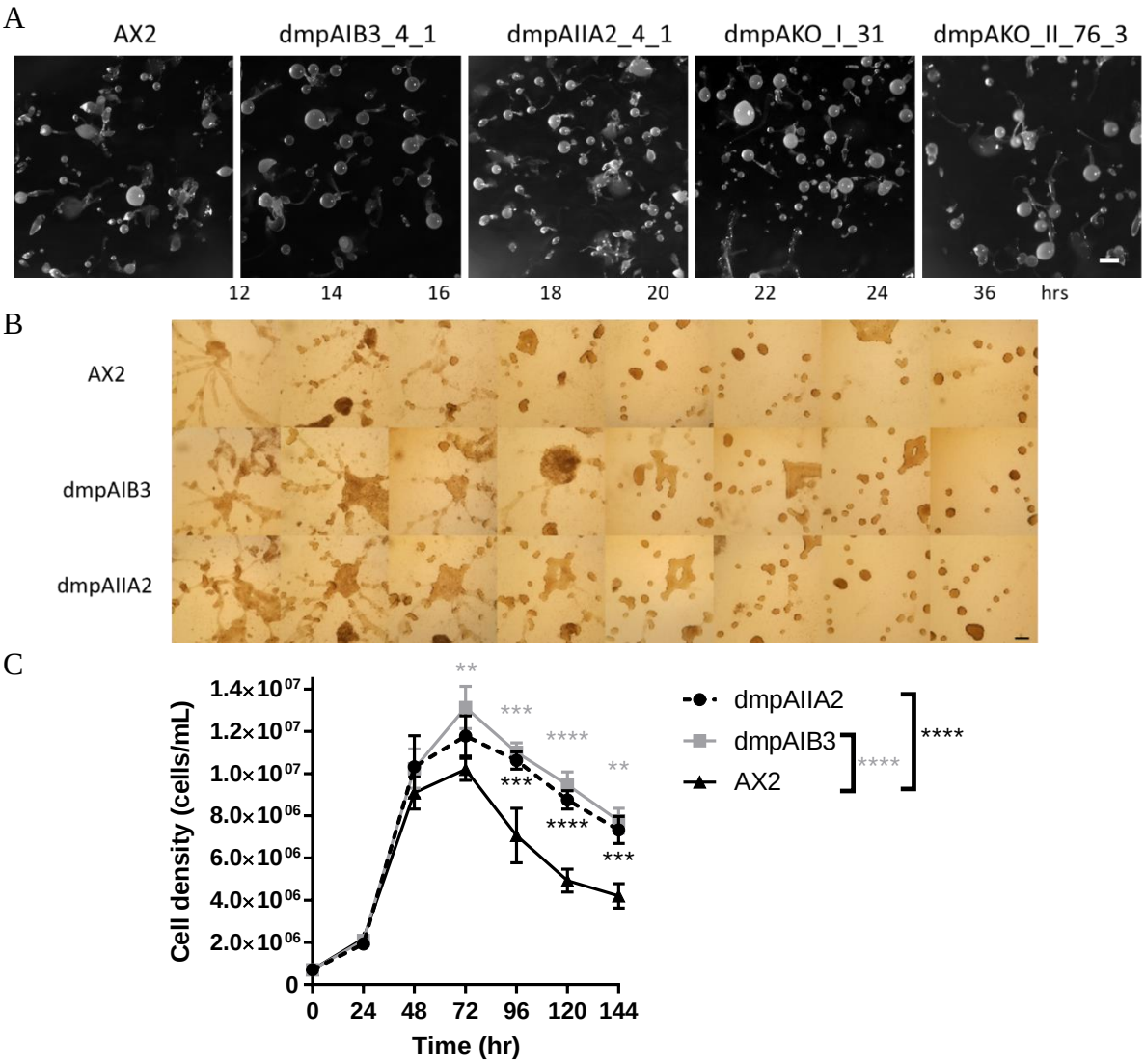


Figure 3.12. Characterization of *dmpA*$^-$ null strains. (A) Nitrocellulose filter development of AX2 and single independent clones of *dmpA*$^-$ cells. Vegetatively growing cells in exponential log phase were harvested as described in the legend to Figure 3.4A. Cells were resuspended at the density of 5×10^7 cells/mL in KK2, then 10 µL of cells were plated onto the nitrocellulose filters with three layers of Whatman paper (around 3.5 cm^2) soaked in 200 µL KK2 a 12-well plate, incubated at 22°C in a dark room and photographed at 24 hrs: CRISPR clones dmpAIB3_4_1 and dmpAIIA2_4_1 and HR clones dmpAKO_I_31 and dmpAKO_II_76_3. N = 2. Scale bar: 1 mm. (B) Under buffer development of *dmpA*$^-$ CRISPR clones: dmpAIB3 and dmpAIIA2. Cells in vegetative growth at the density of 7×10^5 cells/mL were grown for 24 hrs to the exponential log phase. Then, the cells were harvested and resuspended in KK2 at the density of 1.4×10^6 cells/mL in a 12-well plate. The cells were imaged at the times shown. Scale bar: 100 um. N = 2. (C) Growth curve of AX2 and *dmpA*$^-$ CRISPR clones dmpAIB3 and dmpAIIA2. Vegetatively growing cells were seeded at 7×10^5 cells/mL density and grown in shaking suspension for 24 hrs to exponential log phase. Then, they were diluted to 7×10^5 cells/mL in 20 mL normal HL5 medium and noted as time 0 hr. The cells were counted using a haemocytometer every 24 hrs for six days (144 hrs). N = 4. Mean ± S.E.M. Two-way ANOVA: **: P < 0.01; ***: P < 0.001; ****: P < 0.0001.

3.3.6.2 Investigation of cell fate decisions in *dmpA*$^-$ strains

Next, cell fate assays were performed to determine whether disrupting the gene encoding the putative Ca^{2+} channel protein DMP1 influenced cell fate decisions. Mixing experiments showed that *dmpA*$^-$ cells formed fewer spores when developing in chimeras with AX2, consistent in all input mixing ratios. For example, in the 50%L/50%UL ratio, spores formed from the labelled *dmpA*$^-$ lineage (42.2% ± 0.7%) were fewer than the input in chimeric development with parental AX2, whereas more spores originated from labelled AX2 (55.4% ± 1.1%) were produced when mixing with unlabelled *dmpA*$^-$ (Figure 3.13A). In the monolayer stalk induction assays, two independent clones of *dmpA*$^-$ strain: CRISPR clone dmpAIB3 (Upper panel, Figure 3.13B) and HR clone dmpAKOII76 (Lower panel, Figure 3.13B), were transfected with stalk marker *ecmB*-GAL and the assays were performed along with AX2+*ecmB*-GAL as a control. Both *dmpA*$^-$ independent clones were confirmed to have a higher sensitivity to DIF-1, consistent with a stalk tendency.

In summary, different Ca^{2+} channel disrupted strains had distinct cell fate preferences towards spore (*iplA*$^-$) or stalk (*tpc2*$^-$ and *dmpA*$^-$) cell fate. It has been found that *iplA*$^-$ and *tpc2*$^-$ cell lines during vegetative growth have lowered cytosolic Ca^{2+} levels (Chang, 2016) (Figure 3.3), showing no correlation between stalk cell fate bias. Furthermore, these putative Ca^{2+} channels do have different expression levels during development. *dmpA* mRNA transcripts are upregulated at early development (0-6 hrs) and *tpc2* mRNA levels are higher at later development (16-24 hrs), while *iplA* is expressed moderately throughout development with slightly higher expression around 10 hrs (Figure 3.13C). Thus, it is possible that the alteration of Ca^{2+} homeostasis in the mutants during different developmental stages affects the level of Ca^{2+} sequestered in different subcellular stores or Ca^{2+} release from the stores during signalling responses.

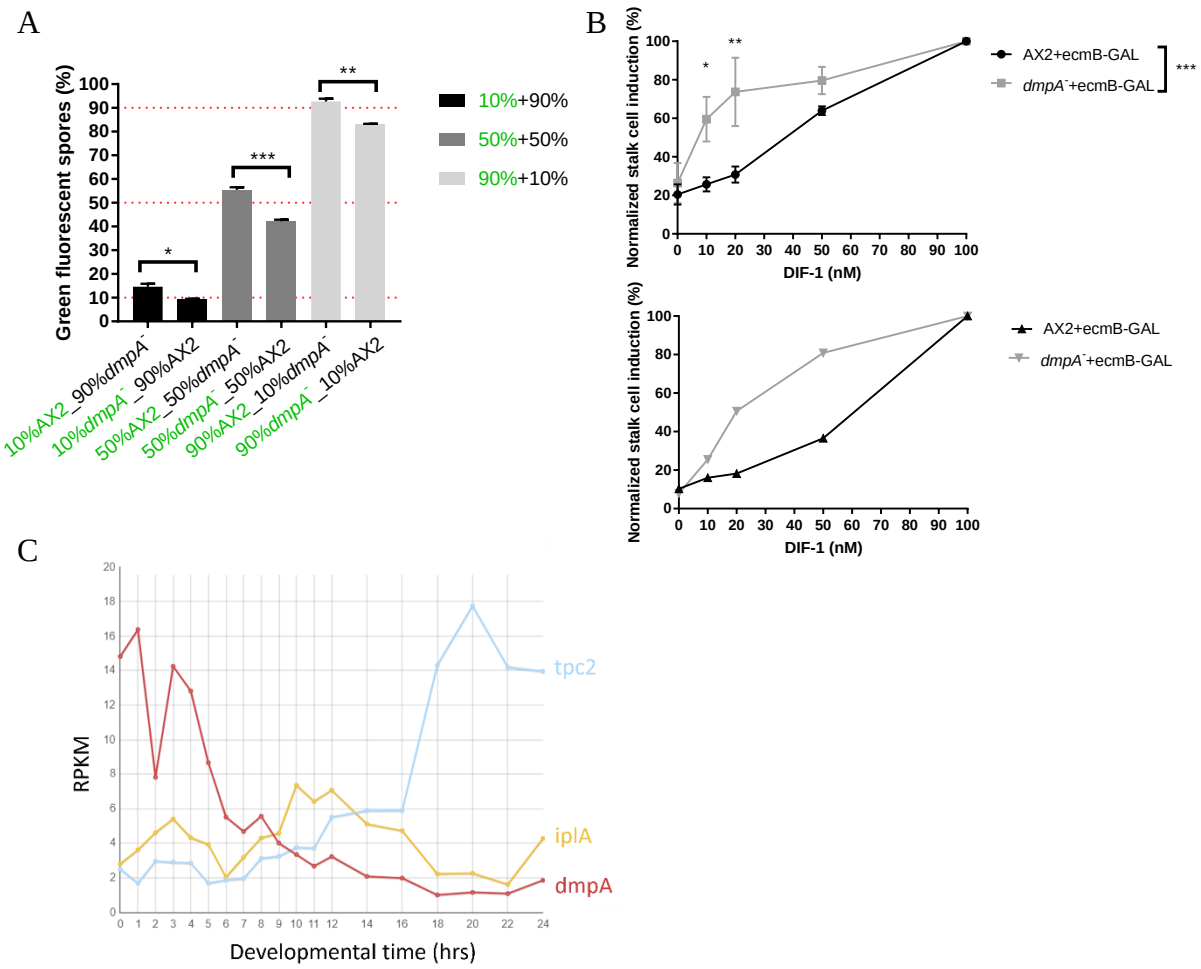


Figure 3.13. Cell fate bias in *dmpA*$^-$ cells. (A) Mixing experiments with AX2 and *dmpA*$^-$ (clone: dmpAIB3) was carried out as previously described in the legend to Figure 3.4A. N = 3. Mean ± S.E.M. Student *t*-test (two-tailed): *: P < 0.05; **: P < 0.01; ***: P < 0.001. (B) Monolayer assays of stalk marker-expressing AX2 and *dmpA*$^-$ (two independent clones, upper panel: dmpAIB3, N = 4 (grey squre); lower panel: dmpAKOII76, N = 1 (grey triangle)) was carried out as described in the legend to Figure 3.5A. *ecmB*-GAL activity in each group was normalized to 100 nM DIF-1 which was defined as 100%. Mean ± S. E.M. Two-way ANOVA: *: P < 0.05; **: P < 0.01; ***: P < 0.001. (C) RNA-seq data of transcript levels of *tpc2*, *iplA* and *dmpA* in filter development time courses. The data and the image were obtained and adapted from Dictybase.org (Rosengarten et al., 2015; Stajdohar et al., 2017).

3.3.7 *tpc2*$^-$ cells still show an effect of glucose growth history on cell fate bias

The nutrient history of *Dictyostelium* cells in vegetative growth generates a cell fate bias (Blaschke et al., 1986; Leach et al., 1973; Thompson and Kay, 2000a) as cells grown in higher levels of glucose have a spore bias. To test whether altering the glucose availability during growth can restore the stalk cell fate bias of *tpc2*$^-$ cells to have no cell fate bias, mixing experiments were performed using both AX2 and *tpc2*$^-$ cells which were incubated for 48-hrs in the presence (G+) or absence (G-) of glucose in HL5 medium before chimeric

development. The mixing of AX2 G+/- cells was a positive control (Figure 3.14A) along with *tpc2*$^{-}$ G+/- mixing (Figure 3.14B). Both AX2 and *tpc2*$^{-}$ cells with G+ history had the same trend at all mixing ratios, favouring a spore cell fate. For instance, 10% labelled G+ AX2 cells mixed with 90% unlabelled G- AX2 cells had 13.9% ± 1.1% green spores (Figure 3.14A). 10% labelled G+ *tpc2*$^{-}$ cells contributed 11.4% ± 0.2% of spores after developing with 90% unlabelled *tpc2*$^{-}$ G- cells (Figure 3.14B). Although the changes were small, the trends of cell fate decision were consistent in all input mixing ratios of both strains whichever population was labelled. This is in agreement with previous literatures reporting that pre-spore cell fate is chosen by AX2 cells grown in nutrient rich medium (Blaschke et al., 1986; Thompson and Kay, 2000a), and was also observed in *tpc2*$^{-}$ G+/- mixing experiments. Comparing the statistical analysis of G+ and G- mixing experiments within these two strains, G+ AX2 cells generally had a stronger spore cell fate tendency compared G+ *tpc2*$^{-}$ cells. This could be glucose deficiency causing partial starvation, making a faster route to stalk cell fate in AX2 cells.

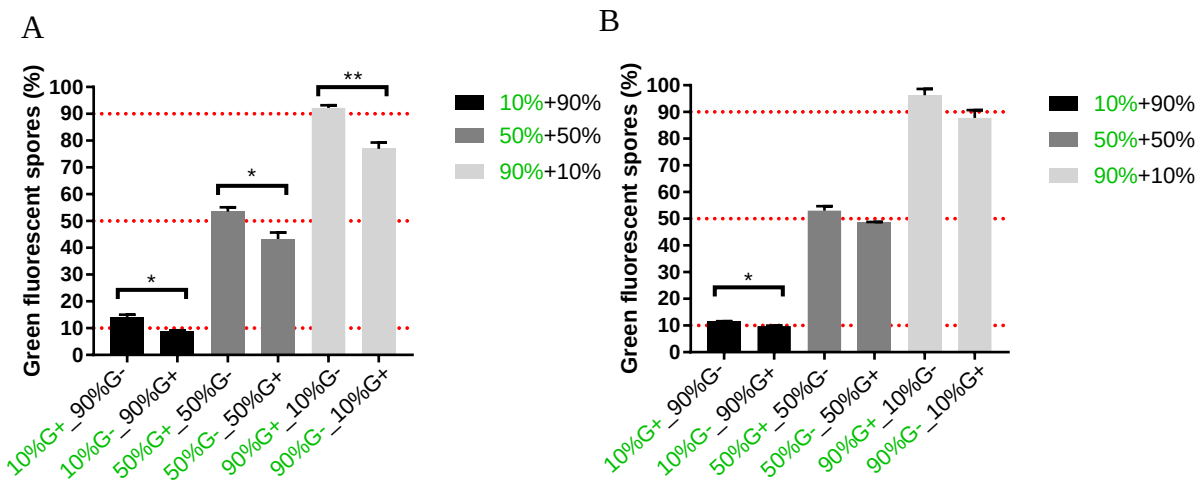


Figure 3.14. Glucose history during growth alters cell fate decisions in mixing experiments. (A) AX2 cells or (B) *tpc2*$^{-}$ cells (clone: TPC22B20) were seeded at the density of 2 × 10^5 cells/mL in shaking HL5 medium in the presence (G+) or absence (G-) of glucose, incubating at 22°C for 48 hrs to reach the exponential growth phase. Mixing experiments were then carried out as previously described in the legend to Figure 3.4A. N = 3. Mean ± S.E.M. Student *t*-test (two-tailed): *: P < 0.05; **: P < 0.01.

3.3.8 Pre-treatment of *tpc2*$^-$ cells with weak base imidazole reversed the cell fate bias

3.3.8.1 Weak bases affect *Dictyostelium* development

Altering acidic vesicle pH using weak bases or weak acids has been reported to influence spore and stalk cell differentiation in *Dictyostelium* cells (Davies et al., 1993; Gross et al., 1983; Gross et al., 1981). As *tpc2*$^-$ cells have reduced acidity in acidic compartments (Chang et al., 2020), it is interesting to investigate whether this altered pH in acidic vesicles accounts for the stalk cell fate bias in *tpc2*$^-$ cells.

Firstly, the effect of the weak base imidazole and NaCl (control for osmotic effects, e.g. about 320 mOsM/kg for NaCl and around 260 mOsM/kg for imidazole in buffers (Marcinkowska et al., 2023; Smith and Whittington, 1988; Venkataraman et al., 2005)) on development of AX2 and *tpc2*$^-$ cells was examined on KK2 agar (Figure 3.15). This development assay was to identify which concentrations of imidazole can be used for cell fate assays without completely arresting development. The development of both strains was inhibited by high concentrations of imidazole with 30 mM treatment leading to development arrest at the aggregate stage in both strains. Both AX2 and *tpc2*$^-$ cells developing at lower imidazole concentrations (10 mM and 20 mM) could complete the developmental cycle. However, there was a slight delay in both strains with 20 mM imidazole treatment and *tpc2*$^-$ seemed to be more affected, for example, a few slug structures shown in *tpc2*$^-$ and later culminant structures in AX2 cells at 24 hrs, indicating that *tpc2*$^-$ cells are more sensitive to the weak base imidazole. Treatment with NaCl to control for osmotic effects showed that both strains formed phenotypically similar fruiting bodies with a similar time course (24 hrs) in the presence of up to 40mM NaCl, while 50 mM NaCl led to a delay in fruiting body formation. No differences were apparent at 20 mM NaCl, the concentration of imidazole that delayed *tpc2*$^-$ development, showing the effect was not due to increased osmotic pressure. In summary, imidazole concentrations lower than 20 mM led to a slightly delayed development in both cells but the development cycle can be completed eventually, and *tpc2*$^-$ cells were more sensitive to imidazole than AX2 cells during development.

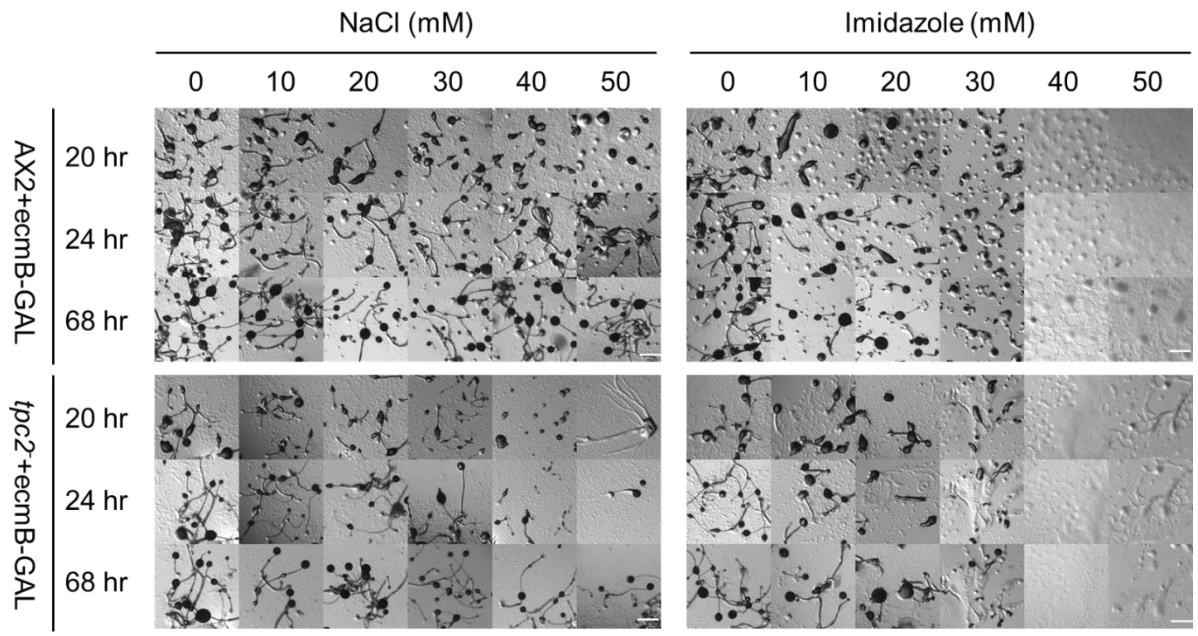


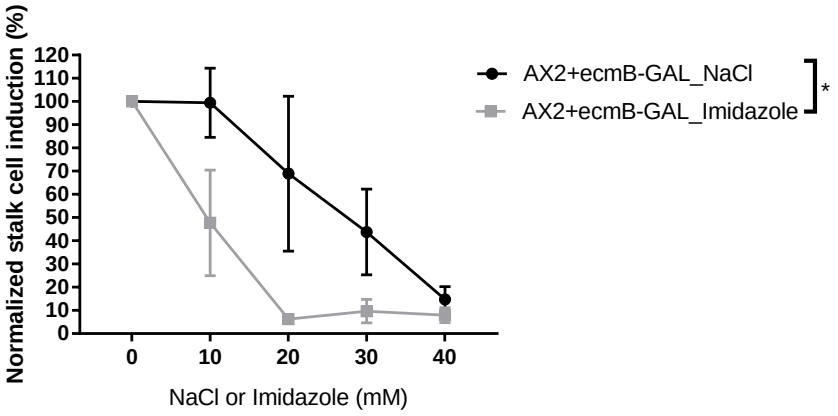
Figure 3.15. Development on agar in the presence of weak base imidazole.
500 µL 1% of KK2 agar was poured in each well of a 24-well plate and 25 µL NaCl or imidazole to achieve final concentrations ranging from 0 to 50 mM was plated on top. Exponentially growing cells AX2+*ecmB*-GAL and *tpc2*$^-$+*ecmB*-GAL were collected, washed in KK2 and resuspended at the density of 5×10^7 cells/mL. 20 µL cell suspensions were plated in each well to develop, and imaged at 20 hrs, 24 hrs and 68 hrs time points. Scale bar: 1 mm. N = 3.

3.3.8.2 Weak bases alter stalk cell fate decisions in *tpc2*$^-$ cells

To validate previous findings that weak bases stimulate spore cell fate in monolayer cultures (Dominov and Town, 1986; Gross et al., 1983) using AX2 cells and determine whether the same effects were seen in *tpc2*$^-$ cells, a long-term treatment of weak base imidazole throughout the development was set up in the monolayer stalk induction assays. Treatments of 0-40 mM imidazole and NaCl throughout the assays were carried out using both AX2 (Figure 3.16A) and *tpc2*$^-$ cells (Figure 3.16B) inducing with 100 nM DIF-1. Both strains subject to imidazole treatment during development showed a reduction in *ecmB*-GAL stalk marker expression compared to the NaCl control, and 20 mM imidazole was sufficient to maximally block marker gene induction in both cell types (6.2% ± 1.4% for AX2 and 4.5% ± 1.1% for *tpc2*$^-$), consistent with the developmental delay in both strains at 20 mM imidazole during agar development (Figure 3.15). Both strains showed a reduction in stalk marker induction by 100 nM DIF-1 in response to increased levels of imidazole and NaCl, while *tpc2*$^-$ cells showed a slightly higher sensitivity to the osmotic effect. In conclusion, the treatment of weak base imidazole raising vesicle pH during development (Davies et al., 1993) inhibited stalk cell formation and

promoted spore fate tendency in AX2 cells in agreement with previous literature (see Chapter 1 section 1.3.3.3), and loss of TPC2 did not affect this bias induced by weak base imidazole.

A



B

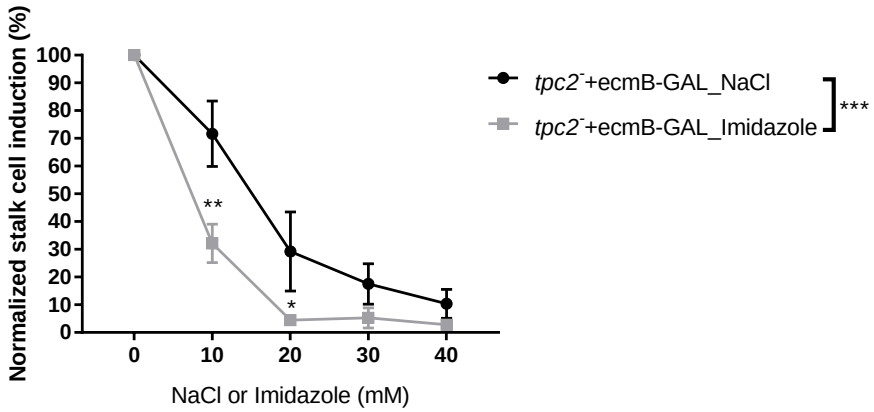


Figure 3.16. Monolayer stalk induction assays in the presence of weak base imidazole. The assays were performed as described in the legends to Figures 3.5A using (A) AX2 (N = 3) and (B) *tpc2*$^{-}$ (N = 3) cells expressing stalk marker *ecmB*-GAL. Cells were exposed to 0-40 mM NaCl or imidazole throughout development and the stalk marker expression was induced by 100 nM DIF-1. Expressions of stalk marker in each group were induced by 100 nM DIF-1 and normalized relative to the no treatment groups (0 mM NaCl or 0 mM imidazole) defined as 100%. Mean ± S.E.M., shown in the table below the graphs. Two-way ANOVA: *: $P < 0.05$; **: $P < 0.01$; ***: $P < 0.001$.

Since weak base imidazole applied to cell development was confirmed to affect stalk cell fate in monolayer assays, next step is to investigate whether altering vesicle pH during growth can influence *tpc2*$^{-}$ cell fate bias as a predisposition effect. 20 mM imidazole was chosen to pre-treat *tpc2*$^{-}$ cells in cell fate assays. AX2 cells were also used as control to show cell fate decisions are influenced by vesicle pH in these conditions.

Mixing experiments were performed by pre-treating AX2 cells with either 20 mM imidazole or osmotic control NaCl for 4 hrs before development in chimeras (Figure 3.17A). In general, imidazole pre-treated cells formed more spores than NaCl pre-treated cells. For example, when 10% imidazole pre-treated cells were labelled, green spores from this lineage were 15.9% ± 2.5%, whereas 10% labelled NaCl pre-treated cells formed 7.4% ± 1.4% spores. All input mixing ratios were observed to have this consistent trend in cell fate bias, although the differences in some groups were not statistically significant, possibly due to the variations in different biological repeats. When *tpc2*$^{-}$ cells were pre-treated for 4 hours with 20 mM imidazole and mixed with AX2 cells with NaCl 4-hr pre-treatment, the cell fate was restored to an unbiased status (Figure 3.17B). Monolayer stalk induction assays in the context of 4-hr imidazole pre-treatment showed a slight decrease in stalk marker expression in both strains, although they were not statistically significant (Figure 3.17C and 3.17D). To summarize, pre-treatment during growth with the weak base imidazole which neutralizes acidic compartments of *Dictyostelium* cells (Davies et al., 1993) predisposes cells to have spore cell fate which is consistent with previous literature (see Chapter 1 section 1.3.3.3). Exposure to 20 mM imidazole for 4 hrs during growth rescued the cell fate bias of *tpc2*$^{-}$ cells when chimerically developing with AX2 cells, indicating that the increased pH in acidic vesicles in *tpc2*$^{-}$ (Chang et al., 2020) has a dominant effect over other cell fate influencing factors to mediate a stalk cell fate. The 4-hr pre-treatment of weak base prior to monolayer stalk induction assay showed a mild tendency of spore cell fate in imidazole-treated groups in both AX2 and *tpc2*$^{-}$ cells. Hence, alteration of vesicle pH with weak base imidazole is a cell fate determinant which might have stronger roles during development than the onset of development, leading to pre-spore cells formation.

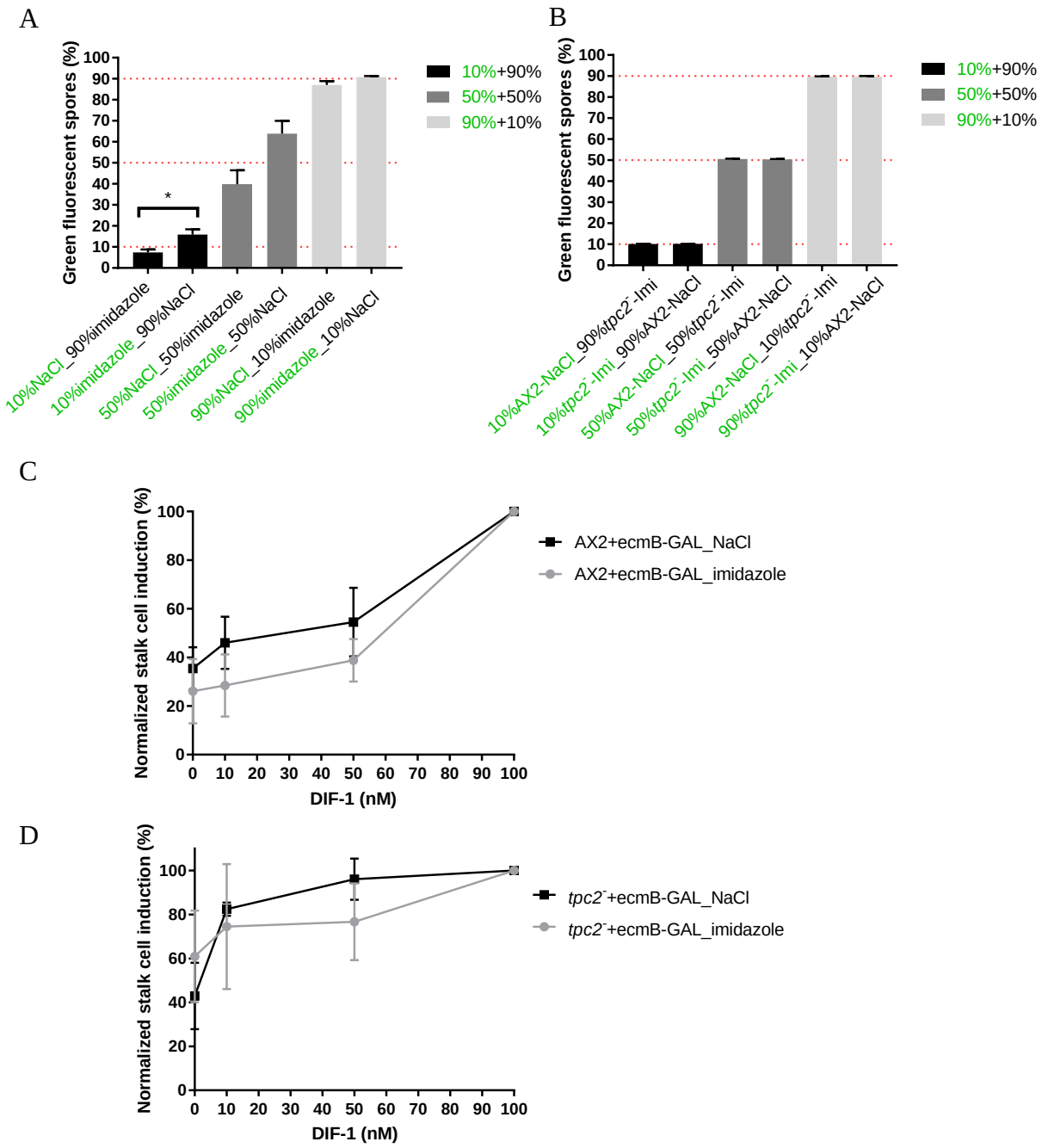


Figure 3.17. Pre-treatment with imidazole affects cell fate decisions. (A) Mixing experiments of AX2 cells with 4-hr pre-treatment with 20 mM imidazole or NaCl (osmotic control). N = 3. Mean ± S.E.M. Student *t*-test (two-tailed): *: P < 0.05. (B) Mixing experiments of AX2 cells with 4-hr pre-treatment with 20 mM NaCl and *tpc2*$^-$ cells with 4-hr pre-treatment with 20 mM imidazole. N = 3. Mean ± S.E.M. The experiments shown in (A) and (B) were performed as described in the legends to Figures 3.4A. (C and D) Monolayer stalk induction assays inducing stalk marker expression with 0-100 nM DIF-1 were performed in monolayer cultures of (C) AX2 cells (N = 3) and (D) *tpc2*$^-$ cells (N = 3) which were 4-hr pre-treated with 20 mM imidazole or NaCl before development. Stalk marker expression was normalized to that seen in 100 nM DIF-1 group (defined as 100%). Mean ± S.E.M. Two-way ANOVA: n.s. The assays were performed as described in the legends to Figure 3.5A.

3.4 Discussion

This chapter mainly has studied:

1) Disruption of the gene encoding different intracellular Ca^{2+} channels (TPC2, IPLA) had altered cell fate bias: stalk cell fate bias in *tpc2*$^{-}$ and spore cell fate bias in *iplA*$^{-}$ cells.
2) *dmpA*$^{-}$ cells with disruption of the gene encoding a putative Ca^{2+} channel DMP1 were generated by two methods (homologous recombination and CRISPR/Cas9 strategies) and shown to have a stalk cell fate bias.
3) *tpc2*$^{-}$ cells had a stalk cell fate bias that could be reversed by the treatment of weak base imidazole.

For constructing *dmpA*$^{-}$ null strains, two methods were used in order to compare the efficiency between the traditional homologous recombination (HR) gene disruption method (Faix et al., 2004) and the CRISPR/Cas9 genome editing system (Sekine et al., 2018). Compared to the HR method, the CRISPR/Cas9 genome editing system was time-saving (less than two months for screening purified clones from candidate pools) and efficient (all six independent clones sent for sequencing had frameshift mutations). The development of strains isolated by both methods was compared and found to be indistinguishable and both showed a stalk cell fate bias in monolayer assays. The development of *dmpA*$^{-}$ strains isolated using both methods were very similar in timing and structures to that seen with the parental AX2 cells. This is different from the previous finding reported by Khosla et al. (2006) using a *dmpA* gene disrupted strain in an AX3 background. Their *dmpA* disrupted cell line was generated using a *dmpA* knockout vector dmpA::bsR (Dictybase plasmid catalog ID: 511), a restriction enzyme mediated integration (REMI) rescue vector (Kupsa and Loomis, 1992), and was reported to have abnormal fruiting body morphologies. We obtained this gene disruption vector dmpA::bsR from Dictybase.org and sequenced it with two standard primers T7F and S6P. The inserted gDNA sequences from *dmpA* were present in the vector but were continuous without the BSR cassette between the two arms as required for homologous recombination gene disruption (data not shown). We transfected this vector into AX2 cells but did not identify any colonies with the aberrant developmental phenotypes reported by Khosla et al. (2006), although they were not tested for disruption of the gene. The difference in phenotypes of the *dmpA*$^{-}$ cells generated here

compared to those previously published could therefore be due to the different genetic background (AX2 vs AX3) (Stajdohar et al., 2017) or the rearranged vector used for disruption could cause unexpected effects in the previously published strain.

Two assays have been used for monitoring cell fate decisions, chimeric mixing experiments for spore cell fate in multicellular development and monolayer stalk induction assay for stalk cell fate. They were adapted and optimized from the work by Thompson and Kay (2000a). Monolayer spore assays have been reported in previous literature (Huang et al., 2006; Thompson et al., 2004; Thompson and Kay, 2000a), but there have been no reports of altered sensitivity to the morphogen for spore cell differentiation as seen in the monolayer DIF-1 stalk induction assays and so are not useful for detecting bias. In Thompson and Kay (2000)'s mixing experiments, cells expressing the semi-constitutive *act15*-GFP were used for imaging at the slug stage and quantifying GFP-tagged spores. Thompson and Kay (2000a) also confirm the G- cells were more responsive to DIF-1 than G+ cells using monolayer stalk induction assays, and another predisposition factor, cell cycle positions (mid-G2 phase and around mitosis) described in Chapter 1 section 1.3.3.2 were also tested, verifying the effectiveness of two assays for cell fate assessment. Therefore, based on these two cell fate assays, a quantifiable system assessing cell fate tendencies from the aspects of spore formation and DIF-1 sensitivity in pre-stalk cells was established. There is also a published dual-fluorescent reporter assay in monolayer development system to detect both pre-stalk (*ecmAO*-RFP, *ecmB*-RFP) and pre-spore markers (*pspA*-RFP) co-expressed in cells in a single assay induced by conditioned medium (Gruenheit et al., 2018). This allows both cell fates to be assessed in one assay as the expression of the two markers can be quantified by FACS. Attempts were made to establish this assay in my hands, however, there were technical limitations with the dual fluorescent reporter system in the monolayer format (Gruenheit et al., 2018). Firstly, more than ten thousand cells were required for sorting by FACS but low cell density in monolayer is fundamental to stay unicellular, thus making parallel comparisons between different cell fate determining conditions difficult. Secondly, cells were generated expressing two available developmental reporter markers, pre-stalk *ecmAO*-RFPmars and pre-spore *cotB*-GFP. However, when the dual-fluorescent cells were harvested from monolayer cultures, a very small number of fluorescent cells observed under fluorescent microscopy which have too low fluorescence intensity to be detected using a microplate reader (data not shown). Therefore, monolayer stalk induction assays with stalk marker *ecmB*-GAL are more robust to quantify

stalk cell marker expression in response to DIF-1 induction. In this thesis, the method of the monolayer stalk induction assay adapted from Thompson and Kay (2000a) was chosen to study stalk cell fate tendency by quantifying DIF-1 responsiveness in microplate reader.

Both mixing experiment and monolayer assays were used to confirm an intrinsic stalk cell fate bias in *tpc2*$^{-}$ cells. Also, glucose availability during growth predisposed stalk and spore cell fate decision is consistent in both AX2 and *tpc2*$^{-}$ cells with both cell fate assays, revealing that glucose absence and presence did not change the stalk cell fate bias in *tpc2*$^{-}$cells. This indicates there might be other factors playing dominant roles in cell fate decisions.

Since *tpc2*$^{-}$ cells have lower cytosolic Ca^{2+} level and increased pH in acidic vesicles (Chang et al., 2020), I then tested whether these factors account for the cell fate bias. *tpc2*$^{-}$ cells tend to choose stalk cell fate compared to parental AX2 cells, which is not consistent with the conclusion of high cytosolic Ca^{2+} correlating to stalk cell differentiation (Azhar et al., 1996). *iplA*$^{-}$ cells also have lower cytosolic Ca^{2+} similar to *tpc2*$^{-}$ (Figure 3.3) (Chang, 2016) but had the opposite cell fate tendency, therefore these findings did not agree with cytosolic Ca^{2+}, at least in vegetative cells, being an important factor of cell fate reported in previous literatures introduced in Chapter 1 section 1.3.3.4. Apart from differences in cellular Ca^{2+} level dependent on cell cycle phases during vegetative growth (Azhar et al., 2001), cytosolic Ca^{2+} levels also vary during development (Hashimura et al., 2022) and these could be the important influencing factor but these have not been measured in these strains for comparison. The cell fate bias seen in *tpc2*$^{-}$ cells, which is inconsistent with previous findings of high cytosolic Ca^{2+} predisposing to a stalk cell fate bias, could be dependent on alterations of Ca^{2+} levels in different intracellular stores, as TPC2 is acidic vesicle-targeted channel (Chang et al., 2020; Wilczynska et al., 2005), while IPLA is located in ER membranes (Lusche et al., 2012; Traynor et al., 2000). However, measuring Ca^{2+} levels in acidic compartments such as endo-lysosomes with the pH 4.3-4.5 (Aubry et al., 1993; Padh et al., 1993) is not feasible as the fluorescent Ca^{2+} sensors are rapidly quenched and restricted by the low pH in acidic vesicles (Lima et al., 2012). Another reason could be the Ca^{2+} channel mutants have differences in aberrant Ca^{2+} release from the intracellular stores, as Ca^{2+} release upon cAMP stimulation is evidently abolished in *iplA*$^{-}$ mutant (Schaloske et al., 2005; Traynor et al., 2000) and only slightly reduced and delayed cAMP-induced Ca^{2+} response was reported in *tpc2*$^{-}$ cells (Chang et al., 2020). The correlations

between the spatiotemporal subcellular Ca^{2+} release and cell fate decision are still too challenging to be tested. Future experiments can test on other Ca^{2+} mutant such as *iplA*$^{-}$ to see whether IPLA has indirect effect on vesicle pH by treating *iplA*$^{-}$ cells with weak acids to increase vesicle pH before cell fate assays, and the vesicle pH can be measured in *Dictyostelium* cells (Aubry et al., 1993; Chang et al., 2020; Padh et al., 1993; Ponsford et al., 2021).

An alternative hypothesis is that the stalk cell fate decision in *tpc2*$^{-}$ might work through altering properties of acidic vesicle, as reduced acidity in vesicles was observed in *tpc2*$^{-}$ cells (Chang et al., 2020). Previous findings reported that ammonia is one of the components accumulated during development (Neave et al., 1983; Schindler and Sussman, 1979; Sternfeld and David, 1979), and weak bases promote spore cell differentiation, although in previous experiments weak base treatment was present throughout the development in monolayer systems (Gross et al., 1983; Neave et al., 1983; Weeks, 1984). Weak bases target intracellular acidic vesicles therefore increasing vesicle pH but have little effect on cytosolic pH measured by pH-sensitive phosphonate probes for ^{13}P-NMR experiments, and it was noticed that weak bases inhibit aggregation (Davies et al., 1993). To test the hypothesis, KK2 agar development experiments were performed with the presence of imidazole in the first place. It showed that higher imidazole concentrations than 20 mM had a strong developmental inhibition on *tpc2*$^{-}$ cells, limiting the concentration for imidazole treatment in cells to 20 mM when investigating cell fate preferences. Therefore, *tpc2*$^{-}$ cells are somewhat more sensitive to weak base imidazole. This is consistent with the previously published data that *tpc2*$^{-}$ cells had an increased pH in acidic vesicles by showing the higher sensitivity to weak base in *tpc2*$^{-}$ development on nitrocellulose filters compared to AX2, and the decreased acidity in acidic vesicles of *tpc2*$^{-}$ visualized by Lysosensor probe imaging (Chang et al., 2020).

Assays testing cell fate decisions were conducted by either incubating cells with weak base during monolayer development or pre-treating the cells with weak base imidazole in 4-hr growth before performing mixing experiments and monolayer assays. When assessing stalk cell differentiation upon continuous imidazole treatment throughout monolayer experiments, both AX2 and *tpc2*$^{-}$ cells have decreased stalk marker expression in 100 nM DIF-1 induction, in agreement with previous literatures that weak bases stimulate spore cell formation (Dominov and Town, 1986; Neave et al., 1983; Sternfeld and David, 1979; Weeks, 1984). *tpc2*$^{-}$ cells in

this case also have slightly higher reduction than AX2 cells at lower imidazole concentrations, indicating the hypersensitivity to weak bases consistent with Chang et al. (2020)'s conclusion. The longer exposure to weak bases cannot be used in mixing experiment as two different pools of cells are mixed together in the development, so cells can only be pre-treated in mixing experiment layout. When *tpc2*$^{-}$ cells were pre-treated with 20 mM imidazole and mixed with AX2 cells for chimeric development, the stalk cell fate bias was rescued, indicating that the vesicle pH drives the cell fate bias observed in *tpc2*$^{-}$ cells. Although not being statistically significant in monolayer assays involving a 4-hr pre-treatment with 20 mM imidazole, the stalk induction levels in imidazole pre-treated cells were less the osmotic control cells. A possible explanation of weak significance of the data might be the alkalinization of acidic vesicles such as endo-lysosomes is a dynamic and reversible process which depends on incubation time (Davies et al., 1993), and 4-hr pre-treatment might not be enough, and following the washing before monolayer assay, the cells might rapidly recover from the effect of weak base. There also might also be some relatively ammonia-resistant acidic vesicles in aerobic *Dictyostelium* cells (Davies et al., 1993). Overall, these results confirm that *tpc2*$^{-}$ chooses a stalk cell fate through a potential mechanism of altering vesicle pH. In future experiments, studying the predisposition effect of altered vesicle pH needs to either use longer pre-treatment or use more weak bases such as methylamine or weak acids such as acetate (Gross et al., 1983) to verify the results.

To further investigate roles of intracellular Ca^{2+} in cell fate decision, *dmpA*$^{-}$ is an alternative putative Ca^{2+} channel mutant to use. The results of cell fate assays using *dmpA*$^{-}$ CRISPR and HR-generated clones showed both have higher DIF-1 responsiveness compared to parental AX2 cells. Mixing experiments also identified *dmpA*$^{-}$ cells to form fewer spores, consistent with the stalk cell fate observed in monolayer assays. However, it is not known whether the mode of action of stalk cell fate preference in *dmpA*$^{-}$ cells is the same as the *tpc2*$^{-}$ cells. Unfortunately, due to the inability to access the microscope facility during Covid restrictions, it has not been possible to monitor Ca^{2+} levels and responses in *dmpA*$^{-}$ cells. mRNA transcript profiles during filter development of *tpc2*, *dmpA* and *iplA* cells from Dictybase also show distinct expression patterns between these three Ca^{2+} channel proteins (Rosengarten et al., 2015; Stajdohar et al., 2017). *tpc2* is mainly expressed in late development (16-24 hrs), while *dmpA* is expressed in early development (0-6 hrs) and *iplA* is expressed uniformly in general but has a higher expression level in early-mid stage of development. In comparison, the expression

level of the pre-spore gene *pspA* increases from 11 hrs, similar to the time of high *iplA* expression levels, whereas the *ecmB* pre-stalk gene has increased expression levels from 16 hrs and reaches maximum at 24 hrs (Rosengarten et al., 2015), correlating with the elevated expression of *tpc2* but not *dmpA*. This suggests that TPC2, IPLA and DMP1 putative Ca^{2+} channels have functions in distinct stages of development. Thus, disrupting one of these channels potentially affects cytosolic Ca^{2+} homeostasis at a certain developmental stage via the sequestered Ca^{2+} levels in different subcellular stores or the release of Ca^{2+} from these compartments, therefore achieving different spore (*iplA*$^{-}$) and stalk (*tpc2*$^{-}$ and *dmpA*$^{-}$) cell fate outcomes. Future experiments should test cytosolic basal Ca^{2+} levels in growing cells and changes in response to cAMP and DIF-1 in *tpc2*$^{-}$, *iplA*$^{-}$ and *dmpA*$^{-}$ strains to correlate to their biased cell fates. To verify the Ca^{2+} changes triggered by cAMP and DIF-1, mutant cells would be transfected with a FRET-based Ca^{2+} indicator YC-Nano15 (Horikawa et al., 2010) available in the lab and imaged with fluorescence microscope following the method used in Chang (2016).

Chapter 4: mTORC1 and cell fate decision

4.1. Introduction

4.1.1 mTORC1 signalling pathway in mammalian cells

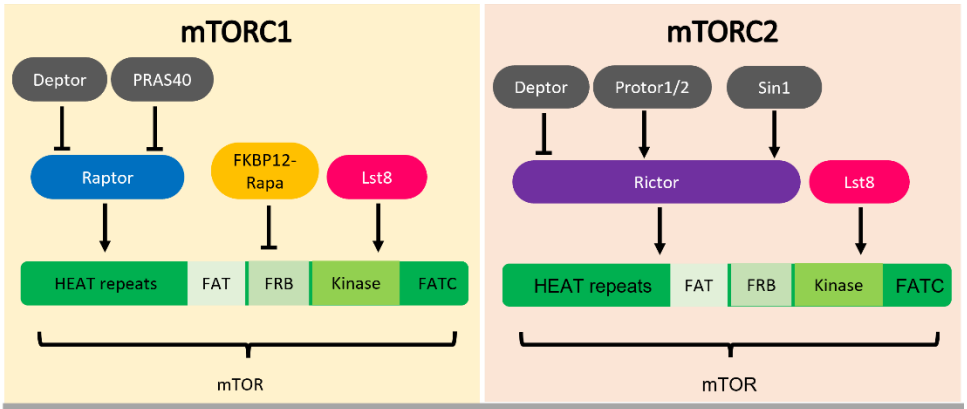
4.1.1.1 Components in mTOR complexes

Mechanistic target of rapamycin (mTOR) is a critical kinase subunit found in mTORC1 and mTORC2 complexes to mediate important cellular processes (Saxton and Sabatini, 2017). It is highly conserved among species from yeast to mammalian cells (Laplante and Sabatini, 2009; Loewith and Hall, 2011). mTORC1 is a master regulator that responds to environmental changes such as nutrient status, stress and energy deprivation, in order to drive cells to undergo autophagy or regulate cell growth (Kim and Guan, 2019; Saxton and Sabatini, 2017). mTORC2 also plays important roles in regulating metabolism and actin cytoskeleton reorganization and has tissue-specific functions verified in mice (reviewed by (Oh and Jacinto, 2011). Both complexes contain shared components such as the mTOR kinase, mammalian lethal with sec-13 protein 8 (Lst8) and DEP-domain containing mTOR-interacting protein (Deptor) and different subunits including regulatory-associated protein of TOR (Raptor) and proline-rich AKT substrate 40 kDa (PRAS40) in mTORC1, and rapamycin insensitive companion of mTOR (Rictor), stress-activated protein kinase-interacting protein 1 (Sin1) and protein observed with rictor 1/2 (Protor1/2) in mTORC2. Protor1/2 and Deptor are two regulatory binding partners of mTOR (Cornu et al., 2013; Laplante and Sabatini, 2012) (Figure 4.1).

4.1.1.2 Main downstream effectors of mTORC1 pathway

There are two well-conserved key downstream substrates of mTORC1 identified, eIF4E binding protein 1 (4E-BP1) that inhibits eukaryotic translation initiation factor 4E (eIF4E) from initiating translation, and ribosomal protein S6 kinase (S6K) with a role in mRNA translation initiation (Burnett et al., 1998; Ma and Blenis, 2009; Nojima et al., 2003; Schalm et al., 2003) (Figure 4.2). Upon mTORC1 phosphorylation, phospho-4E-BP1 is responsible for regulation of cap-dependent mRNA translation and therefore protein synthesis can proceed. Also, S6K activation depends on two-step phosphorylation mediated by c-Jun N-terminal kinase 1 (JNK1) and mTORC1 (Nojima et al., 2003; Zhang et al., 2013a). Activated S6K is involved in cell

growth by regulating crucial cellular processes including ribosomal biogenesis and protein synthesis etc (Fenton and Gout, 2011; Isotani et al., 1999; Jastrzebski et al., 2007; Magnuson et al., 2012). Phosphorylation levels of 4E-BP1 and S6K are commonly considered as *in vivo* mTORC1 activity readouts in mammalian models (Hay and Sonenberg, 2004).



	mTORC1 signalling	mTORC2 signalling
Input signal	Growth factors/insulin, glucose, amino acids, oxygen, stresses	Growth factors/insulin
Activity	**Activation** of protein synthesis, lipid synthesis, nucleotide synthesis, ribosome biogenesis, mitochondrial biogenesis; glycolysis and metabolism; **inhibition** of autophagy and lysosome biosynthesis.	Cell survival, actin/cytoskeletal organization, lipid & glucose metabolism
Key substrate	S6K, 4E-BP1	SGK1, AGC kinases, AKT
Inhibitor	Rapamycin (mTORC1 specific) and other rapamycin analogs; AZD8055 (dual mTORC1/2 inhibitor); BEZ235 (dual mTORC1/2 and PI3K inhibitor)	Chronic rapamycin; AZD8055 (dual mTORC1/2 inhibitor); BEZ235 (dual mTORC1/2 and PI3K inhibitor)
Subcellular localization	Outer lysosome membranes	plasma membrane, mitochondria, endosomal vesicles (subpopulation)

Figure 4.1. Comparison of mammalian mTOR complexes 1 and 2. mTOR is the central player of both mTORC1 and mTORC2 complexes, and it belongs to the family of PI3K-related protein kinase (PIKK). The mTOR protein contains N-terminal tandem HEAT repeats (protein interaction domains of two tandem antiparallel α-helices found in Huntington's disease protein, elongation factor 3, and TOR (FRAP) (Andrade and Bork, 1995)) and at the C-terminus of mTOR is the central 'FRAP/ATM/TRRAP' (FAT) domain (FATC). The FKBP12-rapamycin-binding (FRB) domain locates in between of FAT domain and the catalytic kinase domain (Ma and Blenis, 2009; Yang et al., 2013). Apart from mTOR, other subunits of mTORC1 include Raptor, Lst8, Deptor and PRAS40, and mTORC2 has Rictor, Lst8, Deptor, Protor 1/2 and Sin1 instead. The table below the diagram summarizes the signalling components and main activities performed by mTORC1 and mTORC2. Modified from Saxton and Sabatini (2017).

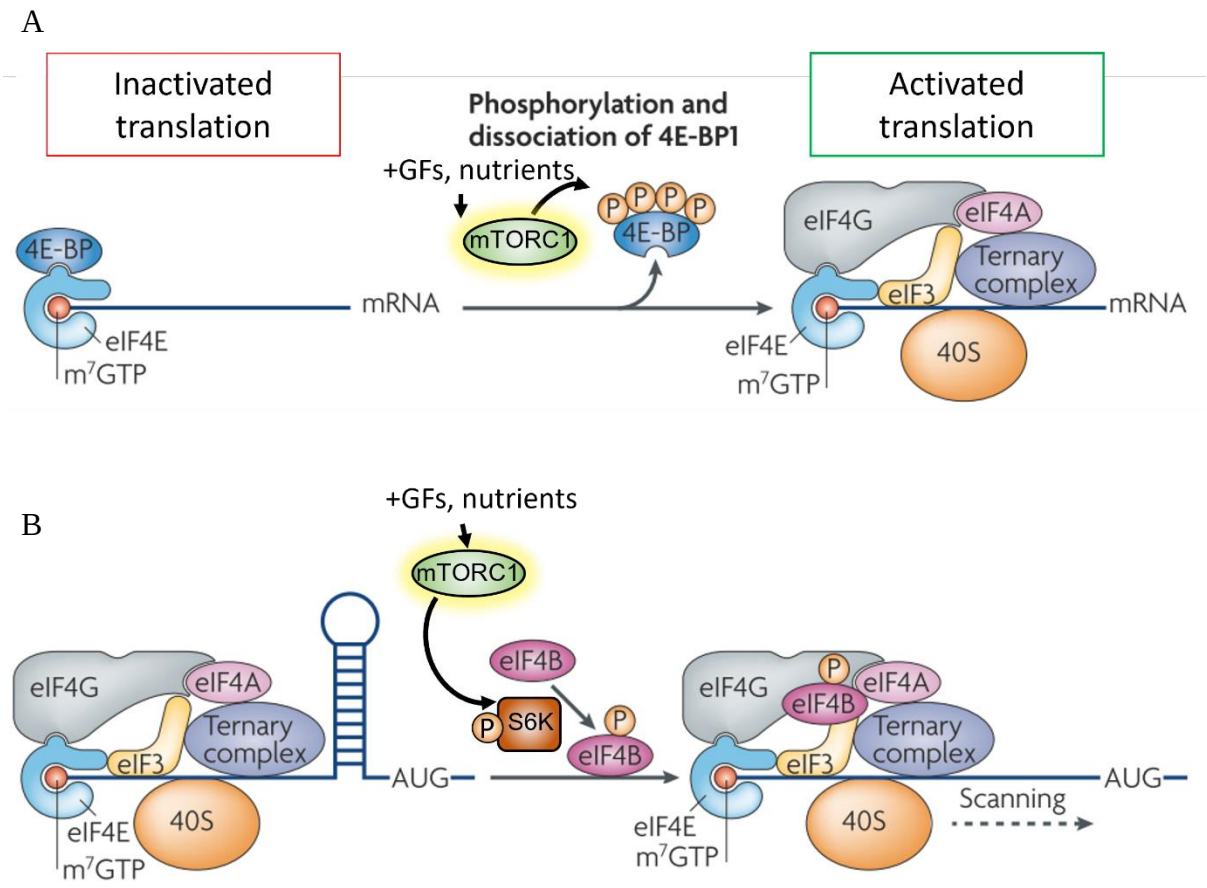


Figure 4.2. Schematic representation of translation regulation by mTORC1. (A) Cap-dependent translation when inactivated is regulated by a translation initiation factor, eIF4E, which is a 5' cap-binding protein negatively regulated by hypophosphorylated 4E-BP1. In this case, it cannot interact with other initiation factors such as eIF4G, thus inhibiting translation. When growth factors (GFs) and nutrients activate mTOR signalling pathway, 4E-BP1 is phosphorylated by activated mTORC1 and released from eIF4E, leading to the recruitment of eIF4G and other initiation factors to 5' cap as well as the 40S ribosomal subunit which is a rate-limiting step of cap-dependent translation. The translation pre-initiation complex is formed to proceed translation initiation. (B) S6K targets and phosphorylates another important translation initiation factor eIF4B, promoting the recruitment of eIF4B to the translation pre-initiation complex to enhance RNA helicase activity of eIF4A for unwinding the 5' untranslated region (UTR) with secondary structures. This allows the 40S ribosomal subunit to efficiently scan the start codon. Adapted from Ma and Blenis (2009).

4.1.1.3 Activation of mTORC1 pathway

Growth factors including insulin, nutrients including glucose and amino acids (AAs) and energy levels are key signals to trigger mTORC1 activation (Figure 4.3). For example, in mammals, the insulin signalling pathway activated by insulin binding to its receptor, which is a member of receptor tyrosine kinase (RTK) family, triggers activation of phosphoinositol-3'-

kinase (also called phosphoinositide 3'-kinase, PI3K), a positive regulator for mTORC1 (Chung et al., 1994; Mendez et al., 1996). To transduce signals for mTOR activation, PI3K generates phosphatidylinositol 3,4,5 triphosphate (PIP_3) which activates the downstream phosphoinositide-dependent protein kinase 1 (PDK1) for stimulating a serine/threonine kinase AKT (or protein kinase B (PKB)) (Brazil and Hemmings, 2001; Kandel and Hay, 1999; Scheid and Woodgett, 2001). Several mTORC1 regulators had been reported in mTORC1 pathway. Negatively regulated by AKT, tuberous sclerosis complex 1/2 (TSC1/2) is a repressor of mTORC1 (Inoki et al., 2002; Ma et al., 2005) and has GTPase-activating protein (GAP) function for Ras homologue enriched in brain (Rheb), a unique member of the small Ras Guanine nucleotide binding protein (G protein) superfamily directly activating mTORC1 located on endo-lysosomal membranes (Aspuria and Tamanoi, 2004; Long et al., 2005). Crystal structures have confirmed that Rheb acts as an activator of mTORC1, while PRAS40 is an inhibitor (Yang et al., 2017). Another mTORC1 regulator, AMP-activated protein kinase (AMPK) is also a well-studied regulator sensing energy and nutrient status, acting antagonistically to mTORC1 in responding to starvation and regulating autophagy (Kim et al., 2011; Long and Zierath, 2006; Zhang et al., 2014). When starved, AMPK promotes autophagy when mTORC1 is inhibited. One mechanism of such signal transduction is dependent on the phosphorylation of the mammalian autophagy-initiating kinase Ulk-1 (Kim et al., 2011).

mTORC1 activation is closely related to amino acid (AA) availability. For instance, solute carrier (SLC) family proteins (SLC7A5-SLC3A2) mediates influx of leucine (Leu) in exchange of glutamine (Gln) in the cytoplasm and lysosomal lumen (Milkereit et al., 2015; Nicklin et al., 2009; Scalise et al., 2018) and SLC38A9 located on lysosomal membrane transports arginine (Arg) and glutamine (Gln) while Leu can also be transported competitively through it (Jung et al., 2015; Rebsamen et al., 2015; Wang et al., 2015).

Moreover, an important mediator of mTORC1 activation, a vacuolar-type H^+-ATPase (v-ATPase)-Ragulator Complex, promotes translocation of mTORC1 to the endo-lysosomal membrane (Kim et al., 2008; Sancak et al., 2010; Sancak et al., 2008; Takahara et al., 2020; Zoncu et al., 2011). Ragulator is a heteropentameric scaffold protein to recruit Ras-related GTP binding protein (Rag GTPase) to anchor on the lysosomal membranes (Bar-Peled et al., 2012). The Rag pathway transduces signals of glucose and AA availability to mTORC1 (Efeyan et al.,

2013). There are four Rag GTPases in mammalian cells (Schürmann et al., 1995; Sekiguchi et al., 2001), and Ragulator has a guanine nucleotide exchange factor (GEF) activity for RagA/B at membranes (Bar-Peled et al., 2012). The Rag proteins function as a pair of heterodimers containing one RagA or RagB and one RagC or RagD protein, and AAs activate the heterodimerization of RagA/B bound to GTP with RagC/D loaded with GDP (Kim et al., 2008; Sancak et al., 2008; Shimobayashi and Hall, 2016). GAP activity towards the Rags 1 (Gator1), interacting with Gator2, regulates RagA/B with its GAP activity, while Gator2 is the negative regulator of Gator1 inhibited by leucine (Leu) bound Sestrin 2 (SESN2) (Bar-Peled et al., 2013; Kim et al., 2015; Shimobayashi and Hall, 2016; Wolfson and Sabatini, 2017). Folliculin (FLCN) and its interacting protein (FNIP) form a complex with GAP activity for RagC/D (Petit et al., 2013; Tsun et al., 2013). Meanwhile, in glucose starvation, the v-ATPase-Ragulator Complex on late endo-lysosomes promote activation of AMPK by accessing to AXIN/LKB1, in total as a metabolic switch from anabolism to catabolism, also mediate an inhibition of GEF activity of Rags leading to disassembly of the Ragulator-Rag anchoring on endo-lysosomes (Hardie et al., 2012; Sancak et al., 2010; Zhang et al., 2014; Zhang et al., 2013b).

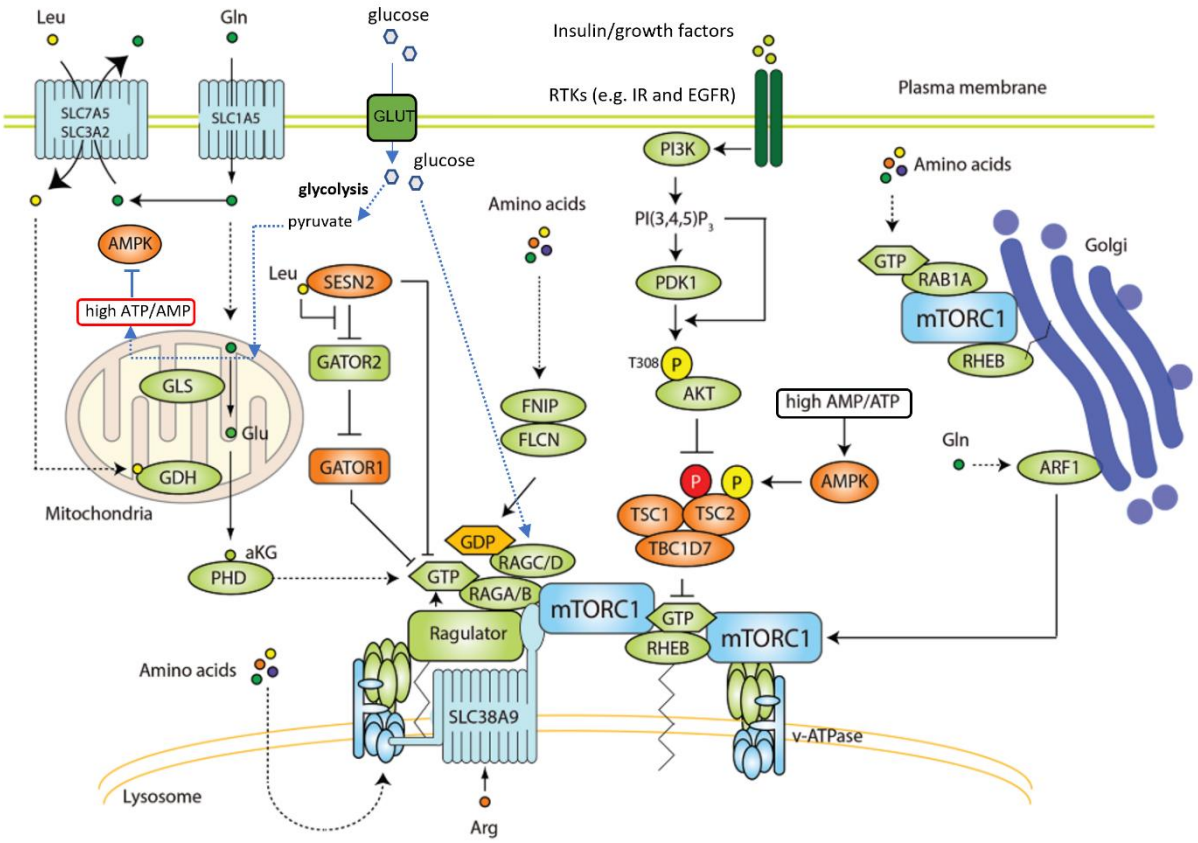


Figure 4.3. mTORC1 activation by extracellular nutrient sources (such as glucose and AAs), energy levels and growth factors or insulin. Growth factors stimulating RTKs (such as insulin receptor (IR) and epidermal growth factor receptor (EGFR)) activate the PI3K-

PDK1-AKT pathway which inhibits the TSC complex, a GAP for Rheb GTPase. When TSC complex is inhibited, Rheb in GTP bound form activates mTORC1 at lysosomal membrane, where Rag GTPases working in heterodimers facilitate mTORC1 recruitment and dimerization of RagA/B with RagC/D is facilitated by amino acids. On the other hand, AMPK is activated when the cell experiences low energy levels (high AMP/ATP ratio, highlighted in a black box) and stimulates TSC to suppress Rheb by phosphorylation. The Ragulator complex anchors Rags to the lysosomal surface and has GEF function for RagA/B, and the active form of Rag GTPases has GTP-bound RagA/B and GDP-bound RagC/D. Upstream of Ragulator-Rags, glutaminolysis promotes RagB loading with GTP. The Gator1 complex functions as a GAP for RagA/B, while Gator2, interacting with Gator1, is an inhibitor of Gator1 and it is negatively regulated by Leu-bound SESN2, a cytoplasmic Leu sensor. FNIP-FLCN complex acts as the GAP for RagC/D. SLC family proteins such as SLC7A5 and SLC3A2 are leucine transporters on PM and lysosomal membranes, while SLC38A9 is an amino acid transporter located on lysosomes and interacts with the Ragulator-Rag complex for activating mTORC1. mTORC1 can also be activated by ADP-ribosylation factor 1 (ARF1) which senses Gln and mediates mTORC1 lysosomal translocation, and v-ATPase also facilitates this recruitment process and promotes mTORC1 activation with or without Rag-associated mechanisms. AAs also recruit and activates mTORC1 at the Golgi by Rab1A and Rheb in a Rag-independent manner. For activating mTORC1, glucose enters from the extracellular environment via a glucose transporter (GLUT) and undergoes glycolysis, and the endpoint product pyruvate is actively transported into mitochondria for participating in energy production (indicated in blue arrows). Therefore, elevated levels of ATP/AMP (highlighted in red box) lead to the inhibition of AMPK and promotes the activation of mTORC1. Glucose can also stimulate the Rag GTPase pathway in a v-ATPase-dependent manner (Efeyan et al., 2013). Phosphorylation in yellow signs indicates an activation and inhibition is indicated in red signs. Adapted from and reviewed by Shimobayashi and Hall (2016).

4.1.1.4 Inhibitors of mTOR complexes

In tumorigenesis and cancers, the PI3K-AKT-mTOR pathway is one of the oncogenic pathways often found to be overactivated (Guertin and Sabatini, 2005, 2007; Ma et al., 2005; Sabatini, 2006; Saxton and Sabatini, 2017; Xu et al., 2014). Many mTOR inhibitors with anti-tumour functions have been proposed to decrease the growth rate of tumours in clinical trials by targeting mTOR pathways (Pongas and Fojo, 2016; Xie et al., 2016a; Zou et al., 2020). A well-known mTORC1 inhibitor, rapamycin, was firstly purified from the bacterium *Streptomyces hygroscopicus* as an antifungal macrolide in the early 1970s (Vézina et al., 1975). Rapamycin has immunosuppressive and antiproliferative effects in cancer biology studies and clinical trials (Bundscherer et al., 2008; Dumont and Su, 1995; Law, 2005; Saunders et al., 2001; Sehgal, 1998; Vézina et al., 1975). It disrupts cell cycle progression in yeasts and mammalian cells (Heitman et al., 1991; Sabers et al., 1995), suppresses proliferation and stimulates autophagy of many tumour cell lines (Aissat et al., 2008; Grewe et al., 1999; Lin et al., 2018; Luan et al., 2002). It also affects cytokine signalling by inhibiting ribosomal p70 S6K

through phosphorylation in mammalian cells (Chung et al., 1992; Dumont and Su, 1995; Price et al., 1992). It is also reported that rapamycin is a potential anti-aging drug and mTOR regulates longevity in animal models (Blackwell et al., 2019; Ehninger et al., 2014; Miller et al., 2014; Neff et al., 2013; Wilkinson et al., 2012). The mode of action of rapamycin includes its key binding partner, an endogenous 12 kDa-FK506-binding protein (FKBP12) which is a peptidyl prolyl cis-trans isomerase well conserved from yeast to mammalian cells (Schreiber, 1991). When rapamycin allosterically binds to FKBP12, a gain-of-function complex is formed to inhibit mTORC1 in yeast and mammalian cells (Chen et al., 1995; Chiu et al., 1994; Sabatini et al., 1994; Sabers et al., 1995). Another member of the FKBP family, FKBP38 binds to mTOR kinase and serves as mTOR kinase inhibitor through a similar interaction between FKBP12-rapamycin complex and mTOR, while GTP-bound Rheb interrupts its binding to mTOR and protects mTOR from being inactivated (Bai et al., 2007). Based on the anticancer properties of rapamycin, analogs of rapamycin which are recognized as "rapalogs" e.g. temsirolimus (CCI-779), everolimus (RAD001) and deforolimus (AP23573) were developed and used in clinical treatments of cancers and solid tumours e.g. renal cell carcinoma and mantle cell lymphoma (Strimpakos et al., 2009; Wander et al., 2011).

There are debates on the limitation of rapamycin-based monotherapies. Although rapamycin is an acute and direct inhibitor for mTORC1 (Brown et al., 1994; Sabatini et al., 1994) and a chronic inhibitor for mTORC2 (Sarbassov et al., 2006; Sarbassov et al., 2005), rapamycin and rapalogs only achieve limited success in combating human cancers with problems of tumour regression or regrow upon cessation of treatment (Bissler et al., 2008; Marsh et al., 2008). It is argued that rapamycin causes cytostatic but not cytotoxic effects on cancer cell growth (Li et al., 2014), as FKBP12-rapamycin inhibition of mTORC1 is subject to phosphorylation (Choo and Blenis, 2009) and this complex does not interact with mTORC2 (Jacinto et al., 2004). Rapamycin only indirectly inhibits mTORC2 through negative feedback regulation of insulin signalling (Kim et al., 2012; Li et al., 2014). Therefore, antitumour therapies in combination with rapalogs and other chemotherapeutic agents or targeted therapies have been suggested in clinical trials to enhance therapeutic effectiveness (Li et al., 2014).

Interests in the application of mTOR pathway in anti-cancer therapies have led to the development of a number of other mTOR inhibitors. While rapamycin is specific for mTORC1,

other broad-spectrum inhibitors which target the PI3K-AKT-mTOR signalling pathway are developed and tested in clinical trials (Chen et al., 2017; Garcia-Martinez et al., 2011; Li et al., 2014; Xu et al., 2014). For example, AZD8055 is an ATP-competitive inhibitor acting on both mTOR complexes 1 and 2 (mTORC1/2) and it has been reported to induce autophagy and caspase-mediated apoptosis, and has an effect to decrease tumour volume in mice models (Chresta et al., 2010; Garcia-Martinez et al., 2011; Houghton et al., 2012; Willems et al., 2012). BEZ235 is another pan-class PI3K/mTOR inhibitor that inhibits these kinases via blocking their ATP-binding clefts and has effects on suppressing tumour cell proliferation (Chiarini et al., 2010; Lang et al., 2020; Maira et al., 2008; McMillin et al., 2009; Pongas and Fojo, 2016; Roper et al., 2011). Although their effects on tumour suppression have been shown in clinical trials, several side effects were also reported with current treatments of mTOR inhibitors and these are not yet approved for cancer therapies (Kaplan et al., 2014; Nguyen et al., 2019; Pallet and Legendre, 2013).

4.1.2 mTORC1 in cell type differentiation and cell fate regulation

Since mTORC1 senses environmental cues and transduces the signals to regulate cell growth, development and metabolism, nutrient-mediated cell differentiation is also under control of mTORC1 activity. For example, in yeast cells, pseudohyphal filamentous differentiation is regulated in a mTOR-associated nutrient-dependent pathway, and rapamycin inhibition of mTORC1 suppresses pseudohyphal development (Cutler et al., 2001). Evidence of mTORC1 involvement in T cell fate decisions through promoting metabolic reprogramming had been studied for years (Patel and Powell, 2017; Waickman and Powell, 2012). mTORC1 signalling in T cells orchestrates metabolic cues and immune information to regulate the activation or maintenance stages (Chi, 2012). Both mTORC1 and mTORC2 involved in glycolysis and lipid biogenesis play important roles in differentiation of follicular helper T (Tfh) cells (Zeng et al., 2016). Specific sets of genes encoding components in metabolism and differentiation programs are expressed dynamically in T cell lineage specification, indicating metabolism actively participates in regulating developmental processes (Chisolm and Weinmann, 2018). mTORC1 as a metabolic checkpoint kinase shapes the identity of cytotoxic T lymphocyte (CTL) revealed by proteomics studies (Hukelmann et al., 2016). Activating mTORC1 mediates T cells to choose an effector fate rather than memory fate (Chi, 2012), while rapamycin promotes memory CD8+ T-cell differentiation (Araki et al., 2010). The mTORC1 antagonist AMPK, controlling a glucose-sensitive metabolic checkpoint in activated T cells, is also important for

regulating T helper 1 (Th1) and Th17 cell development and T cell-mediated adaptive immunity (Blagih et al., 2015). S6K phosphorylation by mTORC1 and an increase of the iron transferrin receptor (CD71) on the cell surface in a mTOR-dependent manner promote the activation of T cells, while inhibition of mTORC1 by rapamycin leads to anergy, an alternative T cell fate (Zheng et al., 2007).

There are also studies linking mTORC1 activity to transitioning from the stem cell quiescent state in response to injury-mediated systematic signals (Rodgers et al., 2014), somatic cell reprogramming via controlling metabolic gene expression and autophagy (Chen et al., 2011; Wu et al., 2015; Zhu et al., 2010). Inhibition of mTORC1 by rapamycin or torkinib (PP242) also stimulates the efficiency of induced pluripotent stem cell (iPSC) reprogramming (Chen et al., 2011). An example of mTOR acting in lineage fidelity of stem and progenitor cells for maintaining tissue homeostasis and integrity is mTORC1-mediated activation of a nutrient-sensing transcription factor ATF4 (Torrence et al., 2021) involved in essential amino acid uptake, which is fundamental to control cell fate conversion from airway secretory cells to the damaged-associated transient progenitors (DATPs)-induced squamous alveolar type 1 (AT1) cells in the lung (Jeon et al., 2022). It has also been reported that mTORC1 antagonizes the activation of small G proteins Rag GTPases C and D in a non-canonical regulation of lysosomal Rag GTPase signalling which coordinates embryonic stem cell (ESC) differentiation (Villegas et al., 2019). Moreover, a recent article reported that during onset of germ layer differentiation in *Xenopus* embryonic development, the transition of pluripotent states to lineage differentiation states orchestrates mTORC1 pathway which is activated by the spatiotemporal membrane polarization-regulated intracellular Ca^{2+} signalling as part of the gene regulatory networks to initiate differentiation programs (Sempou et al., 2022).

4.1.3 mTORC1 signalling in *Dictyostelium*

Dictyostelium has well-conserved machinery of mTOR signalling and components compared to other eukaryotes (Figure 4.4) (Table 4.1). In *Dictyostelium*, hyperactive mTOR via overexpression leads to cell proliferation inhibition (Swer et al., 2016). Upon starvation, mTORC1 activity decrease was reported while AMPK activity was increased, as monitored by phosphorylation of substrates for mTORC1 as an indirect reading of mTORC1 activity or AMPK for a more direct reading of kinase activation, and genes involving in autophagy are upregulated (Jaiswal and Kimmel, 2019; Jaiswal et al., 2019; Rosel et al., 2012). Similar to

mammalian cells, rapamycin has been used to inhibit mTORC1 activity which for example leads to upregulation of autophagy (Calvo-Garrido et al., 2010; Dominguez-Martin et al., 2017) and inhibition of cell proliferation rate in *Dictyostelium* cells (Chang et al., 2020; Jaiswal and Kimmel, 2019). *Dictyostelium* only has an identified gene encoding a homologue of TSC2 but not TSC1, and the mammalian mTORC1 inhibitor PRAS40 is apparently also absent in *Dictyostelium* (Jaiswal et al., 2019). *Dictyostelium* Rheb (DDB_G0277041) is highly conserved with the human Rheb protein and its involvement in the mTORC1 signalling pathway examined looking at the effect of rapamycin on cells overexpressing Rheb under the control of *act15* promoter (Swer et al., 2014) and dominantly-active GTP-bound or non GTP-bound Rheb mutants in phagocytosis, which is the natural approach for *Dictyostelium* to obtain nutrients (Rosel et al., 2012). Increased sensitivity to rapamycin in *rheb*$^-$ cell growth was also reported by Jaiswal and Kimmel (2019).

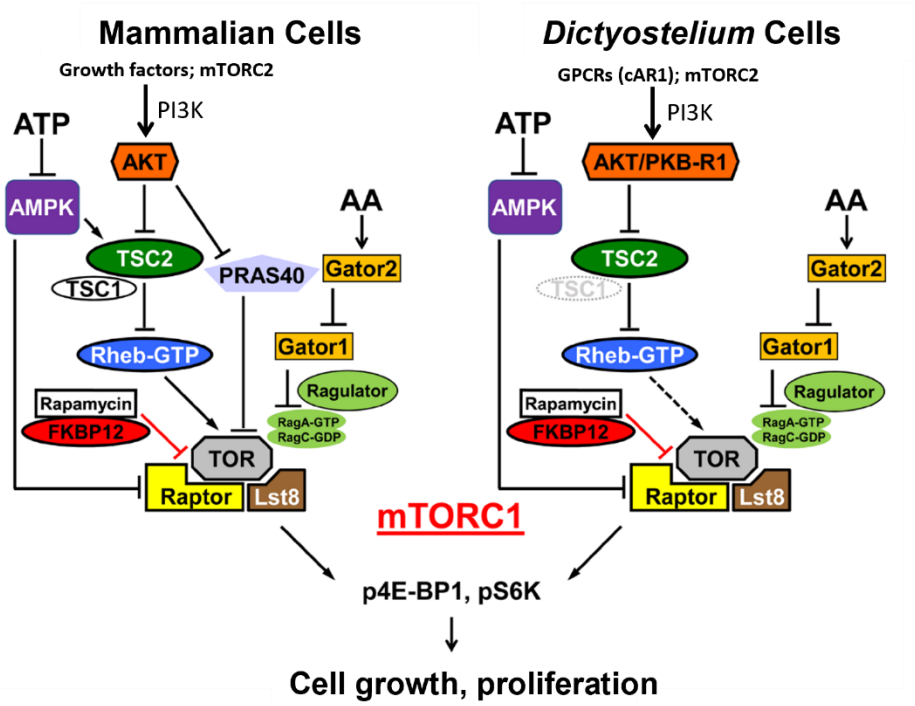


Figure 4.4. Schematic representation of mTORC1 and mTORC2 regulatory pathways in mammalian and *Dictyostelium* cells. mTORC1 in both mammalian and *Dictyostelium* cells contains mTOR kinase, Raptor, Lst8 subunits. Sufficient nutrients and energy sources activate the mTORC1 pathway for promoting cell growth via phosphorylating downstream proteins 4E-BP1 and S6K. The activation of mTORC1 is regulated by amino acid availability through the Gator-Ragulator-RagA/C pathway in mammalian cells, and the homologous sequences were found in *Dictyostelium* genome but have not been investigated functionally and systematically. Rheb when bound by GTP is in its active form and functions as a potent activator of mammalian mTORC1. However, mTORC1 in *Dictyostelium* cells is less dependent on Rheb as only rapamycin-treated cells reveal a function of TSC/Rheb in growth. Growth factors stimulate AKT in mammalian cells and agonist-bound GPCRs (e.g. cAMP receptor) activate AKT/PKB-

R1 in *Dictyostelium* cells via PI3K and mTORC2, which sensitize the Rheb inhibition by TSC1/2, a GAP for Rheb. High ATP level inhibit AMPK which is another important energy and nutrient sensor that antagonizes mTORC1 mediated activation of TSC2 and down-regulates Raptor. *Dictyostelium* TSC2 lacks a phosphorylation site for AMPK, so the inhibitory effect of AMPK on mTORC1 can be achieved by phosphorylating Raptor instead. In both cases of mammalian and *Dictyostelium* cells, endogenous FKBP12 forms a complex with rapamycin to inhibit mTORC1 through competitively bind to mTOR and disrupting the interaction between Raptor and mTOR. Adapted from and reviewed by Jaiswal et al. (2019).

Table 4.1 Components involved in *Dictyostelium* mTOR signalling pathways

Gene name	Gene ID	Protein homologs involved in *Dictyostelium* mTOR pathways	References
tor	DDB_G0281569	mTOR	(Smith et al., 2019; Swer et al., 2016)
lst8	DDB_G0292592	Lst8	(Pergolizzi et al., 2019; Rosel et al., 2012; Senoo et al., 2019)
raptor	DDB_G0270398	Raptor	(Cardenal-Munoz et al., 2017; Jaiswal and Kimmel, 2019)
piaA	DDB_G0277399	PiaA/Rictor	(Pergolizzi et al., 2019; Rosel et al., 2012)
ripA	DDB_G0284611	Rip3/Sin1	(Jaiswal et al., 2019; Rosel et al., 2012; Senoo et al., 2019; Williams et al., 2019)
ragA	DDB_G0288701	RagA/B	(Journet et al., 2012)
lamtor1	DDB_G0292160	LAMTOR1 (component of Ragulator complex)	(Cardenal-Muñoz et al., 2017; Journet et al., 2012; Stajdohar et al., 2017)
mio	DDB_G0276673	MIOS (WD repeats-containing, component of Gator complex)	(Journet et al., 2012)
rheb	DDB_G0277041	Rheb	(Cardenal-Muñoz et al., 2017; Smith et al., 2019; Swer et al., 2014)
snfA	DDB_G0277905	AMPKα (catalytic subunit)	(Jaiswal and Kimmel, 2019; Maurya et al., 2017, 2020; Warren et al., 2020)
tsc2	DDB_G0280527	TSC2	(Jaiswal et al., 2019; Rosel et al., 2012; Serfontein et al., 2011)
pkbA	DDB_G0268620	AKT/PKB	(Meili et al., 1999a; Tanaka et al., 1999)
pkgB	DDB_G0290157	PKBR1/SGK	(Kay et al., 2019; Meili et al., 2000; Senoo et al., 2019; Williams et al., 2019)
pikA	DDB_G0280813 DDB_G0280813	PI3K	(Hoeller and Kay, 2007; Kortholt et al., 2011; Williams et al., 2019)
pdkA, pdkB	DDB_G0281471 DDB_G0284489	PDK1	(Kamimura and Devreotes, 2010; King and Insall, 2009; Liao et al., 2010; Williams et al., 2019)
sesn	DDB_G0279427	SESN (Sestrin-like protein)	(Rafia and Saran, 2019)
febA	DDB_G0291990	4E-BP1	(Morio et al., 2001)

4.1.4 Links between mTORC1 and TPC2 in mammalian models

mTORC1 and TPC2 have been linked in autophagy pathway regulation in mammalian cells. mTORC1 and TPC2 have been reported to have reciprocal activity levels in response to nutrient deprivation, where inactivation of mTORC1 by starvation or pharmacological conditions led to Ca^{2+} and Na^{+} release via TPC2 (Cang et al., 2013; Lin et al., 2015; Ogunbayo et al., 2018). In the lysosomal amino-acid sensing pathway, Ragulator complexes interact with a heterodimer of Rag GTPases, facilitating the anchoring of activated mTORC1 to the lysosomal membranes (Sancak et al., 2010; Sancak et al., 2008). When mTORC1 is activated in an amino acid-sensitive manner (Cang et al., 2013; Kim et al., 2008), mTORC1 is translocated to endo-lysosomal membranes in close vicinity to its activator Rheb required for amino acid-mediated mTORC1 activation (Nobukuni et al., 2005; Sancak et al., 2008; Zoncu et al., 2011).

TPC2 is widely expressed in endo-lysosomal compartments in many species (Calcraft et al., 2009; Furuichi et al., 2001; Ishibashi et al., 2000; Lin et al., 2015) and forms a complex with mTORC1 verified by immunoprecipitation in Cang et al. (2013)'s work. Ogunbayo et al. (2018) reported that in a human embryonic kidney 293 (HEK293) cell line overexpressing hTPC2 (HEK293-hTPC2), mTORC1 inhibition achieved by treatment with mTORC1 inhibitors rapamycin or torin-2 evoked lysosomal Ca^{2+} release via TPC2, and this Ca^{2+} transient was similar to that seen by induction with the Ca^{2+} mobilizing messenger NAADP. However, the Ca^{2+} transients triggered by mTORC1 inhibitors or NAADP from lysosomes mediated by TPC2 in mammalian cells were lost or undetectable in either the myocytes from *tpc2*$^{-/-}$ mice or following a short hairpin RNA (shRNA)-mediated mTOR knockdown in an HEK293-hTPC2 background. Thus, it was confirmed that mTORC1 has a negative regulatory role on Ca^{2+} release from lysosome compartments via TPC2 (Ogunbayo et al., 2018), in agreement of the findings in Cang et al. (2013). TPC2 in the endo-lysosomal system was also found to terminate autophagy through regulating mTORC1 reactivation (Lin et al., 2015; Yu et al., 2010). Thus, mammalian TPC2 links metabolic state and stress-sensing via mTORC1 pathways to lysosome-mediated nutrient homeostasis by regulating many factors, such as intracellular Ca^{2+} level and pH in lysosomes which are also cell fate determinants during cell differentiation in *Dictyostelium* development (see Chapter 1 section 1.3.3.3 and 1.3.3.4).

4.1.5 Links between *Dictyostelium* mTORC1 and TPC2

There is evidence that the lysosomal-targeted Ca^{2+} channel TPC2 can influence mTORC1 activity in *Dictyostelium* cells. Cells lacking the gene encoding TPC2 (*tpc2*$^{-}$) showed a prolonged phosphorylation of the mTORC1 substrate 4E-BP1 compared to parental AX2 after the onset of starvation and the mTORC1 inhibitor rapamycin reverses phenotypes of *tpc2*$^{-}$ cells such as prolonged growth in culture and delay in early aggregation (Chang et al., 2020). In *Dictyostelium*, *tpc2*$^{-}$ cells have increased pH of acidic vesicles and slightly lower cytosolic Ca^{2+} levels and delayed Ca^{2+} release in response to exogenous cAMP (Chang et al., 2020). As intracellular Ca^{2+} level and vesicle pH act as important fate-determinate environmental factors to prime cells to different fate tendencies (Baskar et al., 2000; Kubohara and Okamoto, 1994; Schaap et al., 1996), this raises the possibility that the stalk cell bias seen in *tpc2*$^{-}$ cells might be due to the increased mTORC1 activity during growth. Therefore, it is hypothesized that activity of mTORC1-TPC2 axis is a potential link between cell fate influencing factors in *Dictyostelium* cells (Figure 4.5).

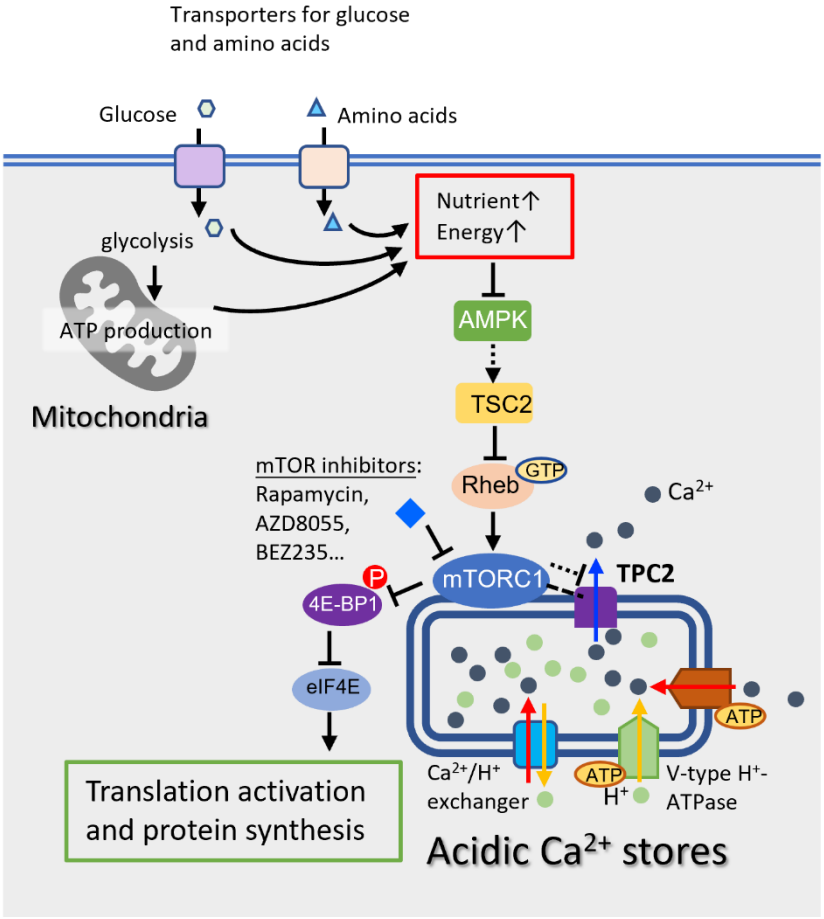


Figure 4.5. The hypothesized model of TPC2-mTORC1 orchestrating cell fate-determining factors in regulating cell fate decisions in *Dictyostelium*. In *Dictyostelium* model, it is hypothesized that TPC2 regulates cell fate decision through mTORC1 activity.

TPC2 is located on acidic Ca^{2+} stores such as endo-lysosomes with a low pH maintained by V-type H^{+}-ATPase and Ca^{2+}/H^{+} exchanger, and TPC2 in mammalian cells is responsible for lysosomal Ca^{2+} release (Galione, 2019; Jin et al., 2020; Morgan et al., 2015). TPC2 is also sensor of luminal pH and Ca^{2+} in mammalian cells (Pitt et al., 2010), while vesicle pH and intracellular Ca^{2+} levels are important cell fate influencing factors in *Dictyostelium* cells. Although have not been proved in *Dictyostelium*, activated mTORC1 in mammalian systems is translocated to lysosomal membranes, sensing environmental cues such as nutrient and energy availability (Sabatini, 2017). Transporters of glucose and amino acids facilitate the uptake of extracellular nutrients into mammalian cells and triggers mTORC1 pathway (Ardestani et al., 2018). Also, mammalian mTORC1 is shown to interact with TPC2 and negatively regulate the release of Ca^{2+} from lysosome through TPC2 (Ogunbayo et al., 2018) and TPC2 impacts mTORC1 reactivation during autophagy termination (Lin et al., 2015). Genetic modulators of mTORC1 activity include its negative regulators TSC2 and AMPK, and an activator Rheb GTPase. The kinase activity of mTORC1 promotes protein synthesis by phosphorylating and inactivating 4E-BP1, a suppressor of mRNA translation, and phospho-4E-BP1 is one way to monitor mTORC1 activity. Pharmacological inhibition of mTORC1 can be achieved by its potent inhibitor rapamycin, and other pan-inhibitors of the mTOR pathway, AZD8055 and BEZ235. Activation in red arrows and inhibition in dark blue symbols are shown, and lighter blue sign indicates the possible interaction. Dashed line shows interaction between proteins or potential effects. Blue arrows and red arrows indicate the movements of Ca^{2+} for increasing or decreasing cytosolic Ca^{2+} levels, while yellow arrows show proton movements around acidic compartments.

4.2. Aims

This chapter aims to determine whether:

(1) mTORC1 activity at the immediate onset of development correlates with factors which affect cell fate decisions.

(2) pharmacological treatment with rapamycin and other general mTOR inhibitors (AZD8055 and BEZ235) to reduce mTORC1 activity cause a cell fate predisposition .

(3) mutations in genes encoding regulators of mTORC1 activity (*ampk* and *rheb*) similarly alter cell fate. Strains overexpressing inducible Rheb and *rheb*$^{-}$ strains were constructed and used alongside available *ampk*$^{-}$ cells to confirm whether upregulation or downregulation of mTORC1 influences cell fate decisions.

(4) activation of mTORC1 later in development has the same effect on cell fate. This was investigated by treating cells with rapamycin during growth or throughout development, and by inducing doxycycline-dependent Rheb OE either during growth or later in development.

4.3. Results

4.3.1 mTORC1 activity is prolonged or higher in cells with a pre-stalk tendency

4.3.1.1 Phosphorylation level of 4E-BP1 remains prolonged in developing cells with a glucose-deficient growth history

One factor known to predispose cells to a stalk cell fate is growth in medium containing low glucose, which was consistently shown for both AX2 and *tpc2*$^{-}$ cells by mixing experiments (Figure 3.14 in Chapter 3). In order to determine if growth in different levels of glucose altered mTORC1 pathway activity at the onset of development, phosphorylation levels of 4E-BP1 were compared. AX2 cells previously grown in HL5 medium with 1% glucose (G+) for 2 days show a rapid decreased phosphorylation level of 4E-BP1 at the onset of starvation, whereas cells that have depleted glucose growth conditions (G-) showed a prolonged high phospho-4E-BP1 level during one-hour starvation (Figure 4.6A). This G+/G- effect was also seen in starved *tpc2*$^{-}$ cells (Figure 4.6B). Jaiswal and Kimmel (2019) also monitored phosphorylation of another potential mTORC1 substrate, S6K, in *Dictyostelium* cells. Therefore, western blot analysis was also carried out using the antibody that they used, phospho-SGK1 (Ser422) antibody, for developing AX2 and *tpc2*$^{-}$ cells (Chang et al., 2020) (Figure 4.6C). This phosphorylation event, like 4E-BP1 phosphorylation, was also higher in *tpc2*$^{-}$ cells. However, NCBI BLAST search failed to reveal an obvious homologue of S6K in the *Dictyostelium* genome, and kinome studies showed that p70 S6K is absent in *Dictyostelium* cells (Goldberg et al., 2006). When using NCBI BLAST tool to verify potential epitopes for the antibody, a gene encoding SGK1 is present and it is thought to be an mTORC2 substrate rather than mTORC1 in mammalian cells (Lu et al., 2010) (Figure 4.1). Therefore, we did not precede with this antibody further. Although the trends are consistent, variation in the phosphorylation levels of 4E-BP1 in each batch of samples harvested during one-hour development meant that the error bars when combining experiments were large. This could be because the phospho-4E-BP1 levels not only reflect the mTORC1 activity but also are subject to phosphatase activity during development. Also, the commercial polyclonal antibody for phospho-4E-BP1 was raised against the mammalian protein, and there can be variations between batches of polyclonal antibodies, so another method to monitor mTORC1 activity is desirable.

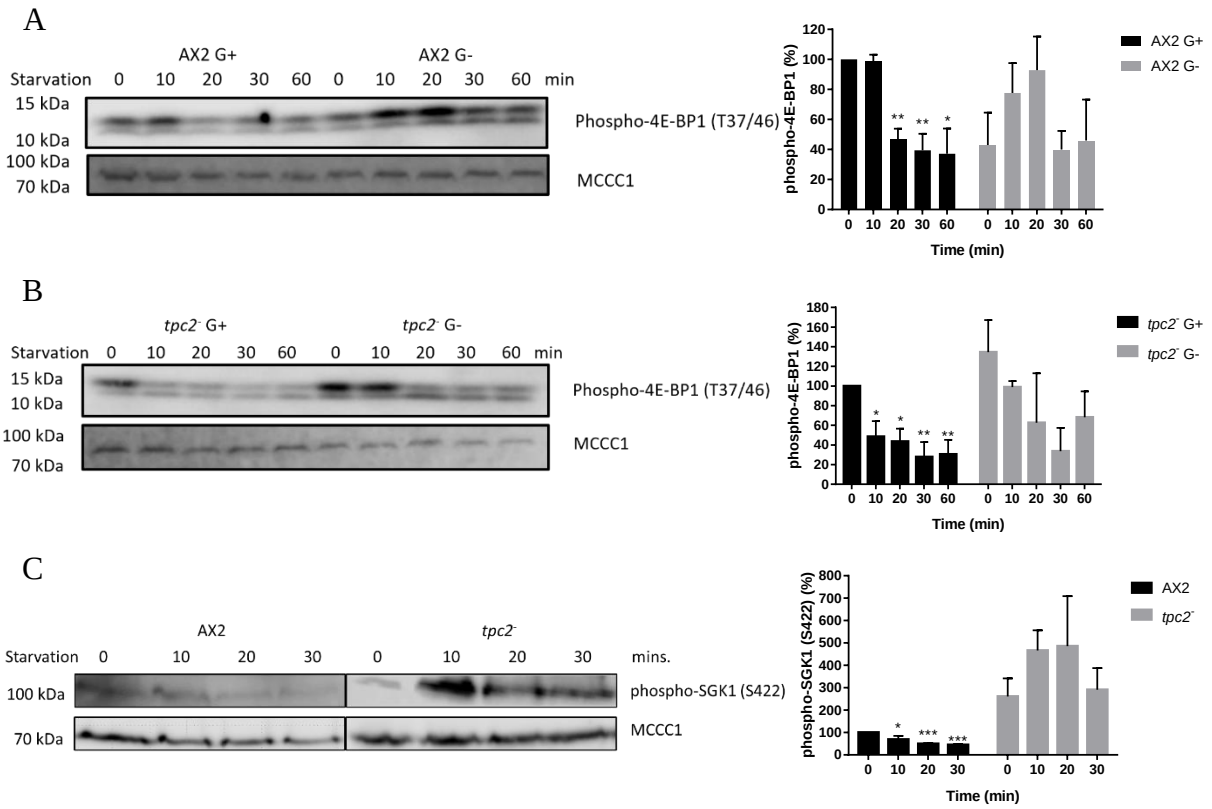


Figure 4.6. mTORC1 activity on starvation of cells grown in glucose rich (G+) or depleted (G-) medium. mTORC1 pathway activity was monitored by the phosphorylation level of its downstream effector 4E-BP1. Western blotting experiments with phospho-4E-BP1 (T37/46) using (A) AX2 cells and (B) *tpc2*$^-$ cells starved for one hour in HKC development buffer were performed. Cells were grown in either normal HL5 medium supplied with 1% glucose (as the control) or without glucose for 48 hours. Then exponentially growing cells were harvested around the density of 2×10^6 cells/mL, washed with HK buffer twice and resuspended in HKC developmental buffer (HK buffer with 250 μM $CaCl_2$) at a density of 1.4×10^7 cells/mL, incubated at 22°C, 120 rpm in HKC for the times shown. At each time point, 2×10^6 cells were collected, lysed in 2× Laemmli buffer and boiled in 95°C for 6 mins. The whole cell lysates were run on 12% denaturing acrylamide separation gels and blotted with p-4E-BP1 (T37/46) (1:1000, Cell Signaling Technology, #9459) (left panels). MCCC1 as loading control (Davidson et al., 2013) was visualised by Streptavidin (1:1000, Streptavidin Alexa Fluor 680, Invitrogen, #S21378). One representative repeat from each experiment, N = 3. The intensities of bands were quantified by Image Studio Lite Software (Ver 5.2) and normalized to 0 min time point of the control condition (e.g. G+) or parental strain (e.g. AX2) defined as 100% (Mean ± S.E.M). Student *t*-test (two-tailed) analyses were performed within the same set and between the non-starved 0 min conditions from different sets: *: $P < 0.05$; **: $P < 0.01$; ***: $P < 0.001$) (right panels). (C) Phosphorylation of a putative S6K substrate was detected by western blots using anti-phospho-SGK1 (Ser 422) (1:500, Abcam, #ab55281) for a time course of up to 30-mins development of AX2 and *tpc2*$^-$ cells. MCCC1 was used for loading control (1:1000). Experiments were performed and analysed as described in (A) and (B) above. One representative repeat shown, N = 3. Adapted from Chang et al. (2020).

4.3.1.2 Rapamycin-induced development to confirm levels of mTORC1 activity

To determine mTORC1 activity levels with an alternative approach, rapamycin sensitivity of cells undergoing under buffer development was assessed. Inhibiting mTORC1 with rapamycin at 500 nM in a 50% strength nutrient medium without glucose (half-strength HL5 medium) has been reported to induce some early developmental events including aggregation (Jaiswal and Kimmel, 2019). This led to an observable rapamycin sensitivity in cells which could be evaluated as a readout of mTORC1 activity. Therefore, to complement the phospho-4E-BP1 western blots for interpreting mTORC1 activity, a rapamycin-induced development assay in half-strength HL5 medium, optimized from Jaiswal and Kimmel (2019), was established as an alternative method to assess mTORC1 activity in cells (Figure 4.7).

This alternative method uses various rapamycin concentrations ranging from 0 to 500 nM in half-strength HL5 to induce aggregation for 22 hrs in exponentially growing cells seeded at a density of 1.4×10^6 cells/mL. A semi-quantitative scoring system was established to score the levels of aggregation in response to each concentration of rapamycin (Figure 4.7A), allowing the rapamycin sensitivity to be assessed. Aggregation under KK2 was a positive control and incubation in complete HL5 (com HL5) was a negative control (Figure 4.7B). To assess whether this rapamycin-induced aggregation assay can show differences in mTORC1 activity in fate-biased mutant strains, rapamycin sensitivity in *tpc2*$^-$ cells was tested compared to AX2 cells (Figure 4.7C). *tpc2*$^-$ had a lower sensitivity to rapamycin in comparison with AX2, for example, when induced by 100 nM rapamycin, AX2 had more aggregates (score 3.0 ± 0.0) than *tpc2*$^-$ (1.7 ± 0.3). Similarly, the rapamycin-induced aggregation assay can show that cells with different predisposition effects towards cell fate decision have different rapamycin sensitivity. For instance, *tpc2*$^-$ cells with glucose depletion history (G-) prior to development were more sensitive to rapamycin, as G+ cells induced by 100 nM rapamycin had a higher aggregation score (2.0 ± 0.0) than G- cells (1.0 ± 0.0) (Figure 4.7D). In both cases of the stalk fate-biased strain *tpc2*$^-$ and G- treatment, the sensitivity towards rapamycin was lower than to the control of AX2 cells and G+ treatment respectively. Dose-dependent inductions of aggregate formation were observed in all groups.

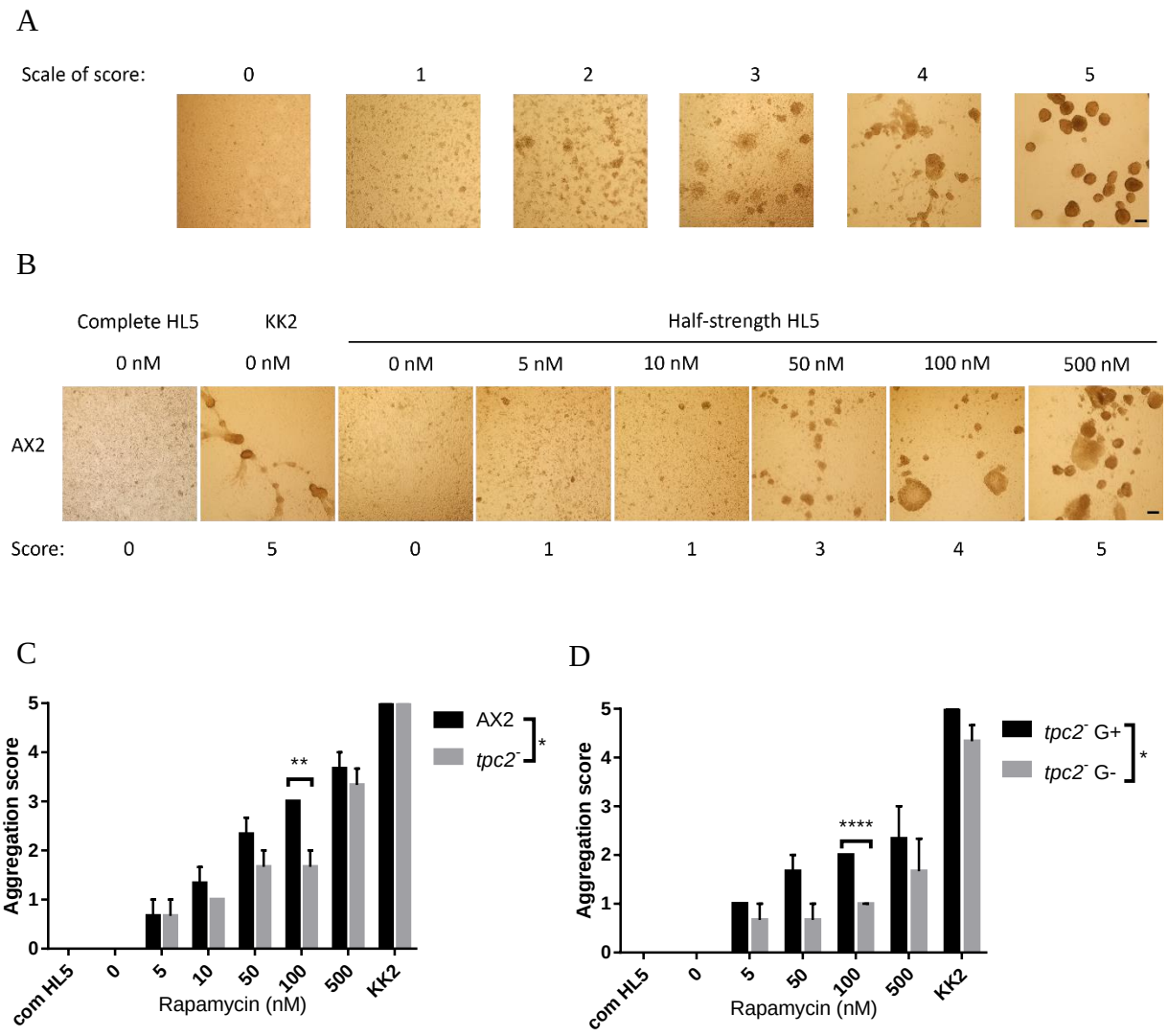


Figure 4.7. Rapamycin-induced aggregation in half-strength HL5 growth medium in fate biased cells. Log-phase cells were washed in KK2 and seeded in a 12-well plate at a density of 1.4×10^6 cells/well. After cells adhered to the bottom of the well for 30 mins, the buffer was replaced with either full-strength/complete HL5 (com HL5) for normal cell growth as a negative control or half-strength HL5, in the presence of various concentrations of rapamycin or vehicle control DMSO (0 nM). A positive control for cell development was included, using KK2 with DMSO to treat cells. After 22-hr incubation at 22°C, the aggregating phenotypes in each well were observed and imaged for analyses. (A) A scaling system using pictures that are representative of different aggregation levels was used as reference to compare other aggregating events in half-strength HL5 in semi-quantification. (B) A representative example of rapamycin-induced aggregation assay in half-strength HL5 medium with AX2 in the presence of various concentrations of rapamycin. (C) AX2 and *tpc2*$^-$ cells were used in rapamycin-induced aggregation assays (N = 3). (D) *tpc2*$^-$ cells were pre-incubated in glucose sufficient (G+, the normal condition) or deficient (G-) HL5 medium for 48 hrs prior to the rapamycin-induced aggregation assay (N = 3). Mean ± S.E.M. Two-way ANOVA: *: $P < 0.05$ and student *t*-test (two-tailed): **: $P < 0.01$.

4.3.1.3 Genetic mutants with distinct cell fate bias have prolonged mTORC1 activity in early development

mTORC1 activity of other fate-biased mutant strains were examined, using phospho-4E-BP1 western blotting and sensitivity to rapamycin-induced aggregation in half strength HL5 medium. It was found that another strain with intrinsic stalk fate bias *dmpA*$^{-}$ (described in Chapter 3, Figure 3.13) shows prolonged 4E-BP1 phosphorylation during one-hour development compared to AX2 cells (Figure 4.8A), as previous reported for *tpc2*$^{-}$ cells (Chang et al., 2020). Moreover, similar to *tpc2*$^{-}$ (Figure 4.7C), *dmpA*$^{-}$ (Figure 4.8B) cells compared to AX2 cells were less sensitive to rapamycin-induced aggregation, for example, at 500 nM rapamycin-induced aggregation, *dmpA*$^{-}$ had a lower aggregation score (2.0 ± 0.0) compared to AX2 cells (3.3 ± 0.3). This was consistent with higher mTORC1 activity needing higher concentrations of rapamycin to reduce to the threshold required to trigger aggregate formation. Therefore, another strain with a stalk cell fate bias also showed increased mTORC1 pathway activity, consistent with this driving the cell fate bias.

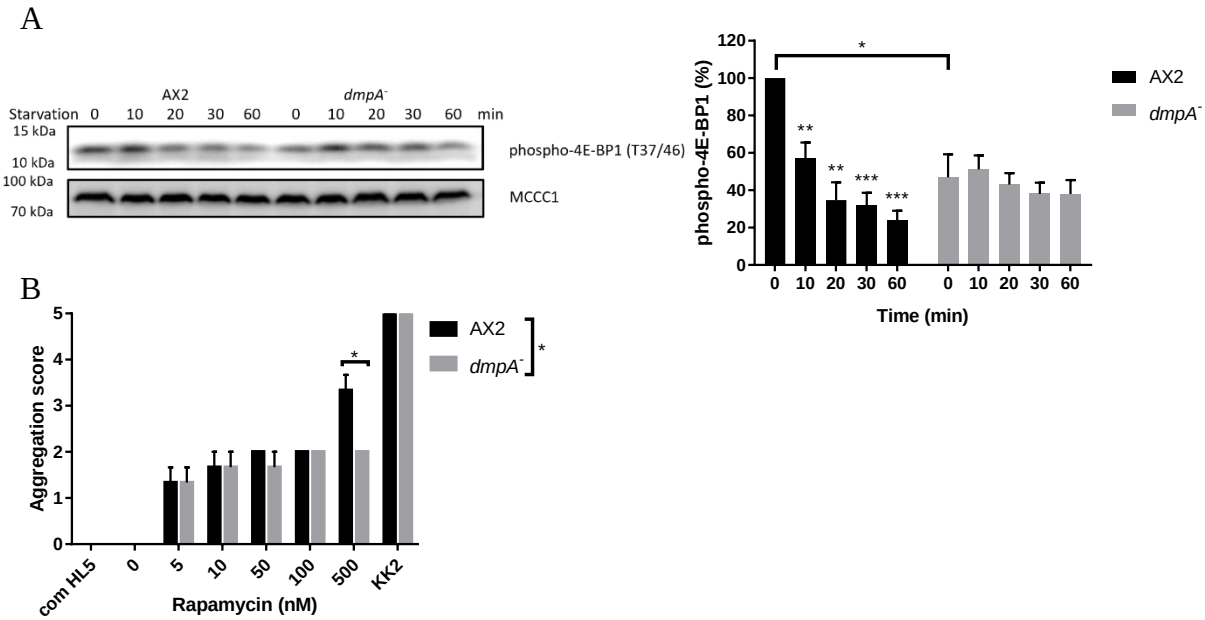


Figure 4.8. mTORC1 activity in stalk fate-biased *dmpA*$^{-}$ strain. (A) Left panel: Western blotting of phospho-4E-BP1 in one-hour developing cells: AX2 and *dmpA*$^{-}$ (clone: dmpkAKO_II_76). MCCC1: Loading control. Experiments were performed as described in the legend to Figure 4.6. One representative repeat was shown, N = 3. Right panel: Quantification of phospho-4E-BP1 level (%) of western blots described in (A). N = 3. Mean ± S.E.M. Student *t*-test (two-tailed): *: P < 0.05; **: P < 0.01; ***: P < 0.001. (B) AX2 and *dmpA*$^{-}$ cells were used in rapamycin-induced aggregation assays in half-strength HL5 medium. Experiments were performed as described in the legend to Figure 4.7. N = 3. Mean ± S.E.M. Student *t*-test (two-tailed) and two-way ANOVA: *: P < 0.05.

4.3.2 Altering mTORC1 activity can influence cell fate decision

4.3.2.1 Pharmacological inhibition of mTORC1 via mTOR inhibitors

Having shown a correlation between the activity of mTORC1 at the onset of starvation with cell fate, the next step was to determine whether altering mTORC1 activity in growing cells can influence cell fate decisions as a predisposition effect. Alongside the established mTORC1 inhibitor rapamycin, two other general mTOR inhibitors AZD8055, a dual mTORC1/2 inhibitor, and BEZ235, a dual PI3K and mTOR inhibitor, were used for testing potential off-target effects of rapamycin.

In order to confirm that rapamycin was exerting its effects through inhibition of mTORC1, the effects of AZD8055 and BEZ235 were assessed. To inhibit mTORC1 activity in *Dictyostelium* cells, 500 nM rapamycin has been previously reported to be effective (Chang et al., 2020; Jaiswal and Kimmel, 2019; Rosel et al., 2012). AZD8055 (500 nM) used in this study was also comparable to concentrations for mTOR inhibition in *Dictyostelium* used by others (Chang et al., 2020; Warren et al., 2020) and in other model organism such as *Arabidopsis* (Dong et al., 2015). Moreover, 1 μM BEZ235 has been reported to have inhibitory effects on mTORC1 activity in human cancer cell lines (Alqurashi et al., 2018; Roper et al., 2011). Western blots showed that phospho-4E-BP1 (T37/46) levels decreased when exponentially growing AX2 cells were treated with all three mTOR inhibitors rapamycin, AZD8055 (Figure 4.9A) and BEZ235 (Figure 4.9B) in HL5 growth medium for up to 15 mins. Whole cell lysates from cells starved for 60 min acted as a positive control showing the reduction in the level of 4E-BP1 phosphorylation during development compared to cells growing in HL5 medium (0 min time point). 500 nM rapamycin, 500 nM AZD8055 and 1 μM BEZ235 in growing AX2 cells all decreased phosphorylation of 4E-BP1 levels to around 30% after 15 minutes (Figure 4.9C). However, 500 nM AZD8055 and 1 μM BEZ235 seemed to cause a more rapid decrease within 5 mins. In 5 mins, 500 nM AZD8055 and 1 μM BEZ235 reduced phospho-4E-BP1 levels to 40.7% ± 15.1% and 48.0% ± 22.5% respectively, while 500 nM rapamycin treated cells had 64.0% ± 4.5%. In general, it is shown that these potent mTOR inhibitors at such concentrations efficiently reduced mTORC1 activity.

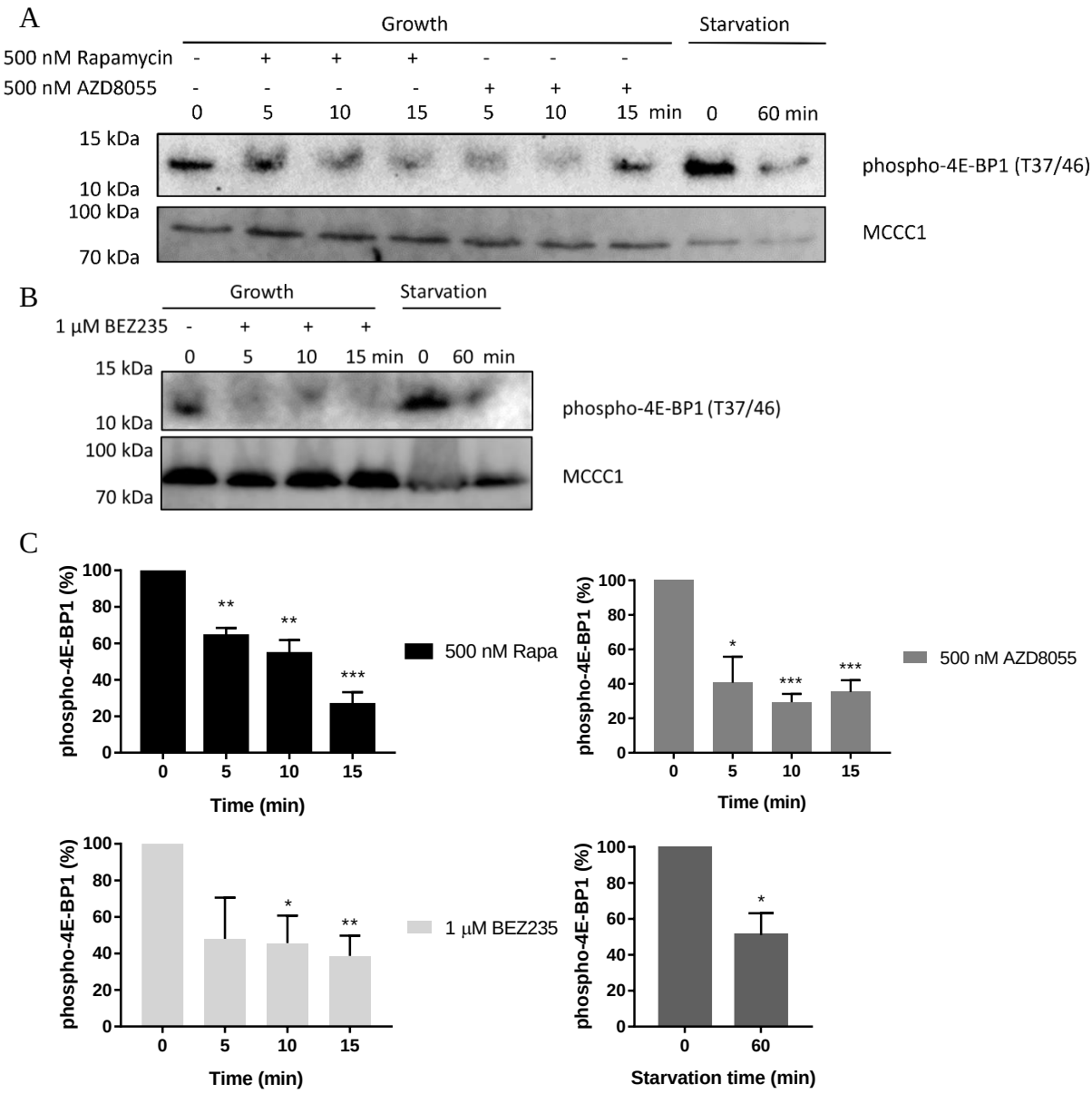


Figure 4.9. Effect of mTOR inhibitors on 4E-BP1 phosphorylation in growing cells. Phosphorylation of mTORC1 substrate 4E-BP1 was detected by western blot (method described in the legend to Figure 4.6). Log-phase AX2 cells were washed twice in KK2, then resuspended into HL5 medium supplied with (A) 500 nM rapamycin, 500 nM AZD8055 or (B) 1 μM BEZ235. Untreated groups were supplied with same volume of vehicle control DMSO instead. The positive controls for reduction of phospho-4E-BP1 level in one-hour starvation was included along with the mTOR inhibitors-treated western blotting experiments. Antibodies used for the western blotting were phospho-4E-BP1 (T37/46) (1:1000) and MCCC1 as loading control (1:1000). One representative repeat from each experiment was shown, N = 3. (C) The quantification of phospho-4E-BP1 level (%) in the western blotting experiments mentioned in (A) and (B) was quantified by normalizing the untreated group (0 min) during the 15-mins treatments of mTOR inhibitors in growth. Phospho-4E-BP1 levels from positive control experiments using AX2 cells for one-hour starvation were also normalized to the cells in growth (0 min time point defined as 100%). N = 3. Mean ± S.E.M. Student *t*-test (two-tailed): *: $P < 0.05$; **: $P < 0.01$; ***: $P < 0.001$.

4.3.2.2 Inhibition of mTORC1 using mTOR inhibitors during growth leads to a spore cell fate bias

To study the predisposition effect of mTORC1 activity at the onset of starvation on cell fate bias, mixing experiments following 4-hr pre-treatment with or without 100 nM rapamycin during growth and labelling were performed, showing that more spores were formed from the rapamycin pre-treated groups in both mixing ratios (10%L/90%UL and 90%L/10%UL) (Figure 4.10A). However, the 45-min dye-labelling involves incubating cells in KK2 development buffer which triggers starvation and enters development. This result therefore cannot separate the effect of rapamycin treatment during the 4-hr growth and during the first 45-min starvation in KK2 during the labelling process. Therefore, another mixing experiment was performed using cells only exposed to 100 nM rapamycin or DMSO vehicle control in the 4-hr pre-treatment (Figure 4.10B). The results of mixing experiments using either the 4-hr 100 nM rapamycin pre-treatment or the 4-hr rapamycin treatment during growth and the first 45-min starvation had similar trends, indicating that 4-hr pre-treatment with rapamycin in growth is sufficient to predispose cells to a spore cell fate in mixing experiments.

Similarly, in the monolayer stalk induction assay, when AX2 cells containing the stalk marker *ecmB*-GAL were pre-incubated with 500 nM rapamycin for 4 hrs before developing in monolayers, stalk marker induction in response to concentrations of DIF up to 100 nM was almost undetectable compared to the untreated cells (Figure 4.11A). For example, at 100 nM DIF-1 induction, untreated AX2 cells had drastically higher stalk marker expression than that seen in cells with 500 nM rapamycin pre-treatment history. Pre-treatment with a range of concentrations of rapamycin was then assessed in AX2 cells (Figure 4.11B). Stalk marker induction by 100 nM DIF-1 dramatically decreased between 10 nM to 100 nM rapamycin pre-treatment from 91.0% ± 2.0% to 10.5% ± 3.5%, while 100 nM and 500 nM rapamycin pre-treatment diminished the stalk marker expression to a similarly low level (10.5% ± 3.5%, and 7.5% to 1.5%, respectively). This was seen for both 50 nM and 100 nM DIF-1. A narrower range of rapamycin concentrations (0-100 nM) was then further examined using 100 nM DIF-1 for inducing pre-stalk marker expression, showing a dose response in reduction of stalk marker induction (Figure 4.11C). In the pre-treatment group with 50 nM and 100 nM rapamycin, cells induced by 100 nM DIF-1 had reduction of pre-stalk marker expressions to 62.6% ± 8.5% and 29.6% ± 8.9%, respectively. The same trends of the reduction of pre-stalk

marker expression were observed in response to AZD8055 (Figure 4.11D) and BEZ235 (Figure 4.11E) 4-hr pre-treatment, although the results were not significantly different, while 500 nM AZD8055 and 1 μM BEZ235 still led to a significant decrease in phospho-4E-BP1 levels (Figure 4.9). The decreases of pre-stalk marker expression were less significant than the trend observed in rapamycin, it might be because these pan-inhibitors AZD8055 and BEZ235 may also inhibit the activity of mTORC2 and perhaps other upstream kinases like PI3K in mTOR signalling pathway. Their known effects on mTORC2 meant that they could not be tested in mixing experiments as mTORC2 is implicated in chemotaxis, aggregation and cell migration in both *Dictyostelium* and mammalian cell models (Jacinto et al., 2004; Lee et al., 2005; Li et al., 2012). In conclusion, pharmacologically altering mTORC1 activity prior to the onset of development using inhibitors rapamycin, AZD8055 and BEZ235 led to a spore cell fate bias.

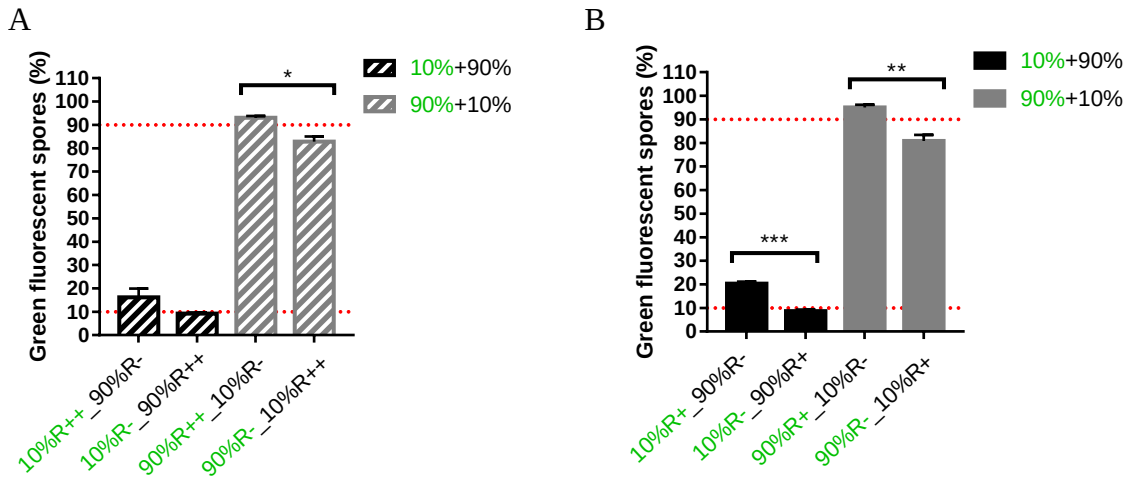


Figure 4.10. 4-hr pre-treatment of growing cells with rapamycin before starvation influences cell fate. Exponentially growing cells were treated with 100 nM rapamycin or DMSO vehicle control for 4 hrs in HL5 growth medium before harvesting and mixing for chimeric development as described in the legend to Figure 3.4A. (A) Mixing experiments using cells 4-hr pre-treated with rapamycin or DMSO and also exposed to rapamycin (R++) or DMSO (R-) during in CellTracker dye-labelling process (45-min starvation in KK2) (diagonal line-patterned bars). (B) Mixing experiments using rapamycin (R+) or DMSO (R-) vehicle control to pre-treat AX2 cells for 4 hrs before development (solid bars). The input ratios in (A) and (B) were 10% labelled cells mixed with 90% unlabelled cells (10%L/90%UL) and 90% labelled cells mixed with 10% unlabelled cells (90%L/10%UL). The labelled portions were highlighted in green. N = 3. Mean ± S.E.M. Student *t*-test (two-tailed): *: $P < 0.05$; **: $P < 0.01$; ***: $P < 0.001$.

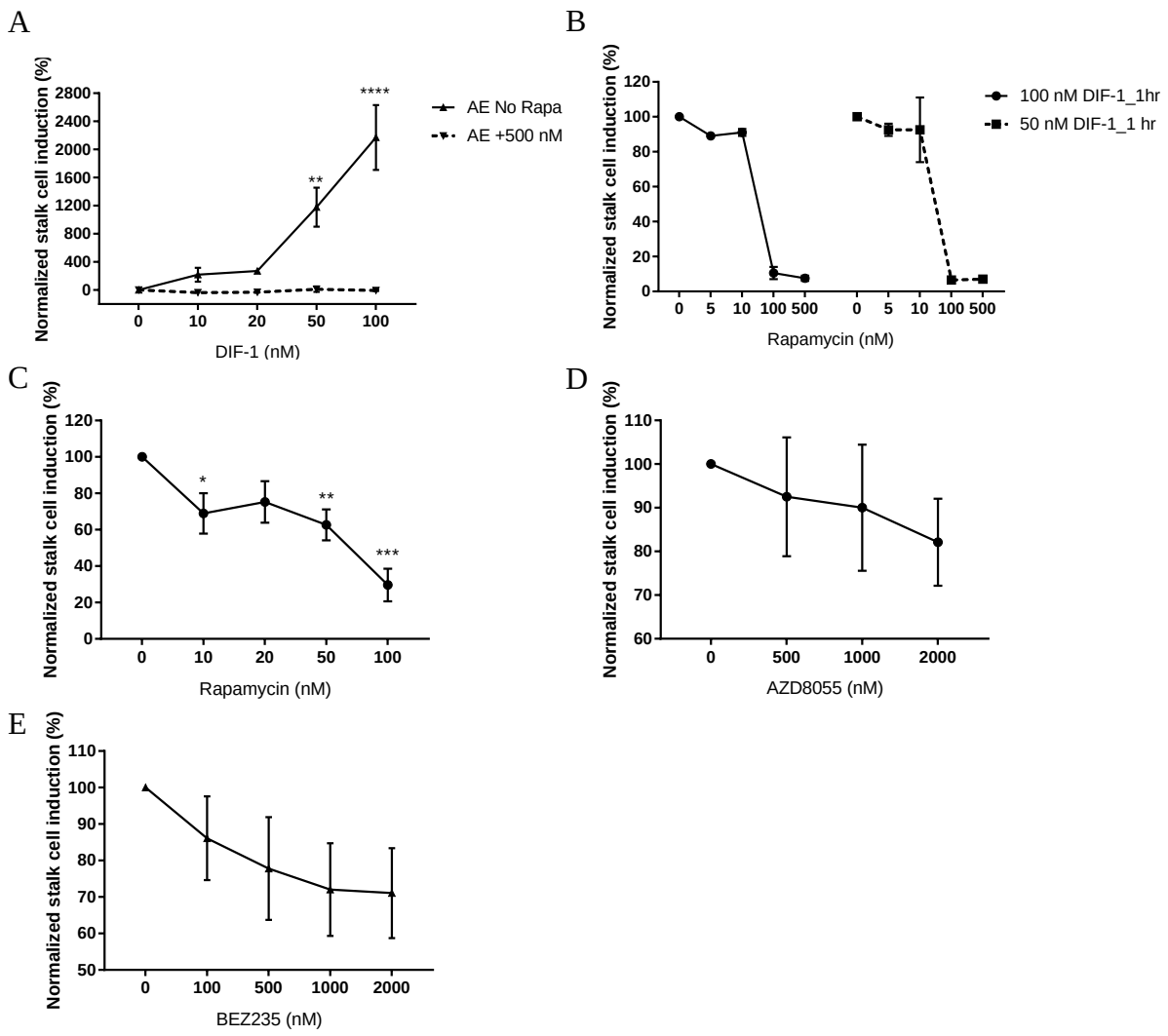


Figure 4.11. Inhibition of mTORC1 during growth inhibits pre-stalk gene induction. Monolayer stalk induction following 4-hr pre-treatment with mTOR inhibitors. (A) AX2 cells with *ecmB*-GAL pre-stalk marker were grown to log-phase, then growth medium was replaced by 500 nM rapamycin (or vehicle control DMSO) supplemented HL5 medium for 4-hr preincubation at 22°C, 220 rpm. After pre-treatment, cells were used to perform monolayer stalk induction assay as described in the legend to Figure 3.5A. The pre-stalk marker expression level induced by a range of DIF-1 concentrations (0-100 nM) were normalized to untreated group with no DIF-1 induction (0 nM) defined as 0%. Mean ± S.E.M., N = 2. (B) With the same experimental approach as in (A), monolayer stalk induction assays were performed using AX2 cells pre-treated with various concentrations of rapamycin (0-500 nM) as a pre-treatment for 4 hrs. 50 nM or 100 nM DIF-1 were used to induce pre-stalk marker expression which were normalized to the rapamycin-untreated group (0 nM) as 100%. Mean ± S.E.M., N = 2. (C) Pre-stalk marker expression of AX2 cells pre-treated with 0-100 nM rapamycin were assessed by monolayer assays (N = 4), where the expression levels were normalized to the untreated (0 nM) group. Similarly, other general mTOR inhibitors (D) AZD8055 (N = 4) and (E) BEZ235 (N = 4) were used for 4-hr pre-treatment in monolayer stalk induction assays. The stalk marker expression levels in C, D and E were normalized to untreated groups (0 nM, defined as 100%). Mean ± S.E.M. Student *t*-test (two-tailed): *: $P < 0.05$; **: $P < 0.01$; ***: $P < 0.001$; ****: $P < 0.0001$.

4.3.3 Genetic alteration of mTORC1 activity influences cell fate decisions

Even though a number of inhibitors that are reported to have mTORC1 as a common target were used, and treatment with all three led to a reduction in 4E-BP1 phosphorylation and a decreasing trend in stalk cell induction, it is always possible that these compounds are not specific for mTORC1 activity. Therefore, genetic approaches were taken to verify these results. In *Dictyostelium* mTORC1 signalling pathway, upstream regulators that change mTORC1 activity include activators e.g. Rheb, and repressors e.g. TSC2 and AMPK (Figure 4.4). To genetically alter mTORC1 activity, different strains containing disruption or overexpression of mTORC1 regulators were used.

4.3.3.1 Alteration of mTORC1 activity by manipulating the mTORC1 antagonist AMPK with a genetic mutant strain of AMPK (*ampk*$^-$)

An *ampk*$^-$ strain in which the gene was disrupted using a CRISPR/Cas9 approach in an AX3 background was generously provided by Professor Robin Williams, Royal Holloway University of London. This *ampk*$^-$ null strain has a 14-bp deletion in the second exon of the gene encoding the AMP-activated protein kinase alpha subunit (SnfA) (Warren et al., 2020). This frameshift mutation introduces a premature stop codon in exon 2 which results in disrupted translation to generate a truncated protein lacking catalytic activity (Figure 4.12A). The small deletion means that the *ampk*$^-$ null strain has lost a BamHI site which was used to verify the strain following PCR of a fragment flanking this site and digestion of the PCR product with BamHI (Figure 4.12B). This 14-bp deletion in *ampk*$^-$ null strain was further confirmed by sequencing the resulting PCR fragment (data not shown). To verify the catalytic subunit of AMPK protein was absent in *ampk*$^-$ cells as previously published (Warren et al., 2020), western blots using an antibody against the phosphorylation of AMPK at T172 was performed with both AX3 and *ampk*$^-$ cells during one-hour starvation to induce development. The phospho-AMPK levels in AX3 cells during the first 20 mins of starvation increased, and as predicted, no phospho-AMPK was apparent in the *ampk*$^-$ null cells (Figure 4.12C and 4.12D). Meanwhile, mTORC1 activity was assessed by western blots of phospho-4E-BP1 at T37/46. *ampk*$^-$ cells when starved for one hour in all biological repeats had a relatively prolonged and higher phosphorylation level in 4E-BP1 than seen in AX3 cells, although it was not statistically significant (Figure 4.12C and 4.12D). This is consistent with loss of AMPK leading to increased and prolonged the 4E-BP1 phosphorylation levels following starvation.

Due to the lack of significant quantification in western blots, an alternative approach to assess the activity of mTORC1 in cells was to assess their sensitivity of cell growth to inhibition by rapamycin. This rapamycin-inhibited growth assay has been used previously (Chang et al., 2020) where sensitivity correlated with increased 4E-BP1 phosphorylation. When 50 nM or 100 nM rapamycin present in HL5 medium, AX2 cells grew much slower for 24 to 48 hrs (Figure 4.13), in agreement with the findings reported in Chang et al. (2020). Thus, rapamycin inhibits cell growth and can be used to monitor rapamycin sensitivity as an indirect way to assess mTORC1 activity during growth at the stage when rapamycin treatment leads to cell fate bias. To determine whether *ampk*$^{-}$ cells have increased mTORC1 activity compared to AX3 cells during growth, inhibition of growth of AX3 and *ampk*$^{-}$ by 50 nM or 100 nM rapamycin was analysed (Figure 4.14). Both strains showed inhibition of growth in the presence of rapamycin. However, comparison between AX3 and *ampk*$^{-}$ cells showed that the *ampk*$^{-}$ cells consistently showed a lower degree of growth inhibition at both 50 and 100nM rapamycin and at 24 and 48 hours. For example, incubating in HL5 with 50 nM rapamycin for 48 hrs, *ampk*$^{-}$ cell growth reached 0.8 ± 0.1 relative to the untreated compared to 0.4 ± 0.0 for AX3 cells, consistent with *ampk*$^{-}$ cells having an increased level of mTORC1 activity compared to AX3 cells.

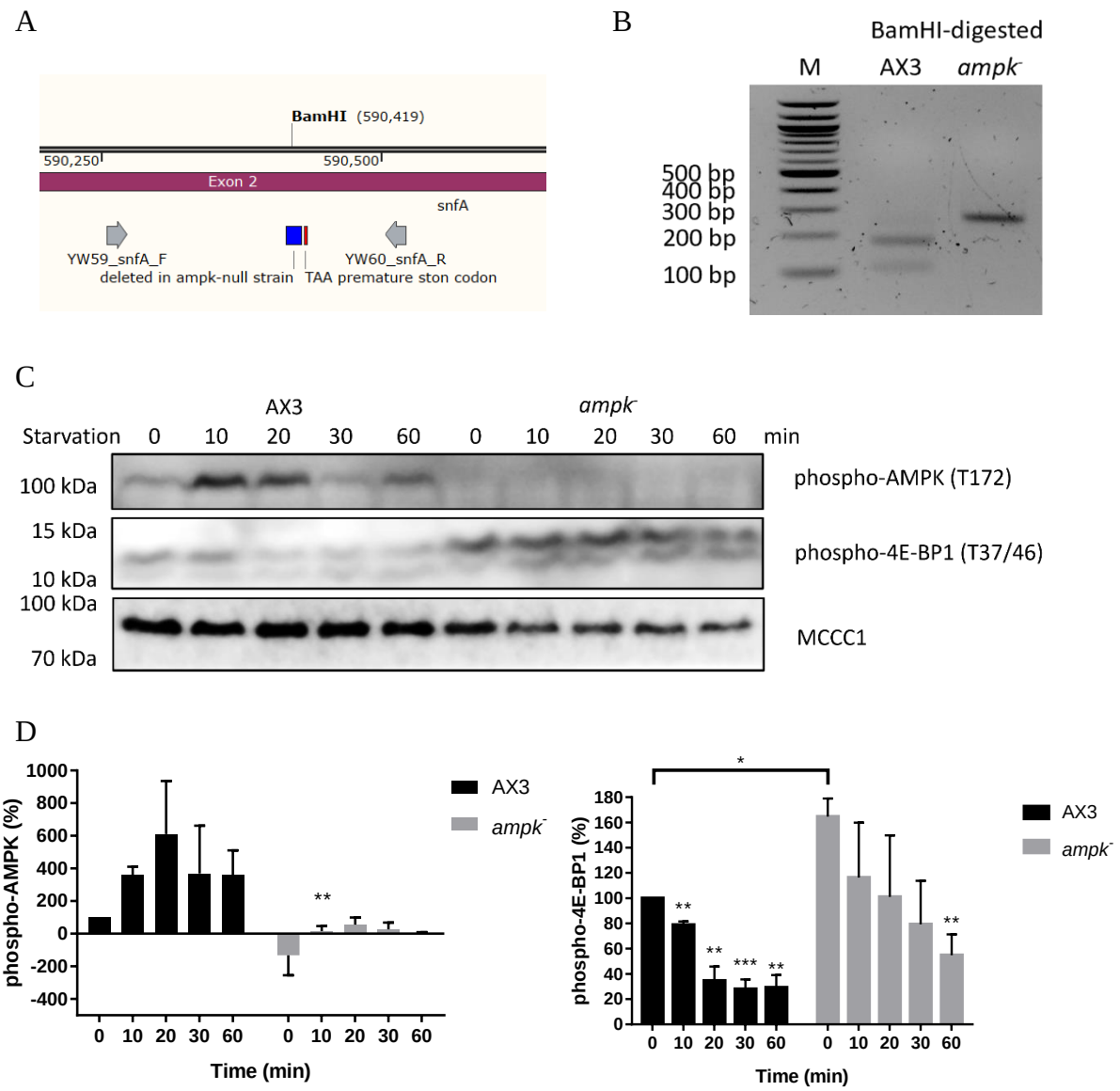


Figure 4.12. Verification of *ampk*⁻ strain. The *ampk*⁻ cell line was provided by Williams Lab, Royal Holloway University of London (Warren et al., 2020). (A) PCR primers YW59 and YW60 were designed to flank the deleted sequence of the *snfA* gene encoding the AMP-activated protein kinase alpha subunit. YW59 and YW60 primers amplified a wildtype product of 267 bp from AX3 or a 253 bp band from *ampk*⁻ genomic DNA. (B) Agarose gel electrophoresis of BamHI-digested PCR fragments from AX3 and *ampk*⁻. PCR fragments amplified by YW59 and YW60 were digested with BamHI restriction enzyme, generating two bands in AX3 (165 bp + 102 bp) but only one band without digestion in *ampk*⁻ strain (253 bp). M: Quick-load 100 bp (NEB). (C) Western blotting of cells for up to one-hour development of AX3 and *ampk*⁻ cells using the method as described in the legend to Figure 4.6 with phospho-AMPK (T172) (1:2000, Cell Signaling Technology, #2531) and phospho-4E-BP1 (T37/46) (1:1000) antibodies. MCCC1: Loading control (1:1000). One representative blot shown, N = 3. (D) Quantification of three repeats of western blots described in (C). Phosphorylation levels in AMPK (left panel) or 4E-BP1 (right panel) in both AX3 and *ampk*⁻ were normalized to 0 min time point in AX3 (in growth) defined as 100%. N = 3. Mean ± S.E.M. Student *t*-test (two-tailed): *: P < 0.05; **: P < 0.01; ***: P < 0.001.

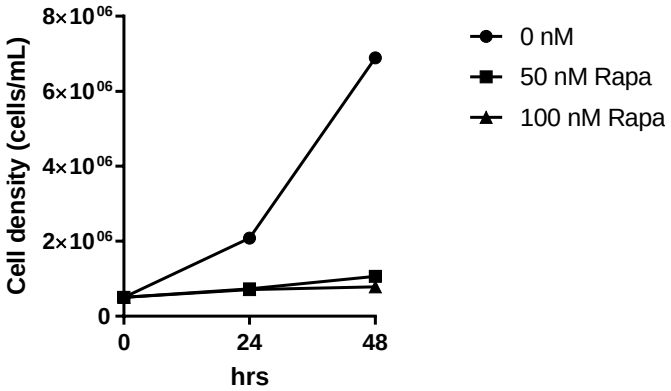


Figure 4.13. Rapamycin inhibits cell growth of AX2. Growth curve of AX2 cells treated with or without 50 nM and 100 nM rapamycin for up to 48 hours. Exponentially growing cells were used to set up cultures at the density of 5×10^5 cells/mL and cells were counted every 24 hours using a haemocytometer. One representative experiment of two is shown, N = 2.

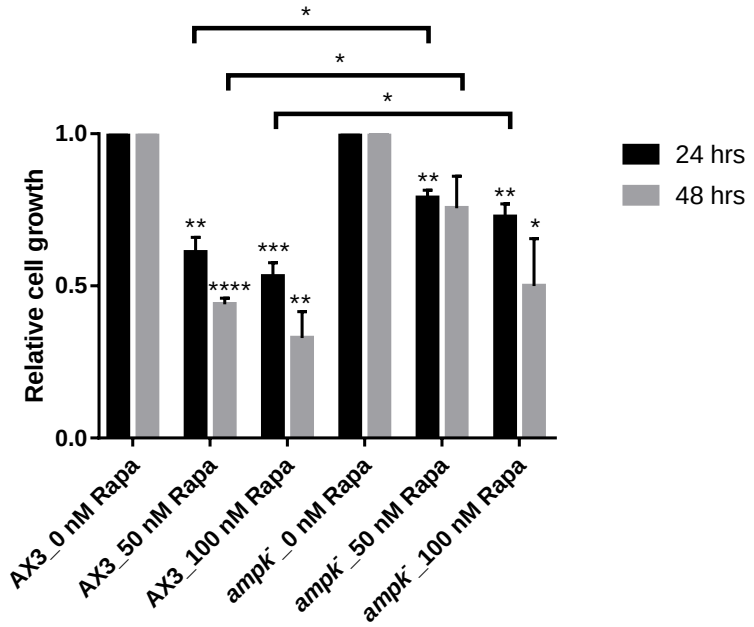


Figure 4.14. Rapamycin sensitivity of AX3 and *ampk*⁻ cells during growth. AX3 and *ampk*⁻ cells were harvested from log-phase growth, washed and resuspended to 7×10^5 cells/mL in HL5 medium containing 0, 50 or 100 nM rapamycin. The number of cells were counted at 24 hrs and 48 hrs. The relative cell growth in each of the rapamycin treated groups within each strains were normalized to the untreated group (0 nM) at the same time point which was considered as 1 (no inhibition). N = 3. Mean ± S.E.M. Student *t*-test (two-tailed) was used to compare rapamycin treated groups and the untreated groups within and between the same set: *: P < 0.05; **: P < 0.01; ***: P < 0.001; ****: P<0.0001.

4.3.3.2 Alteration of mTORC1 activity by manipulating expression of Rheb, an activator of mTORC1

4.3.3.2.1 Construction of Rheb overexpressing strains

To construct a strain in which it is possible to turn mTORC1 activity on and off, the positive regulator Rheb was chosen, as it is a direct activator when in GTP-bound form (reviewed in (Takahara et al., 2020)). A useful toolkit of tetracycline/doxycycline controllable vectors with selectable markers has already been established in *Dictyostelium* (Blaauw et al., 2000; Veltman et al., 2009). Therefore, overexpression (OE) of Rheb was designed under the control of a doxycycline regulatable system with two types of doxycycline regulated vectors (Figure 4.15): the pDM310 dox-on (containing transactivator rtTA-M2$_s$) and pDM309 dox-off (containing transactivator tTA) constructs (Veltman et al., 2009). The principle of doxycycline regulating transcription relies on the binding of transactivator to the inducible promoter, regulated by the binding of doxycycline to the transactivator, which turns gene transcription on or off depending on the type of transactivator with high specificity and affinity (Veltman et al., 2009).

To confirm that AX2 cDNA was free from genomic DNA (gDNA) contamination, PCR was performed on AX2 gDNA or cDNA templates with primers spanning the Rheb intron (YW43 and YW44), producing single bands: 656 bp and 564 bp respectively (Figure 4.16A). After confirming the quality of AX2 cDNA template, PCR was performed with cDNA using YW43 and YW45 primers to amplify the entire Rheb coding sequence (Figure 4.16B). In this case, BglII and SpeI restriction enzyme sites, the sequences to code for a FLAG tag and a stop codon were added at the 3' end of the Rheb coding sequence to form the Rheb_FLAG cDNA cassette (588 bp). This cassette was inserted into both vectors and the final constructs were verified to be correct by both restriction enzyme digests and sequencing (data not shown). These constructs were transfected into AX2 cells via electroporation and 10 μg/mL G418 used as a selectable marker to obtain pools of transformants containing the Rheb_FLAG dox-on or dox-off constructs.

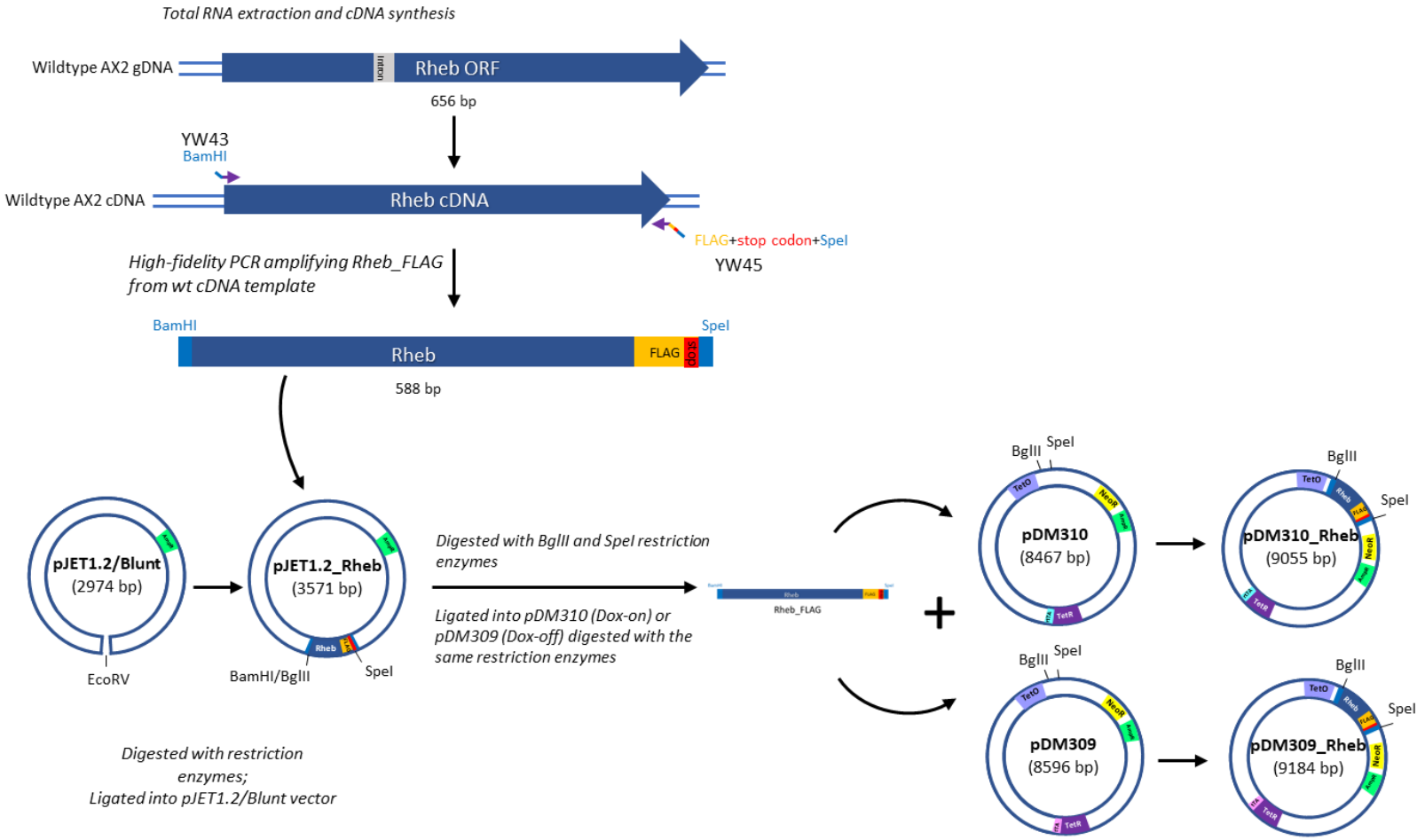


Figure 4.15. Schematic representation of cloning strategy for dox-on/dox-off inducible Rheb overexpression vectors. AX2 cells were harvested and lysed in Trizol for total RNA extraction and cDNA synthesis. cDNA was used as the template for amplifying Rheb cDNA using primers to incorporate two unique restriction digesting enzyme site (BglII at 5' end and SpeI at 3' end), a FLAG tag and a stop codon (YW43 and YW45). Then, the Rheb_FLAG cDNA was cloned into an intermediate pJET1.2 cloning vector (Thermo Scientific, #K1231). After confirmation by sequencing, the Rheb_FLAG cDNA cassette was digested and cloned into the destination vectors: pDM310 (dox-on) and pDM309 (dox-off) where BglII and SpeI are unique sites for restriction digestion.

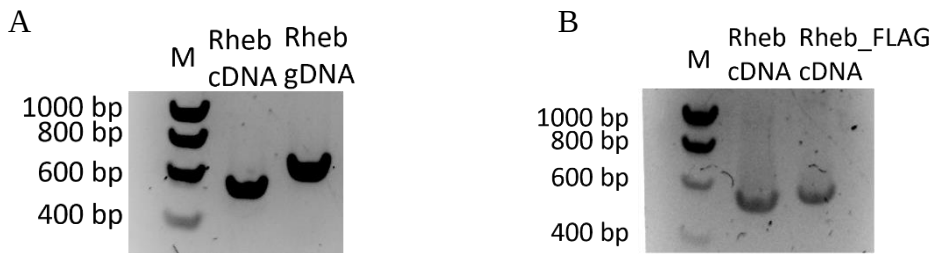
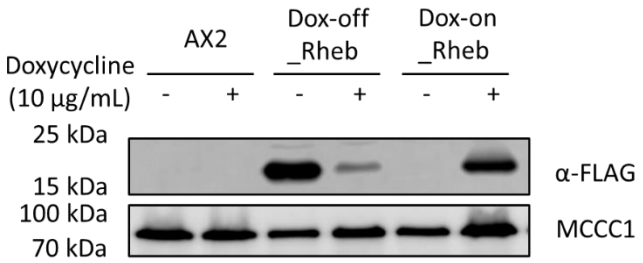


Figure 4.16. Verification of Rheb_FLAG cassette. Agarose gel electrophoresis (1%, stained with EtBr) of Rheb PCR product amplified from gDNA or cDNA templates. (A) PCR products of Rheb cDNA or gDNA using primers YW43 and YW44. Single bands 656 bp from gDNA and 564 bp from cDNA were generated. (B) PCR products of Rheb cDNA with YW43 and YW45 primers. YW45 is the reverse primer that has the FLAG tag, stop codon and SpeI restriction enzyme cutting sites in the overhang. The sizes of the bands from cDNA were 564 bp without the FLAG tag sequences and 588 bp where FLAG tag was added. Marker (M): HyperLadder 1kb (Bioline).

4.3.3.2.2 Verification of Rheb_FLAG overexpressing strains

To verify whether don-on and dox-off systems were behaving as expected, the expression of Rheb_FLAG in the dox-on and dox-off Rheb_FLAG OE strains were examined by western blot using α-FLAG antibody. Three-day growth in a 6-well plate with or without 10 μg/mL doxycycline confirmed the successful induction of Rheb_FLAG expression in the dox-on strain and reduction of expression in the dox-off strain, both having bands with the expected size of 22 kDa (Figure 4.17A). In a shorter time-course to determine the kinetics of induction or loss of expression (0-6 hrs) where a treatment of 10 μg/mL doxycycline was supplied in HL5 in cell shaking suspension (Figure 4.17B), the dox-on strain (310_Rheb) had an obvious increase of Rheb_FLAG expression which reached the maximum around 4 hrs to 6 hrs. However, the dox-off strain (309_Rheb) did not show an obvious decrease in protein levels within 6 hrs, possibly because Rheb_FLAG is quite stable and protein degradation takes time. This indicated that dox-on cells are more ideal to mediate a change in Rheb levels in a short preincubation time with doxycycline. It was also worth mentioning that there was some detectable Rheb_FLAG expression in the dox-on strain in the absence of doxycycline (Figure 4.17B), suggesting that the control of Rheb_FLAG expression by doxycycline-regulated vectors is not very tight. Overall, both dox-on and dox-off Rheb_FLAG OE strains were controllable in a doxycycline-dependent manner in growth cultures and expression was maintained during the first hour following the onset of development.

A



B

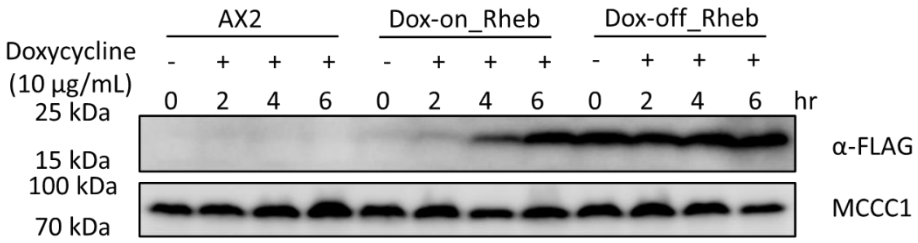


Figure 4.17. Doxycycline-regulated expression of Rheb_FLAG. Western blotting experiments were performed to detect expression of Rheb_FLAG (expected size: 22 kDa) in doxycycline regulatable strains, 309_Rheb_FLAG (Dox-off_Rheb) and 310_Rheb_FLAG (Dox-on_Rheb), and AX2 as negative control with no FLAG expression. (A) 1×10^5 log-phase cells were seeded into a 6-well plate and grown for 3 days in HL5 with or without 10 µg/mL doxycycline. Then, from each condition, 2×10^6 cells were harvested and lysed in 2× Laemmli buffer and boiled for 95 °C, 6 min. The whole cell lysates were used for western blots. N = 2. (B) Log-phase cells were incubated in shaking suspension in HL5 medium with or without 10 µg/mL doxycycline at 22°C, 220 rpm. 2×10^6 cells were taken from the suspension every 2 hrs and whole cell lysates were harvested before running western blots. N = 2. Antibodies used in the blots were: α-FLAG (1:1000, Sigma, #F7425), MCCC1: Loading control (1:1000). One representative blot for each experiment, N = 2.

4.3.3.2.3 Characterization of Rheb_FLAG overexpressing strains and construction of mutated Rheb_FLAG_E40K strain

To investigate whether overexpressing Rheb can alter mTORC1 activity, the dox-on_Rheb_FLAG OE strain was used. Phosphorylation levels of 4E-BP1 in AX2 and dox-on_Rheb_FLAG OE strains at the onset of development were assessed using western blotting. However, different batches of developing samples, dox-on, dox-off or even AX2 control cells were not consistent in phospho-4E-BP1 level (data not shown). As these results were not interpretable, constructing a constitutively active version of Rheb to increase the overexpression activity could be one solution. It has been reported that in mammalian models

such as Chinese hamster ovary (CHO) cells, mutating the Rheb sequence at specific sites E40K or T23M generates a supposedly constitutively active version of Rheb which then promotes the rate of protein synthesis as well as recombinant protein production and secretion in the ER (De Poi et al., 2021). Comparison of the protein coding sequences of Rheb orthologues in several organisms revealed a high level of conservation including the amino acid residues of interest: E40 and T23 (Figure 4.18).

A construct to drive expression of a potentially constitutively active Rheb was generated using site-directed mutagenesis from wildtype Rheb_FLAG cDNA sequence (Figure 4.19A). In the intermediate vector pJET1.2_Rheb, site-directed mutagenesis was performed to create two constitutively active constructs: T23M and E40K. Using non-overlapping primers, the mutation of interest E40K was achieved by replacing from **G**AA (glutamic acid) in the wildtype Rheb coding sequence to **A**AA (lysine) codon, while mutating T23M required a codon change from A**CA** (threonine) to A**TG** (methionine). The sequencing results showed that E40K was successfully mutated in Rheb_FLAG cDNA, while T23M construct did not have a successful mutation on sequencing (data not shown), so this was taken no further. The mutated Rheb_FLAG_E40K coding sequence was cloned into the dox-on vector pDM310 (dox-on_Rheb_FLAG_E40K). Following the generation of a pool of transformed cells, western blotting experiments were performed to confirm whether Rheb_FLAG expression is maintained in the dox-on_Rheb_FLAG, dox-on_Rheb_FLAG_E40K and dox-off_Rheb_FLAG cells at the early onset of development for one hour. Cells were exposed to either 10 μg/mL doxycycline or not for 6 hrs prior to one-hour starvation (Figure 4.19B). During starvation, both dox-on cells with doxycycline induction and dox-off cells without doxycycline treatment express Rheb_FLAG for the first hour of development. To verify the developmental phenotypes of Rheb_FLAG OE strains, nitrocellulose filter development of dox-on and dox-off strains were performed (Figure 4.19C and D). AX2 and dox-on strains were exposed to 10 μg/mL doxycycline throughout the development, while relatively smaller fruiting bodies were observed following development of dox-on_Rheb_FLAG_E40K strain (Figure 4.19C). Figure 4.19D showed that AX2 and dox-off strains were developed without doxycycline treatment. All strains showed similar developmental timing as in AX2 cells.

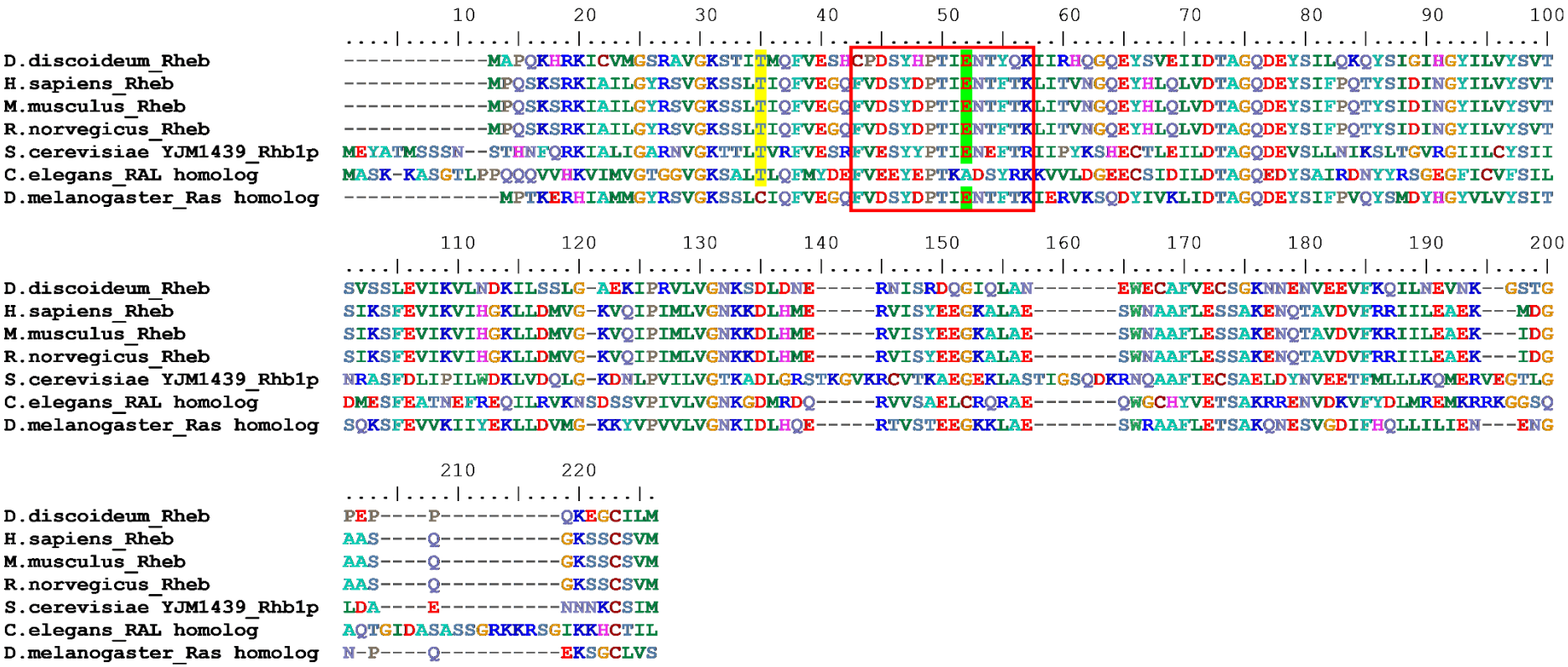
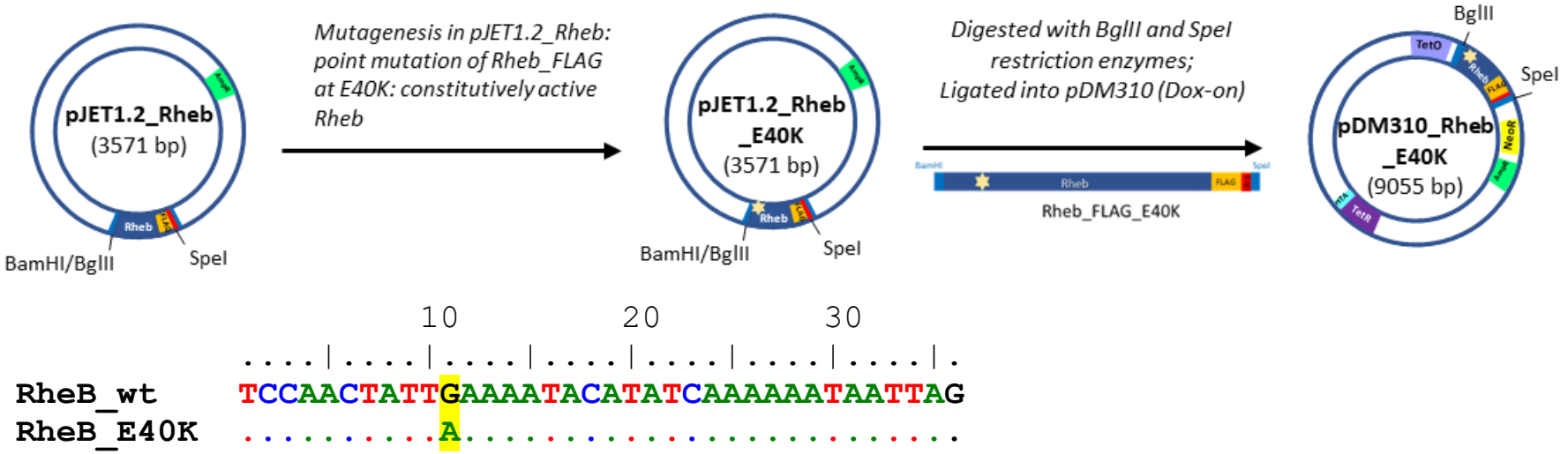
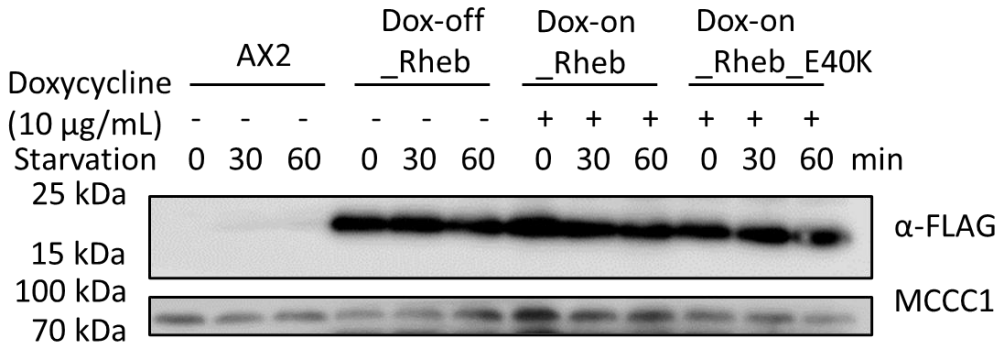


Figure 4.18. Alignment of Rheb orthologues in different species. GTP-binding protein Rheb sequences from *Dictyostelium* (*Dictyostelium discoideum*, GenBank: EAL69022.1), mouse (*Mus musculus*, NCBI ref seq: NP_444305.2), rat (*Rattus norvegicus*, NCBI ref seq: NP_037348.1) and yeast (Saccharomyces cerevisiae, GenBank: AJQ34567.1) contain the conserved threonine (T23, highlighted in yellow) and glutamic acid (E40, highlighted in green) residues of interest. Fruit flies (*Drosophila melanogaster*, NCBI ref seq: NP_730950.2) only have the conserved glutamic acid residue while worms (*Caenorhabditis elegans*, NCBI ref seq: NP_001254867.1) only have the conserved threonine residue. Clustal Omega and BioEdit were used to generate and plot the alignment results. Sequences in red box indicates the effector domain of Rheb (reviewed by (Parmar and Tamanoi, 2010)).

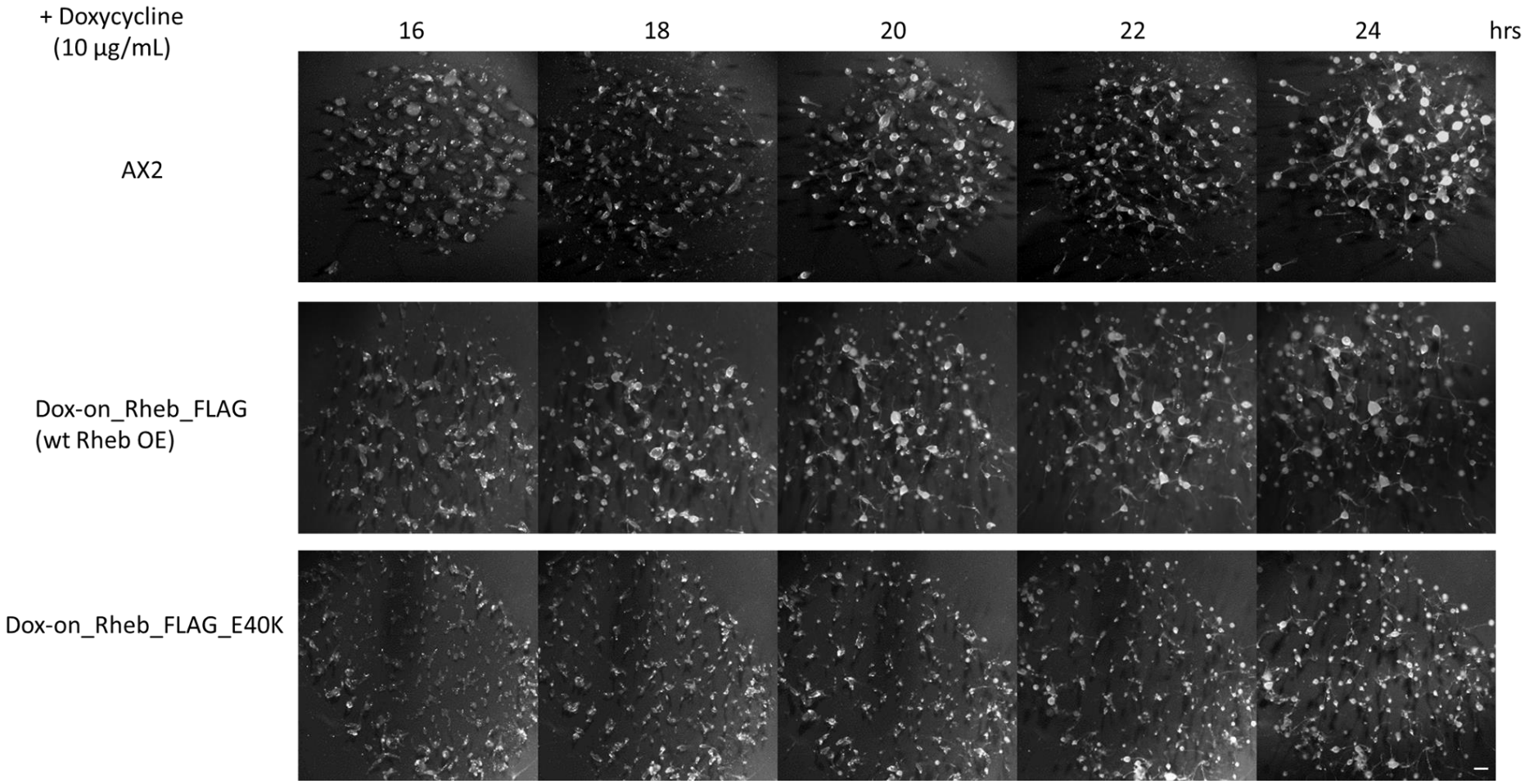
A


pJET1.2_Rheb
(3571 bp)
Rheb
FLAG
BamHI/BglII
SpeI
Mutagenesis in pJET1.2_Rheb:
point mutation of Rheb_FLAG
at E40K: constitutively active
Rheb
pJET1.2_Rheb
_E40K
(3571 bp)
Rheb
FLAG
BamHI/BglII
SpeI
Digested with BglII and SpeI
restriction enzymes;
Ligated into pDM310 (Dox-on)
Rheb
FLAG
Rheb_FLAG_E40K
BglII
SpeI
pDM310_Rheb
_E40K
(9055 bp)
TetO
Rheb
FLAG
NeoR
TetR
10
20
30
RheB_wt TCCAACTATTGAAAATACATATCAAAAAATAATTAG
RheB_E40K ....A.....................

B


Doxycycline
(10 µg/mL)
Starvation
AX2
Dox-off
_Rheb
Dox-on
_Rheb
Dox-on
_Rheb_E40K
- - - - - - + + + + + +
0 30 60 0 30 60 0 30 60 0 30 60 min
25 kDa
15 kDa
100 kDa
70 kDa
α-FLAG
MCCC1

C


+ Doxycycline
(10 µg/mL)
16
18
20
22
24
hrs
AX2
Dox-on_Rheb_FLAG
(wt Rheb OE)
Dox-on_Rheb_FLAG_E40K

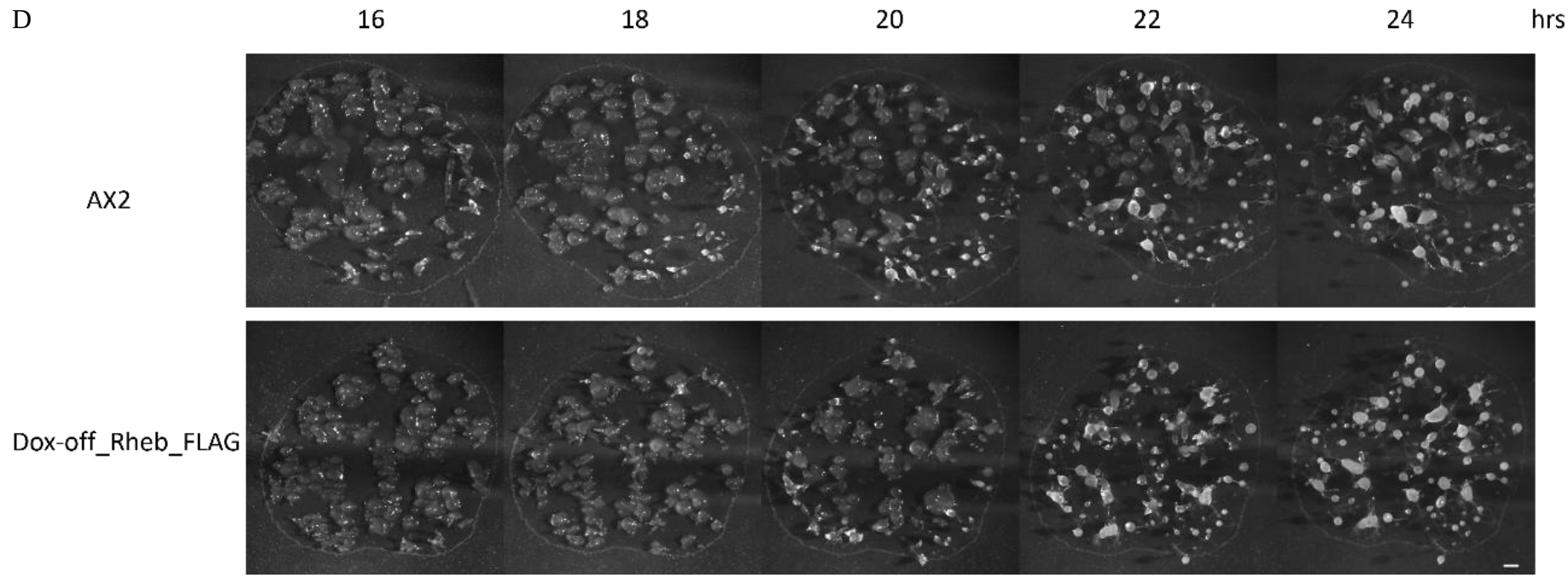


Figure 4.19. Construction of a Rheb_FLAG_E40K strain and verification of development of Rheb_FLAG OE strains. (A) A schematic representation of cloning strategy for Rheb_FLAG_E40K in the dox-on (pDM310) background is shown in upper panel. Site-directed mutagenesis kit (NEB, E0554S) using non-overlapping primers designed with NEBaseChanger online tool were used to mutate Rheb_FLAG in the intermediate cloning vector pJET1.2_Rheb. Lower panel shows the alignment of sequencing result: Rheb_E40K substituting the wildtype codon **G**AA (glutamic acid) to **A**AA (lysine). (B) Doxycycline-regulated expression of Rheb_FLAG during development in dox-off_Rheb_FLAG strain, dox-on_Rheb_FLAG strain and mutated dox-on_Rheb_FLAG_E40K strain. Log-phase cells were pre-incubated in HL5 with or without 10 µg/mL doxycycline for 6 hrs before triggering one-hour starvation in developmental buffer HKC. Whole cell lysates were collected every 30 mins and analysed on western blots as described in the legend to Figure 4.6. Antibodies used in the blots were: α-FLAG (1:1000), MCCC1: Loading control (1:1000). One representative blot for each experiment, N = 2. (C) Development of dox-on_Rheb_FLAG OE strains (OE of wt Rheb_FLAG and Rheb_FLAG_E40K, N = 2) and (D) dox-off_Rheb_FLAG (no doxycycline, N = 1). Dox-on_Rheb_FLAG strains were growing in HL5 with 10 µg/mL doxycycline for 24 hrs to log phase, then were incubated in KK2 with 10 µg/mL doxycycline throughout development on nitrocellulose membrane for 24 hrs in a 12-well plate at the density of 5×10^7 cells/mL, while dox-off_Rheb_FLAG cells were treated the same but without doxycycline treatment during growth and development. Images were taken in the indicated time points. Scale bar: 1 mm.

To assess the mTORC1 activity in dox-on_Rheb_FLAG_E40K which was predicted to have constitutively active Rheb overexpression, phospho-4E-BP1 levels were analysed by western blot. The pattern of phosphorylation of 4E-BP1, again, remained inconsistent between different sample batches (two example blots shown in Figure 4.20). Due to the weak signals detected in the western blots, it is difficult to see whether dox-on_Rheb_FLAG_E40K increased mTORC1 activity. Given that western blotting with phospho-4E-BP1 (T37/46) were inconsistent in different batches of developing Rheb OE cells, alternative approaches were used to assess mTORC1 activity.

To investigate the activity of mTORC1 in Rheb OE strains with an alternative method, rapamycin sensitivity was assessed in growing cells, as reduced sensitivity to rapamycin in cell growth has been shown to correlate with increased phospho-4E-BP1 level at early onset of development (Chang et al., 2020). As 10 μg/mL doxycycline was used to induce the expression of Rheb_FLAG in dox-on strains, it is important to know whether addition of doxycycline in HL5 growth medium affects the rapamycin-inhibition growth assay. Figure 4.21A showed that AX2 cells with and without doxycycline had no difference in growth inhibition when exposed to 0, 50 or 100 nM rapamycin for 24 hrs and 48 hrs. This suggests that the presence of doxycycline did not affect rapamycin inhibition of AX2 cell growth. Using the same method, doxycycline-induced Rheb_FLAG OE strains, wt Rheb_FLAG and Rheb_FLAG_E40K were slightly less sensitive to rapamycin, which is more apparent at 48 hrs (grey bars) (Figure 4.21B). Also, while comparing the two Rheb_FLAG OE strains, OE of Rheb_FLAG_E40K led to slightly less inhibition than OE of wt Rheb_FLAG at 24 hrs but this effect disappeared by 48 hrs (Figure 4.21B).

In rapamycin-induced aggregation assays, doxycycline-induced Rheb overexpression in dox-on strains had a lower aggregation score compared to AX2 and the dox-on strains without doxycycline induction (Figure 4.21C). For example, with 100 nM rapamycin treatment, AX2, dox-on_Rheb_FLAG and Rheb_FLAG_E40K without doxycycline activation (-Dox) had a score of 2.3 ± 0.3, 2.0 ± 0.6 and 1.7 ± 0.7, while doxycycline-treated (+Dox) dox-on strains with OE of Rheb_FLAG or Rheb_FLAG_E40K had a score of 1.0 ± 0.0. In terms of the comparison between dox-on Rheb_FLAG OE strains with +Dox induction, both have lower

scores compared to -Dox conditions or AX2 cells. However, at 500 nM rapamycin, dox-on_Rheb_FLAG_E40K in +Dox condition had subtly fewer aggregating events (1.0 ± 0.0) than that observed in dox-on_Rheb_FLAG (1.3 ± 0.3), but the difference was not statistically significant. To sum up, during growth and aggregation induced by rapamycin treatment, dox-on Rheb OE strains which overexpressed wt Rheb_FLAG and mutated Rheb_FLAG_E40K were less sensitive to rapamycin, which is consistent with their mTORC1 activities being relatively high compared to AX2 cells. The mutated dox-on_Rheb_FLAG_E40K strain is quite similar to dox-on_Rheb_FLAG strain in terms of rapamycin sensitivity but might potentially be slightly less sensitive to high rapamycin concentrations (e.g. 500 nM) in the 24-hr treatment in growth media.

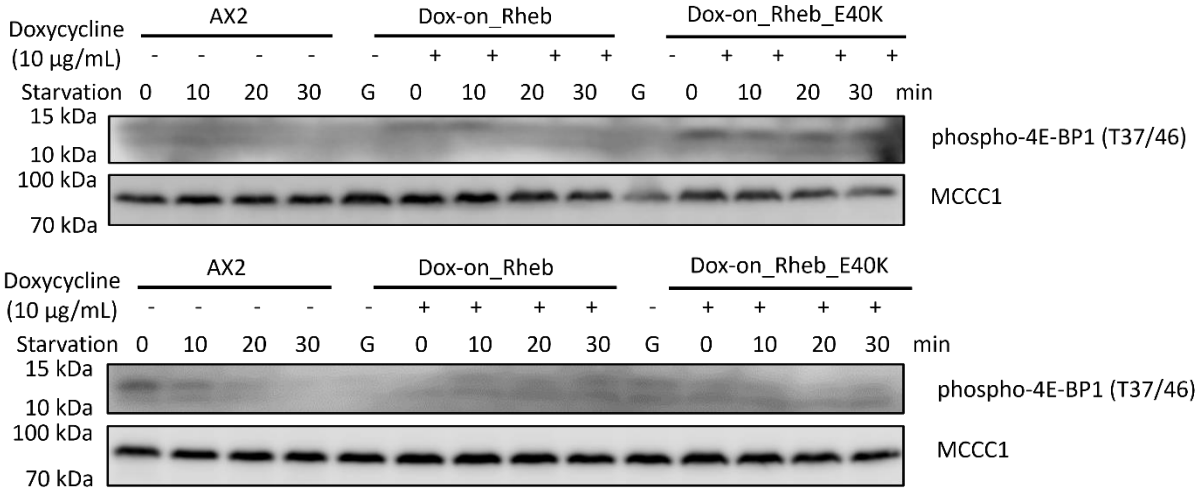


Figure 4.20. mTORC1 pathway activity of dox-on_Rheb_FLAG and dox-on_Rheb_FLAG_E40K investigated by phosphorylation levels of 4E-BP1 and AMPK. Two example blots from 3 repeats blotting with phospho-4E-BP1 (T37/46). Cells growing exponentially were harvested from HL5 medium and developed in HKC developmental buffer triggering starvation. Whole cell lysates were collected in both growing stage (G) and at 10-min intervals following starvation as described in the legend to Figure 4.6. α-FLAG (1:1000). Antibodies: phospho-4E-BP1 (T37/46) (1:1000). MCCC1: Loading control (1:1000).

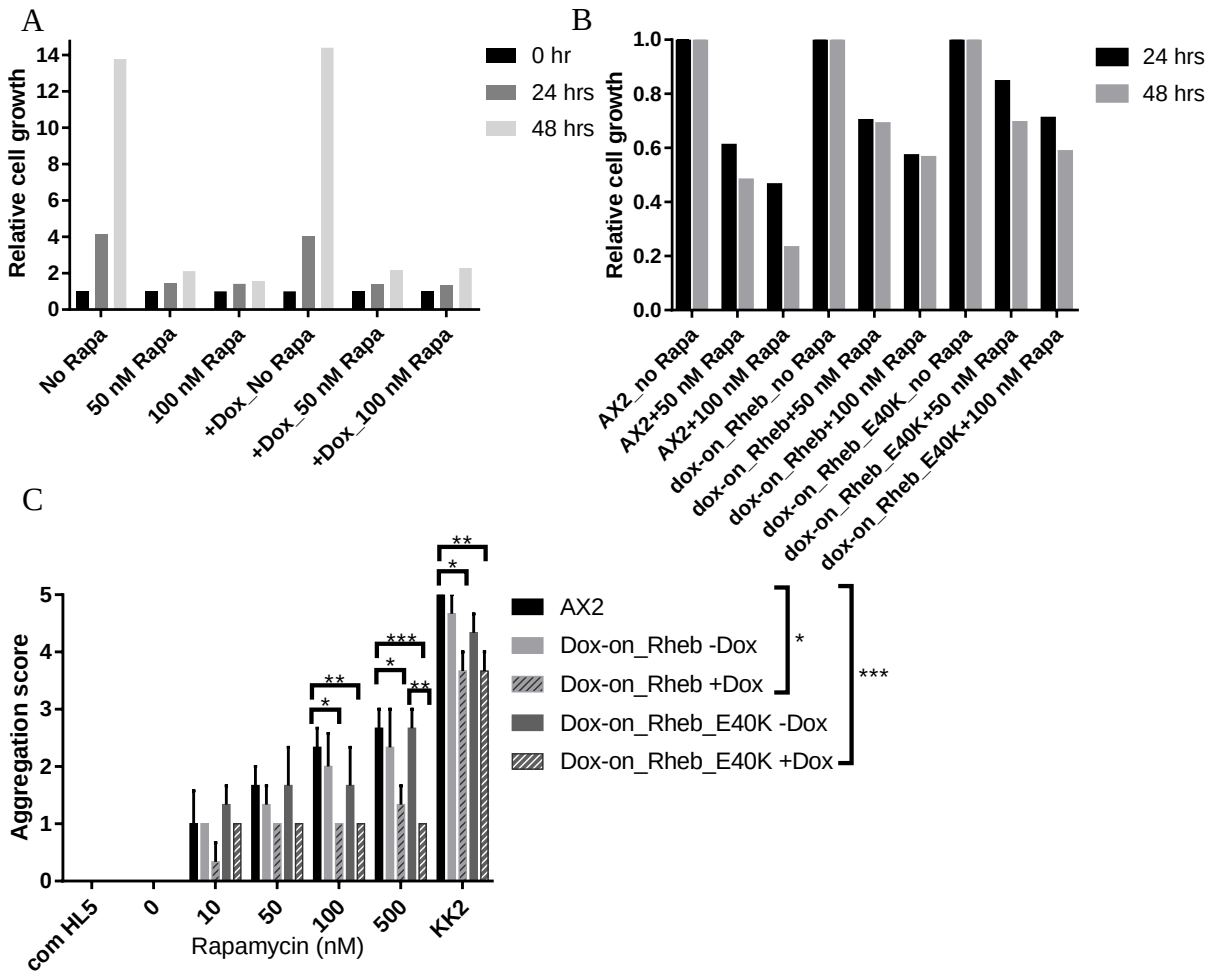


Figure 4.21. Rapamycin sensitivity of Rheb_FLAG OE strains during growth and early development. (A) Rapamycin-inhibited growth assays: vegetatively growing AX2 cells at a density of 5×10^5 cells/mL were pre-cultured with or without 10 μg/mL doxycycline for 24 hrs and grown to log phase. After washing with KK2 twice, cells were resuspended to 5×10^5 cells/mL in HL5 (0 hr) with 0 nM (No Rapa, DMSO control), 50 nM and 100 nM rapamycin, in the presence or absence of 10 μg/mL doxycycline throughout the assay. The number of cells were counted over 2 days in shaking suspension at 22°C at 24 and 48 hrs and then normalized to the untreated groups (No Rapa) which were defined as 1. First three groups: no doxycycline was added before or during the growth assay. Last three groups (+Dox): cells were incubated with 10 μg/mL doxycycline before the assay for 24 hrs and throughout the assay. N = 1. (B) Rapamycin-inhibited growth assays using AX2 and dox-on Rheb_FLAG OE strains. AX2, dox-on_Rheb_FLAG and dox-on_Rheb_FLAG_E40K were all incubated in 10 μg/mL doxycycline for 24 hrs before the assay and throughout the assay. Method of this experiment was performed as described in (A). One representative data set, N = 3. (C) Rapamycin-induced aggregation assays were performed in AX2, dox-on_Rheb_FLAG and dox-on_Rheb_FLAG_E40K cells. This method was described as the legend to Figure 4.7. Cells were pre-incubated in HL5 with or without 10 μg/mL doxycycline for 24 hrs (+Dox: diagonal line-patterned bars; -Dox: solid bars). Exponentially growing cells were washed and plated into 12-well plates at a density of 1.4×10^6 cells/mL in half-strength HL5 medium containing various concentrations of rapamycin or DMSO control. KK2 group (developmental buffer) and full-strength HL5 (complete HL5) group were positive and negative controls accordingly, supplied with DMSO as vehicle control. N = 3. Mean ± S.E.M. Two-way ANOVA: *: $P < 0.05$; **: $P < 0.01$; ***: $P < 0.001$.

4.3.3.2.4 Construction and characterization of a Rheb gene disrupted strain (*rheb*$^-$)

To further investigate the role of Rheb in activating mTORC1 activity and the correlation between mTORC1 activity changed by Rheb and cell fate decisions, a gene disrupted *rheb*$^-$ mutant strain was made via a CRISPR/Cas9 method using the pTM1285 all-in-one CRISPR vector (Sekine et al., 2018) (described in Chapter 3, Figure 3.10). Two sets of complimentary sgRNA oligonucleotide pairs were designed: YW55+YW56 and YW57+YW58, and the insertion of into the vector confirmed by PCR (Figure 4.22). AX2 cells were co-transfected with both gene disruption vectors harbouring different guide RNAs and transiently selected in G418 for three days before plating onto SM agar plates in serial dilutions for isolating single colonies after about 5 days. 13 single colonies of potential *rheb*$^-$ mutants were picked from agar plates and their genomic DNA was extracted for screening to identify frameshift mutations. Three out of 13 candidates were confirmed to have insertions and deletions by sequencing results, causing frameshifts compared to the wildtype *rheb* coding sequence (Figure 4.23A). The amino acid sequences translated from these mutants were aligned against the wildtype Rheb, showing that the frameshift mutations generated several pre-mature stop codons and thus producing truncated and therefore non-functional proteins (Figure 4.23B).

These *rheb*$^-$ mutants I-12, I-10, I-3 were further purified into independent clones via serial dilutions and confirmed by sequencing a PCR fragment of the *rheb* gene again. Following total RNA extraction and cDNA synthesis, at the mRNA transcript level, the *rheb*$^-$ independent clones had lower *rheb* mRNA levels compared to the AX2 *rheb* transcript level analysed by semi-quantitative RT-PCR, with single bands of 558 bp as expected (Figure 4.23C). The cDNA endogenous control *ig7* has single bands with the expected size of 190 bp, confirming no gDNA contamination as YW29 and YW30 primers span an intron (547 bp) and could have generated a 737-bp PCR product if amplified from gDNA template (Figure 3.4C). Even though there is still some *rheb* mRNA in *rheb*$^-$ strains, based on the sequencing data, premature stop codons were introduced by frameshift mutations during CRISPR genome editing event, possibly leading to nonsense-mediated mRNA decay of remaining transcripts (Figure 4.23B). The developmental timing and structures of two of the independent clones (*rheb*$^-$_I_12_1 and *rheb*$^-$_I_3_1) were similar to AX2 cells (Figure 4.23D and 4.23E).

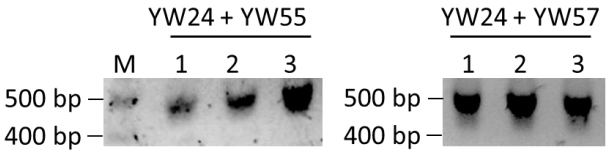
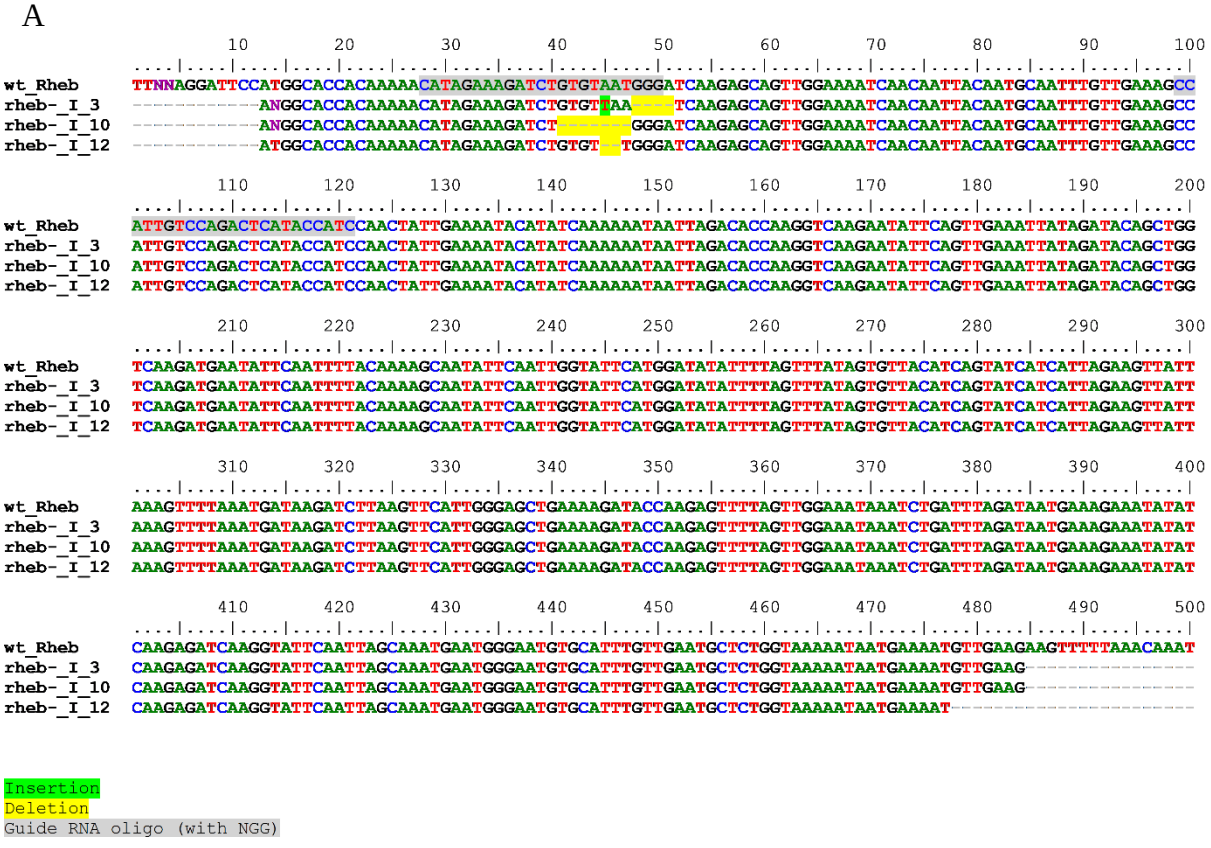


Figure 4.22. Verification of sgRNA insertion into pTM1285 vector for CRISPR-Cas9 mediated *rheb* gene disruption. Forward primer YW24 (upstream of sgRNA) and reverse primer YW55 or YW57 (oligo in reverse direction) were used to perform PCR experiments, generating a 500-bp band, visualised on 1% EtBr agarose gel. YW24 is a forward primer annealing to the Cas9-GFP coding sequence upstream of sgRNA and the reverse guide RNA oligonucleotides (YW55 and YW57) act as reverse primers. M: Quick-load 100 bp DNA ladder (NEB).

A



B

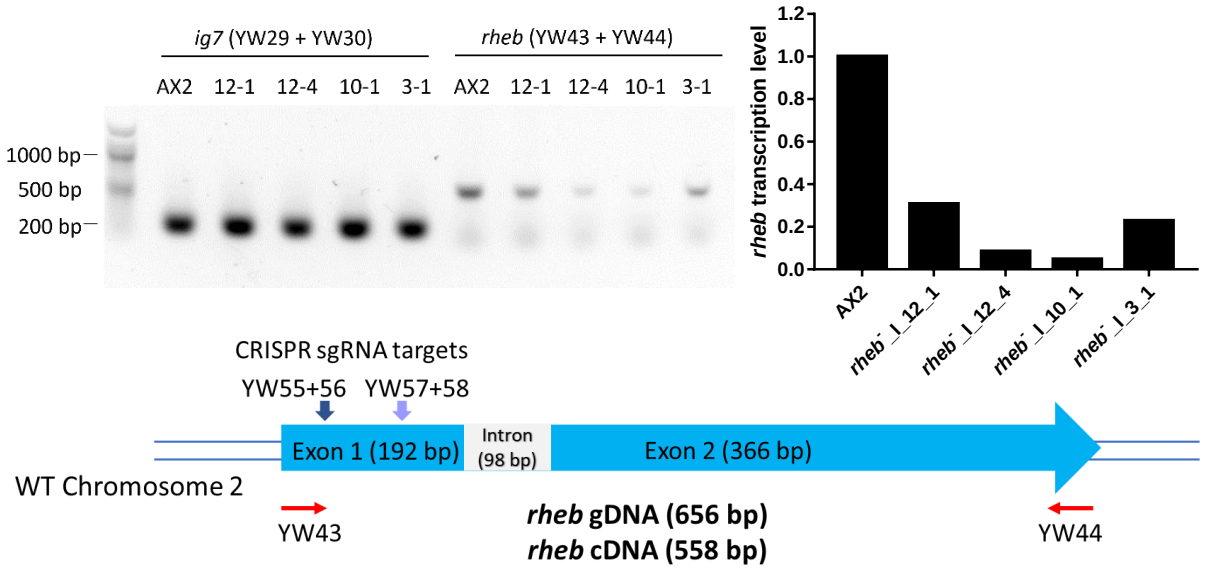
```
wt_Rheb_protein      MAPQKHRKICVMGSRAVGKSTITMQFVESHCPDSYHPTIENTYQKIIRHQGQEY----SV  56
rheb-_I_12_protein   MAPQKHRKICVGIKSSWKI-N----NYNAIC*KPLSRLIPSNY*KYISKNN*TP----RS  48
rheb-_I_10_protein   MAPQKHRKIW-DQEQLENQ-QLQCNLLKAIVQTHTIQLLKIHIKK*LDTKVKNIQLKL*I  56
rheb-_I_3_protein    MAPQKHRKICVNQEQLENQ-QLQCNLLKAIVQTHTIQLLKIHIKK*LDTKVKNIQLKL*I  57
                     *********    .             ::         :     * :  :

wt_Rheb_protein      EIIDTAGQDEYSILQKQYSIGIHGY-IL------VYSVTSVSSLEVIKVLNDKILSSLGA  109
rheb-_I_12_protein   RIFS*NYRYSWSR*IFNFTKAIFNWYSWIYFSL*CYISIIIRSY*SFK**DLKFIGS*KD  101
rheb-_I_10_protein   QLVKMNIQFYKSNIQL----------VFMD--IF*FIVLHQYHH*KLLKF*MIRS---  96
rheb-_I_3_protein    QLVKMNIQFYKSNIQL----------VFMD--IF*FIVLHQYHH*KLLKF*MIRS---  97
                     .:..   :   *                      :    : .    *  .  :: *

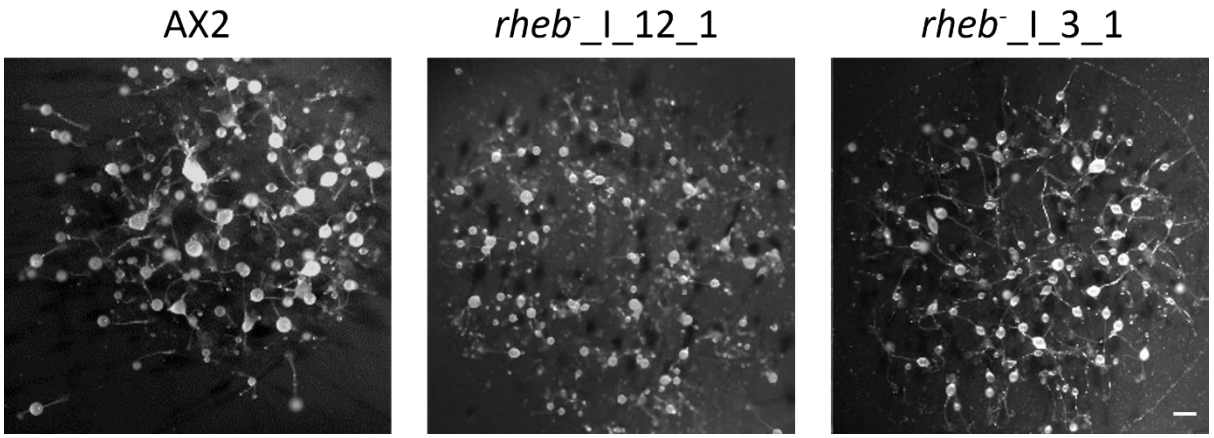
wt_Rheb_protein      EKIPRVLVGNKSDLDNERN---IS--RDQGIQLANEWECAFVECSGKNNENVEEVFKQIL  164
rheb-_I_12_protein   TKSFSWK*I*FR**KK-----YIKRSRYSISK*MG-------MCIC--*MLW-*---K--  134
rheb-_I_10_protein   --*VHWELKRYQEF*LEINLI*IMKEIYQEIKVFN-------*QMNGNVHLL-NALVKIM  142
rheb-_I_3_protein    --*VHWELKRYQEF*LEINLI*IMKEIYQEIKVFN-------*QMNGNVHLL-NALVKIM  143
                                 *     .  :  .                        :

wt_Rheb_protein      NEVNKGSTGPEPPQKEGCILM*  185
rheb-_I_12_protein   -**K------------------  135
rheb-_I_10_protein   KMLK------------------  146
rheb-_I_3_protein    KMLK------------------  147
                        :
```

C



D



E

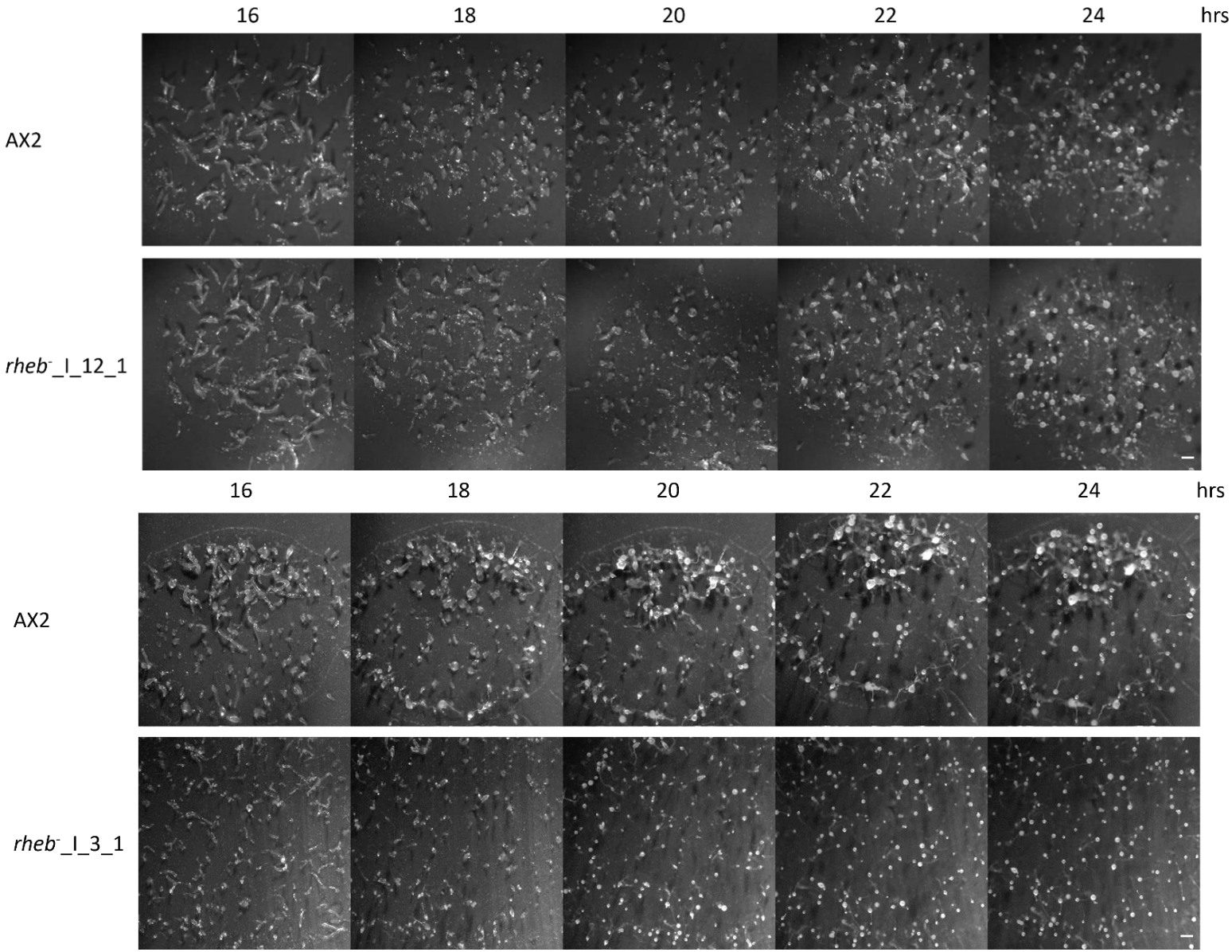


Figure 4.23. Verification of CRISPR/Cas9-mediated gene disrupted *rheb*$^-$ strains. (A) The sequencing results from PCR products of gDNA from *rheb*$^-$ mutants aligned to wildtype Rheb sequence. (B) Amino acid sequence alignment of *rheb*$^-$ mutant and wildtype Rheb proteins. Clustal Omega and BioEdit software were used to generate alignment results. Premature stop codons are highlighted in red. (C) Assessing transcript level of Rheb in AX2 and *rheb*$^-$ independent clones. Upper left panel: Total RNA from parental AX2 and single clones of *rheb*$^-$_I_12 (12-1 and 12-4), *rheb*$^-$_I_10 (10-1) and *rheb*$^-$_I_3 (3-1) were extracted with Trizol and purified for cDNA synthesis. Reverse transcription PCR (RT-PCR) was performed to amplify Rheb coding sequences using primers YW43 and YW44 along with the endogenous control *ig7* using primers YW29 and YW30 for 35 PCR cycles. The products were analysed on a 1% EtBr agarose gel with the marker Quick-load 100 bp DNA ladder (NEB). Upper right panel: the *rheb* PCR product levels were quantified by normalizing the *rheb* band intensity in comparison with *ig7* control with ImageJ software. Lower panel: A schematic gene map of the wildtype *rheb* in chromosome 2 and primer positions. The gene map of *ig7* endogenous control is shown in Figure 3.4D. (D, E) Development of *rheb*$^-$ CRISPR/Cas9 strain on nitrocellulose membranes. Exponentially growing cells were harvested and washed in KK2 twice. Cells then were resuspended to the density of 5×10^7 cells/mL and 10 µL of cells were plated onto the nitrocellulose membrane and three layers of Whatman filter paper soaked in 200 µL KK2 in 12-well plates. (D) Fruiting bodies structures from AX2 and two clones of *rheb*$^-$ were observed in the 24 hrs time point. (E) Images from different time points during development were taken at the brightfield microscope. Scale bar: 1 mm. Two independent clones were tested: *rheb*$^-$_I_12_1 (N = 3) and *rheb*$^-$_I_3_1 (N = 2).

4.3.3.2.5 Investigation of mTORC1 activity in *rheb*$^-$ strain

mTORC1 activity in *rheb*$^-$ cells was characterized using western blotting with phospho-4E-BP1 and rapamycin sensitivity assays in growth or under-buffer development. The phosphorylation of 4E-BP1 in *rheb*$^-$ cells remained unchanged throughout the first hour of development, while the phosphorylation level in AX2 cells decreased (Figure 4.24A). However, when comparing phospho-4E-BP1 levels in growth before the start of the development (0 min), *rheb*$^-$ cells had a lower phosphorylation level (14.9% ± 5.4%) than in AX2 cells (defined as 100%) and overall levels at all time points were low as well (right panel, Figure 4.24A). The rapamycin sensitivity growth assay showed that the rapamycin sensitivity of the *rheb*$^-$ cells was similar to AX2 at 24 hrs and 48 hrs (Figure 4.24B). However, when the degrees of rapamycin-induced aggregation were assessed at 22 hrs, *rheb*$^-$ cells were prone to aggregation in half-strength HL5 medium at lower concentrations of rapamycin compared with AX2 (Figure 4.24C). For example, at 50 nM rapamycin treatment, AX2 cells had an aggregation score of 1.0 ± 0.0 compared to 3.0 ± 0.6 for *rheb*$^-$ cells. In conclusion, although *rheb*$^-$ null cells had similar cell growth inhibition in response to rapamycin treatment compared to AX2 cells, *rheb*$^-$

cells were more sensitive to rapamycin induction of aggregation in half-strength HL5.

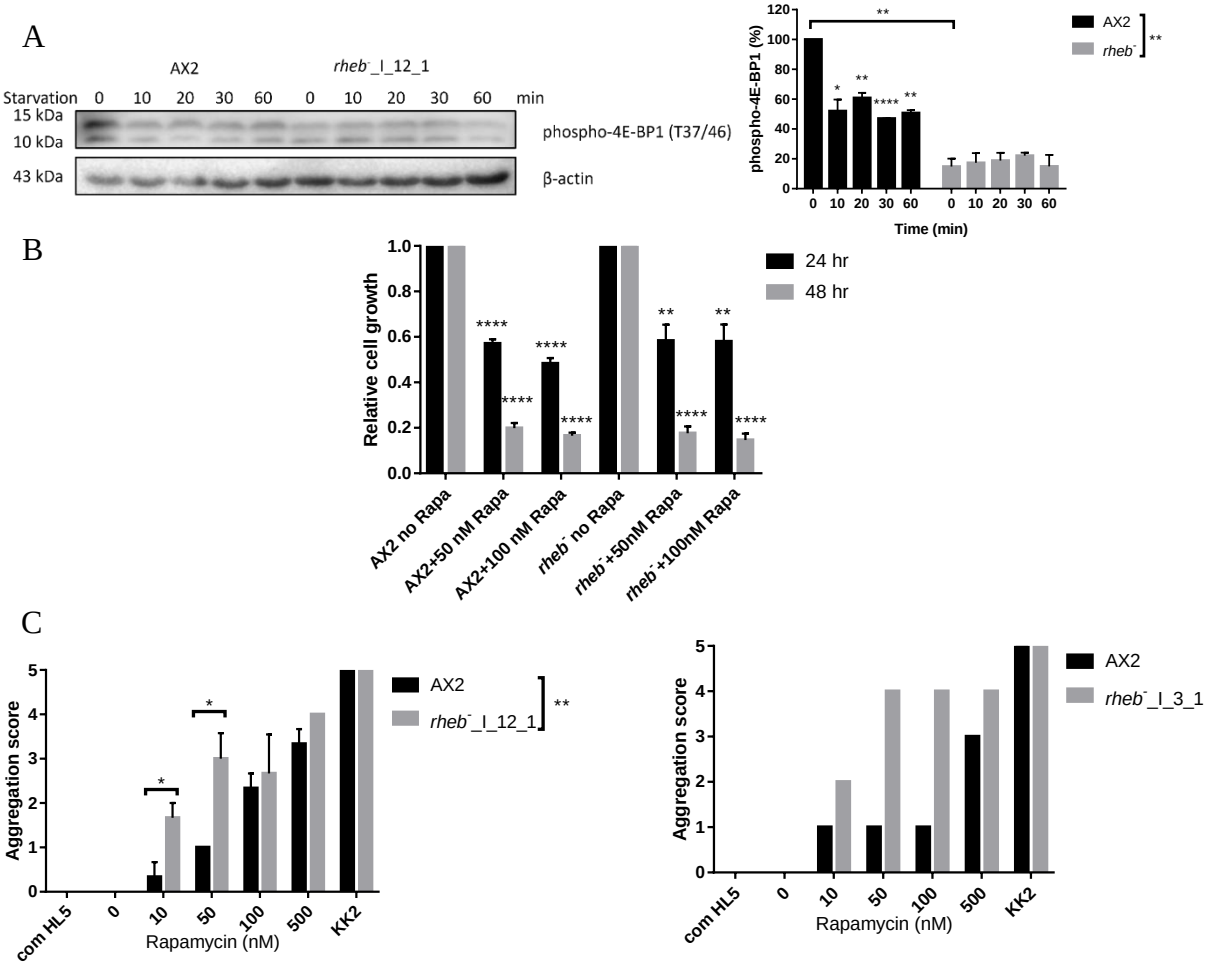


Figure 4.24. Assessing mTORC1 pathway activity of *rheb*⁻ strain. (A) Left panel: western blots of phospho-4E-BP1 in AX2 and *rheb*⁻ (clone: *rheb*⁻_I_12_1) cells starved in developmental buffer HKC for one hour. The method and statistical analysis were described in the legend to Figure 4.6. Whole cell lysates were collected in different time points for western blotting against phospho-4E-BP1 (T37/46). Antibodies included phospho-4E-BP1 (T37/46) (1:1000) and β-actin which was used as loading control (1:10000, Santa Cruz Biotechnology, sc-47778). N = 2. Mean ± S.E.M. Student *t*-test (two-tailed): *: P < 0.05; **: P < 0.01; ****: P < 0.0001. Right panel: Quantification of two repeats of western blots described in (A). Phosphorylation levels of 4E-BP1 in both AX2 and *rheb*⁻ were normalized to 0 min time point (in growth) of AX2 defined as 100%. Student *t*-test (two-tailed): *: P < 0.05; **: P < 0.01. Two-way ANOVA: **: P < 0.01. (B) Rapamycin sensitivity in growth of *rheb*⁻ (clone: *rheb*⁻_I_12_1). This rapamycin-induced growth assay was performed as described in the legend to Figure 4.14. N = 3. Mean ± S.E.M. Student *t*-test (two-tailed): **: P < 0.01; ****: P < 0.0001. (C) AX2 and *rheb*⁻ strains were assessed in rapamycin-induced aggregation assays. This aggregation assay was performed as described in the legend to Figure 4.7. Left panel: clone: *rheb*⁻_I_12_1 was assessed in rapamycin-induced aggregation assays, N = 3. Two-way ANOVA: **: P < 0.01. Right panel: an independent clone *rheb*⁻_I_3_1 was tested once to confirm the phenotype, N = 1.

4.3.3.3 Cell fate decisions in genetic mutants involved in the mTORC1 pathway

4.3.3.3.1 Loss of AMPK leads to a stalk cell fate tendency

The increased mTORC1 activity in growing *ampk*$^-$ cells, led to the prediction that *ampk*$^-$ cells would also have a stalk cell fate bias compared to AX2 and AX3 parental cells. Mixing experiments of AX2 and *ampk*$^-$ cells (Figure 4.25A) as well as AX3 and *ampk*$^-$ cells (Figure 4.25B) confirmed this. For example, when 50% *ampk*$^-$ cells were labelled with CellTracker and mixed with 50% unlabelled AX2, the final proportion of fluorescent spores which were originated from *ampk*$^-$ were less than half of the total spores (31.6% ± 10.6%), whereas when 50% wildtype cells were labelled, more than 50% of the total spores had green fluorescence (78.6% ± 2.3%). The same trend of fewer spores produced from *ampk*$^-$ cells was also revealed in the 10%L/90%UL mixing ratio (Figure 4.25A), and this trend is consistent with the observation in the mixing experiments of AX3 and *ampk*$^-$ (Figure 4.25B). These results both showed that *ampk*$^-$ cells form fewer spores in mixed aggregates.

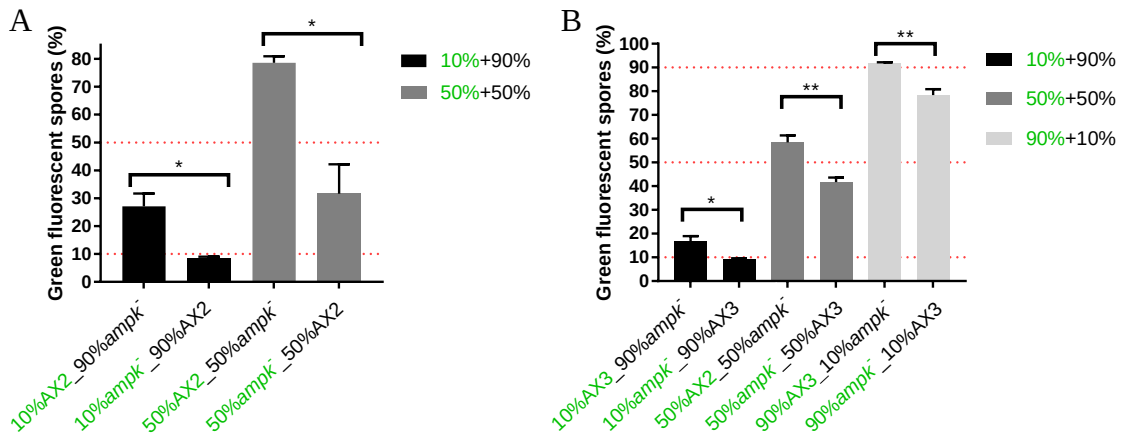


Figure 4.25. Cell fate tendency in *ampk*$^-$ compared to AX2 and AX3 cells. Mixed development of *ampk*$^-$ and AX2 (A, N = 3) or AX3 (B, N = 3) cells in chimeric mixing experiments were performed. The experiments were carried out as described in the legend to Figure 3.4A. Mean ± S.E.M. Student *t*-test (two-tailed): *: P < 0.05; **: P < 0.01.

4.3.3.3.2 Loss of Rheb in the *rheb*$^-$ strain leads to a spore cell fate bias

Cell fate assays were used to validate whether cells in the absence of functional Rheb have the opposite trend in cell fate tendency to that seen in the *ampk*$^-$ strain. Mixing experiments of AX2 and *rheb*$^-$ cells showed that *rheb*$^-$ strains tended to choose a spore cell fate when mixed with AX2 cells (Figure 4.26A and 4.26B). For instance, when 50% labelled AX2 cells mixed and

developed with 50% unlabelled *rheb*$^{-}$ (clone: *rheb*$^{-}$_I_12_1), fewer green spores from the AX2 lineage were formed (45.9% ± 0.9%). However, when 50% labelled *rheb*$^{-}$ cells were developed with 50% unlabelled AX2, more green spores were generated from *rheb*$^{-}$ (51.8% ± 0.7%) (Figure 4.26A). When using a monolayer assay to assess stalk cell fate tendency, the *ecmB*-GAL pre-stalk marker expression induced by different concentrations of DIF-1 in the *rheb*$^{-}$ strain was less than in AX2 cells (Figure 4.26C), such as at 50 nM DIF-1 induction, AX2 cells had higher pre-stalk marker expressed (100.6% ± 1.5%) compared to *rheb*$^{-}$ (93.0% ± 2.4%). Although the changes between AX2 and *rheb*$^{-}$ strains in both assays were small, they were statistically significant. These results concluded that loss of Rheb in *rheb*$^{-}$ mutants affected cell fate decisions in cells: lack of Rheb drives cells to favour a spore cell fate.

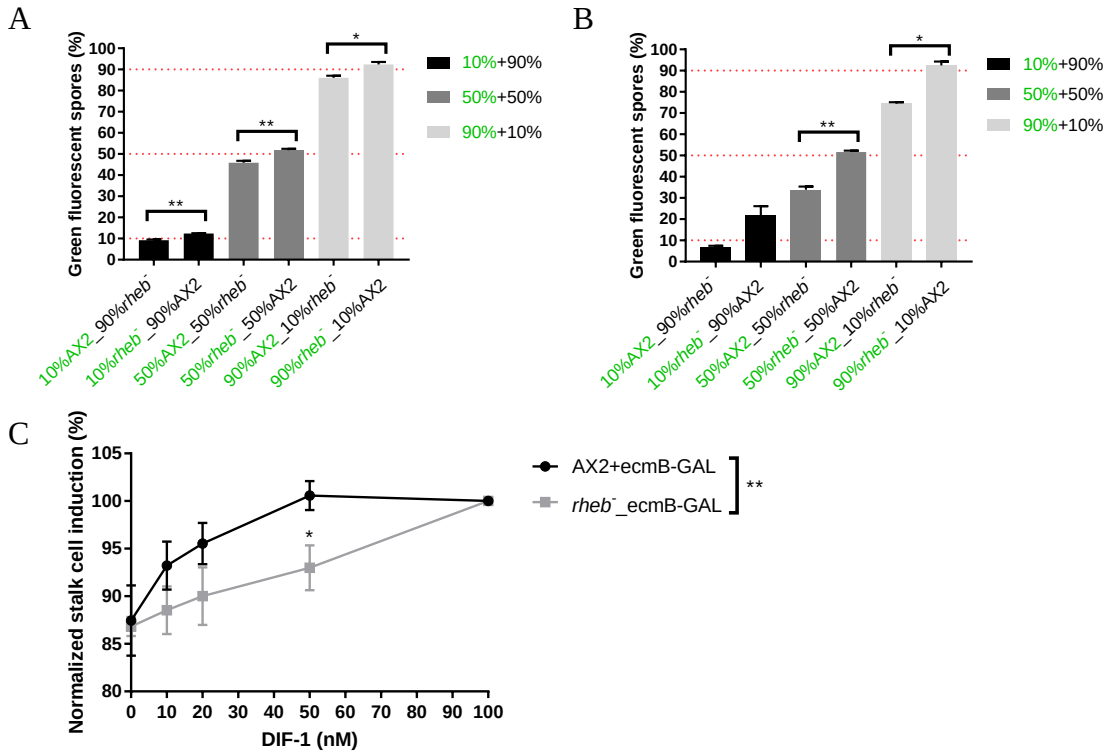


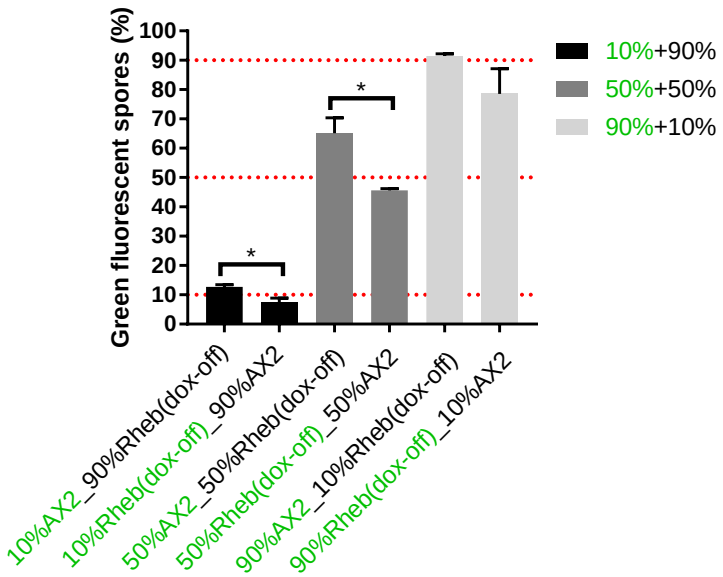
Figure 4.26. *rheb*$^{-}$ strains have a spore fate bias. In mixing experiments (A and B), AX2 or *rheb*$^{-}$ cells (A: clone: *rheb*$^{-}$_I_12_1 (N = 3) and B: clone *rheb*$^{-}$_I_3_1 (N = 2)). The method used for this experiment was performed as described in the legend of Figure 3.4A. Mean ± S.E.M. Student *t*-test (two-tailed): *: P < 0.05; **: P < 0.01. (C) Monolayer stalk induction assays of AX2 and *rheb*$^{-}$ cells (independent clone: *rheb*$^{-}$_I_12_1) were performed as described in the legend to Figure 3.5A. N = 4. Mean ± S.E.M. Two-way ANOVA: **: P < 0.01. Student *t*-test (two-tailed): *: P < 0.05.

4.3.3.3.3 Overexpressing Rheb in Rheb_FLAG OE strains results in a stalk cell fate tendency

To further investigate mTORC1 pathway activity in cell fate decisions via overexpression of Rheb, cell fate tendencies were assessed in dox-on_Rheb_FLAG OE strains. In chimeric mixing experiments, the higher proportion of green spores implied a stalk cell fate tendency in each OE strain. When AX2 and dox-off_Rheb_FLAG OE strains were developed together in 10%L/90%UL mixing ratios, 10% labelled AX2 formed 12.7% ± 0.8% spores while 10% labelled dox-off_Rheb_FLAG OE strains formed 7.6% ± 1.3% (Figure 4.27A).

Similarly, when labelled doxycycline-induced dox-on Rheb_FLAG OE strains mixed with unlabelled AX2 in 10%L/90%UL mixing ratio, fewer spores were formed from the dox-on Rheb OE strains that overexpressed wildtype Rheb (dox-on_Rheb_FLAG) (9.1% ± 0.6%) and dox-on_Rheb_FLAG_E40K (8.8% ± 0.7%) (Figure 4.27B). It was also noticed that when comparing 10% labelled AX2 mixed with 90% unlabelled dox-on Rheb OE strains, not only did AX2 cells contribute more than 10% green spores when developing with dox-on_Rheb_FLAG (10.9% ± 0.01%), but also AX2 cells seemed to contribute a higher proportion of spores when mixing with dox-on_Rheb_FLAG_E40K cells (18.4% ± 0.1%). Likewise, when 10% unlabelled AX2 cells mixed with 90% labelled dox-on_Rheb_FLAG OE cells, both Rheb OE strains made less than 90% green spores. However, WT Rheb overexpressing cells showed a small reduction in spores to 86.5% ± 1.9%, comparing to the mutated form (E40K) of Rheb overexpressing strain which showed a greater reduction to 72.9% ± 2.6%. This indicated that overexpression of Rheb_FLAG_E40K might lead to a stalkier cell fate tendency than overexpression of wildtype Rheb which already generated a stalk cell fate bias compared to AX2 cells. To summarize, the stalk cell fate biases of Rheb OE strains reported here were consistent with the results shown in the previous section, as they lead to the opposite cell fate bias to disruption of the *rheb* gene in both mixing experiments (Figure 4.26A and B) and monolayer stalk induction assay (Figure 4.26C).

A



B

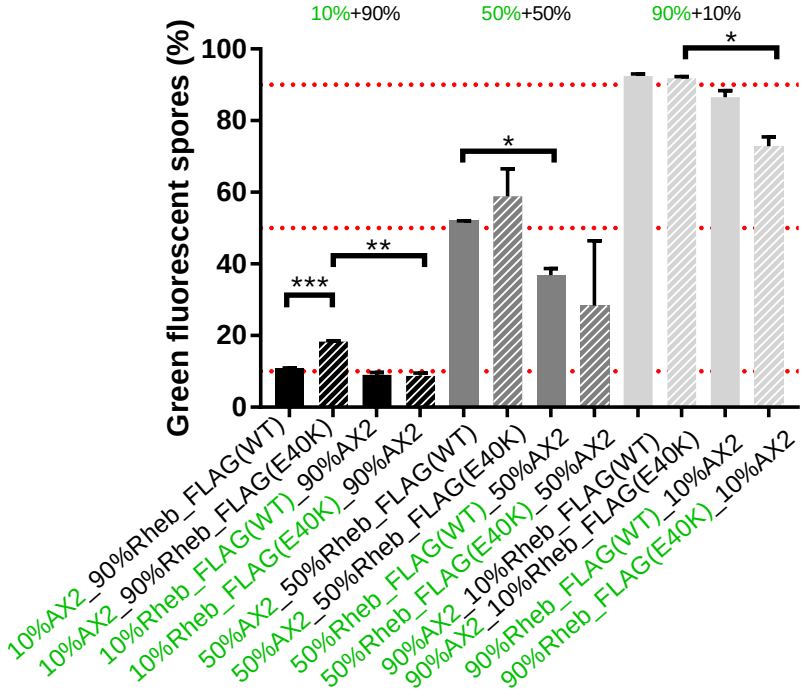


Figure 4.27. Doxycycline-regulatable Rheb_FLAG OE strains show a stalk cell bias in mixtures with AX2 cells. The mixing experiments with these strains were carried as described in the legend to Figure 3.4A. (A) Dox-off_Rheb_FLAG OE strains were mixed with AX2 for chimeric development. N = 3. Mean ± S.E.M. (B) AX2 and dox-on strains: dox-on_Rheb (wt Rheb) and dox-on_Rheb_FLAG_E40K (mutated Rheb) were all treated with 10 µg/mL doxycycline for 24 hrs before development and also with doxycycline during mixing experiments. During the experiments, starved cells in mixtures developed on the nitrocellulose filters which were soaked in KK2 buffer with 10 µg/mL doxycycline. Solid bars: AX2 mixed with OE of wt Rheb strain (dox-on_Rheb); diagonal line-patterned bars: AX2 mixed with OE of mutated Rheb strain (dox-on_Rheb_FLAG_E40K). Black bars: 10%L/90%UL; dark grey bars: 50%L/50%UL; light grey bars: 90%L/10%UL. N = 2. Mean ± S.E.M. Student *t*-test (two-tailed): *: $P < 0.05$; **: $P < 0.01$; ***: $P < 0.001$.

4.3.3.3.4 Investigation of whether mTORC1 pathway activity has a predisposition effect in cell fate bias

To further understand the roles of mTORC1 in cell fate decisions, it was important to explore whether mTORC1 pathway activity was playing a role in predisposition during growth (i.e. activity during growth and the onset of development) or it is the pathway activity later during development that influences cell fate. Previously results showed that in both the mixing assays and monolayer stalk induction assay, pre-treating cells with rapamycin for 4 hrs was sufficient to generate the bias (Figure 4.10 and 4.11). On the other hand, cells with prolonged rapamycin treatment and Rheb OE strains are expected to have altered mTORC1 activity throughout the development process. To test the effect of mTORC1 activity during development, cells were exposed to rapamycin throughout monolayer stalk induction assay rather than pre-treatment before development, and as a result, stalk marker expression in cells was increased upon induction with 50 nM or 100 nM DIF-1 (Figure 4.28). For example, when induced by 100 nM DIF-1, developing cells treated with 100 nM rapamycin had almost two-fold higher stalk marker expression (208.4% ± 0.6%) compared with those treated with 10 nM rapamycin (109.2% ± 8.8%) or no rapamycin (defined as 100%). The stalk cell fate tendency upon prolonged rapamycin treatment throughout monolayer stalk induction assay was the opposite to the 4-hrs rapamycin predisposition effect which led to a spore cell fate tendency. It is not possible to investigate this using mixing experiments, as all cells in the mixture would be exposed to rapamycin if present throughout development.

Moreover, it has been reported that extended treatment with rapamycin in mammalian cell models has an inhibitory effect on other protein kinase activities such as mTORC2 and AKT/PKB (Sarbassov et al., 2006). The inducible Rheb overexpression system might help to delineate whether the effect of prolonged rapamycin treatment was a direct consequence of mTORC1 pathway activity. Dox-on Rheb_FLAG OE strains were therefore used as an alternative approach for studying cell fate decisions with altered mTORC1 activity only during development. When turning on Rheb overexpression using doxycycline treatment only during development, 10% labelled dox-on cells overexpressing wt Rheb_FLAG or mutated Rheb_FLAG_E40K were mixed with 90% unlabelled AX2 cells (which should not be affected by the presence of Dox) in mixing experiments (Figure 4.29A). The numbers of green spores originating from dox-on Rheb OE strains were less than 10% (the input ratio), and the

Rheb_FLAG_E40K OE strain formed even fewer spores (7.3% ± 1.2%) than wt Rheb_FLAG OE strain (9.0% ± 0.3%), while AX2 in 10% labelling mixed with 90% unlabelled dox-on strains had 17.8% ± 2.7% and 21.6% ± 4.7% green spores when mixed with wt Rheb_FLAG and mutated Rheb_FLAG_E40K OE strains respectively. These results indicates that increased level of Rheb only in development disposed cells to choose a stalk cell fate in chimeric development with AX2. This is opposite to the observation on rapamycin treatment during the monolayer stalk induction assay. However, in growth conditions where dox-on Rheb OE strains were cultured in doxycycline-free HL5 medium, there were bands in FLAG western blots (Figure 4.29B) revealing leaky expression. Therefore, there might be some Rheb overexpression leakage from the dox-on regulatory system even incubated in the absence of doxycycline in those dox-on Rheb strains. It is possible that even a small amount of leaking Rheb overexpression penetrating the control of doxycycline during growth could be enough to induce cells to choose a stalk cell fate.

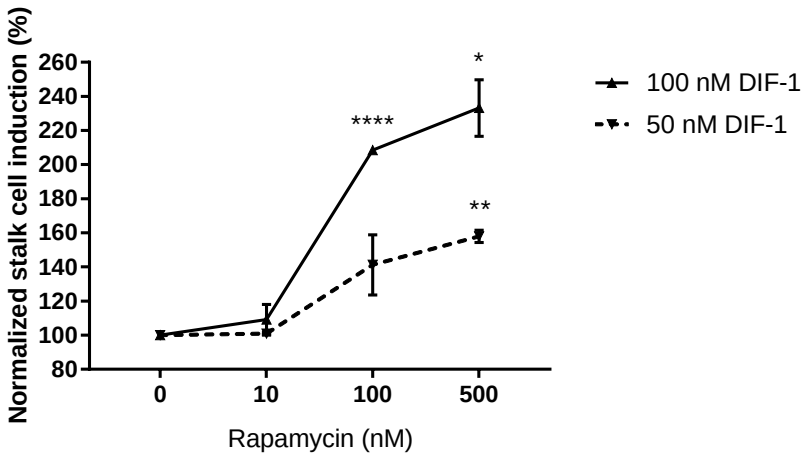


Figure 4.28. Pre-stalk marker-expressing cells exposed to rapamycin throughout development show a stalk cell fate bias. Monolayer stalk induction assays were performed as described in the legend to Figure 3.5A with rapamycin treatment all the time during development. Log-phase AX2 cells with *ecmB*-GAL construct were harvested and plated in the 96-well plate format with a range of rapamycin concentrations (0-500 nM) applied throughout the monolayer DIF-1 assay. N = 2. Mean ± S.E.M. Student *t*-test (two-tailed): *: $P < 0.05$; **: $P < 0.01$; ****: $P < 0.0001$.

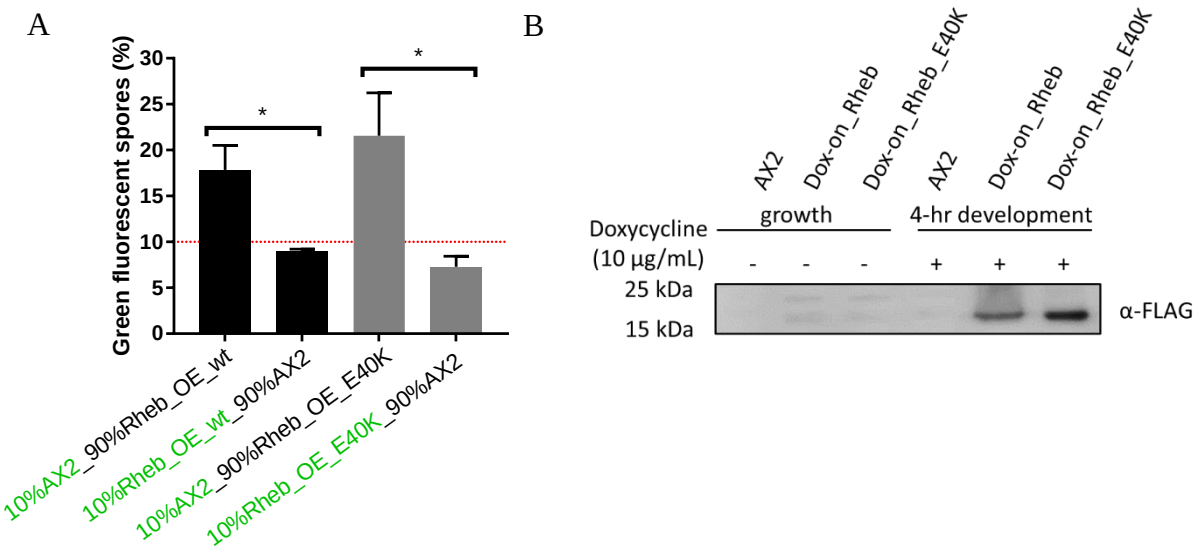


Figure 4.29. Rheb overexpression regulated in a doxycycline-dependent manner during development changed cell fate. Rheb_FLAG OE strains (wt Rheb OE: dox-on_Rheb_FLAG; mutated Rheb OE: dox-on_Rheb_FLAG_E40K) were used. (A) Mixing experiments of AX2 and dox-on Rheb OE strains (in AX2 genetic background) were carried out as described in the legend to Figure 3.4A but in the presence of 10 µg/mL doxycycline only during development. After labelling, the mixtures that contained 10% labelled mixed with 90% unlabelled cells were incubated with 10 µg/mL doxycycline at 120 rpm, 22°C for four hours to allow cells to overexpress Rheb_FLAG. Then, the mixtures were plated onto the nitrocellulose filters soaked in KK2 buffer with 10 µg/mL doxycycline. N = 3. Mean ± S.E.M. Student *t*-test (two-tailed): *: $P < 0.05$. (B) Western blotting of α-FLAG in AX2 and Rheb_FLAG OE strains (dox-on_Rheb_FLAG and dox-on_Rheb_FLAG_E40K) from growth in HL5 medium without doxycycline and four-hour development in KK2 buffer with 10 µg/mL doxycycline. The method of harvesting whole cell lysates was described in the legend to Figure 4.6. N = 1.

4.3.3.3.5 Leakage of Rheb OE in the dox-on regulatable system in dox-free conditions during growth potentially affects cell fate decisions during development

Although the opposite cell fate tendencies were shown in cells either pre-treated with rapamycin during growth or exposed to longer-term rapamycin treatment during development, it was impossible to use the inducible expression of Rheb_FLAG to confirm the importance of the timing of pathway activation due to the low level of expression of dox-on Rheb_FLAG OE construct in the absence of doxycycline. To reduce the consequence of leakage of Rheb_FLAG overexpression from the dox-on inducible construct, the dox-on constructs were introduced into *rheb*$^-$ cells to reduce the level of Rheb expression overall. Pools of transformants of *rheb*$^-$_dox-on_Rheb_FLAG and *rheb*$^-$_dox-on_Rheb_FLAG_E40K were examined for expression of Rheb_FLAG following 10 µg/mL doxycycline treatment during growth via western blotting

(Figure 4.30A). Dox-on Rheb_FLAG and Rheb_FLAG_E40K constructs in the *rheb*$^-$ background responded to doxycycline induction and were switched on after 2-hr incubation with doxycycline, and mutated *rheb*$^-$_dox-on_Rheb_FLAG_E40K had slightly stronger expression levels compared to *rheb*$^-$_dox-on_Rheb_FLAG. Mixing experiments were conducted using cells pre-incubated in KK2 with doxycycline for 4-hr development by mixing *rheb*$^-$_dox-on_Rheb_FLAG OE cells and AX2 cells in different ratios (Figure 4.30B). These *rheb*$^-$_dox-on Rheb_FLAG OE cells showed a similar stalk cell tendency as previously shown for cells expressing the Rheb_FLAG in an AX2 background (Figure 4.29A), with fewer spores formed from 10% labelled *rheb*$^-$_Rheb_FLAG OE cells (9.2% ± 0.7% from Rheb_FLAG and 9.0% ± 0.6% from Rheb_FLAG_E40K) mixed with 90% unlabelled AX2 cells. Also, cells undergoing doxycycline treatment in shaking suspension during the first four hours of development in KK2, prior to plating on nitrocellulose with doxycycline were confirmed to express Rheb_FLAG and Rheb_FLAG_E40K in the *rheb*$^-$ background (Figure 4.30C). However, there still could be a residual overexpression of Rheb_FLAG in growing cells that can override any late developmental effects as leaky expression is detectable when intensifying the contrast of the western blot image (lower panel in Figure 4.30C), and the pDM310 dox-on inducible construct use a strong *act15* promoter to drive target gene expression (Veltman et al., 2009).

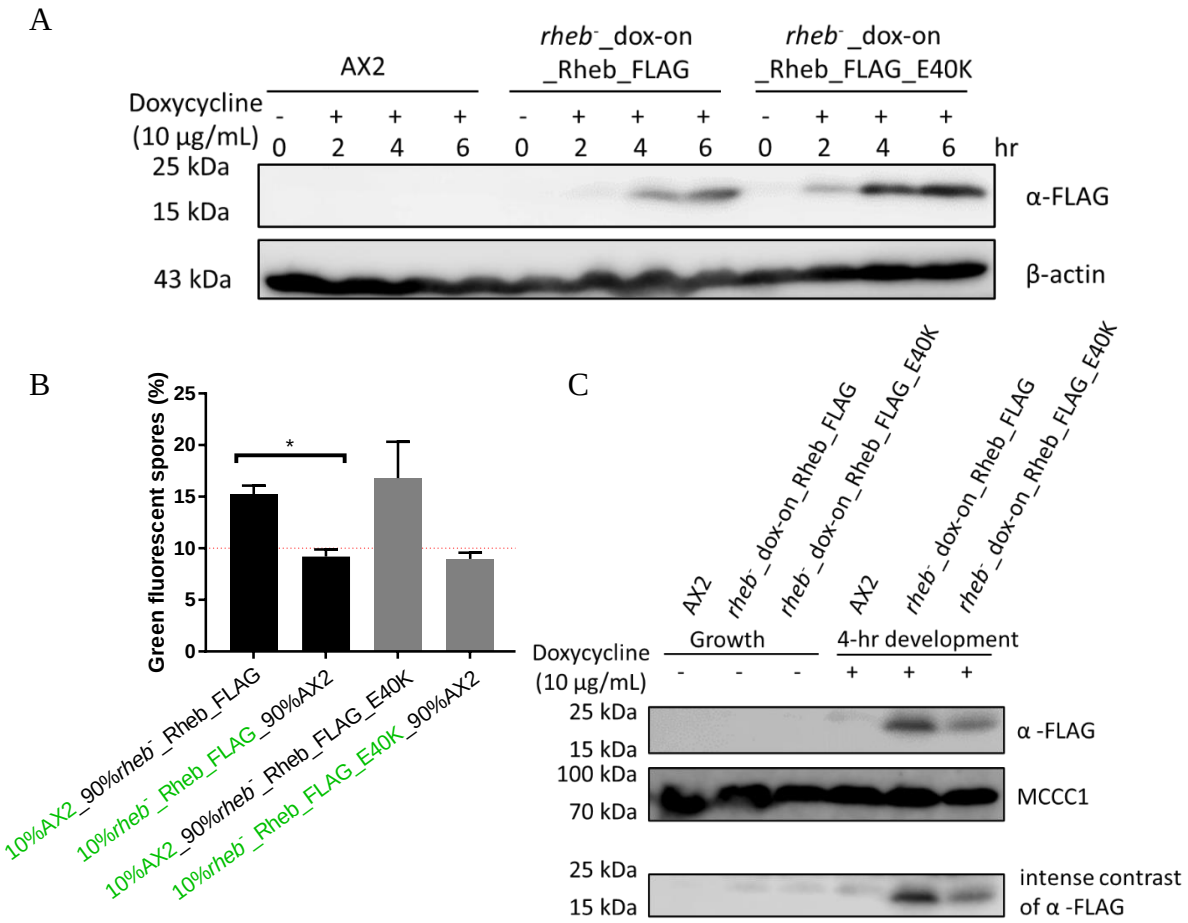
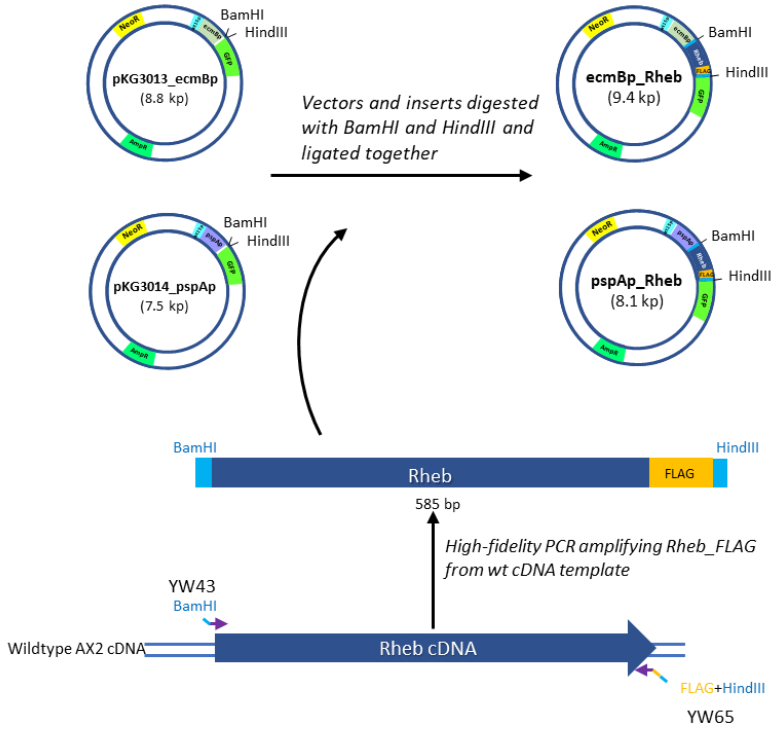


Figure 4.30. Verification of the expression of dox-on dependent Rheb_FLAG OE constructs in *rheb*⁻ background and cell fate preference. (A) Western blotting experiments of α-FLAG were carried out using whole cell lysates of growing AX2 and *rheb*⁻_dox-on Rheb_FLAG OE strains (wt Rheb_FLAG and mutated Rheb_FLAG_E40K) in the presence or absence of 10 µg/mL doxycycline as described in the legend to Figure 4.17B. Loading control: β-actin. One representative blot, N = 2. (B) Mixing experiments of AX2 and cells with *rheb*⁻_dox-on Rheb_FLAG OE cells which turned on Rheb_FLAG expression in development only. The method for the experiments was described in the legend to Figure 4.29A. N = 2. Student *t*-test (two-tailed): *: $P < 0.05$. (C) Western blotting of α-FLAG using AX2 and *rheb*⁻_dox-on_Rheb_FLAG OE strains incubated in HL5 medium without doxycycline and developed in KK2 buffer with 10 µg/mL doxycycline for four hours. The method for collecting whole cell lysates was described in the legend to Figure 4.6. One representative blot, N = 2.

4.3.3.3.6 Developmentally regulated promoters driving Rheb_FLAG expression can be used to study the effect of mTORC1 pathway during development in cell fate decisions

Another strategy to potentially generate strains with less leaky expression during growth is to express Rheb under the control of developmental promoters, such as the *ecmB* pre-stalk and *pspA* pre-spore promoters (Figure 4.31A). Using both constructs expressing Rheb in late development could also be helpful to understand whether mTORC1 pathway activity at later stages in development influences cell fate decisions in pre-spore or pre-stalk cells. So far, only ecmBp_Rheb_FLAG has been successfully made and confirmed by sequencing (Figure 4.31B).

A



B



Figure 4.31. Cloning of ecmBp_Rheb_FLAG and pspAp_Rheb_FLAG. (A) Schematic representation of cloning strategy for ecmBp_Rheb_FLAG and pspAp_Rheb_FLAG. pKG3013 harbours the *ecmB* pre-stalk promoter sequence, while pKG3014 contains a pspA pre-spore promoter sequence. Rheb_FLAG was amplified from AX2 cDNA using YW43 and YW65 primers which incorporated a FLAG-tag sequence as well as restriction sites BamHI and HindIII at 5' and 3' ends accordingly. This Rheb_FLAG fragment was then cloned into these two developmental expression vectors. (B) Schematic representation of final ecmBp_Rheb construct. This was verified by sequencing a single positive candidate (E-005 colony) out of 30 colonies, using a primer from the EGFP at the N-terminus. The *ecmB* promoter sequence and initiating ATG was in frame with Rheb cDNA and EGFP. Annotation was made using SnapGene.

4.4. Discussion

This chapter shows:

1) mTORC1 pathway activity can be monitored by different approaches: western blotting of phospho-4E-BP1 levels and rapamycin sensitivity assays in growth or under-buffer development. High mTORC1 activity is correlated to stalk cell fate bias in cells with nutrient deficient history (G-) or genetic mutants *dmpA*$^{-}$, *ampk*$^{-}$, Rheb_FLAG OE. Low mTORC1 activity correlates to spore cell fate bias shown in *rheb*$^{-}$ cells.
2) Pharmacological alteration using 4-hr pre-treatment with mTOR inhibitors (rapamycin and two other inhibitors, AZD8055 and BEZ235 which are more complicated to interpret as they inhibit mTORC2 as well as mTORC1 and are less potent in mTORC1 inhibition compared to the effect of rapamycin), and genetic modulation (*ampk*$^{-}$, Rheb_FLAG OE and *rheb*$^{-}$ strains) of mTORC1 pathway activity alter cell fate decisions.
3) Although the levels of the changes between wildtype and Rheb mutants in general were small, the *rheb* null cell line (*rheb*$^{-}$) constructed using CRISPR/Cas9 method was confirmed to be spore cell fate-biased, while using doxycycline regulated expression vectors pDM309 and pDM310 to generate wt Rheb_FLAG and mutated Rheb_FLAG_E40K OE constructs in both AX2 and *rheb*$^{-}$ genetic backgrounds caused stalk cell fate tendencies.
4) 4-hr pre-treatment of rapamycin in cell growth and prolonged rapamycin treatment throughout monolayer development have the opposite cell fate biases, indicating altered mTORC1 activity in growth and later development have different effects on cell fate, probably involved in protein synthesis regulation at different stages preparing for spore formation or vacuolation during stalk formation. Rheb OE during development leads to stalk cell fate bias, but leaking expression could potentially affect the cell fate bias assessment.

mTORC1 as a well-conserved master regulator senses environmental stress and cellular nutrient and energy status, transducing signals to execute important biological processes such as autophagy and protein/lipid biogenesis. A role for mTORC1 in cell fate determination has

been reported in mammalian T cells (Chi, 2012; Zheng et al., 2007) as well as an involvement in regulation of stem cell reprogramming via suppressing glycolytic gene expression (Chen et al., 2011; Ryall et al., 2015). Considering the translocation of mTORC1 to the surface of lysosomes when activated by amino acids in mammalian cells (Shimobayashi and Hall, 2016), this proximity of mTORC1 and the lysosomally-targeted TPC2 Ca^{2+} channel protein support a potential interplay between mTORC1 and TPC2 in response to cellular stresses. TPC2 has a regulatory role in termination of autophagy by interacting with mTORC1 and controlling mTORC1 reactivation in skeletal muscle (Lin et al., 2015). Meanwhile, a negative regulatory role for mTORC1 on TPC2 cation channel activation had been reported repeatedly in mammalian systems such as HEK293 cells and TPC2 knockout mice (Cang et al., 2013; Ogunbayo et al., 2018). It has also been shown that in *Dictyostelium tpc2*$^{-}$ cells have prolonged higher levels of phosphorylation of the mTORC1 substrate 4E-BP1 as cells enter development triggered by starvation (Chang et al., 2020). Consistent with an increased mTORC1 pathway activity, *tpc2*$^{-}$ cells also required higher concentrations of rapamycin to inhibit growth in culture (Chang et al., 2020) and to induce aggregation in the rapamycin-induced aggregation assay reported here. Since *tpc2*$^{-}$ cells have altered vesicle pH (Chang et al., 2020) and are more sensitive to weak bases shown in both Chang et al. (2020) and in previous chapter, it is not known whether it is vesicle pH, mTORC1 activity or some other factor that leads to *tpc2*$^{-}$ to choose stalk cell fate. Despite reports of lysosomal pH regulating mTORC1 activity in osteoclast differentiation (Hu et al., 2016) and mTORC1 governing circadian clock-associated metabolic protein synthesis to sense intracellular pH via lysosome distribution through Rheb (Walton et al., 2019), these pathways are not characterised in *Dictyostelium* cells yet. Thus, to further investigate the underlying mechanism by which lack of TPC2 increases mTORC1 pathway activity, future experiments could include measurement of phospho-4E-BP1 level and the degree of rapamycin-induced aggregation in cells which are pre-treated with weak bases to answer the question whether weak bases changing vesicle pH have the potential to alter prolonged mTORC1 pathway activity in *tpc2*$^{-}$ cells.

In *Dictyostelium* which has a growth-to-development transition upon starvation, mTORC1 together with its metabolic antagonist AMPK have been studied in response to glucose withdrawal using AX3 cells (Jaiswal and Kimmel, 2019). In agreement with this, AX2 cells that were pre-incubated in glucose deficient HL5 for 48 hrs had relatively high mTORC1 pathway activity during the first hour of development, which is shown in *tpc2*$^{-}$ cells here as

well. Another stalk cell fate-biased putative Ca^{2+} channel mutant, *dmpA*$^{-}$, also has high mTORC1 pathway activity in response to starvation during the first hour of development and is less sensitive to rapamycin-induced aggregation in half-strength HL5. The intriguing stalk cell fate tendencies observed in both *tpc2*$^{-}$ and *dmpA*$^{-}$ cells could support the hypothesis that mTORC1/TPC2 signalling plays a role in regulating cell fate decisions.

In order to investigate whether mTORC1 pathway activity was a determining factor in cell fate decisions, mTOR inhibitors or genetic mutants of mTORC1 regulators AMPK and Rheb, were used to alter mTORC1 activity in pharmacological and genetic contexts to determine if this was sufficient to cause a cell fate bias. Using monolayer stalk induction assays, cells pre-treated with rapamycin had reduced pre-stalk marker *ecmB* promoter-driven expression. The broader-spectrum mTOR inhibitors AZD8055 and BEZ235 might also disrupt other kinases such as PI3K and the mTORC2 complex (Roper et al., 2011; Willems et al., 2012), and pre-treatment with these inhibitors showed a larger variation in the pre-stalk marker expression, although they also gave a reduction trend. Moreover, treating cells with inhibitors for both mTORC1 and mTORC2 such as AZD8055 and BEZ235 could reduce cell mobility, as the mTORC2/AKT pathway has been shown to control cell migration in *Dictyostelium* via activation by Rho GTPase family RacE protein in their GDP-bound form and the defects in mTORC2-mediated AKT phosphorylation observed in RacE null cells can be rescued by $RacE_{T25N}$-GDP (Senoo et al., 2019), which challenges the conventional point of view that G protein bound to GDP is inactive. It was also reported that targeting mTORC2 rather than mTORC1 could reduce migration of breast cancer cells (Li et al., 2012). Therefore, rapamycin-induced aggregation assays and mixing experiments could not be interpreted when cells were treated with the more general dual mTORC1/2 inhibitors such as AZD8055 and BEZ235. Overall, treatment with all three of these mTORC1 inhibitors led to reduced phospho-4E-BP1 levels within 15 mins during cell growth in HL5 medium, suggesting that the inhibitors can reduce mTORC1 activity. Mixing experiments using 4-hr rapamycin pre-treatment of AX2 cells mixed with untreated cells also showed that rapamycin treatment during growth leads to spore cell fate tendency, consistent with observations in the monolayer stalk induction assay.

mTORC1 activity in strains containing genetic changes in mTORC1 regulators including the *ampk*$^{-}$ and Rheb_FLAG OE as well as *rheb*$^{-}$ were also studied, initially by western blotting for

phospho-4E-BP1 (T37/46) to confirm an alteration in mTORC1 activity. However, these phospho-specific antibodies were often problematic when analysing samples from *Dictyostelium* cells, as the commercial antibodies were originally designed against the mammalian protein sequence and different batches of polyclonal antibodies were more or less useful in *Dictyostelium* extracts, perhaps having slightly altered specificity for different epitopes in the same target protein. We also tried to detect other sites of mTORC1-phosphorylated substrate such as phospho-4E-BP1 (T70) which did not give consistent signals between biological repeats (data not shown) and phospho-S6K using the same antibody as mentioned in Jaiswal and Kimmel (2019). S6K belongs to AGC family which is a well-studied Ser/Thr kinase in mammals (Jastrzebski et al., 2007; Magnuson et al., 2012), but it has been reported to be absent in *Dictyostelium* (Goldberg et al., 2006). In Jaiswal and Kimmel (2019)'s work, an anti-phospho-SGK1 (Ser 422) antibody was used to detect S6K phosphorylation in *Dictyostelium* cells. SGK1 is a serum- and glucocorticoid-induced protein kinase belonging to the protein kinase A, protein kinase G, protein kinase C (AGC) kinase family, and it is an mTORC2 substrate in mammalian cells (Garcia-Martinez and Alessi, 2008; Lu et al., 2010). Using human SGK1 sequence (Uniprot: P23443) to cross-reference *Dictyostelium* database with BLASTp program, the most similar *Dictyostelium* protein is PkgB (encoded by *pkgb* gene: DDB_G0290157) with the highest score, and this belongs to SGK protein kinase family (Williams et al., 2019). The human SGK1 sequence contains an S422 residue in the F**S**$_{422}$YAP amino acid sequence, but *Dictyostelium* PkgB has threonine instead of serine in this sequence. There are another two proteins containing the F**S**YAP sequence identified in BLASTp search using human SGK1 against *Dictyostelium* database. One is an AKT family protein kinase encoded by DDB_G0288795, similar to mammalian kinase domains in AKT/PKB and yeast GAD8 and SCH9; the other was a PDK1 family protein kinase PdkB (encoded by DDB_G0284489) which is similar to mammalian PDK. AKT/PKB kinase is well-studied as a downstream effector of mTORC2 in other models (Frias et al., 2006; Sarbassov et al., 2006; Sarbassov et al., 2005; Senoo et al., 2019). Such results indicate that this substrate reports on mTORC2 activity rather than mTORC1. In our hands, the anti-phospho-SGK1 (S422) used by Jaiswal and Kimmel (2019) did show that *tpc2*$^{-}$ cells had an increased phosphorylation level of this mTORC2 substrate SGK1 on starvation, although this was not significant (Chang et al., 2020). However, due to doubt about the pathway involved, alternative approaches to measure mTORC1 pathway activity were desirable. Rapamycin sensitivity to inhibition of growth and or induction of aggregation in half-strength HL5 could indirectly provide information on

mTORC1 activity in cells. It is possible that the half-strength HL5 which has a reduced level of amino acids such as leucine could sensitize the mTORC1 pathway and allow rapamycin-induced aggregation through Sestrin/Gator regulation. As expected, *rheb*$^{-}$ cells were prone to aggregation in half-strength HL5 medium at lower concentrations of rapamycin compared with AX2, correlated to a lower level of mTORC1 activity. However, *rheb*$^{-}$ cells have similar rapamycin-mediated growth inhibition compared to parental AX2 cells, consistent with a minor role of Rheb in cell growth reported in Rosel et al., 2012. Rheb_FLAG OE strains on the other hand showed less sensitivity to rapamycin in both rapamycin-induced growth inhibition and aggregation assays, indicating higher levels of mTORC1 in these cell lines. The *ampk* null cells also showed relatively less sensitivity to rapamycin-induced growth inhibition compared to parental AX3 cells, correlating with the higher and prolonged phospho-4E-BP1 levels in the early onset of development. Therefore, the rapamycin sensitivities assessed in cell growth and early development in these alternative methods correlate to the phospho-4E-BP1 levels revealing mTORC1 pathway activity in mutants.

When investigating cell fate decisions in the genetic mutants with altered mTORC1 activity, loss of AMPK was reported to result in a stalk cell fate tendency. A limitation of multicellular development assays used to evaluate *ampk*$^{-}$ cell fate tendency and its rapamycin sensitivity in early development is that AMPK regulates cell migration (Cunniff et al., 2016) via phosphorylation of substrates such as CLIP-170 at microtubule tips for microtubule polymerization (Nakano et al., 2010) and an α-actinin-binding protein Pdlim5 in the Rac1-Arp2/3 signalling pathway at the cell periphery (Yan et al., 2015). Assays including mixing experiments and rapamycin-induced aggregation require cell migration, which could be problematic for *ampk*$^{-}$ cells. With the absence of AMPK activity, cell movement could have been disrupted as well, which was consistent with the observation of slower development in mixing experiments with 90% labelled *ampk*$^{-}$ and 10% unlabelled AX3 cells (data not shown). In rapamycin-induced aggregation, *ampk*$^{-}$ cells showed no aggregates although parental AX3 cells did (data not shown).

As mentioned earlier, when verifying mTORC1 activity in Rheb mutant cell including *rheb*$^{-}$ and dox-on Rheb_FLAG OE strains, they all showed the expected results in rapamycin-induced aggregation assays: *rheb*$^{-}$ cells had a high aggregation score while dox-on Rheb_FLAG OE

cells had a reduced aggregation score compared to parental cells. However, although *rheb*$^{-}$ cells compared to AX2 cells showed hypersensitivity to rapamycin in rapamycin-induced aggregation assays, they were not more sensitive to rapamycin during growth, indicating that Rheb has little effect on mTORC1 during *Dictyostelium* cell growth, which is consistent with previous literature (Rosel et al., 2012). Compared to the reduced rapamycin sensitivity in growing dox-on Rheb_FLAG OE, it is suggested that Rheb overexpression leads to larger mTORC1 pathway activity changes than loss of Rheb. Moreover, inconsistency in phospho-4E-BP1 levels as mTORC1 activity readouts were observed using dox-on Rheb OE, while the level of phospho-4E-BP1 in *rheb*$^{-}$ during development were barely changed, and notably *rheb*$^{-}$ has a lower basal phospho-4E-BP1 level in vegetative growth compared to parental AX2. These results indicated that Rheb might have a relatively little impact on activating mTORC1 in *Dictyostelium*, which matched the findings that *Dictyostelium* Rheb suppressing phagocytosis was dependent on the existence of mTORC2 and it might also be less important during cell growth for mTORC1 activity (Rosel et al., 2012). In other organisms such as *S. pombe* or mammalian cells, Rheb can also have mTORC1-independent roles (Aspuria et al., 2007; Karbowniczek et al., 2004; Otsubo and Yamamato, 2008).

Comparing two doxycycline-regulated versions of Rheb_FLAG OE when transfected into AX2 background, the dox-off promoter led to a slow kinetics in response to doxycycline to reduce levels of Rheb_FLAG protein, so this is not useful for rapid changes of expression. This could potentially be solved by creating a more unstable version of Rheb protein with a short half-life. In mixing experiments, overexpression of Rheb_FLAG in dox-on strains upon doxycycline induction led to stalk cell fate bias in mixing experiment, which might be working through mTORC1 activity development. However, the regulation of expression of Rheb_FLAG under the control of dox-on promoter was not tight, as there was leakage of expression seen in dox-on Rheb_FLAG OE strains without doxycycline induction, complicating data interpretation. To overcome this, the dox-on_Rheb_FLAG OE expression constructs were introduced into the *rheb*$^{-}$ background, but the level of expression from the strong promoter might still lead to an overall overexpression of Rheb_FLAG relative to the normal levels of Rheb seen in parental cells. On the other hand, *rheb*$^{-}$ cells showed a spore cell fate preference in mixing experiments and monolayer stalk induction assays as predicted.

It is also reported that GTP-bound Rheb in a cell line expressing Rheb^{Q46L}, equivalent to a constitutively active Rheb mutation, and non-GTP-bound Rheb^{D60I} variant mimicking the *rheb* null state were used to study mTORC2 activity by assessing phagocytosis rates, as more efficient phagocytosis is correlated to lower mTORC2 activity (Rosel et al., 2012). We intended to get this dominantly active GTP-bound Rheb^{Q46L} construct (which is a more usual way to lock these G proteins in an active status) from Dictybase for comparison with the mutant I made, however, it was unavailable in stock and impossible to ship during the COVID pandemic situation. Therefore, we could try the dominantly active Rheb^{Q46L} cell line to control mTORC1 activation in future experiments in parallel to verify whether Rheb^{Q46L} can serve as a potential constitutively active Rheb strain on changing cell fate decision during development without the expression leakage problem seen in dox-on_Rheb_FLAG_E40K strain.

Moreover, changing mTORC1 activity could be achieved by manipulating the key components in this complex, such as overexpressing the TOR kinase in *Dictyostelium* (Swer et al., 2016) or knockdown of raptor by RNAi in tet-off system (Rosel et al., 2012). It would be desirable to assess the cell fates bias in other genetic mutants of mTORC1 components such as a CRIPSR/Cas9 knockout *tor*$^{-}$ strain (Ogasawara et al., 2022) available from Dr. T. Muramoto (pers. comm.). It would also be useful to generate mutants with altered mTORC2 activity and perform monolayer stalk induction assays to see if mTORC2 activity also has a cell fate effect.

When trying to investigate the effect of mTORC1 activity on cell fate only during growth or development, experiments were carried out treating cells with rapamycin at different times. Inhibition of mTORC1 activity by extended rapamycin treatment throughout development in the monolayer stalk induction assay led to a stalk cell fate tendency, which is the opposite of the spore cell fate tendency seen following pre-treatment of cells with rapamycin before development. Therefore, it was hypothesized that mTORC1 plays different roles in cell fate decisions before development compared to the later stages in development. To confirm these alternate roles for mTORC1 at different stages, one approach is to induce Rheb_FLAG OE in development only using the dox-on system. However, the potentially high Rheb_FLAG basal level of expression from the strong *actin15* promoter in the dox-on inducible system made the results hard to interpret. Thus, a limitation of using dox-on Rheb_FLAG OE constructs is that the background OE in growing cells of Rheb_FLAG might be sufficient to cause a stalk cell

fate bias. Therefore, an alternative approach is to use developmental promoters (which might be more tightly switched off during growth) to drive the expression of Rheb in later stages of development. A construct with a pre-stalk promoter driving Rheb_FLAG expression (ecmBp_Rheb_FLAG) was made and is ready to be introduced into cells for future cell fate experiments, such as mixing experiments with *rheb*$^{-}$ cells and cells following expression of ecmBp_Rheb_FLAG in the *rheb*$^{-}$ background. With the FLAG tag as a reporter, Rheb expression under the control of the *ecmB* promoter can be traced throughout development. *Dictyostelium* Rheb has been reported to be ubiquitously expressed in all subtypes of pre-stalk cells including pstA, pstAB and pstO, and its expression localized to the pre-stalk regions during development (Swer et al., 2014). However, driving expression of Rheb_FLAG in prespore cells using a prespore specific promoter will be an important control for these experiments. Using developmentally controlled promoters to express Rheb_FLAG or dominant active GTP-bound Rheb^{Q46L} may also reveal the importance of a certain cell types in regulating cell any fate decision mediated by mTORC1 activity in later development. In summary, investigating the roles of mTORC1 in regulating cell fate decision from a spatial-temporal perspective during development can be crucial to understand this underlying mechanism of cell fate bias.

Chapter 5: Gene expression regulation and cell fate decision

5.1. Introduction

5.1.1. Gene expression regulating cell type differentiation in development

Spatiotemporal regulation of gene expression allows a specific set of genes to be expressed in the correct place at the correct time, playing fundamental roles in regulating cell differentiation, pattern formation and organogenesis in the development of a multicellular organism such as *Drosophila melanogaster* (Tomancak et al., 2007). Genes that prime the cells to undergo differentiation have been studied in mammalian cells. For example, Tcf15 which is a basic helix-loop-helix (bHLH) transcription factor negatively regulated by inhibitor of DNA binding/differentiation proteins, is considered as a marker expressed in pluripotent cells for the transition from pluripotency state to somatic lineage commitment, as it has upregulated expression in embryonic stem cells when transiting from a naïve state to a primed state (Davies et al., 2013). Ras, a small GTPase protein which is also known to regulate cell cycle and differentiation is another mechanism of gene expression regulation affecting development (Coleman et al., 2004; Crespo and Leon, 2000; Schubbert et al., 2007). A general example is Ras signalling stimulates the activation of transcriptional regulators involved in cell cycle progression, such as cyclin D (Pruitt and Der, 2001), and dysregulation of the Ras pathway results in developmental disorders and cancers (Fernández-Medarde and Santos, 2011; Schubbert et al., 2007). In *Dictyostelium*, Ras proteins such as RasD and RasG are highly related to mammalian Ras proteins (Khosla et al., 2000; Reymond et al., 1984; Robbins et al., 1989). It is also long known that RasD influences stalk and spore cell proportioning in development (Louis et al., 1997; Reymond et al., 1986), as the pre-stalk cells have higher RasD expression levels compared to pre-spore cells (Jermyn et al., 1987). Mutants with constitutively active RasD and RasG proteins with G12T mutations play a role in pre-stalk cell differentiation (Jaffer et al., 2001). Moreover, high RasD activity can predispose towards a stalk cell fate, as a lower mRNA transcript levels of RasD primes growing cells to be pre-spore cells later in development, while upregulated expression leads to stalk cell fate (Chattwood et al., 2013). A

guanine nucleotide exchange factor for RasD (RasGEF), GefE, (Wilkins et al., 2000; Wilkins et al., 2005) stimulates RasD during phototaxis (Wilkins et al., 2005) and activates the heterogeneously distributed RasD which underpins a salt-and-pepper pattern in lineage priming during position-independent differentiation (Chattwood et al., 2013). This resembles the observation in mouse embryogenesis which has two main cell types in the inner cell mass (PrE and EPI) with stochastic and intermingled expression patterns, as the responsiveness to morphogenic signals such as the PrE inducing factor, fibroblast growth factor (FGF), is heterogenous, probably through variations in cellular intrinsic threshold to FGF (Grabarek et al., 2012; Yamanaka et al., 2010).

5.1.2. Potential biomarkers for prediction of predisposition of cell fate determination in growing cells

The ability to predict cell fate tendency has attracted interest in recent years with studies on potential biomarkers to predict cell fate decisions affected by predisposition factors. For example, in development of blood cell lineages, multiple transcription factors were identified to be potential biomarkers revealing cell fate states during blood cell development stages and together with cell-specific gene expression profiles, the integrated lineage-specific expression pattern correlates transcription factors and genes expressed in different stages to unravel a regulatory network of haematopoiesis (Nazarieh et al., 2021). In *Dictyostelium* cells, disruption of the genes encoding RasD and GefE lead to spore cell fate bias when developing with parental controls in chimeric mixing experiments and a reduction of DIF-1 sensitivity in *gefE*$^{-}$ cells was shown in monolayer stalk induction assays, while FACS analysis showed a lower number of DIF-1 responsive cells in *gefE*$^{-}$ genetic background compared to AX3 indicated by *ecmA*-GFP expression, supporting GefE being a modulator in intrinsic DIF threshold control (Chattwood et al., 2013). Moreover, constitutively activated RasD overexpression in *gefE*$^{-}$ or AX3 background alters cell fate bias to a DIF-1-mediated pre-stalk cell fate tendency, indicating that GefE-RasD activity is coordinated into a gene regulatory network for regulating cell fate decisions in DIF-1 dependent lineages (Chattwood et al., 2013). A buffering system to compensate for perturbation of cell cycle dynamics due to extrinsically changing environmental cues was proposed to explain the underlying mechanism of the GefE-RasD regulatory network in this process (Gruenheit et al., 2018). Studied by RNA-seq, reciprocal gene expression profiles during growth were identified in fate-biased cells either due to distinct

nutrient history, glucose sufficient (G+) or deficient (G-), or different GefE levels (AX3 or *gefE*$^{-}$) (Gruenheit et al., 2018). From this gene expression profile study, the expression ratio of *rrgA* (DDB_G0268600) to *rigA* (DDB_G0274655) in growing cells has been suggested to act as a biomarker for prediction of cell fate bias before entering development (Gruenheit et al., 2018). These two genes are representative Ras-dependent genes that have maximal expression levels during multicellular development (Gruenheit et al., 2018; Rosengarten et al., 2015). The *rigA* gene shares sequence similarity with a gene encoding human histidine-rich glycoprotein involved in many signalling pathways regulating important physiological activities such as angiogenesis and immune processes (Gruenheit et al., 2018; Jones et al., 2005), while *rrgA* also known as *uduB* is related to a protein found at the *Dictyostelium* centrosome (Reinders et al., 2006) and involved in a signalling pathways in early development revealed from genome-wide analysis (Strmecki et al., 2007). The ratio of *rrgA* to *rigA* transcript levels from qPCR experiments was confirmed to predict cell fate preferences caused by alteration of nutrient and pH levels in the growth media. When cells were grown in medium lacking glucose with a pre-stalk bias, the expression ratio of *rrgA/rigA* was relatively high, whilst when pH level was increased during cell growth to give a prespore bias, the expression ratio of *rrgA* to *rigA* became relatively lower (Gruenheit et al., 2018). Thus, during vegetative growth, the ratio of *rrgA* to *rigA* genes expressed via the RasD regulatory network activity could be useful markers to predict cell fate bias in cells.

5.1.3. Post-translational modifications (PTMs) on histones controlling gene transcription influence cell differentiation

Histone modifications, a well-studied form of PTMs, have been reported to impact on gene expression (Alberts, 2002; Lawrence et al., 2016). An important contribution of histone PTMs is to chromatin structure remodelling that changes gene expression without altering nucleotide sequences. In eukaryotes, DNA is wrapped around an octameric core histone complex and packaged into nucleosomes containing two sets of histone H2A, H2B, H3 and H4 proteins (Luger et al., 1997; Oudet et al., 1975), and histone H1 is bound to the nucleosome as a linker to stabilize the higher-order chromatin structure (Allan et al., 1980; Oudet et al., 1975). Histone PTMs at the N-terminal ‘tails’ of histones change the chromatin environment and therefore directly regulate gene transcription by controlling the accessibility to underlying DNA (reviewed by (Alberts, 2002; Lawrence et al., 2016; Morales et al., 2001; Strahl and Allis,

2000)). These chromatin modifications decorating histone tails, including methylation, acetylation, phosphorylation, ubiquitylation, sumoylation, ADP ribosylation etc. (reviewed in (Kouzarides, 2007; Lawrence et al., 2016)), and functions of these modifications include regulation of transcription and therefore influence gene expression. Gene expression changes associated with different types of histone modification greatly contribute to regulation of important cellular processes, such as DNA repair and DNA replication, by remodelling chromatin structures such as via acetylation on histone 3 at lysine 14 (H3K14) and histone 1 at lysine 18 (H1K18) (Suka et al., 2001; Zhang et al., 2002). An example is acetylation on histone H4 via the histone acetyltransferase (HAT) called ESA1 promotes DNA double-stranded break repair in yeast (Bird et al., 2002).

Chromatin modelling via histone PTMs has been reported to play roles in cell differentiation and fate determination (Becker et al., 2016; Morales et al., 2001). Histone acetylation is commonly associated with euchromatin which has loosened chromatin structure (Grant, 2001; Singh et al., 2020), such as histone H4 acetylation at lysine 16 (H4K16ac) which mediates the mobilization of the mono-nucleosome, therefore activating gene transcription and maintaining euchromatin (Shogren-Knaak et al., 2006; Suka et al., 2002). Levels of histone acetylation that control the degree of chromatin accessibility are often higher in undifferentiated embryonic stem cells (Paul and Knott, 2014; Yao et al., 2020). Some sites of histone methylation are enriched in compact chromatin structures like heterochromatin. For example, di- and tri-methylation of histone 3 at lysine 9 (H3K9me2/me3) have been found to associate with heterochromatin, leading to gene silencing (Rosenfeld et al., 2009). During development, trimethylated histone 3 lysine 9 (H3K9me3)-decorated heterochromatin at protein-coding genes are rearranged and lost compared to the uncommitted stage, allowing cell type-specific genes to be expressed for cell fates to be established at early stages of organogenesis and lineage maintenance to take place (Becker et al., 2016; Nicetto et al., 2019). In mouse embryonic stem cells (ESCs), a methyltransferase Dot1L is important for deposition of methylation on histone 3 lysine 79 (H3K79me), and distinct levels of di- and tri-methylation on H3K79 in mice oocytes are seen at different stages of early embryonic development (Ooga et al., 2008), while deficiency of Dot1L in transcriptome studies showed dysregulation of genes involving in endoderm differentiation, cell cycle regulation and cell proliferation (Barry et al., 2009).

In *Dictyostelium*, histone modifying enzymes and their corresponding modifying activities are well conserved (Chubb et al., 2006a; Kaller et al., 2006; Muller-Taubenberger et al., 2011). *Dictyostelium* also has a homologue of Dot1, a lysine methyltransferase 4 (KMT4), generating the H3K79me2 mark on histone, and loss of *dotA* gene encoding Dot1 leads to defects in growth and development as well as a reduced level of recovery from ultraviolet radiation (UV)-induced DNA damage (Muller-Taubenberger et al., 2011). Different chromatin modification patterns including H3K4 methylation and H3K27 acetylation change at the growth-to-development transition (Wang et al., 2021).

5.1.4 *Dictyostelium* methyltransferase Set1 is responsible for H3K4me3 mark

Set1 is an example of histone methyltransferase (HMT) mediating H3K4 methylation through its catalytic SET domain associated with gene expression regulation, such as activating *PPH3* gene (Bernstein et al., 2002; Santos-Rosa et al., 2002) and silencing locus of mating types, telomeres (Nislow et al., 1997) as well as ribosomal RNA gene (rDNA) in yeast cells (Briggs et al., 2001). The scaffolding structure of Set1 allows the binding of other SET domain-associated components in a H3K4 methyltransferase complex (Luciano et al., 2017; Roguev et al., 2001).

Similarly, the *Dictyostelium* homologue of Set1 contains a C-terminal SET domain that places mono-, di- and tri-methylation marks on histone H3 at lysine 4 residue (H3K4) (Chubb et al., 2006a). Highly conserved across species, H3K4 methylation is enriched at gene promoters and transcriptionally active regions (Noma et al., 2001; Strahl et al., 1999), while the methylation states in different developmental phases are varied. *set1*$^{-}$ cells lack all detectable H3K4 methylation on the two highly expressed H3 variants H3a and H3b and this leads to precocious aggregation and rapid early development compared to parental AX2 cells (Chubb et al., 2006a). At the same time, *set1*$^{-}$ cells show mis-expression of genes in genomic clusters and importantly premature activation of genes involved in the development programme during growth with sufficient nutrients, indicating Set1 plays an important role in producing extracellularly secreted prestarvation factor for perceiving the growth environment (Chubb et al., 2006a). The H3K4 methylation also has a ‘memory’ effect where components of the transcription

machinery and chromatin modifications pre-exist from past transcriptional events and allow re-initiation of transcription of temporarily accessible genes (Chubb et al., 2006b; Muramoto et al., 2010). Similar transcriptional memory effect was also reported in yeasts, as H3K4me3 marks placed by Set1 persistently exist even after inactivation of transcription and dissociation of Set1 from the chromatin, which reflects the recent activity of RNA polymerase II (Ng et al., 2003).

H3K4 di- and trimethylation marks are profoundly enriched at promoter regions and coding regions of actively expressing genes whose promoters are decorated by acetylation marks (Bernstein et al., 2002; Noma et al., 2001; Santos-Rosa et al., 2002; Zhou et al., 2011). Set1 has been reported to facilitate transcription and maintain gene expression by precluding recruitment of a histone deacetylase via placing H3K4 methylation marks at the coding regions of the genes with acetylated promoters (Bernstein et al., 2002). Alternatively, histone H3 proteins containing H3K4me3 have been proposed to be the site of dynamic turnover of acetylation. This coupling of H3K4 tri-methylation and dynamic acetylation has been identified in a number of eukaryotic systems, such as mice and yeast (Bian et al., 2011; Crump et al., 2011; Hazzalin and Mahadevan, 2005; Taverna et al., 2006).

One complex that delivers acetylation by recognizing H3K4me3 is the Spt-Ada-Gcn5 acetyltransferase (SAGA) complex, a chromatin modifying complex mediating transcription activation (Koutelou et al., 2010). Initially characterized in yeast and highly conserved among eukaryotes, the SAGA complex contains multiple components and modules which have distinct functions to regulate histone modification (Liu et al., 2008; Mischerikow et al., 2009). General control non-derepressible 5 (Gcn5) is a well-conserved catalytic subunit of a histone acetyltransferase (HAT) module in the SAGA complex with a bromodomain to catalyse acetylation of lysine residues on H3, leading to transcriptional activation (Cieniewicz et al., 2014; Koutelou et al., 2010; Ringel et al., 2015). Tandem mass spectrometry of yeast core histones showed co-ordinated changes in acetylation and methylation levels in a deletion mutant of Gcn5, as global acetylation levels on different lysine residues on H3 dramatically diminished in *gcn5*Δ cells (e.g. levels of H3K9Ac and H3K14Ac each decreased by ~40%), alongside an overall reduction of 30% in H3K4me3 levels (Jiang et al., 2007). SAGA-associated factor 29 (Sgf29) is well-conserved SAGA subunit which contains a chromodomain

to bind histone tails and a tandem Tudor domain which specifically binds H3K4me3 (Koutelou et al., 2010; Li et al., 2010; Sanders et al., 2002; Soffers and Workman, 2020; Vermeulen et al., 2010). In yeast, Sgf29 acts as a reader of H3K4me2/3 marks in chromatin and recruits SAGA to promoter regions via its tandem Tudor domain, facilitating subsequent acetylation via the HAT module in the SAGA complex (Ringel et al., 2015) (Figure 5.1). Deletion of the gene encoding Sgf29 decreases the acetylation of H3K9 (H3K9ac) and recruitment of SAGA to its target genes (Bian et al., 2011).

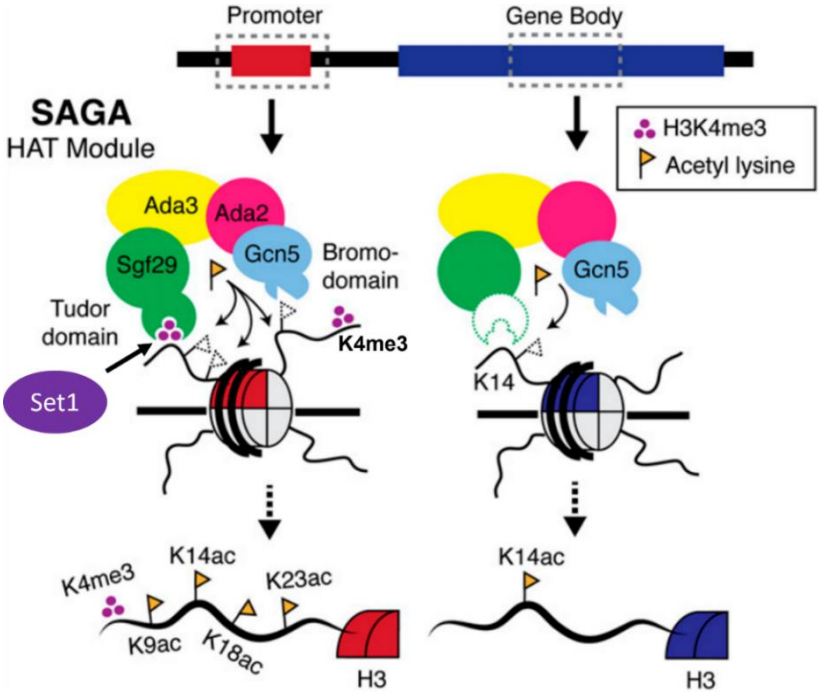


Figure 5.1. Schematic representation of the H3K4me3-mediated acetylation on H3K by SAGA complex. At the promoter sequence of the gene, enrichment of H3K4me3 marks deposited by Set1 via its HMT activity and recognized by the tandem Tudor domain in Sgf29 primes the processive acetylation at multiple lysine residues through HAT module (containing catalytic Gcn5, Ada2/Ada3 and Sgf29 subunits) in SAGA complex. This leads to hyperacetylation of histone H3. Within the gene bodies, bromodomain-containing Gcn5 preferentially catalyses H3K14 acetylation through its intrinsic lysine specificity. Adapted from Ringel et al. (2015).

Treatment of cells with the histone deacetylase inhibitor trichostatin A (TSA) elevates histone acetylation on H3K14 and H3K9 in *Dictyostelium* cells (Hsu et al., 2012; Huang et al., 2021). Following addition of TSA, the first histones to be acetylated are the ones already modified by H3K4me3, before other H3 proteins. This dynamic acetylation revealed by inhibition of the histone deacetylases (HDAC), is lost in the *set1*$^{-}$ mutant, indicating that Set1-mediated H3K4me3 primes sequential H3 acetylation (H3Ac), consistent with the situation in other eukaryotes (Hsu et al., 2012). In *Dictyostelium*, a putative orthologue of Sgf29 was identified

and shown to specifically target H3K4me3 to direct histone acetylation to nucleosomes already marked with this modification. It serves as a link between H3K4me3 and acetylation at promoter regions, and the *sgf29*$^{-}$ cells lose this link (Huang et al., 2021). At the onset of TSA treatment, *sgf29*$^{-}$ cells have delayed TSA-induced accumulation of H3K9ac and H3bK14ac and loss of H3K4me3-mediated rapid acetylation on H3 (Huang et al., 2021).

Investigation of Set1 and its deposition of H3K4me3 marks is a starting point to understand whether these methylation and acetylation histone modifications regulating gene expression can influence cell fate decisions. Using gene disrupted mutant strains of Set1, which deposits H3K4me3 marks, and mutants of genes encoding SAGA subunits such as Sgf29 which recognizes H3K4me3 marks and Gcn5 which places histone acetylation marks, the roles of these histone modifications in expression of predisposition biomarkers such as *rrgA* and *rigA*, as well as cell fate determination mechanisms can be elucidated.

5.1.5 Histone variants

In addition to histone modifications influencing gene expression regulation, in metazoans variants of histones present in association with different genes potentially provides another layer of complexity in regulating essential biological processes including development and cell-type determination (Elsaesser et al., 2010; Wiedemann et al., 2010). *Dictyostelium* contains a variety of histone variants similar to those found in vertebrates, and there are three characterized single-copy genes of H3 variants, H3a, H3b and H3c in *Dictyostelium* genome (Dubin et al., 2010; Hsu et al., 2012; Stevense et al., 2011). In higher eukaryotes, it is common to have multiple copies of H3 genes with high redundancy contributing to expression of three major H3 variants and other minor variants (Elsaesser et al., 2010; Hake and Allis, 2006; Wiedemann et al., 2010). However, it was found that mammalian H3 variants which only have few amino acid differences might be responsible for various H3 variant-specific activities, governing cell-type specific differentiation (Brown et al., 1985; Tagami et al., 2004). For example, centromeric silencing involves centromere associated H3s (e.g. CENP-A) (Black et al., 2004; Dubin et al., 2010) and transcriptionally silencing heterochromatin structure is associated with H3.1 and H3.2 (Hake and Allis, 2006; Jacob et al., 2014; Wunsch and Lough, 1987), while H3.3 variant is enriched at transcriptionally active euchromatin structure (Ahmad and Henikoff, 2002; Vermaak et al., 2003).

Typically, histone variants have a specific collection of modifications, and this has been seen in *Dictyostelium*. For instance, H3K9 acetylation is preferentially placed on H3b rather than in H3a in *Dictyostelium* (Hsu et al., 2012). There is interplay between H3a and H3b variants revealing variant specificity in terms of histone modification, which is observed by introducing substitution mutations from lysine 4 to alanine (K4A). For instance, in a strain with H3aK4A introduced into the endogenous H3a gene confirmed by loss of the mono-, di- and trimethylation on H3aK4 (Hsu et al., 2012; Muramoto et al., 2010), the H3bK4me3 mark is also completely lost and mono-/di-methylation levels of H3bK4 are preserved but reduced (Hsu et al., 2012). However, when K4A is introduced into the endogenous copy of the gene encoding H3b, the H3bK4A mutant strain has detectable although reduced H3aK4me3 level, and the levels of acetylation on K9 and K14 are also decreased (Hsu et al., 2012). The H3aK4 methylation mark is also important in transcription memory, as H3aK4A depletes the inheritance of reporter gene *act5* transcription (Muramoto et al., 2010). In this chapter, the role of K4 methylation of the H3b variant in cell fate decisions was investigated using the H3bK4A gene replacement strain.

5.2 Aims

This chapter aims to investigate whether:

(1) the cell fate bias in genetically altered strains are predispositions seen in growth or later effects through assessing the ratio of expression of *rrgA* and *rigA* during growth as a biomarker to reveal any predisposition on cell fate tendency before cells undergo development.

(2) H3K4me3 is important in *Dictyostelium* cell fate decisions. *set1*$^{-}$ and strains with loss of the *set1* gene complemented by expression of catalytically active or inactive Set1 provide information on control of the *rrgA/rigA* expression ratio and cell fate decisions when H3K4me3 is lost.

(3) the effect of H3K4me3 on regulating cell fate decisions is working through the established pathway of targeting H3K acetylation to the same histone tails mediated by Sgf29 and Gcn5. Mutant cell lines *gcn5⊿bromo* and *sgf29*$^{-}$ were used to investigate how disrupting histone acetylation can direct cells to choose a different fate.

(4) the cell fate decision dependent on histone modifiers is a predisposition effect using TSA, an inhibitor of histone deacetylases to stimulate the acetylation level on histones during growth or has an effect later during development by pre-treating cells with TSA for four hours.

(5) high mTORC1 activity and stalk cell fate preference correlate with altered H3K4me3 in *set1*$^{-}$ and H3bK4A cells as well as cells with glucose deficient growth history.

5.3 Results

5.3.1 Cell fate bias can be predicted by assessing the gene expression ratio of two markers: *rrgA* and *rigA*

In pre-spore and pre-stalk preferential conditions, the expression ratio of a pair of reciprocally expressed genes, *rrgA* and *rigA,* has been suggested to predict cell fate biases (Gruenheit et al., 2018). The expression ratio of *rrgA/rigA* in growing cells is relatively low in cells with a spore-biased fate but relatively high in stalk-biased cells. For instance, AX3 cells grown in high pH or high glucose levels leading to spore cell fate have a relatively low *rrgA/rigA* ratio compared to cells in low pH or low glucose (Gruenheit et al., 2018). Primers designed to detect expression from the *rigA* and *rrgA* genes as well as from the control *ig7* were validated using AX2 gDNA (Figure 5.2A). The cycle threshold (CT) values from qPCR experiments using SYBR green dye were plotted against cDNA (log10[DNA]) in serial dilutions. Linear regression analysis was performed, showing a good linearity between CT values and cDNA concentrations. This indicated that the primer sets were efficient for quantification (Figure 5.2B). The melt-curve analyses programmed after each qPCR experiment were also performed (data not shown), to verify that single and specific PCR products were generated.

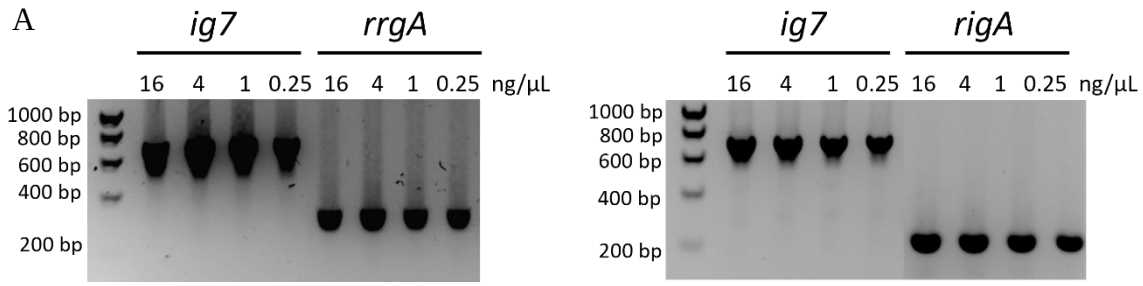
After verifying the primer quality, qPCR experiments with comparative ΔΔCt data analysis were conducted to test whether the relative gene expression levels of *rrgA* and *rigA* correlate with cell fate bias with different predispositions (Gruenheit et al., 2018). AX2 cells were grown in HL5 medium in normal glucose levels (G+) or deficient in glucose (G-) for two days before total RNA extraction for cDNA synthesis. G- cells showed a relatively high expression level of *rrgA* compared to *rigA* (Figure 5.3A), which was consistent with the findings reported by Gruenheit and colleagues (2018).

Cells pre-treated in conditions of different pH of the growth medium (Figure 5.3B) and different vesicle pH altered by the weak base imidazole (Figure 5.3C) were also assessed following either 4-hr or 24-hr treatment. With 24-hr treatment at pH 7.5 or 20 mM imidazole in HL5, growing cells had low *rrgA/rigA* ratios which correlated to spore cell fate tendency, which is in agreement with the result reported in Gruenheit et al. (2018). However, cells with

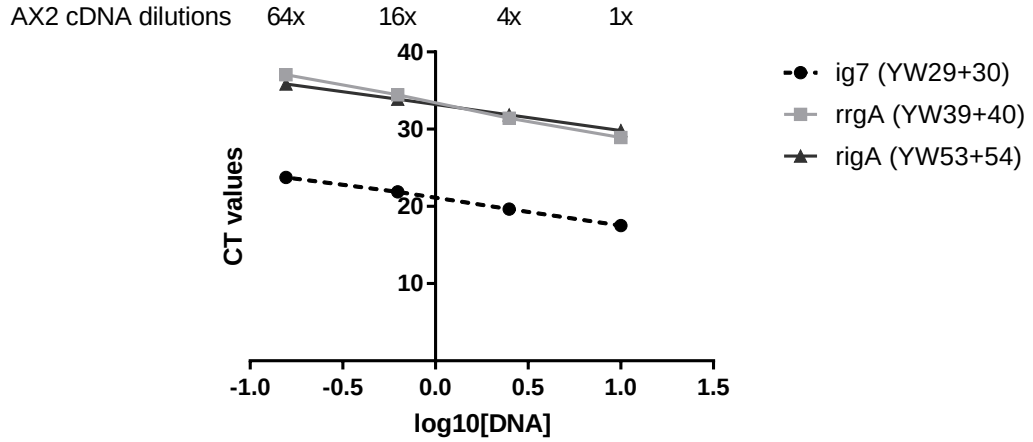
shorter 4-hr treatment at higher pH or weak base imidazole showed the opposite ratio of *rrgA/rigA* expression to that predicted by the observed cell fates. This suggests that 4-hr treatment is not sufficient to cause a detectable change in mRNA levels which will depend on the rate of mRNA degradation as well as synthesis, although 4 hours is enough to give the change in fate bias. Thus, the relative levels of *rrgA* and *rigA* gene expressions were not the cause of cell fate bias as extensive time was required for altering mRNA transcript ratios.

To investigate whether spore fate decisions mediated by low mTORC1 activity were correlated with low *rrgA/rigA* expression ratios, qPCR experiments were performed using exponentially growing AX2 cells incubated with mTOR inhibitors. Cells were treated for 24-hrs with 100 nM rapamycin, 100 nM or 500 nM AZD8055 and 100 nM or 1 μM BEZ235 before harvesting for assessing *rrgA/rigA* expression ratio (Figure 5.3D). Cells treated with 100 nM rapamycin, 100 nM AZD8055 and 500 nM AZD8055 tended to have a low *rrgA/rigA* expression ratio, consistent with the expected spore cell fate tendency. Although 100 nM BEZ235 treatment generated a higher *rrgA/rigA* expression ratio, a 10-fold higher BEZ235 concentration led to the overall *rrgA/rigA* expression ratio dropping and indicated the expected spore cell fate tendency. It should be noted that AZD8055 and BEZ235 could have more complicated inhibitory effects on other kinases in mTOR pathway. Nonetheless, higher concentrations of these two general mTOR inhibitors showed lower *rrgA/rigA* expression ratios with smaller variations, correlated with the expected spore cell fate prediction.

A



B



Primer sets	ig7 (YW29+30)	rrgA (YW39+40)	rigA (YW53+54)
Equation	Y = -3.464*X + 21.04	Y = -4.551*X + 33.4	Y = -3.351*X + 33.17
R squre (goodness of fit)	0.9985	0.9987	0.9999
P value of slope from non-zero	0.0007	0.0006	<0.0001

Figure 5.2. qPCR primer validation using AX2 gDNA and cDNA templates. (A) PCR primers for *ig7* (YW29+YW30), *rrgA* (YW39+YW40) and *rigA* (YW53+YW54) were validated using serial dilutions of AX2 gDNA in a 35-cycle PCR experiment. The PCR products were resolved on a 1% agarose gel and visualised with EtBr staining. Marker: HyperLadder 1kb. (B) qPCR experiments using comparative ΔΔCt method were performed. 2 × 10^6 exponentially growing AX2 cells at a density of 2 × 10^6 cells/mL were lysed and total RNA extracted using TRIzol method (Thermo Fisher, 15596026). AX2 cDNA synthesized from the total RNA with SuperScript IV reverse transcriptase (Thermo Fisher, 18090010) was serially diluted and used as a template for qPCR. qPCR experiments were performed following the manufacturer's protocol of SYBR™ Green PCR Master Mix (Applied Biosystems, 4309155). The absolute quantitation of the copies of qPCR product was analysed by assessing CT values with cDNA template in serial dilutions (log10[DNA] (ng/µL)). In the table, the linear regression analyses for each primer sets were performed to evaluate the linearity of qPCR in the table and the equations reveals the slope and y intercept which can be used for quantification.

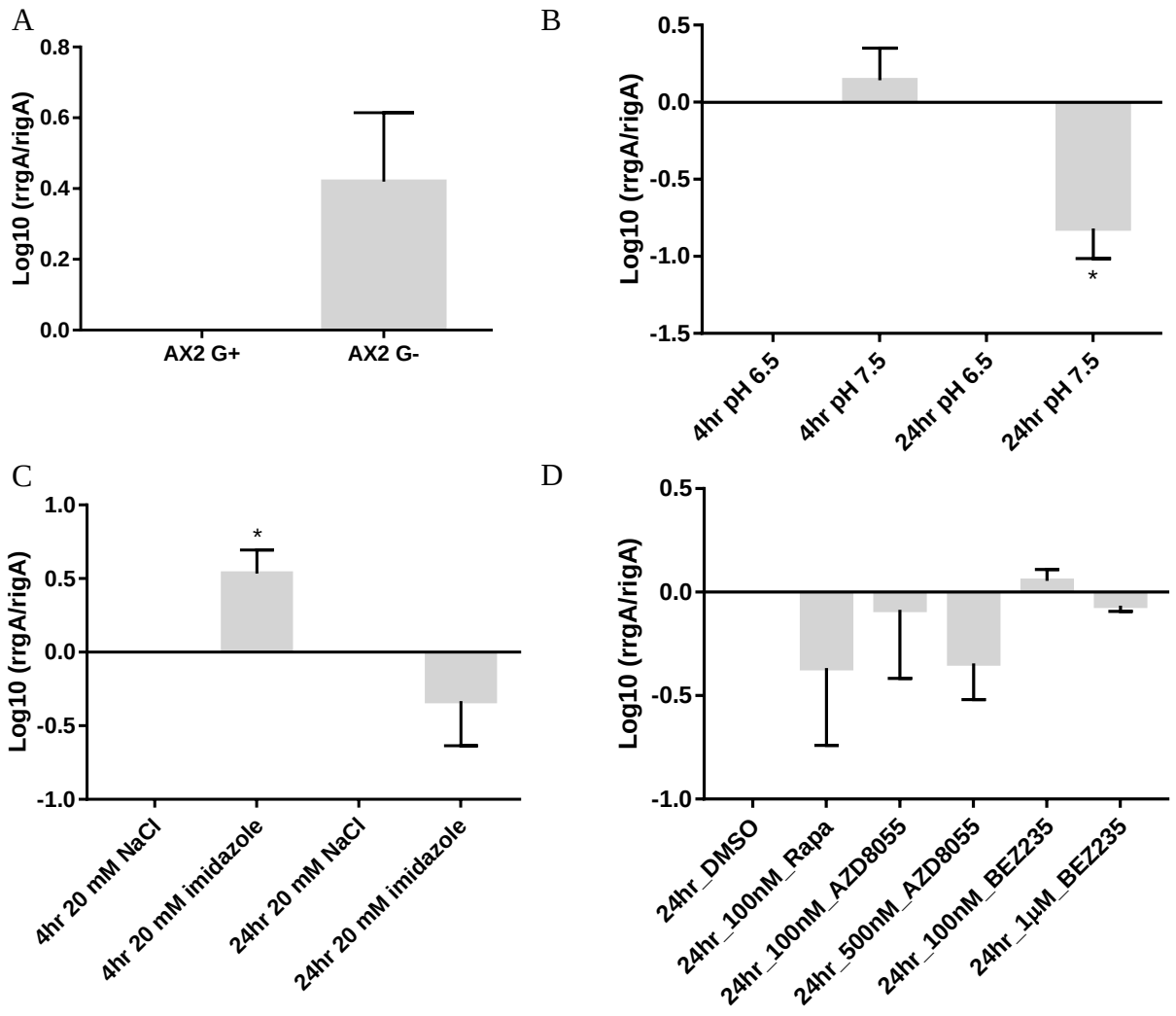


Figure 5.3. *rrgA/rigA* expression ratios in AX2 cells with different nutrient history, pH in growth medium, vesicle pH levels and mTORC1 inhibitor treatments. (A) Vegetatively growing AX2 cells were cultured in shaking suspension in HL5 medium with different nutrient history for 48 hrs: glucose sufficient (G+, the untreated calibrator control) and glucose absent (G-). Then, 2×10^6 exponentially growing AX2 cells were harvested and lysed in TRIzol for total RNA extraction, following by cDNA synthesis with SuperScript IV reverse transcriptase. SYBR Green dye-based qPCR experiments were performed as described in the manufacturer's protocol using cDNA templates to assess expression of *rrgA* (primers: YW39+YW40) and *rigA* (primers: YW53+54) in comparison to endogenous control *ig7* (primers: YW29+YW30). In each qPCR experiment, comparative ΔΔCt analyses were conducted as described in Schmittgen and Livak (2008) designating the AX2 G+ control as the untreated calibrator group for each biological repeat, i.e. the *rrgA/rigA* expression ratio is set to be 1 for the calibrator AX2 G+ control (thus, log10 of the calibrator group is 0). The relative *rrgA/rigA* expression ratio of G- cells were analysed by comparing gene expression ratio variations to the AX2 G+ calibrator control. N = 4. Mean ± S.E.M. (B) AX2 cells were incubated in shaking suspension in HL5 medium at pH 6.5 (control, the pH of HL5 medium) or pH 7.5 for either 4 hrs or 24 hrs. *rrgA/rigA* expression ratios were analysed by qPCR as described for panel (A). Conditions of pH 6.5 for both 4 hrs and 24 hrs treatments were taken as the calibrator control. N = 3. Mean ± S.E.M. Student *t*-test (two-tailed): *: $P < 0.05$. (C) AX2 cells in shaking suspension were incubated in HL5 medium with 20 mM NaCl (osmotic control) or 20 mM imidazole for either

4 hrs or 24 hrs. qPCR analyses for *rrgA/rigA* expression ratios were performed as described for panel (A). Conditions of 20 mM NaCl for both 4 hrs and 24 hrs treatments were considered as the calibrator control. N = 3. Mean ± S.E.M. Student *t*-test (two-tailed): *: $P < 0.05$. (D) *rrgA/rigA* expression ratios of exponentially growing AX2 cells upon mTOR inhibitor treatment for 24 hrs were analysed via qPCR as described for panel (A), where untreated AX2 (DMSO group) was set as the calibrator control. Different concentrations of mTOR inhibitors used to treat cells were: 100 nM rapamycin, 100 nM AZD8055, 500 nM AZD8055, 100 nM BEZ235 and 1 μM BEZ235 compared to DMSO (vehicle control). Mean ± S.E.M. N = 3.

5.3.2 Cell fates altered by intrinsic genetic factors have distinct *rrgA/rigA* gene expression ratios

To see whether intrinsic cell fate biases could be predicted in genetic mutants by assessing the *rrgA/rigA* expression ratio, stalk cell fate-biased strains were assessed. Two strains shown to have a pre-stalk tendency, *tpc2*$^-$ (Figure 3.4 and 3.5) and *dmpA*$^-$ (Figures 3.13) had an expected high *rrgA/rigA* expression ratio in growing cells compared to AX2 cells (Figure 5.4A).

iplA$^-$ cells have spore cell tendency in chimeric mixing experiments and tend to have reduced DIF-1-induced stalk marker expression at low DIF-1 concentrations (Figure 3.6). However, the *rrgA/rigA* expression ratio in growing *iplA*$^-$ cells is significantly higher than in AX2 cells (Figure 5.4B), which is not the predicted ratio. This was also seen in RNA from cheater strain *fbxA*$^-$ (previously called *chtA*$^-$). FbxA, encoded by *chtA*, is a protein with an F-box domain, and the *fbxA*$^-$ mutant prefers a pre-spore cell fate when chimerically developing with parental AX3 cells (Ennis et al., 2003). Similarly, the *rrgA/rigA* expression ratio in growing *fbxA*$^-$ cells is relatively high compared to AX3 cells, which would indicate a stalk cell fate rather than spore cell fate (Figure 5.4C). To confirm the cell fate preference, mixing experiments of *fbxA*$^-$ and AX2 cells were performed, and more spores were formed from *fbxA*$^-$ cells (Figure 5.5A), in agreement with previous studies (Ennis et al., 2003; Ennis et al., 2000). For instance, with 50%L/50%UL input, 56.7% ± 1.1% spores originated from labelled *fbxA*$^-$ cells were formed when mixing with unlabelled AX2 cells, while only 37.0% ± 1.1% spores from labelled AX2 cells mixed with unlabelled *fbxA*$^-$ cells were observed. However, monolayer stalk induction assays using ecmB-GAL stalk marker whose expression is induced by DIF-1 showed the opposite tendency: the *fbxA*$^-$ cells have higher expression levels of the stalk marker than the level in AX2 cells at all DIF-1 concentrations (Figure 5.5B). Even the untreated, *fbxA*$^-$ cells have an intrinsically higher stalk marker induction level (33.9% ± 7.6%) than that observed in

AX2 cells (8.3% ± 1.4%), indicating a strong pre-stalk tendency rather than spore tendency in *fbxA*$^{-}$ cells in this alternative assay. This stalk induction assay correlates with the observation of a high *rrgA/rigA* expression ratio in growing *fbxA*$^{-}$ cells compared to parental AX3. It is also noticed that AX3 should have been used in cell fate assays in comparison with this *fbxA*$^{-}$ strain as a more appropriate control than another parental AX2 strain. Interpretation of the expression ratio in genetic mutants could be more complex as it could be that FbxA and IPLA have one role in cell fate bias in growing cells before development, but this could be overridden by their involvement in other cell fate decision mechanisms in later development. The difference between the mixing and monolayer experiments for *fbxA*$^{-}$ cells also reveals that multicellular development may add extra complexity to the decision-making process, or monolayer assay with DIF-1 addition could artificially rescue mutants with lower levels of DIF production. In chimeric mixing experiments, cells undergo multicellular development that is practically unmodified or with a minimal manipulation, while monolayer stalk induction assay resembles an *in vitro* system for inducing cell type differentiation, which involves artificial conditions such as externally adding signalling molecules cAMP and DIF-1. Thus, cell fate bias revealed by mixing experiments could be more representative.

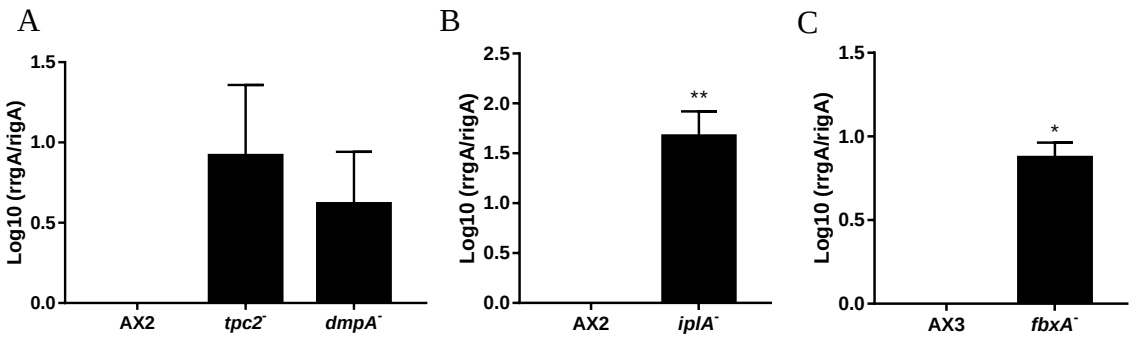


Figure 5.4. *rrgA/rigA* expression ratios in genetic mutants to verify cell fate prediction. Exponentially growing cells in HL5 shaking suspension were grown to a density of 2×10^6 cells/mL before harvesting for total RNA extraction and cDNA synthesis. qPCR experiments and data analyses of *rrgA/rigA* expression ratios were performed as described in the legend to Figure 5.3A. (A) *rrgA/rigA* expression ratios in AX2 and the stalk cell fate-biased genetic mutants: *tpc2*$^-$ (clone: TPC22B20) and *dmpA*$^-$ (clone: dmpAKOII76) cells were analysed. AX2 was the calibrator control to assess the ratios in mutants. N = 3. Mean ± S.E.M. (B) *rrgA/rigA* expression ratios of *iplA*$^-$ (clone: iplAI2D) and AX2 (calibrator control) were examined. N = 3. Mean ± S.E.M. Student *t*-test (two-tailed): **: P < 0.01. (C) *rrgA/rigA* expression ratios of *fbxA*$^-$ and AX3 cells (calibrator control) were examined. N = 2. Mean ± S.E.M. Student *t*-test (two-tailed): *: P < 0.05.

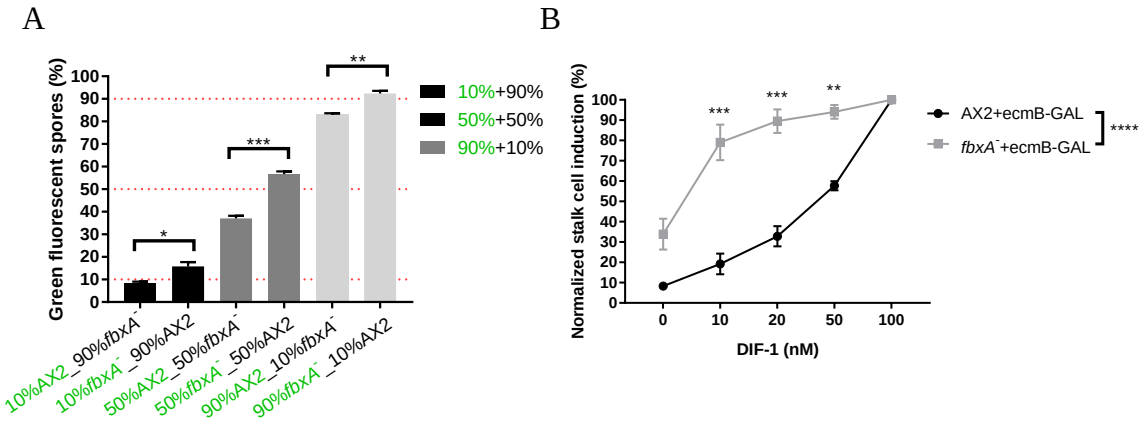


Figure 5.5. Cell fate preference in the *fbxA*$^-$ strain. (A) Mixing experiments of AX2 and *fbxA*$^-$ cells in chimeric development. The experiments were performed as described in the legend to Figure 3.4A. N = 3. Mean ± S.E.M. Student *t*-test (two-tailed): *: P < 0.05; **: P < 0.01; ***: P < 0.001. (B) Monolayer stalk induction assay of AX2 and *fbxA*$^-$ cells with stalk marker *ecmB*-GAL. The assays were conducted as described in the legend to Figure 3.5A. Two-way ANOVA: ****: P < 0.0001.

5.3.3 Genetic predisposition of cells lacking the H3K4 methyltransferase Set1 in cell fate decisions

5.3.3.1 *Dictyostelium set1*$^-$ cells have an intrinsic stalk cell fate bias

In *Dictyostelium*, cells lacking the Set1 are known to have an altered transcription pattern in growing cells and express a number of genes characteristic of early development whilst still growing. This led us to investigate the *rrgA/rigA* expression ratio in the *set1*$^-$ strain to see if this was involved in cell fate decisions. The *set1*$^-$ strain contains a BSR cassette inserted upstream of the catalytic C-terminal SET domain, causing ablation of all detectable mono-, di- and tri-methylation on H3K4 (Chubb et al., 2006a). Firstly, the ratio of *rrgA/rigA* expression in growing *set1*$^-$ cells was determined relative to parental AX2 cells (Figure 5.6A). A high *rrgA/rigA* ratio was observed in *set1*$^-$ cells, suggesting that *set1*$^-$ cells would have a stalk cell fate. This stalk tendency in *set1*$^-$ was then assessed in the two cell fate assays. In mixing experiments, when labelled *set1*$^-$ cells were mixed and developed with unlabelled AX2 cells in 10%L/90%UL ratios, fewer green spores originating from *set1*$^-$ cells were formed (6.5% ± 0.5%), whereas when AX2 cells were labelled and mixed with unlabelled *set1*$^-$ cells in the 10%L/90%L input ratio, more green spores from AX2 were formed (15.9% ± 1.1%) (Figure 5.6B). The same trend was seen when mixing at other ratios. Monolayer stalk induction assays which assessed stalk marker gene expression showed that *set1*$^-$ cells tend to be more sensitive to DIF-1 induction of *ecmB*-GAL expression compared to AX2 cells. When induced by 20 nM DIF-1, for example, *set1*$^-$ cells had an elevated level (84.3% ± 5.6% of the level seen at 100 nM) of pre-stalk marker gene expression compared to AX2 (44.5% ± 10.6%) (Figure 5.6C).

In order to determine whether the catalytic activity of the Set1 was responsible for the stalk cell fate-biased phenotype, cell fate decisions of the *set1*$^-$ cells complemented by expression of wildtype (wt) GFP-Set1 and catalytically dead versions of GFP-Set1 were analysed. The GFP-tagged rescue vectors of *set1*$^-$ (Chubb et al., 2006a), express GFP-Set1 fusion proteins either wildtype to restore the function of the SET methyltransferase domain or a GFP-Set1 protein containing one of two mutations N1425Q and C1474A in to generate catalytically dead protein which could still provide a scaffolding function. The GFP-Set1 rescue plasmids pJRC119 (GFP-Set1), pJRC89 (GFP-Set1:N1425Q) and pJRC88 (GFP-Set1:C1474A) with selectable G418 resistance marker, obtained from the *Dictyostelium* stock centre, were transfected into *set1*$^-$ cells and, following selection in G418, in order to confirm expression of the transgenes,

total RNA from pools of rescue strains were extracted from growing cells for cDNA synthesis. RT-PCR of AX2 and the GFP-Set1 rescue strains was performed using YW46 and YW47 primers which confirmed the expression of the GFP-Set1 fusion constructs in the rescue strains (Left panel, Figure 5.7A). YW29 and YW30 primers were also used for amplifying *ig7* endogenous control (Figure 3.4D) with cDNA templates which generated single bands with expected size (190 bp) (Right panel, Figure 5.7A), showing no gDNA contamination as no band was detected at 737 bp. To check protein expression, fluorescence microscopy was used to detect green fluorescence in the *set1*$^{-}$ rescue strains (Figure 5.7B). Western blot analysis confirmed that H3K4me3 was restored in cells rescued by expression of GFP-Set1 compared to the catalytically dead mutants N1425Q and C1474A (Figure 5.7C). While the *set1*$^{-}$ mutant has a high *rrgA/rigA* ratio consistent with its stalk cell fate preference, the *set1*$^{-}$ rescue strain complemented by expression of wt catalytically active GFP-Set1 had a low *rrgA/rigA* ratio compared to *set1*$^{-}$ (Figure 5.6A). Expression of the catalytically dead mutant GFP-Set1:C1474A showed high *rrgA/rigA* ratio similar to *set1*$^{-}$ (Figure 5.6A). Cells rescued by expression of wt GFP-Set1 no longer demonstrated a cell fate bias (Figure 5.8). For example, when labelled GFP-Set1 and unlabelled AX2 cells were mixed in 50%L/50%UL ratio, 50.5% ± 0.1% spores were formed from GFP-Set1, and similar results were observed in other mixing ratios. However, cells expressing the catalytically dead GFP-Set1 mutants retained stalk cell fate tendency (Figure 5.8). For instance, in 50%L/50%UL ratio there were 45.6% ± 0.5% spores derived from GFP-Set1:N1425Q while 46.0% ± 1.7% spores were formed from GFP-Set1:C1474A. It was also noticed that the catalytically dead N1425Q and C1474A mutants slightly formed more spores when chimerically developed with AX2 comparing to *set1*$^{-}$ strain. For instance, when mixing with unlabelled AX2 at 10%L/90%UL input ratios, 7.1% ± 0.3% spores were formed from labelled *set1*$^{-}$, while labelled GFP-Set1:N1425Q formed 9.3 ± 0.1% spores and labelled GFP-Set1:C1474A formed a similar number (9.2% ± 0.6%), although less than the spores formed from GFP-Set1 rescue (10.2% ± 0.2%). Despite these observations revealing both catalytically dead mutants show stalk cell fate preferences as seen in the *set1*$^{-}$ strain, the relevant functions of Set1 in changing cell fate biases were not clear. Set1 protein may also function in cell fate decisions independently of its catalytic activity, perhaps as a scaffolding protein.

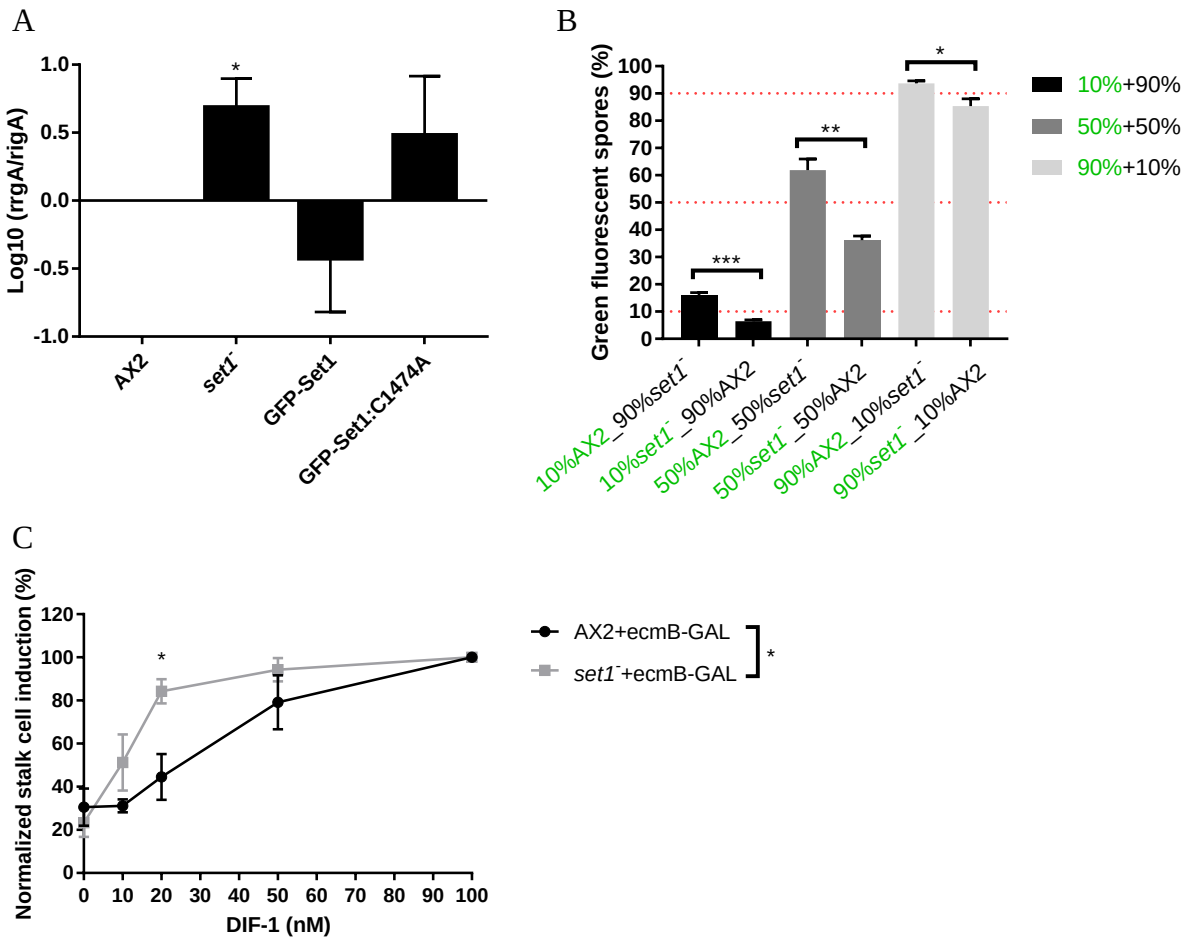


Figure 5.6. Stalk cell fate bias is predicted and observed in *set1*⁻ cells and the rescue cells with altered HMT activities. (A) *rrgA/rigA* expression ratios in *set1*⁻ cells and its rescue strains expressing GFP-Set1 (wildtype) and GFP-Set1:C1474A (catalytically dead) compared with AX2 (the calibrator control), were analysed as described in the legend to Figure 5.3A. N = 3. Mean ± S.E.M. Student *t*-test (two-tailed): *: P < 0.05. (B) Mixing experiments of AX2 and *set1*⁻ cells. The experiments were performed as described in the legend to Figure 3.4A. N = 4. Mean ± S.E.M. Three repeats were carried out by M. Papayova, and one repeat was from my work. Student *t*-test (two-tailed): *: P < 0.05; **: P < 0.01; ***: P < 0.001. (C) Monolayer stalk cell induction assays of AX2 and *set1*⁻ cells. AX2 and *set1*⁻ cells were transfected with *ecmB*-GAL stalk marker construct induced by different concentrations of the stalk inducer DIF-1 as described in the legend to Figure 3.5A. N = 4. Mean ± S.E.M. Student *t*-test (two-tailed) and two-way ANOVA: *: P < 0.05.

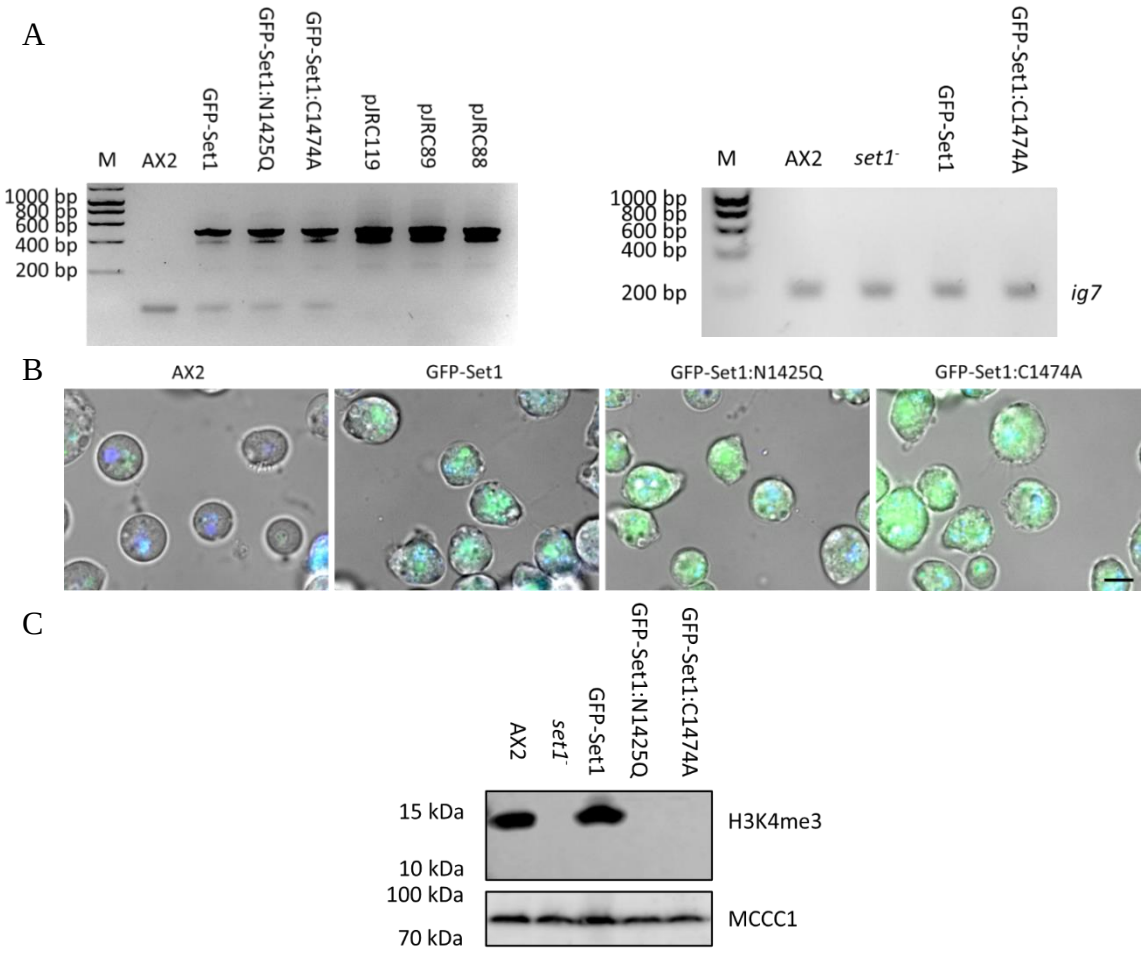


Figure 5.7. Verification of expression of GFP-Set1 in *set1*$^{-}$ cells. (A) Left panel: RT-PCR of GFP-Set1 rescue strains using cDNA templates. The forward primer YW46 was designed against the coding sequence of GFP at the C terminus, and the reverse primer YW47 was designed against the coding sequence of Set1 at the N terminus, and the PCR product from these primers was 552 bp. cDNA from RNA extracted from growing AX2 cells and cells transfected with constructs to drive expression of GFP-Set1, GFP-Set1:N1425Q, GFP-Set1:C1474A were synthesized as templates for verifying expression of the rescue constructs. Positive controls were the GFP-Set1 rescue plasmids: pJRC119, pJRC89 and pJRC88. Right panel: an example of confirming cDNA quality for PCR using endogenous control gene *ig7* amplified by primers YW29 and YW30 with the expected size of 190 bp. These results were visualized on 1% EtBr-stained electrophoresis agarose gel. M: the ladder HyperLadder 1kb. (B) Images from fluorescent microscopy of cells expressing the different rescue constructs with 100× oil lens. Vegetatively growing cells were cultured in shaking HL5 medium at 220 rpm, 22°C to log phase, then washed and resuspended in KK2 at 2 × 10^5 cells/mL. 1mL cell suspension was plated into a μ-Dish 35 mm imaging dish (ibidi) and 50 μg/mL Blue fluorescent dye Hoechst (Sigma, #33342) was applied to stain nucleic acids in cells. Green fluorescence showed the expression of GFP-Set1 rescue constructs. Scale bar: 10 μm. One representative repeat was shown, N = 2. (C) Western blot to detect H3K4 tri-methylation (H3K4me3) in AX2, *set1*$^{-}$ and rescue strains GFP-Set1, GFP-Set1:N1425Q and GFP-Set1:C1474A. 5 × 10^5 cells seeded into HL5 shaking medium were grown to exponential log phase for 24 hrs at 22°C, 220 rpm. Then, 2 × 10^6 growing cells were harvested and lysed in 2× Laemmli buffer at 95 °C, 6 min. Antibodies for the western blots: H3K4me3 (homemade, 1:1000) and MCCC1 (loading control, 1:1000). One representative blot was shown, N = 3.

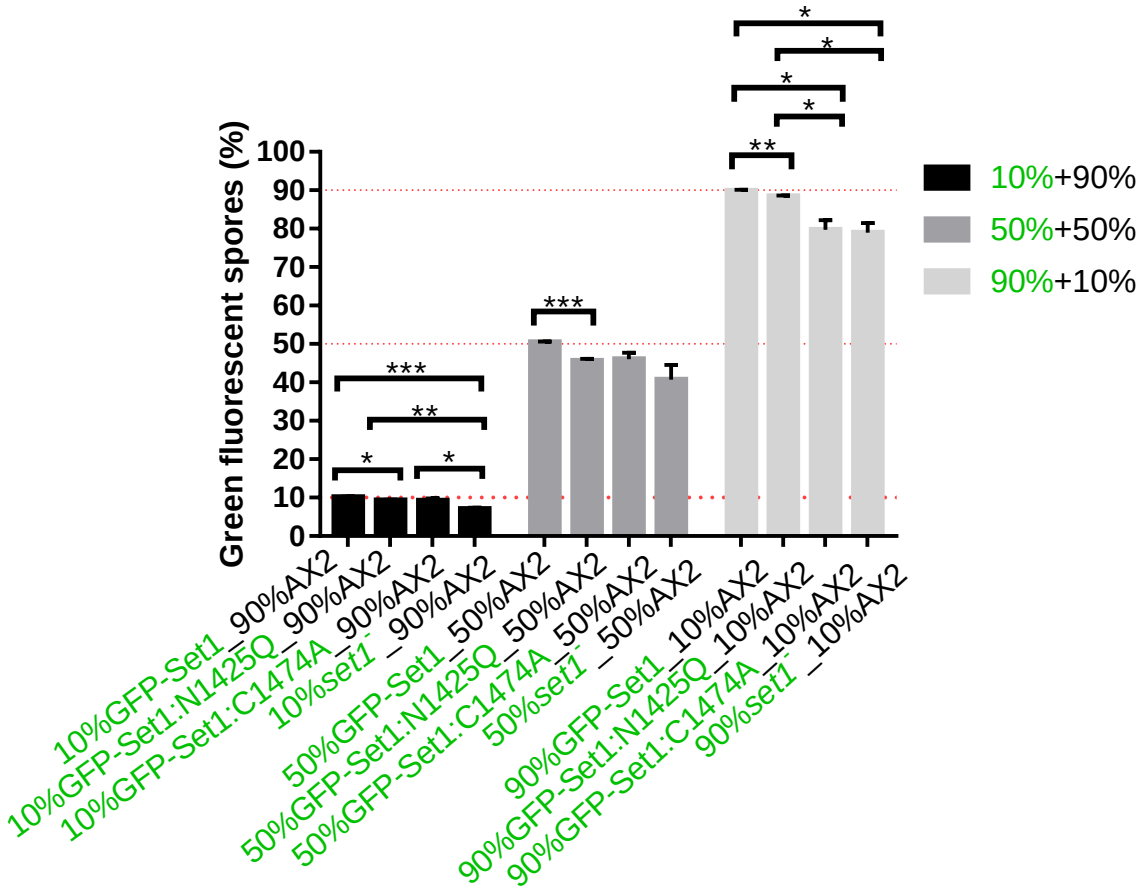


Figure 5.8. Expression of active GFP-Set1 restores balanced cell fate decision. Chimeric mixing experiments of labelled GFP-Set1 rescue cells (catalytically active GFP-Set1 and catalytically dead mutants GFP-Set1:N1425Q, GFP-Set1:C1474A) or *set1*$^{-}$ cells mixed with unlabelled AX2 cells were performed as described in the legend to Figure 3.4A. The quantifications in various input mixing ratios 10%L/90%UL, 50%L/50%UL, 90%L/10%UL were included. N = 3. Mean ± S.E.M. Student *t*-test (two-tailed): *: P < 0.05; **: P < 0.01; ***: P < 0.001.

5.3.3.2 H3bK4A cells have an intrinsic stalk cell fate bias revealing the importance of the H3K4me3 mark in cell fate decisions

The stalk cell fate tendency of *set1*$^{-}$ cells is dependent on catalytic activity of Set1. H3K4 is the best established Set1 substrate but other substrates could be present. In order to test whether H3 was the substrate involved in the bias, strains in which mutation of H3K4 to alanine (H3K4A) in the endogenous H3 genes, to prevent methylation of the protein, can be used. In *Dictyostelium*, methylation on both H3K4 variants can be detected, while H3 variant-dependent selective modifications were also reported (Hsu et al., 2012). For example, AX2 cells H3K4me3 deposition is preferentially on the H3b histone variant, and acetylation of H3K9 also predominantly marks H3b and has a greater apparent increase on H3b upon TSA treatment

compared to H3a (Hsu et al., 2012). In the *H3b/c*$^{-/-}$ mutant strain, where only H3a is expressed, the residual K4-trimethylation on H3a variant is also hyperacetylated on TSA treatment, demonstrating that H3K4me3 marks both H3 variants for dynamic acetylation (Hsu et al., 2012). In H3aK4A mutant, all K4 trimethylation marks in both H3a and H3b were lost, while replacing endogenous H3b with the mutated version, H3bK4A mutant leads to loss of H3bK4me3 but still has moderate H3aK4me3 levels although reduced (Hsu et al., 2012).

To investigate whether ablation of H3K4me3 restricted to the H3b variant is involved in defining stalk cell fate tendency, the mutant strain H3bK4A which lost all methylation marks on H3bK4 (Hsu et al., 2012) was used. This mutant has the endogenous lysine-4 residue (codon AAA) replaced by alanine (codon GCA) in the histone variant H3b locus, with a BSR cassette inserted after the stop codon generated via gene replacement (Hsu et al., 2012). Western blotting of H3K4me3 confirmed the H3bK4A strain, showing both AX2 and H3bK4A cells had detectable trimethylation on K4 of the H3a variant, whereas H3bK4me3, shown at a slightly lower position on the blot, was not detectable in the H3bK4A gene replacement cells (Figure 5.9A). This is consistent with the previous literature. In parental AX2 cells, the amount of K4 tri-methylation in H3a was more than the amount shown in H3b position, probably due to the higher abundance of H3a than H3b in *Dictyostelium* cells (Hsu et al., 2012). Similar to *set1*$^{-}$cells, H3bK4A cells prefer a stalk cell fate bias as it forms less spores when chimerically developing with AX2 cells (Figure 5.9B). For example, in the 50%L/50%UL ratio, more spores were formed from labelled AX2 (59.7% ± 3.9%) than from labelled H3bK4A mutant cells (40.7% ± 3.3%), and this trend is consistent in other mixing ratios. The preferential stalk cell fate of H3bK4A is also predicted by the *rrgA/rigA* expression ratio in growing cells which is relatively high compared to AX2 cells (Figure 5.9C). Thus, loss of H3bK4me in H3bK4A strain leads to a stalk cell fate bias revealed by mixing experiments and the biomarker prediction. Since Set1 is the methyltransferase responsible for depositing all H3K4me, H3K4me2 and H3K4me3 marks in *Dictyostelium* cells (Chubb et al., 2006a), this is consistent with Set1 working, at least in part, through methylation of H3bK4 in determining the ratio of expression of *rrgA* to *rigA* and in stalk cell fate tendency.

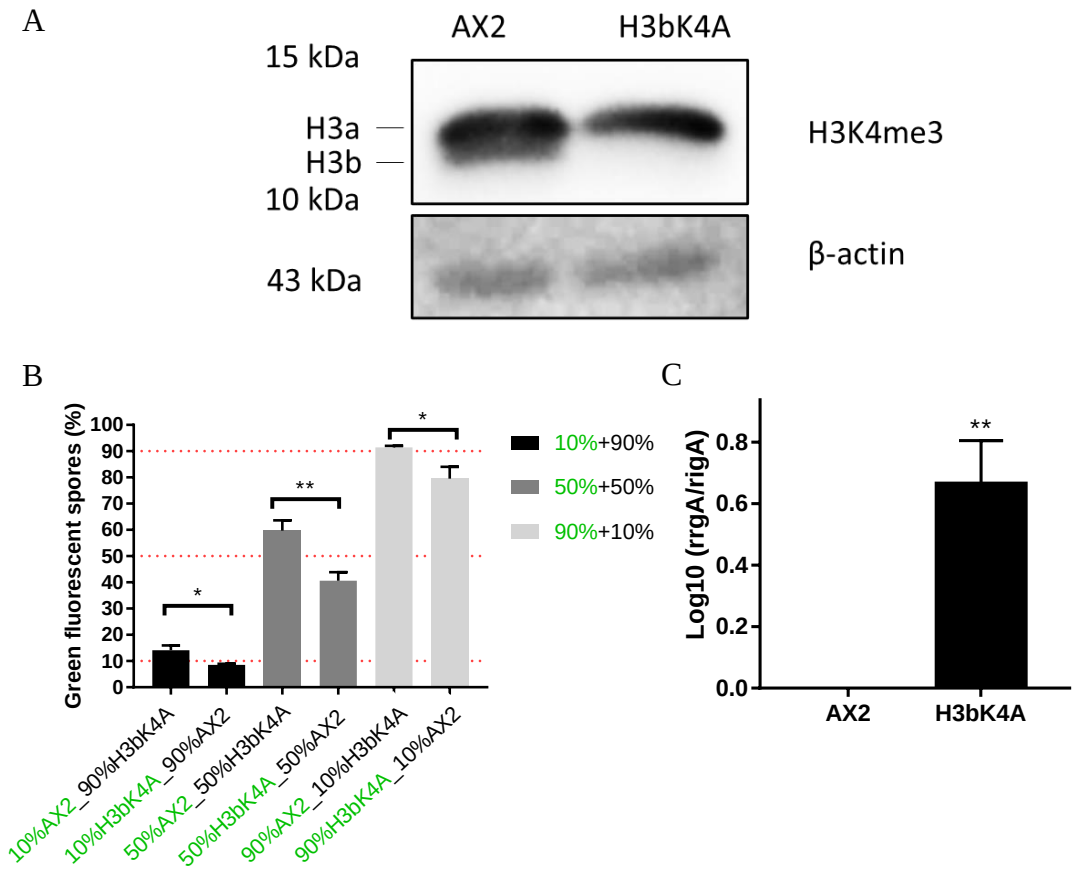


Figure 5.9. Verification of H3bK4A mutant cells and their cell fate tendency. (A) Western blotting of H3K4me3 in growing AX2 and H3bK4A cells were performed as described in Figure 5.7C. Antibody detecting H3K4me3: 1:1000; MCCC1: loading control, 1:1000. One representative blot was shown, N = 3. (B) Mixing experiments of AX2 and H3bK4A cells were conducted as described in the legend to Figure 3.4A. N = 4. Mean ± S.E.M. Student *t*-test (two-tailed): *: P < 0.05; **: P < 0.01. (C) *rrgA/rigA* expression ratios in H3bK4A and AX2 cells were determined by qPCR experiments performed as described in the legend to Figure 5.3A. AX2 was the calibrator control for comparing the relative expression ration observed in H3bK4A mutant. N = 3. Mean ± S.E.M. Student *t*-test (two-tailed): **: P < 0.01.

5.3.4 Histone acetylation coupled to the H3K4me3 mark affects cell fate decisions

Conserved with other eukaryotes, the H3K4me3 mark in *Dictyostelium* recruits the Gcn5 HAT in the SAGA complex via the tandem Tudor domain of Sgf29 subunit for subsequent acetylation at the same histone proteins (Huang et al., 2021). According to the developmental transcriptomic studies, expression of *sgf29* reaches a maximal level around 10 hrs of development, whereas *gcn5* is moderately expressed throughout development (Rosengarten et al., 2015). To investigate whether loss of H3K4me3-directed histone acetylation is responsible for the cell fate bias seen in the absence of H3K4me, genetically mutated strains of SAGA subunits were assessed. These mutants used in this study are an *sgf29*$^{-}$ gene

disrupted strain constructed via homologous recombination in AX2 genetic background (Huang et al., 2021) and the hypermorph mutant *gcn5⊿bromo* obtained from the Genome Wide *Dictyostelium* Insertion (GWDI) library generated by REMI-seq technique (Gruenheit et al., 2021) containing a plasmid insertion to disrupt expression of the C-terminal bromodomain in an AX4 background (Gruenheit et al., 2021; Huang, 2020). This strain has reduced HAT activity observed by decreased basal levels of H3K9ac and H3K14ac (Huang, 2020)). In chimeric mixing experiments, when developing with control AX2-bsR or AX4-bsR cells, both *sgf29*$^{-}$ (Figure 5.10A) and *gcn5⊿bromo* cells (Figure 5.10B) formed fewer spores, indicating a stalk-biased cell fate. For instance, in the 10%L/90%UL mixing ratio, labelled *sgf29*$^{-}$ cells formed 8.2% ± 0.7% spores when mixed with unlabelled control AX2-bsR, and labelled AX2-bsR formed twice as many spores than that (16.7% ± 1.8%), which is similar to the mixing experiment between *gcn5⊿bromo* and AX4-bsR, such as 10% labelled *gcn5⊿bromo* forming 7.7% ± 0.3% spores and 10% labelled AX4-bsR forming 16.4% ± 2.9% spores. Moreover, the *rrgA/rigA* expression ratios were higher in both *sgf29*$^{-}$ and *gcn5⊿bromo* growing cells compared to their parental control cells (Figure 5.10C), correlating with the observation of stalk cell fate preferences. Therefore, this data is consistent with H3K4me3 exerting its effect on cell fate though recruitment of Gcn5 via Sgf29, leading to H3Ac.

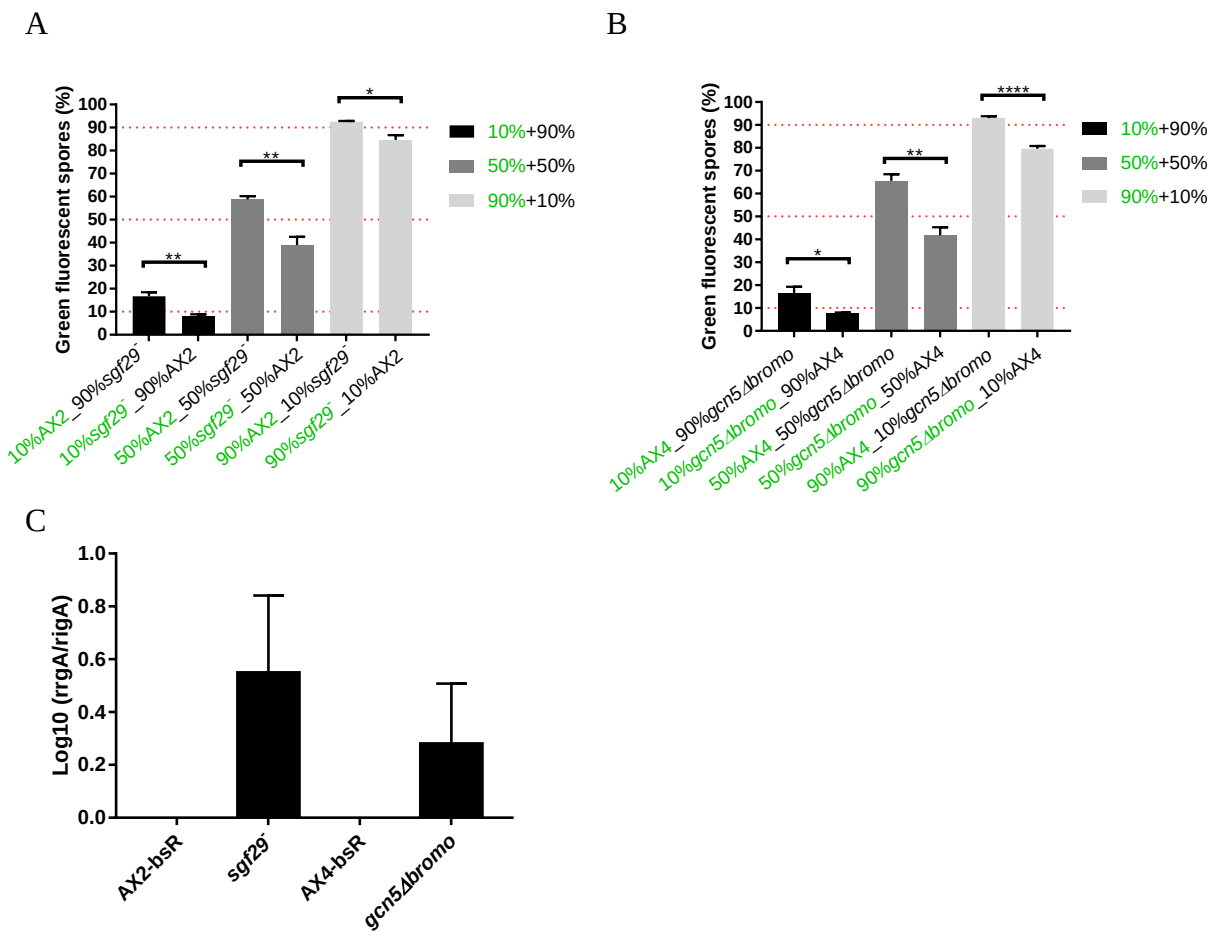


Figure 5.10. Intrinsic cell fate bias in *sgf29*$^{-}$ and *gcn5⊿bromo* mutants. (A) Mixing experiments of AX2-bsR and *sgf29*$^{-}$ cells as well as (B) mixing experiments of AX4-bsR and *gcn5⊿bromo* cells were performed as described in the legend to Figure 3.4A. N = 4. Three repeats were carried out by M. Papayova, and one repeat was from my work. Mean ± S.E.M. Student *t*-test (two-tailed): *: P < 0.05; **: P < 0.01; ****: P < 0.0001. (C) *rrgA/rigA* expression ratios in *sgf29*$^{-}$, AX2-bsR (calibrator control for *sgf29*$^{-}$), *gcn5⊿bromo* and AX4-bsR (calibrator control for *gcn5⊿bromo*) were examined by qPCR. The method was described in the legend to Figure 5.3A. N = 3. Mean ± S.E.M.

5.3.5 Pharmacologically altered histone acetylation via treatment with TSA during growth leads to a cell fate bias

The genetic mutant strains used here have altered methylation and acetylation of histone H3 during both growth and development. Another way to assess the effect of histone acetylation on cell fate is to pharmacologically manipulate the histone acetylation level via treatment with an inhibitor of HDACs, TSA. This can be used to pre-treat cells to determine if the cell fate tendency seen is a bias apparent in growing cells or is solely due to effects during development. AX2 cells can complete the development cycle but form smaller fruiting bodies at 24 hrs when continuously exposed to 250 nM TSA during development, whereas the development is

completely inhibited by 4 μM TSA on agar (Huang et al., 2021). 4-hr treatment with TSA during growth has been shown to increase acetylation levels on H3 in *Dictyostelium* (Hsu et al., 2012).

To investigate whether the cell fate tendency is influenced by the increased global histone acetylation on H3 during growth, and since assessment of spore cell fate tendency in chimeric mixing experiment relies on spore formation, a moderate concentration of TSA (400 nM) was chosen for pre-treatment of AX2 cells before mixing with untreated cells (Figure 5.11A). AX2 cells pre-treated with 400 nM TSA for four hours during growth had reduced spore formation compared to the untreated group, for example, in the 10%L/90%UL mixing ratio, labelled TSA-pre-treated AX2 formed 9.3% ± 0.5% spores, which is less than those formed from labelled DMSO-treated cells (14.9% ± 1.9%), indicating a stalk cell fate tendency in cells with high histone acetylation levels, and this trend was seen in other mixing ratios. One explanation is that this time of pre-treatment with this concentration of TSA is not sufficient.

Monolayer stalk induction assays were also performed. A stalk cell fate-biased strain *tpc2*$^{-}$ was included to determine if it can change its cell fate preference upon increased histone acetylation in growth. 4 μM TSA has been reported to rapidly increase level of H3Ac in *Dictyostelium* growth and development (Hsu et al., 2012; Huang et al., 2021). However, when pre-treated with 4 μM TSA for four hours, AX2 and *tpc2*$^{-}$ cells did not show a significant difference in pre-stalk cell marker *ecmB*-GAL expression between TSA-treated or untreated cells, and *tpc2*$^{-}$ cells still had unchanged stalk cell fate bias compared to AX2 cells regardless of the pre-treatments (Figure 5.11B). It is possible that the time of 4-hr growth with higher TSA concentration was still not enough to change cell fates.

Moreover, when grown in HL5 supplied with TSA for either 4 hrs or 24 hrs, AX2 cells showed different *rrgA/rigA* expression ratios (Figure 5.11C). Cells with 24-hr incubation with 400 nM TSA had a higher *rrgA/rigA* expression ratio compared to the untreated group, which is consistent with stalk cell fate bias in TSA pre-treated cells observed in mixing experiments. 4-hr treatment did not show the expected cell fate tendency, indicating that longer time is required for gene expression changes in response to TSA, similar to the pH effect described earlier.

To conclude, although loss of Set1-mediated H3K4me3 was reported to lose or delay TSA-mediated H3Ac (Hsu et al., 2012; Huang et al., 2021), and loss of Set1 or lack of H3K4me3 generates a stalk cell fate preference, increasing histone acetylation upon TSA pre-treatment in growth predisposes a stalk cell fate rather than spore cell fate in chimeric mixing experiments and cell fate-predicting *rrgA/rigA* expression ratio assessment. Cell fate decisions in both AX2 and *tpc2*$^{-}$ upon 4-hr TSA pre-treatment in monolayer stalk induction assay remain unchanged. This might show that the predisposition effect due to histone acetylation rather than later effect during development has different consequences for cell fate decisions, or that elevation of global H3Ac may have little effect on the DIF-1-associated pre-stalk cell lineage differentiation.

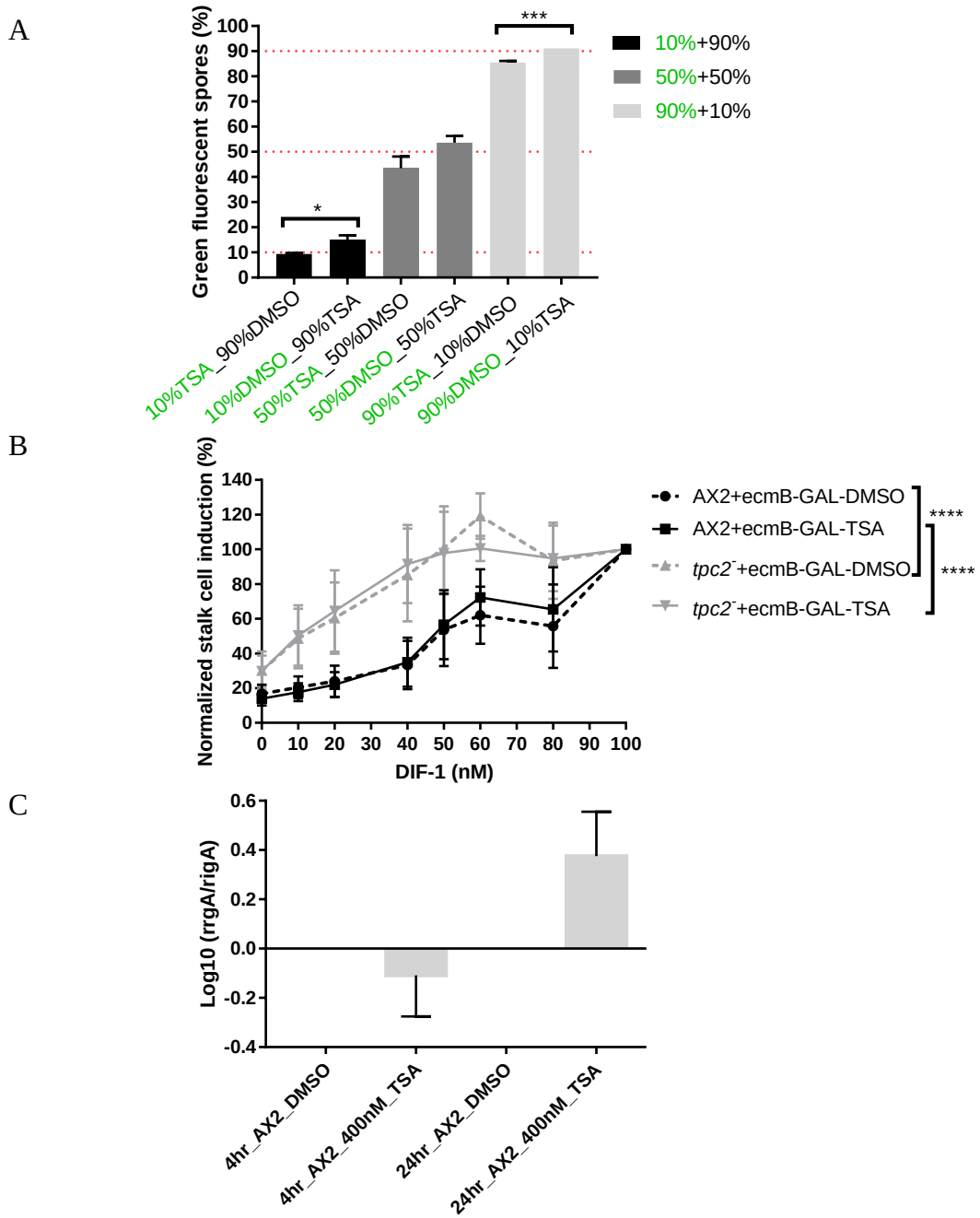


Figure 5.11. Pre-treatment with TSA alters cell fate bias. AX2 cells growing exponentially were either 4-hr pre-treated with TSA or vehicle control DMSO in HL5 medium before performing cell fate assays. (A) Mixing experiments of AX2 cells with 400 nM TSA pre-treatment history. The method for chimeric development in mixtures was described in the legend of Figure 3.4A. N = 3. Mean ± S.E.M. Student *t*-test (two-tailed): *: $P < 0.05$; ***: $P < 0.001$. (B) Monolayer stalk induction assays of cells with 4-hr pre-treatment of 4 μM TSA. AX2 cells and *tpc2*$^{-}$ cells transfected with stalk marker *ecmB*-GAL were used. The method of this assay was conducted as described in the legend of Figure 3.5A. N = 3. Mean ± S.E.M. Two-way ANOVA: ****: $P < 0.0001$. (C) *rrgA/rigA* expression ratios in growing AX2 cells following 4-hr or 24-hr 400 nM TSA treatment were assessed by qPCR. The method was described in the legend to Figure 5.3A. DMSO vehicle control groups in 4-hr and 24-hr treatment were set as calibrator controls. N = 2. Mean ± S.E.M.

5.3.6 Loss of histone H3K4 methylation leads to increased mTORC1 activity during growth and early development

To investigate whether the stalk cell fate bias observed in the situations with loss of H3K4me3 correlate with high mTORC1 pathway activity, as discussed in Chapter 4, mTORC1 pathway activity in *set1*$^-$ cells was examined. *set1*$^-$ cells have a high level of mTORC1 pathway activity during growth and at the onset of development as determined by the phosphorylation of 4E-BP1 compared to AX2 cells (Figure 5.12A). Consistent with this, in the rapamycin-induced aggregation assay, *set1*$^-$ cells were relatively insensitive to the ability of low rapamycin concentrations to trigger aggregation in half-strength HL5 with a lower aggregation score at 5 nM and 10 nM rapamycin: (both of them scored 1.0 ± 0.6) compared to AX2 cells (1.3 ± 0.3 and 1.7 ± 0.3, respectively) (Figure 5.12B). However, the aggregation score of *set1*$^-$ cells dramatically decreased at 50 nM rapamycin (0.3 ± 0.3) compared to AX2 cells (2.0 ± 0.0) and no aggregating structures were apparent in higher rapamycin concentrations (100 nM and 500 nM) (Figure 5.12B). This suggests that a longer-term treatment with high rapamycin concentrations for 22 hrs in this assay may have other effects. For example, it might also alter mTORC2 activity in the *set1*$^-$ mutant which was not seen in other strains. H3bK4A cells also tend to be less sensitive to rapamycin-induced aggregation in half-strength medium conditions, only showing aggregate structures when induced with 50 nM or higher rapamycin concentrations (Figure 5.12C). For example, at 100 nM rapamycin induction, H3bK4A cells had a lower score (1.3 ± 0.3) than AX2 cells (2.3 ± 0.3) (although not being statistically significant). Hence, ablation of H3K4me3 results in increased mTORC1 activity, indicating that histone modification regulating gene expression might change cell fate through mTORC1.

Conversely, AX2 cells with different nutrient history in vegetative growth have unchanged levels of H3K4me3 (Figure 5.12D), comparing G+ control cells to G- cells, which choose a stalk cell fate over spore cell fate and tend to have higher mTORC1 activity levels as revealed by rapamycin sensitivity reported in Chapters 3 and 4. Since the predisposition of glucose levels in growth and histone methylation both influence cell fate decisions through altering mTORC1 activity, it is possible that mTORC1 pathway is at the downstream of H3K4 methylation, which need further investigation.

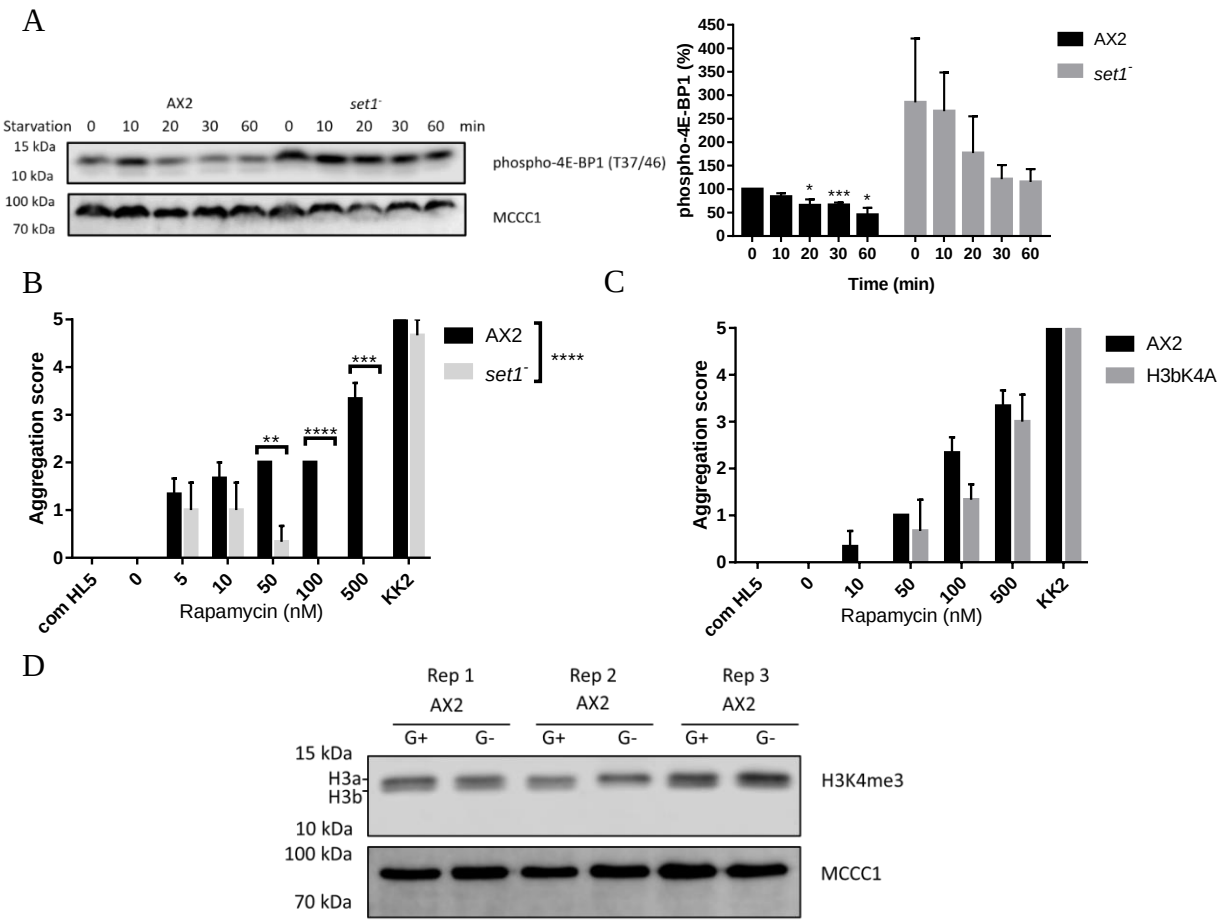


Figure 5.12. mTORC1 activity in *set1*⁻ cells. (A) Western blotting of phospho-4E-BP1 in AX2 and *set1*⁻ cells for time points up to one hour following starvation were carried out as described in the legend to Figure 4.6. One representative repeat, N = 4. Mean ± S.E.M. Antibodies for western blots: phospho-4E-BP1 (1:1000) and MCCC1 (loading control, 1:1000). (B) Rapamycin sensitivity of *set1*⁻ and (C) H3bK4A compared to AX2 cells assessed in half-strength HL5 medium. The rapamycin-induced aggregation assays were carried out and the aggregation events were assessed by a semi-quantified scoring system as described in the legend of Figure 4.7. N = 3. Mean ± S.E.M. Student *t*-test (two-tailed) and two-way ANOVA: *: P < 0.05; **: P < 0.01; ***: P < 0.001; ****: P < 0.0001. (D) H3K4me3 levels in AX2 cells grown in different nutrient history. Exponentially growing AX2 cells were grown in glucose sufficient G+ medium or glucose deficient G- medium in HL5 for 48 hrs before harvesting for H3K4me3 western blot analysis as described in the legend to Figure 5.7C. Three biological repeats (Rep 1, 2 and 3) are shown.

5.4 Discussion

This chapter has determined that:

1) The ratio of *rrgA* and *rigA* reciprocal expression during growth can be used to predict the predisposition of cell fate bias: a high *rrgA/rigA* ratio correlates to a stalk cell fate bias (growth history with low pH/vesicle pH, low glucose and TSA treatment; mutants *tpc2*$^{-}$, *dmpA*$^{-}$, *set1*$^{-}$ and *set1*$^{-}$ cells rescued by expression of catalytically dead mutant GFP-Set1:C1474A, H3bK4A, *sgf29*$^{-}$, *gcn5⊿bromo* cells). A low *rrgA/rigA* ratio predicts a spore cell fate (growth history with high pH/vesicle pH, high glucose, treatment with mTORC1 inhibitors; rescue strain *set1*$^{-}$ expressing GFP-Set1). This expression ratio is a biomarker for indicating cell fate decisions prior to development rather than the cause of cell fate bias. Therefore, the high *rrgA/rigA* expression ratios in *fbxA*$^{-}$ and *iplA*$^{-}$ strains which are the opposite to that expected for their spore cell fates in mixing experiments could indicate complicated roles of FbxA and IPLA in growing and developmental stages.
2) *set1*$^{-}$ and *set1*$^{-}$ cells expressing the catalytically inactive mutants GFP-Set1:N1425Q or GFP-Set1:C1474A are shown to have stalk cell fate biases compared to *set1*$^{-}$ cells rescued by expression of GFP-Set1 and parental AX2.
3) H3K4me3 and H3Ac influence cell fate decisions through a Set1-Sgf29-Gcn5 signalling pathway. Mutant strains including *set1*$^{-}$ and H3bK4A with all or partial loss of H3K4me3 and mutants of HAT module components in SAGA complex *sgf29*$^{-}$ and *gcn5⊿bromo* all had stalk cell fate bias.
4) The stalk cell fate bias in cells with a growth history of HDAC inhibitor TSA pre-treatment, however, was not as predicted.
5) mTORC1 pathway activity is potentially downstream of H3K4me3 methylation, as loss of Set1 leads to high mTORC1 pathway activity. Future directions to study this pathway can investigate whether the expression levels of mTORC1 regulators (e.g. Rheb and AMPK) or components of mTORC1 complex (e.g. mTOR and Raptor) are altered. The expressions of the genes encoding mTORC1 subunits or positive regulators might be upregulated to increase the amount of mTORC1 complex and/or its activity.

Gene expression is strictly regulated by different mechanisms at multidimensional levels, such as chromatin structure, regulatory elements in DNA sequences, transcription factors etc. (Bannister and Kouzarides, 2011; Koch, 2015; Remenyi et al., 2004; Strahl and Allis, 2000). Robust gene expression regulation in a spatiotemporal manner is important in organism development. Among different model organisms, histone modifications such as methylation and acetylation are well-conserved PTMs that have chromatin remodelling roles and therefore, by being associated with specific genes, regulating gene expression involved in processes such as development (Bannister and Kouzarides, 2011; Wu et al., 2021). Cell fate is one outcome that could be affected by gene expression associated with histone PTMs, such as H3K9me3-decorated heterochromatin involvement in gene silencing during cell fate determination by sequestrating and suppressing specific genes inappropriate to the commitment of other lineages by shielding gene regulatory sequences from active transcription factors (Becker et al., 2016; Rugg-Gunn et al., 2010).

This chapter revealed that cell fate biases can be changed by manipulating histone modifications. The effect of alteration of histone methylation on H3K4 were tested with genetic disruption of Set1 coding sequences in *set1*$^{-}$ and *set1*$^{-}$ rescue strains expressing wt GFP-Set1, or catalytically dead mutants N1425Q and C1474A (Chubb et al., 2006a) as well as H3bK4A gene replacement strains (Hsu et al., 2012). Disruption of the SET catalytic domain leads to loss of histone H3K4 methylation, but SET domain-containing lysine methyltransferase family members could also methylates other non-histone proteins, such as transcription factors and ribosomal proteins, and regulate their cellular functions (Del Rizzo and Trievel, 2011; Huang and Berger, 2008; Mahesh et al., 2020; Sugeedha et al., 2021). The stalk cell fate bias seen in *set1*$^{-}$ cells can be rescued by expressing GFP-Set1, but the unbalanced stalk cell fate was persistently seen when expressing the catalytically dead GFP-Set1:N1425Q and C1474A mutant proteins in the *set1*$^{-}$ cells. This indicates that the stalk fate-biased phenotype of the *set1*$^{-}$ cells, at least in part, is due to the defect in HMT catalytic activity, therefore, Set1 is not just through acting as a scaffold in a complex. A strain with gene replacement to express only the H3bK4A mutant protein only losing the H3K4me modification on H3b variant (Hsu et al., 2012) also prefers stalk cell fate, indicating that H3K4me mediates cell fate regulation. However, it does not rule out an additional involvement of other targets of Set1, or modification on H3a variant may also play a role, since H3aK4A strain has been reported to have completely no lysine 4 tri-methylation on both H3a and H3b variants, while H3bK4A still has apparent but

decreased level of K4me3 on H3a variant (Hsu et al., 2012). Both *set1*$^{-}$ and H3bK4A strains have relatively high mTORC1 activity, as defined by rapamycin-induced aggregation assays, which correlates with the observation in Chapter 4 that high mTORC1 activity leads to stalk cell fate bias. However, G+ and G- treatment during cell growth, which have altered mTORC1 activity shown in Chapter 4, have similar H3K4me3 levels. Total histone H3K4 methylation level on nucleosomes associated with all genes is completely lost in *set1*$^{-}$ cells (Chubb et al., 2006a) and H3b-associated H3K4me3 is completely lost in the H3bK4A mutant (Hsu et al., 2012). It is therefore possible that the histone modifications on nucleosomes associated with specific genes play important roles in directing cell fate decisions through the ultimate effector mTORC1 and relevant genes, but this would not be apparent when assessing the total levels of histone modification in all histone H3 detected in whole cell lysates by western blotting. However, it is possible that loss of H3K4me3 acts to alter expression of certain genes that, in turn activate mTORC1 activity or that mTORC1 activity alters the histone modifications at a subset of important genes for defining cell fate bias.

To understand whether the established pathway by which H3K4me3 recruits the histone acetyltransferase Gcn5 via Sgf29 is involved in the stalk cell fate bias, the cell fate preference in strains containing mutations of these key components of the SAGA histone acetyltransferase complex, *sgf29*$^{-}$ and *gcn5⊿bromo* were investigated. It was confirmed that loss of Sgf29 and reduction of Gcn5 leads to a preferential stalk cell fate decision similar to *set1*$^{-}$ cells. This is consistent with the importance of pathway coupling H3K4me3 and H3Ac modifications, influencing cell fate decision by SAGA complex-mediated gene expression regulation. In summary, Set1, Sgf29 and Gcn5 could work together to regulate a particular pattern of gene expressions and thus affect cell fate decisions, although it cannot be ruled out that Set1 and Set1-mediated H3K4me3 may affect cell fate through other mechanism.

To distinguish whether histone modifications affect cell fate during growth or development, pre-treating cells with different inhibitors of histone modifiers could help. However, inhibitors of histone modifiers can have multiple targets involved in other important biological activities. For example, the HDAC inhibitor TSA is a broad-spectrum inhibitor of class I and II HDACs, and there is precedent for TSA not only potently promoting cell differentiation but also triggering cell cycle arrest at G1 and G2 phase in rat fibroblasts even at a low concentration

(Furumai et al., 2001; Yoshida et al., 1990). In *Dictyostelium*, pharmacologically increased histone acetylation levels can be achieved via treatment of growing cells with the TSA (Hsu et al., 2012), thus it was used to test if this change during cell growth could lead to cell fate alterations. It was surprising that TSA treatment in growth predisposes cells to a stalk cell fate tendency in mixing experiments but does not showing any tendency of intrinsic cell fate changes in the monolayer stalk induction assay for both AX2 and *tpc2*$^{-}$ cells. It is worth mentioning that mixing experiments involve more complex cell-cell communications and multiple signals during multicellular development to impact on cell fate decision-making, e.g. promoting cells to form more spores and less likely to form stalk cells, while monolayer stalk induction assays only look at a DIF-1 induced stalk cell differentiation tendency *in vitro*. It might also be that histone acetylation affects later developmental activities that give rise to changes in cell fate decisions, which cannot be assessed with pre-treatment of TSA during growth.

Limitations of TSA treatment in cell fate assays exist. As discussed earlier, high TSA concentration treatment of cells during development has been reported to have acute inhibitory effect on development, leading to developmental delay and reduced number of later multicellular structures (Huang et al., 2021), which might be a potential problem in mixing experiments even though using a moderate concentration of TSA (400 nM). Moreover, it is hard to directly compare the effect of increased histone acetylation through TSA treatment to the strains with reduced histone acetylation levels, as these altered histone acetylation levels in these two situations can affect histones associated with different genes with differential effects. Future experiments need to include longer exposure to TSA treatment during growth and only in development during monolayer cell fate assays to investigate whether elevated histone acetylation in development cause alternative cell fate bias. Other HDAC inhibitors such as valproic acid (VPA) (Göttlicher et al., 2001) and suberoylanilide hydroxamic acid (SAHA) (Finnin et al., 1999) which were reported to regulate cell differentiation and cell growth in mammalian models and clinical studies (Cheng et al., 2019) have been also used in *Dictyostelium* (Huang et al., 2021; Xu et al., 2007) and can be used to verify the effect of histone acetylation modification on cell fate decisions.

These changes in histone PTMs are presumed to work through changes in gene expression to

lead to a predisposition effect on cell fate decisions. The ratio of expression of two genes *rrgA* and *rigA* during growth has been proposed to function as a potential cell fate marker (Gruenheit et al., 2018). Therefore, an assay was established to assess the expression ratio by qPCR and analysed with a comparative ΔΔCt method. To verify that this ratio could predict cell fate bias before entering development, cell fate influencing factors which mediate a stalk cell fate bias were tested, such as glucose deficient history (48 hrs) and low pH history (24 hrs) in growing cells and these indeed were shown to have high *rrgA/rigA* expression ratios. This was then tested on cells with a spore cell fate preference mediated by the treatment during growth with the mTORC1 inhibitor rapamycin and general mTOR inhibitors AZD8055 and BEZ235 and it was found that these correlated with lower *rrgA/rigA* expression ratio. TSA pre-treatment was also tested which gave a high *rrgA/rigA* expression ratio consistent with fewer spore cells formed in mixing experiments. However, the length of treatment was found to be important, as *rrgA/rigA* expression ratios in cells in 4-hr pre-treatment conditions do not correlate with the cell fate assay results, while 24-hr treatments lead to a more accurate prediction of cell fates. This indicates that this ratio of these two mRNA transcript levels is not the cause of cell fate bias and that changes in the mRNA levels of these genes require sufficient time to happen that the cell fate bias. Gruenheit et al. (2018) concluded that the genes involved in RasD regulatory network have the potential to influence signalling in response to external signals, which forms a buffering mechanism for compensating the perturbation of cell cycle dynamics. Thus, in my experiments the alteration of *rrgA* and *rigA* expression ratios is more likely to be a consequence of cell fate changes upon the effect of cell fate determinants.

As well as alteration of extrinsic conditions during growth, genetic mutants that have a cell fate preference were also tested. A high *rrgA/rigA* expression ratio seemed to be predictive in some stalk cell fate-biased strains such as *tpc2*$^{-}$ and *dmpA*$^{-}$ cells as well as *set1*$^{-}$ cells. Rescue of *set1*$^{-}$ cells by expression of wildtype but not catalytically dead GFP-Set1 showed a low *rrgA/rigA* ratio, consistent with its loss of cell fate decision bias. This high ratio was also reported in *sgf29*$^{-}$, *gcn5⊿bromo* and H3bK4A mutant strains compared to their parental controls which all have stalk cell fate biases. However, in some other strains, the correlation was lost. The *fbxA*$^{-}$ and *iplA*$^{-}$ strains both have a high *rrgA/rigA* expression ratio in vegetative growth that did not correlate with their spore cell fate bias in mixing experiments with AX2 cells. However, in monolayer stalk induction assays, *fbxA*$^{-}$ cells showed an increased stalk marker expression induced by low DIF-1 concentrations. This is contrary to the spore cell fate preference shown

in chimeric development in mixtures with AX2 cells and these mixing experiments are consistent with previous findings (Ennis et al., 2003). The *fbxA*$^{-}$ strain has been found to form pre-stalk cells when developing in low densities or not in chimeras (Ennis et al., 2003) and the monolayer assay for stalk cell differentiation requires low cell number to avoid multicellular structure formation. Also, *fbxA* mRNA levels reported in RNA-seq experiments were low before 10-hr development and dramatically increased in later development stages (Rosengarten et al., 2015). Therefore, FbxA might influence cell fate decisions in later development, revealing the importance of distinguishing predisposition and developmental effect on cell fate bias alteration. This is challenging to do in mutant strains where alterations are found during growth and development.

One limitation of using the *rrgA/rigA* expression ratio to predict cell fate is that these two genes play roles in cell fate buffering system only when the RasD activity in the cell cycle regulatory network is perturbated by extrinsic factors in growth or genetic factors (Gruenheit et al., 2018). Another pair of genes involved in the RasD responsive network, *rrgB* and *rigB* have been shown to have a similar ability in cell fate prediction in response to altered RasD states (Gruenheit et al., 2018). If only genes involved in the GefE-RasD regulatory network are used for cell fate prediction, other cell fate determinants that alter cell fates via different mechanisms could be missed, as there could be multiple signalling pathways, not just the one aspect of cell cycle in a complicated regulatory network of complicated cell fate decisions. Thus, it may be more predictive to assess the transcription level of multiple genes shown to be differentially expressed in cells with fate bias. Expression levels of lineage-specific transcription factors have been shown to be involved in regulating embryonic stem cell fates (Casey et al., 2018; Morris, 2016; Yamamizu et al., 2013) and equivalent genes might also be candidates in *Dictyostelium* to indicate cell fate bias under various contexts. A combinatorial cell fate assessment platform is required to study cell fate decision-making process by separating predisposition and later development effects of cell fate determinants using longer or shorter treatments of drugs as well as developmentally-regulated genetic changes in multiple cell fate assays.

Chapter 6. Does iron have a role in early development and influence cell fate decisions?

6.1 Introduction

6.1.1 Iron has essential roles in organisms' growth and development

Iron is an important transition metal ion abundant in living cells and its sensitivity towards oxygen and reactive oxygen species (ROS) including H_2O_2 makes it an important cellular redox sensor which is well conserved (Outten and Theil, 2009; Sigel and Sigel, 1998). Existing in many forms in the cellular environment, iron coordinates with proteins physiologically and biochemically in different ways, either as individual ions, ferrous (Fe^{2+}) and ferric (Fe^{3+}), or via a cofactor such as in iron-sulfur (Fe-S) clusters or heme groups in proteins (Andreini et al., 2018; Ciofi-Baffoni et al., 2018). Iron is required as a common protein co-factor involved in many cellular processes such as DNA/RNA synthesis (Boldt, 1999), oxidative phosphorylation and the citric acid cycle (Oexle et al., 1999). In turn these can lead to changes in cell behaviour such as cell cycle progression (Le and Richardson, 2002), T cell-mediated immune responses to virus infection (Frost et al., 2021) and bacterial infection resistance (Bozzaro et al., 2013; Buracco et al., 2017). Iron and its binding proteins have a role in T cell activation, for example, upon activation of CD4+ helper and CD8+ cytotoxic T cells (which are two main lineages of T cells) (Karimi et al., 2021), upregulated expression levels of iron transport proteins such as the transferrin receptor 1 (TfR1, also known as CD71) and iron sensing proteins such as iron-responsive element-binding protein 1 (IREB1) are observed in T cell effector states compared to naïve states (Howden et al., 2019). Excessive iron overload which is pathological and arises from mutations in iron regulatory genes, causing diseases such as hereditary hemochromatosis, and the patients usually have much higher risks of developing cancer due to dysregulation in iron homeostasis (Torti et al., 2018). For instance, high expression levels of TfRs facilitating iron uptake are observed in different types of cancers (Singh et al., 2011), while expression of ferroportin 1 (Fpn1) which is the only known cellular iron exporter, is downregulated (Hentze et al., 2010; Rouault, 2006). Excessive intracellular iron levels via hijacking the mechanisms of iron homeostasis by iron regulatory proteins are

exploited by cancer cells, leading to cancer progression and tumour metastasis (Guo et al., 2021; Shang et al., 2020). Iron chelators such as deferoxamine (DFO) have been used as anticancer agents for treating neuroblastoma (Donfrancesco et al., 1990), showing the importance of iron in tumour growth.

Iron is a vital nutrient source involved in cell differentiation and development. One example is erythroblast development, and erythroid precursor cell differentiation into mature haemoglobin-containing red blood cells greatly depends on a ferritin iron source supported by macrophages (Leimberg et al., 2008). Exogenous iron in the culture medium can also modulate osteoclast lineage differentiation from hematopoietic stem cells, increasing proliferation of the progenitor fate of osteoclast cells with macrophage-like phenotypes and decreasing osteoclast development (Xie et al., 2016b). T cell differentiation is closely regulated by iron during T cell-mediated immune responses against pathogen infections. For example, iron stimulates the expression of T cell immunoglobulin and mucin containing protein-3 (TIM-3) which is a negative regulator of the immune checkpoint for T cell priming, and thus inhibiting the differentiation of naïve CD4+ T helper cells to the effector T helper type 1 (Th1) lymphocytes, producing interferon-gamma (IFNγ) for intracellular pathogenic infection control (Pfeifhofer-Obermair et al., 2021). There are also studies reporting that iron homeostasis in cells is regulated by mTOR signalling which links metabolism and inflammation to iron-mediated pathways. Iron chelator treatment reduces mTORC1 activity in cancer cell lines (Shang et al., 2020). mTORC1 activates its downstream effector, tristetraprolin (TTP) which plays a part in anti-inflammatory responses, to modulate the stability of the TfR1 controlling cellular iron influx (Bayeva et al., 2012). mTORC1 is also involved in regulating differentiation of memory CD8+ T cells, where rapamycin treated naïve CD8+ T cells have an increased quantity and quality of memory precursor effector cells (Araki et al., 2010). Also, reduced expression of important glycolytic enzymes including hexokinase 2 pyruvate kinases, lactate dehydrogenase and phosphofructokinase 1 in activated CD8+ T cells were observed upon rapamycin treatment (Finlay et al., 2012). Changing iron levels in T cells can alter mTORC1 activity, for instance, in CD8+ T cells decreased iron levels result in a reduction of mTORC1 activity (Frost et al., 2021).

6.1.2 The effects of iron in *Dictyostelium*

Relatively little is known about specific roles for iron in *Dictyostelium*. The *Dictyostelium* genome encodes iron-regulated proteins highly conserved with mammalian versions, including two iron transporter orthologues of natural resistance-associated macrophage proteins (Nramps). Nramp1 is mainly located on phago-lysosomes (similar to macrophages), and Nramp2 exclusively on contractile vacuoles, both of which facilitate iron transport energised by the proton gradient generated by the vacuolar type-H^+-ATPase (Bozzaro et al., 2013; Peracino et al., 2013). Thus, iron transport is closely related to vesicle pH in acidic compartments containing proton pumps, and vesicle pH is one of the important cell fate influencing factors discussed in previous chapters (Clarke et al., 2002; Davies et al., 1996; Davies et al., 1993; Gross et al., 1983). Nramp1 has a role in phagocytosis and defending *Dictyostelium* cells against bacterial infection (Buracco et al., 2017). Upregulated expression of the *nramp1* gene is observed when cells are incubated with bacteria during growth as Nramp1 mediates iron efflux from phagosomes to induce iron starvation and killing of pathogenic bacteria, and the expression level of *nramp1* decreases during *Dictyostelium* development (Peracino et al., 2013; Peracino et al., 2006). Nramp2 on the other hand has shown to be exclusively expressed on contractile vacuoles which are potential labile iron stores, indicating a role in adapting to environmental changes and regulating osmolarity (Bozzaro et al., 2013; Peracino et al., 2013). As in higher eukaryotic cells, host-pathogen interactions depend on iron homeostasis in *Dictyostelium* cells. The roles of iron in defence mechanisms against bacterial invasion has been studied in the phagocytic *Dictyostelium* model which harbours similar iron-related genes to macrophages (Bozzaro and Eichinger, 2011; Peracino et al., 2013), and cells in iron depletion or overload growth conditions are more resistant or sensitive to *Legionella pneumophila* infection (Buracco et al., 2017). Pathogens such as *Escherichia coli* express virulence genes to exploit iron uptake metabolism and escape from the predation by *Dictyostelium* (Adiba et al., 2010).

Little is known about the importance of iron in development of *Dictyostelium*, however, a recent report describes a role for sulphur and in particular its importance in proteins containing Fe-S clusters in early development (Kelly et al., 2021). Many proteins contain Fe-S clusters, linking iron and sulphur metabolism. Cysteine which provides a source of sulfur, is important for Fe-S protein assembly, and depletion of cysteine triggers growth arrest in *Neisseria*

meningitidis pathogen (van de Waterbeemd et al., 2013). In *Dictyostelium*, it has been known for a long time that cysteine depletion is one of the triggers for development (Marin, 1976). Cells with cysteine depletion growth history have higher demand of cysteine during development than normal starved cells (Kelly et al., 2021). One important iron-dependent enzyme, nitrogen fixation 1 (NFS1), which is well-conserved in eukaryotes, is a cysteine desulfurase that extracts sulfur from cysteine to synthesize Fe-S clusters (Alvarez et al., 2017; Biederbick et al., 2006).

Reduction in NFS1 expression by small interfering RNAs (siRNA) in *Dictyostelium* promotes aggregation and the cells do not respond to cysteine-mediated aggregation rescue (Kelly et al., 2021). Upon starvation, ROS accumulate in *Dictyostelium* cells, leading to the sequestration of cysteine, prioritizing synthesis of antioxidant glutathione (GSH) and stopping Fe-S cluster synthesis involved in mitochondrial metabolism and therefore required for cell proliferation (Kelly et al., 2021). Such ROS-mediated sulfur restriction during *Dictyostelium* starvation sets limits for the activity of enzymes containing Fe-S clusters which could be limiting upon iron and sulfur starvation, and the antagonistic role of cysteine in aggregation, with the consequence of low Fe-S cluster production, dictates the decision to enter development (Kelly et al., 2021). The importance of iron availability is less well understood. Iron depletion and iron overloading over 0.2 mM have been reported to inhibit *Dictyostelium* cell growth (Bozzaro et al., 2013; Buracco et al., 2017), while development of cells which have been pre-incubated with 200 μM iron in minimal medium leads to fragmented elongated streams before forming multiple mounds that eventually form fruiting bodies in normal timing (Buracco et al., 2017).

Since both iron and mTOR have essential roles in regulating cell differentiation in mammalian T cells in adaptive immunity (Araki et al., 2010; Frost et al., 2021; Teh et al., 2021) and cysteine-regulated Fe-S cluster synthesis is involved in early development upon nutrient starvation in *Dictyostelium* (Kelly et al., 2021). It is of interest to study whether iron is an essential nutrient to affect the entry into development and cell fate decisions in *Dictyostelium* development. This iron-dependent cell fate project was inspired by our collaborator Prof. Hal Drakesmith's Lab.

6.2 Aims

This chapter is to investigate:

(1) whether the level of iron (source ferric chloride ($FeCl_3$)) impacts on *Dictyostelium* aggregation
(2) whether growth of cells with and without $FeCl_3$ influences cell fate. This will be investigated using cell fate assays: mixing experiments and monolayer stalk induction assays as well as determining the cell fate marker *rrgA/rigA* expression ratio

6.3 Results

6.3.1 The consequence of altering iron levels during growth and early development

6.3.1.1 High concentrations of iron inhibit aggregation

To assess the effect of the presence of excess iron on aggregation during *Dictyostelium* development, different concentrations of $FeCl_3$ were added to an under-buffer aggregation assay and the aggregate formation of AX2 cells was assessed at different time points (Figure 6.1A). KCl osmotic and chloride ion control groups (0-100 μM) showed cells aggregating effectively from 16 to 24 hrs. Using the scoring system to assess the aggregates at 22 hrs with the method described in the previous rapamycin-induced development assay (Figure 6.1B), it was shown that in control experiments aggregates formed at all KCl concentrations, for example, at 50 μM and 100 μM, the aggregates are scored at 5.0 ± 0.0. However, $FeCl_3$ treated groups had lower aggregation scores at 22 hours or a delay in aggregation at concentrations of $FeCl_3$ above 10 μM. At 22 hrs, 50 μM and 100 μM $FeCl_3$-treated groups have significantly fewer aggregates with scores of 1.3 ± 0.3 and 0.7 ± 0.3 respectively. Although there would be other osmotic controls better than KCl for $FeCl_3$ treatment, this preliminary data shows that the presence of extracellular iron suppresses aggregation formation in cell development.

Moreover, at 24 hrs, aggregates in $FeCl_3$-treated groups detached from the dish bottom and disaggregated. Although it was consistently seen in all three repeats, the reason for this phenomenon of disaggregation over time is unknown but could be a cell-cell adhesion blockage in response to iron. To examine whether the cells were alive in the presence of $FeCl_3$ during KK2 development, trypan blue staining was conducted to check the cell viability during $FeCl_3$ treatment at 6-hr development in KK2 (Figure 6.1C). Trypan blue dye cannot penetrate the intact cell membranes of live cells, leaving a clear cytoplasm excluding the dye, and the dye only stains the dead cells which have damaged membranes so they take on a blue colour (Strober, 2015). The cells incubated with $FeCl_3$ were not blue in colour following treatment with trypan blue dye compared to the positive control cells with blue colour, indicating that the cells survived in concentrations of $FeCl_3$ up to 100 μM.

To test whether iron deficiency during vegetative growth can affect cell development later on, customized minimal medium (Franke and Kessin, 1977) which had iron (100 μM $FeCl_3$)

removed from the standard FM minimal medium recipe (specially made by Formedium). For the pre-treatment groups with or without iron, vegetatively growing AX2 cells in HL5 medium were grown in the iron-free minimal medium in the presence or absence of additional 100 μM $FeCl_3$ (minimal medium +/-Fe^{3+}) for 24 hrs (Figure 6.2A). Both groups of cells grew much slower than when in HL5, with extended doubling times of around 26 to 28 hrs (data not shown) consistent with previous findings (Buracco et al., 2017; Peracino et al., 2013). It was confirmed that cells with or without iron during 24-hr pre-treatment can form aggregates equally well under KK2 development at 22 hrs (Right panel, Figure 6.2A).

In order to determine whether iron depletion is sufficient to trigger aggregation while in minimal medium, cells grown with and without iron pre-treatment were plated in iron-free minimal medium containing various $FeCl_3$ concentrations (Figure 6.2B). Scoring aggregation in iron-free conditions (0 μM $FeCl_3$) at 22 hrs (Figure 6.2C) showed that 24 hrs pre-treatment in minimal medium (-Fe^{3+}) was sufficient to trigger loose aggregate formation at 22 hrs (score of 3.0 ± 0.0) compared to cells pre-treated in standard minimal medium (+Fe^{3+}) which have a lower aggregation score (1.0 ± 0.0). The re-addition of $FeCl_3$ when plating rescued this aggregation in growth medium at 10 μM (1.5 ± 0.5) and 100 μM (0.0 ± 0.0) $FeCl_3$. In comparison to iron-starved pre-treated cells, cells pre-treated in standard minimal medium (+Fe^{3+}) generally formed very few aggregates in all iron concentrations. For example, in the presence of 1 μM $FeCl_3$, the aggregate score from cells with iron pre-treatment (0.5 ± 0.5) is lower than from iron-starved pre-treated cells (2.5 ± 0.5). Consistently, the addition of low iron concentrations such as 0.1 μM $FeCl_3$ induced some aggregates in iron-added pre-treated cells (1.0 ± 0.0) whereas higher iron concentrations did not, and aggregation of cells with iron-added growth history was not induced when they were incubated in normal levels of iron (100 μM $FeCl_3$) in standard minimal medium. Trypan blue staining was also performed to check the viability of cells pre-incubated in iron-free minimal medium (Figure 6.2D), which confirmed that the cells were alive.

These observations show that iron starvation is sufficient to induce aggregation in minimal medium and this can be suppressed by adding iron back. The requirement for $FeCl_3$ to inhibit aggregation is seen with 22 hrs, as cells plated with usual iron levels, will form some aggregates

following plating for 22 hrs in minimal medium in the absence of iron.

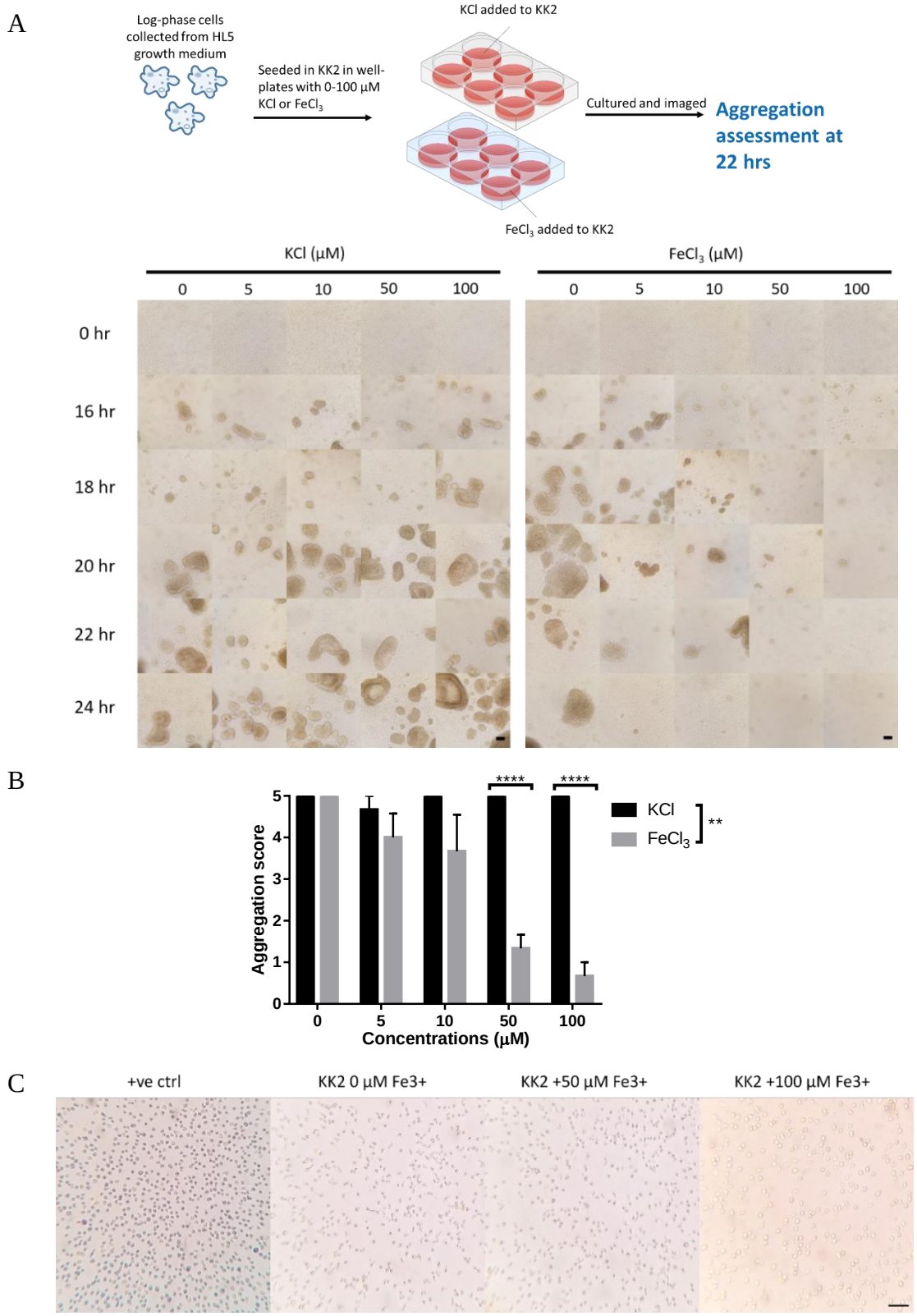
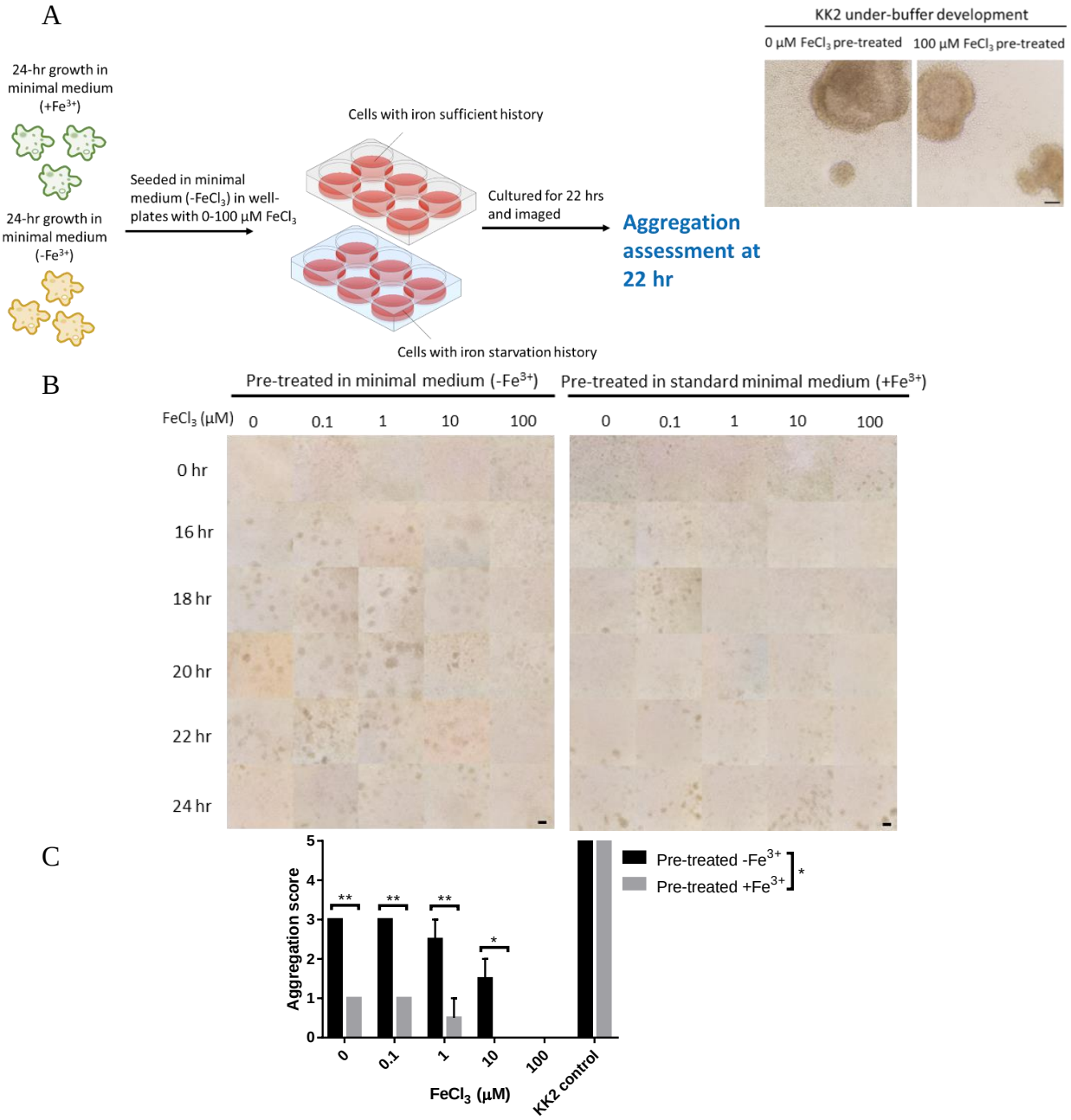


Figure 6.1. Effect of iron on early development in KK2 buffer. (A) Upper panel: Schematic representation of KK2 under-buffer development assays with iron addition: exponentially growing AX2 cells were harvested, washed twice in KK2 buffer and resuspended to 1.4×10^6 cells/mL. 1 mL cells per well were plated into a 12-well plate in KK2 with different $FeCl_3$ or KCl (control) concentrations (0-100 µM). Images from several time points were taken in

brightfield. Lower panel: One representative repeat shown, N = 3. Scale bar: 1 mm. (B) Scoring of aggregates at 22 hrs development in KK2 as described in panel (A). The aggregation scoring system was used as for analysing the rapamycin-induced development assay in the legend to Figure 4.7. N = 3. Mean ± S.E.M. Student *t*-test (two-tailed) and two-way ANOVA: **: P < 0.01; ****: P < 0.0001. (C) The viability of AX2 cells in under-buffer development for 6 hrs tested with trypan blue staining. AX2 cells grown to exponential log phase in HL5 medium were collected for under-buffer development in KK2 with 0, 50 and 100 μM $FeCl_3$ described in panel (A). After 6-hr development, 1 mL of cells at the density of 1.4×10^6 cells/mL were harvested by removing the growth medium, and the cell pellets were resuspended in 200 μL KK2 and 200 μL 0.4% trypan blue dye (Sigma-Aldrich, 72-57-1), incubating at 22°C for 5 mins before imaging. Positive control: 2×10^6 AX2 cells grown at exponential log phase in HL5 medium were incubated at 37°C for 5 hrs. Scale bar: 1 mm. N = 1.



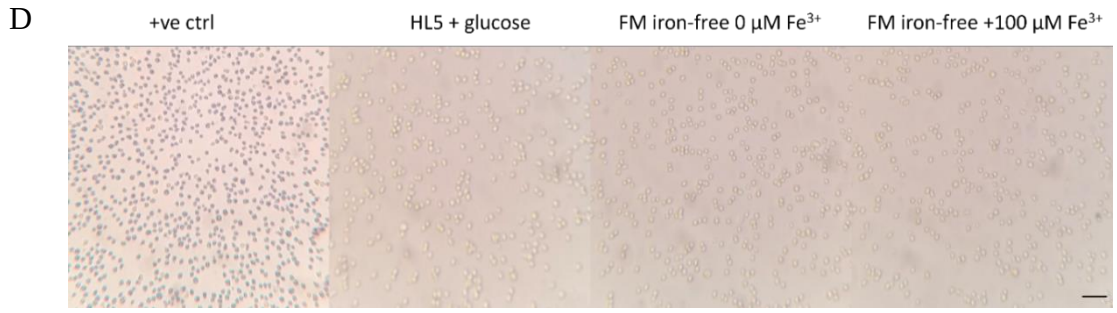


Figure 6.2. Iron depletion is sufficient to trigger aggregate formation in FM minimal medium. (A) Left panel: Schematic representation of minimal medium aggregation assay induced by iron starvation. To pre-treat the cells with different iron history during growth, exponentially growing AX2 cells in standard HL5 medium were harvested, washed twice in KK2 buffer and resuspended to 1×10^6 cells/mL in iron-free minimal medium with or without 100 μM $FeCl_3$ for 24-hr incubation. These cells were then washed twice in KK2 buffer and seeded into 12-well plates at a density of 1.4×10^6 cells/mL in either KK2 control groups (Right panel of A) which verified aggregation at 22 hrs of the cells with different iron history during growth (N = 1, scale bar: 1 mm), or in (B) iron-free minimal medium supplied with various concentrations of $FeCl_3$. 100 μM $FeCl_3$ added into iron-free minimal medium in the assays represents the standard minimal medium conditions. Images from times from 16 to 24 hrs were collected. One representative repeat shown, N = 2. Scale bar: 1 mm. (C) Scoring of aggregation formation from cells pre-treated in minimal medium (+/- Fe^{3+}) at 22 hrs in the aggregation assays described in (B). The aggregation scoring system described in the legend to Figure 4.7 was used. N = 2. Mean ± S.E.M. Student *t*-test (two-tailed) and two-way ANOVA: *: $P < 0.05$; **: $P < 0.01$. (D) The viability of AX2 cells in the minimal medium assay was assessed at 6 hrs by trypan blue staining. Cells in iron-free minimal medium which had growth history of iron-free minimal medium with or without 100 μM $FeCl_3$ for 24 hrs were stained with 0.4% trypan blue as described in the legend to Figure 6.1C. The positive control was described in the legend to Figure 6.1C. Scale bar: 1 mm. N = 1.

6.3.1.2 The effect of iron depletion on *Dictyostelium* cell fate decisions

To study whether iron starvation during vegetative growth can influence cell fate decisions, cell fates of AX2 cells pre-incubated in iron-free minimal medium with or without 100 μM $FeCl_3$ for 24 hrs were investigated. The results of mixing experiments showed that the presence of standard levels of $FeCl_3$ promoted cells to form more spores than the counterpart grown in iron-free conditions. For example, in the mixing ratio of 10%L/90%UL, cells from iron-added pre-treatment groups formed 14.7% ± 1.2% spores, whereas cells with iron starvation growth history only formed 6.7% ± 0.5% spores (Figure 6.3A). However, monolayer stalk induction assays showed that AX2 cells with a 100 μM $FeCl_3$ deficient history in 24-hr growth showed lower induction of the stalk cell marker *ecmB*-GAL (Figure 6.3B). Upon 50 nM DIF-1 induction, the expression level of stalk marker in cells with iron starvation growth history (Pre-treated -Fe^{3+}) is 67.4% ± 14.3% which is lower than the level seen in cells pre-incubated with

iron-supplied minimal medium (Pre-treated $+Fe^{3+}$) (93.0% ± 6.2%). This suggests that stalk cell induction is reduced as well as spore cell induction when cells have iron depletion growth history.

The *rrgA/rigA* expression ratios of cells incubated in minimal medium with or without iron for 24 hrs were examined using qPCR and comparative ΔΔCt analysis (Figure 6.3C). High *rrgA/rigA* expression ratios were observed in cells without iron for 24 hrs in growth compared to those incubated in minimal medium with standard 100 μM $FeCl_3$ supplied. This would be consistent with a stalk cell fate bias in cells with iron-free growth history as seen in mixing experiments. However, as these iron-depleted cells did not show increased sensitivity to DIF-1, it is possible that they are quite fragile and less healthy. An alternative is that the bias seen in mixing experiments is not due to differential DIF-1 sensitivity in stalk cell induction, but perhaps due to differential sensitivity to spore cell induction.

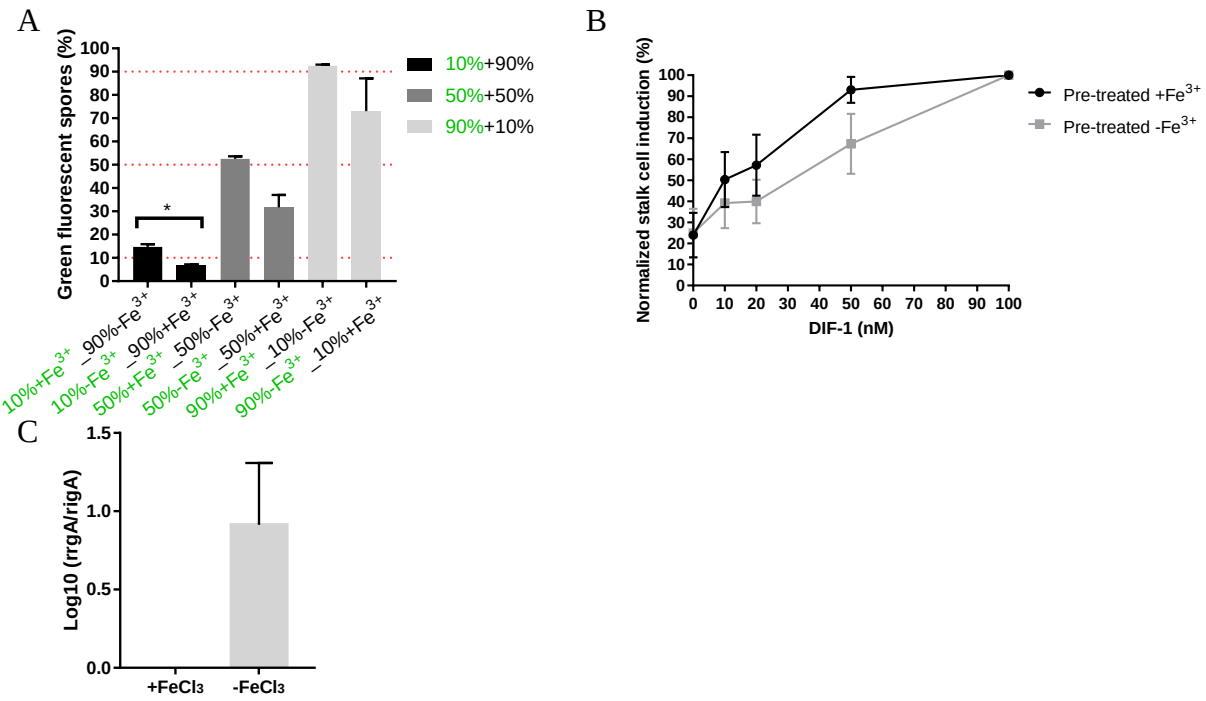


Figure 6.3. Effect of iron depletion on cell fate of AX2 cells. (A) Mixing experiments of AX2 cells pre-incubated with (+Fe^{3+}) or without (-Fe^{3+}) 100 μM $FeCl_3$ in iron-free minimal medium for 24 hrs. The method of chimeric development by mixing labelled or unlabelled cells was described in the legend to Figure 3.4A. N = 2. Mean ± S.E.M. Student *t*-test (two-tailed): *: P < 0.05. (B) Monolayer stalk induction assays of stalk marker expression in AX2 cells with 24-hr pre-treatment with or without 100 μM $FeCl_3$ in minimal medium were performed as described in the legend to Figure 3.5A. Expression of the stalk marker *ecmB*-GAL induced by DIF-1 concentrations were normalized to that seen in 100 nM DIF-1 defined as 100 %. N = 3. Mean ± S.E.M. (C) *rrgA/rigA* expression ratios in cells with different iron pre-treatment conditions for 24-hr growth in iron-free minimal medium. qPCR experiments with the comparative ΔΔCt method were performed to assess the ratio of *rrgA/rigA* as described in the legend to Figure 5.3A. Exponentially growing AX2 cells were incubated in shaking suspension in iron-free minimal medium with or without 100 μM $FeCl_3$. The 100 μM $FeCl_3$ pre-treatment group was set as the calibrator control for cells incubated in iron-free minimal medium (-Fe^{3+}) during vegetative growth. N = 3. Mean ± S.E.M.

6.3.2 mTORC1 activity in *Dictyostelium* cells with different iron pre-treatment history

mTORC1 activity has been reported to influence T cell differentiation and activation (Araki et al., 2010; Teh et al., 2021) and iron depletion reduces mTORC1 activity in CD8+ T cell and human cancer cells (Frost et al., 2021; Shang et al., 2020). Since in Chapter 4 it was shown that high mTORC1 activity at the onset of development correlates with a stalk cell fate bias, it is interesting to know whether iron depletion conditions in iron-free minimal medium have altered mTORC1 pathway activity. Western blotting of phospho-4E-BP1 levels were performed (Figure 6.4), using AX2 cells grown in iron-free minimal medium with or without 100 μM $FeCl_3$ for 24 hrs before harvesting for development. Although quantification of the

phospho-4E-BP1 levels over one-hour of starvation did not show a significant difference compared to the sample collected in growth (0 min time point), there was a very large level of variation. The iron-starved cells tended to have persistently higher 4E-BP1 phosphorylation levels throughout one-hour of starvation, again indicating a stalk cell fate, consistent with the reduced spore formation and high *rrgA*/*rigA* expression ratio.

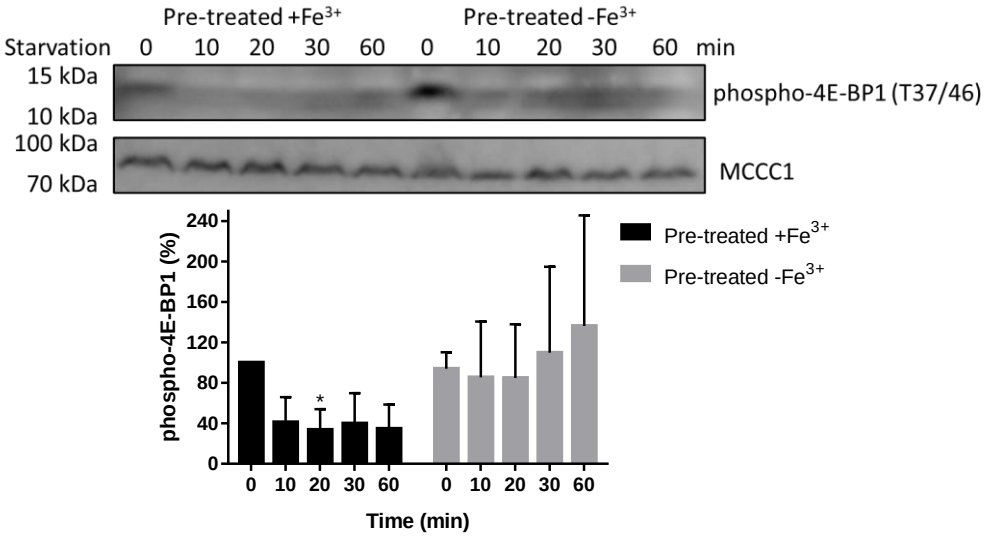


Figure 6.4. 4E-BP1 phosphorylation levels in developing cells which had an iron depletion growth history. Upper panel: Exponentially growing AX2 cells were incubated with or without 100 μM $FeCl_3$ during a 24-hr pre-treatment in iron-free minimal medium (Pre-treated +/- Fe^{3+}) before harvesting whole cell lysates at intervals during one-hour development in HKC development buffer. Phosphorylation levels of 4E-BP1 were detected by western blots performed and analysed as described in the legend to Figure 4.6. One representative blot shown, N = 3. Lower panel: phospho-4E-BP1 levels at each time point was quantified and normalized to 0 min time point of sample pre-treated with $+Fe^{3+}$ minimal medium defined as 100%. Student *t*-test (two-tailed): *: $P < 0.05$. N = 3. Mean ± S.E.M.

6.4 Discussion

This chapter investigates how iron affects development of *Dictyostelium* cells. Iron overload during development in KK2 inhibits aggregate formation, while iron depletion history makes cells prone to form aggregates when they are not starved. Chimeric mixing experiments, qPCR detecting *rrgA/rigA* expression ratio and phospho-4E-BP1 western blots examining mTORC1 activity suggested a stalk cell fate bias of iron-starved cells, while monolayer stalk induction assays did not agree, possibly because cells are less healthy in the first place when cultured in iron-depleted minimal medium.

T cell differentiation has been shown to be influenced by iron levels (Pfeifhofer-Obermair et al., 2021), while mTORC1 activity has also been reported to interfere immune responses by modulating T lymphocyte differentiation (Frost et al., 2021; Howden et al., 2019; Shang et al., 2020). Despite the roles of iron being well-studied using mammalian disease models for investigating cancer, metabolism and immunity (Abbaspour et al., 2014; Guo et al., 2021; Oexle et al., 1999; Pfeifhofer-Obermair et al., 2021; Rouault, 2006), the research into iron and relevant iron-associated proteins in *Dictyostelium* cells has few publications and predominantly focusses on host-pathogenic interactions using *Dictyostelium* as a phagocyte model (Bozzaro et al., 2013; Buracco et al., 2017; Peracino et al., 2006). A recent paper has reported that starvation-mediated accumulation of ROS leads to high demand for antioxidants synthesized by cysteine, and limited sulfur metabolism in *Dictyostelium* cells promotes multicellular development via sequestrating cysteine and reducing iron-sulfur synthesis (Kelly et al., 2021).

To further understand if there is a role for iron in *Dictyostelium* cell fate decisions, this project was inspired by Prof. Hal Drakesmith who initiated a collaboration on investigating *Dictyostelium* cell developmental responses to iron depletion or excess iron. It has been already shown that in *Dictyostelium* cells, iron overload or depletion can inhibit cell growth (Bozzaro et al., 2013; Buracco et al., 2017; Peracino et al., 2013). Development of cells on non-nutrient agar following 24-hr growth in iron overloaded (200 μM $FeCl_3$) conditions leads to aberrant phenotypes such as multiple mounds resulting from fragmented large streams (Buracco et al., 2017). Here we report that in KK2 under-buffer development, excess iron addition ranging

from 0 to 100 μM suppresses aggregate formation, and the aggregates dissolve after 24 hrs, which is to some extent consistent with previous findings that iron overloaded cells have abnormal development on agar with streams breaking up (Buracco et al., 2017). The reason is not known but might be that cell adhesion molecule expression is affected upon longer exposure to iron in developmental buffer, or more possibly free radical oxidation caused by extracellular iron increasing oxidative damage and leading to the fragmentation of the extracellular matrix as commonly reported in studies of lung diseases (Chuang et al., 2014; Eble and de Rezende, 2014; Galaris et al., 2019; Yao et al., 2010).

Depletion of iron for 24 hours in the presence of nutrients and amino acids is sufficient to trigger some aggregate formation in minimal medium. While iron-depletion history in growth promotes cells to form aggregates in iron-free minimal medium, cells grown in standard minimal medium supplied with 100 μM $FeCl_3$ are unable to aggregate in the absence of Fe^{3+} in minimal medium, suggesting that iron sufficient history can allow cells to resist aggregation when iron is removed from minimal medium. In comparison, cysteine which is a source of sulfur extracted by NFS1 for Fe-S cluster synthesis, antagonizes aggregation, and when cells lacking NFS1 via siRNA knockdown enter development, they aggregate more rapidly compared to the control cells and adding cysteine can no longer oppose aggregation in *nfs1*-scilenced cells (Kelly et al., 2021). This is comparable to our data where iron-depleted cells tend to form aggregates in non-starved minimal medium. Thus, it is possible that the sulfur availability in regulating *Dictyostelium* development can be a secondary effect of iron changes in production of Fe-S clusters. To test this idea, future experiments could investigate whether cysteine inhibits aggregation in iron-starved cells which are pre-incubated in iron-free minimal medium. In this case, *nfs1* knockdown cell line could be used to see whether they can still resist cysteine-mediated aggregation inhibition when pre-treated in iron deficient condition.

In the future, expression levels of genes which are known to be induced by different signalling pathways in early aggregation, such as cAMP-independent genes *carA* and *pdsA* whose expression is triggered upon starvation (Masaki et al., 2013) and cAMP pulse-dependent genes *acaA* and *csaA* (Loomis, 2014), could be examined in developing cells with iron presence or absence to see whether iron affects particular aspects of aggregation. Attempts were tried using

developing cells in KK2 with or without $FeCl_3$ (10 and 50 μM) collected at 0, 3, and 6 hrs, but the expressions of *carA*, *pdsA*, *acaA* and *csaA* analysed with qPCR showed no significant difference in these conditions (M. Teh, pers. comms).

In experiments to determine if iron depletion generated a cell fate bias, mixing experiments showed fewer spores formed from iron-starved cells than cells growing in standard minimal medium. This stalk fate bias is consistent with a high *rrgA/rigA* expression ratio determined by qPCR and a trend of relatively high 4E-BP1 phosphorylation in early development shown by western blotting of cells with iron depletion growth history (although not statistically significant). However, this is opposite to the findings in human tumour cell line Rh30 and lung cancer cell line A549. When they are pre-starved with $FeSO_4$ for one hour, iron chelators ciclopirox olamine (CPX) and Dp44mT-mediated reduction of mTORC1 activity revealed by phospho-S6K and phospho-4E-BP1 levels was observed in both cell lines, while cells pre-cultured in 10 μM $FeSO_4$ supplied growth medium did not have obvious decreases in mTORC1 activity (Shang et al., 2020). Also, when CD8+ T cells pre-cultured in iron-free complete medium and supplied with holotransferrin (which is an iron source in mammalian cell culture) back to the medium later, levels of phospho-S6 ribosomal protein (Ser235/236) detected by flow cytometry indicate that mTORC1 activity is reduced in low iron conditions (Frost et al., 2021). This indicates that iron and mTORC1 signalling may have a complex relationship during growth and early development and may differ in different cell types.

In our monolayer stalk induction assay, although not significantly different between cells with and without iron in pre-treatment, showed if anything a reduced level of stalk marker expression induced by DIF-1 in iron-depleted cells. One interpretation of this is that the cells are not healthy (although they are still alive as determined by trypan blue staining) so they have a reduced capacity to make spores in the mixing experiment and express stalk markers in the monolayer. However, they clearly can do both, almost as well as cells with iron in the monolayer assay.

There could also be a complicated number of roles for iron in cell fate decisions, complicating interpretation of the assays. Kelly et al. (2021) interpreted the effects of cysteine and GSH on

aggregation to be mediated through Fe-S cluster proteins. However, proteins dependent on iron alone could have a separate role. To exemplify, lack of iron might alter DIF-1 metabolism, for example, via modulating oxidation of DIF-1 metabolites (Traynor and Kay, 1991; van Es et al., 1994).

Further investigation into the roles of iron in cell fate decisions might include other iron sources such as ferrous ion (Fe^{2+}) or other ferric ion salts (e.g. ferric sulphate) and manipulation of iron levels in HL5 medium using iron chelators such as DFO. Investigating cell fate bias in cells with altered expression of Nramp1/2 may also be useful to investigate cell fate decisions as they regulate iron efflux (Peracino et al., 2006). The *nramp1* gene has low expression levels throughout development but has high levels in growth, while *nramp2* expresses at a low level in growth but slightly increases at 6 hrs development (equivalent to the aggregation stage) before decreasing again, followed by relatively lower levels in further multicellular stages (Peracino et al., 2013). Expressions of pre-stalk genes *ecmA* and *ecmB*, on the other hand, start to increase from about 8 hrs of development (Rosengarten et al., 2015). The single and double *nramp1/2* gene disrupted strains have higher sensitivity to iron starvation and are less sensitive to iron overload (especially the double mutant) in growth, and have developmental defects such as delayed aggregation in single or double mutants, large aggregating streams resulting in increased multi-tipped aggregate formation in the double mutant (Peracino et al., 2013). Moreover, lack of both *nramp* genes in *Dictyostelium* gives rise to taller fruiting bodies in average with longer stalk structures but the proportion of sori and stalk is reported to be unchanged (Peracino et al., 2013), although no quantification data was shown. Since Nramp1 was reported to colocalize with vacuolar type-ATPase on CV membrane, disrupting *nramp1* alters iron homeostasis between cytoplasm and intracellular iron stores such as CV (Peracino et al., 2013), so determining cell fate bias in these strains in different iron conditions would be useful to clarify the effect of iron.

Chapter 7: General discussion and Future work

7.1 General summary and discussion

Two main cell assays were chosen for assessing cell fate tendencies throughout this thesis because they monitor both spore and stalk cell fates: mixing experiments as a lineage tracing method examining spore cell numbers in a multicellular context and monolayer stalk induction assays assessing DIF-1 sensitivity in isolation. Combining these assays, a range of information on cell fate decisions from various aspects of development in multicellular and monolayer formats can be obtained and analysed.

(1) To investigate the role of cellular Ca^{2+}, I have studied cell fate decisions in putative Ca^{2+} channel mutant strains *tpc2*$^{-}$ and *iplA*$^{-}$: loss of TPC2 leads to a stalk cell fate bias, while loss of IPLA results in an alternative spore cell fate preference. Both of these strains have reduced basal cytosolic Ca^{2+} levels in growing cells, suggesting that this is unlikely to be the underlying factor. However, as revealed by experiments later in the thesis using rapamycin treatment to alter cell fate bias, it may be that the cell fate bias in growing cells is overridden by events later in development. This indicates the difficulty of the assays to separate temporal cell fate decision events in genetic mutants during growth and development. Expressing proteins from inducible promoters or systems to destroy proteins rapidly using targeted proteolysis could be used to determine this.

(2) It was reported that *tpc2*$^{-}$ cells were hypersensitive to weak bases in development and have reduced acidity in acidic vesicles (Chang et al., 2020). Here I report that stalk cell fate bias of these cells can be reversed by increasing the pH in acidic vesicles via weak base imidazole treatment, suggesting that the vesicle pH can be a dominant cell fate influencing factor over other factors such as the altered Ca^{2+} levels mediated by loss of TPC2.

(3) Since *tpc2*$^{-}$ cells at early onset of starvation were also reported to have prolonged mTORC1 activity in *Dictyostelium* (Chang et al., 2020), and there is an established interaction between mTORC1 and acidic vesicles, we hypothesized that mTORC1,

which interacts with TPC2 and regulates TPC2-mediated lysosomal Ca^{2+} release in mammalian systems, has functions in cell fate decisions in *Dictyostelium* via its interplay with TPC2. To analyse this correlation between high mTORC1 pathway activity and stalk cell fate bias, stalk cell fate-biased cell lines and cells with glucose depletion history during growth (which could trigger starvation early that leads to cells prone to following autophagy, acidification or vacuolation processes) were assessed, showing higher levels of phospho-4E-BP1 as the readout of mTORC1 activity during the first hour of development. As no other substrates are known in *Dictyostelium* and due to inconsistencies in detection, alternative methods for interpreting mTORC1 pathway activity were also used involving assessing the sensitivity of cells to the mTORC1 inhibitor rapamycin to trigger aggregation in reduced strength medium and to inhibit vegetative growth. In general, these different approaches generate results agree with the information obtained from western blots when available, confirming the correlation between lower rapamycin sensitivity and higher mTORC1 pathway activity in stalk-biased cells. It is also better to use more than one method to detect mTORC1 activity as this can reinforce the evidence from different aspects verifying the role of mTORC1 pathway activity in cell fate decisions.

(4) Alteration of mTORC1 activity was investigated using gene modulation of mTORC1 regulators including the activator Rheb and the antagonistic regulator AMPK. Overexpression strains of Rheb were constructed using doxycycline regulated dox-on and dox-off constructs, although dox-on constructs have better kinetics to respond to doxycycline in switching on the FLGA-tagged Rheb expression. These cells showed an expected stalk cell fate tendency in correlation with less sensitivity to rapamycin. The genetic disrupted mutant of AMPK (*ampk*$^{-}$ from Williams lab) and Rheb (*rheb*$^{-}$) were both constructed with CRISPR/Cas9 strategy, and as expected, *ampk*$^{-}$ cells which had higher mTORC1 activity and were less sensitive to rapamycin in growth preferred stalk cell fate, while *rheb*$^{-}$ cells which were more sensitive to rapamycin in under-buffer aggregation assays tended to have spore cell fate. These results suggested that during growth and development of *Dictyostelium*, AMPK has antagonistic role to mTORC1 as seen in higher eukaryotes. However, Rheb has been reported to have roles in regulating mTORC2-dependent phagocytosis and could be

less important for regulating mTORC1 pathway during cell growth in *Dictyostelium*, although it is the potent activator for mTORC1 in mammalian cells (Rosel et al., 2012). My data also showed little or no change of rapamycin sensitivity of *rheb*$^{-}$ cells during vegetative growth which is in agreement with this previous report. Overall, genetic manipulations of the mTORC1 pathway activity provide information that mTORC1 pathway activity is a potential regulatory component in cell fate decisions. Expressing a GTP-bound Rheb variant to endogenously introduce constitutively active Rheb or pharmacological activation of mTORC1 could be alternative ways to study whether hyperactivation of mTORC1 affects cell fates.

(5) Interestingly, cell fate experiments with pharmacological mTOR inhibitors reveal that the same pathways might lead to a different cell fate bias during growth or development. Rapamycin pre-treatment during growth predisposes cells to a spore cell fate, while prolonged treatment throughout monolayer development leads to a stalk cell fate tendency. This spore cell fate predisposition in monolayer assays was also seen using the other two pan mTOR pathway inhibitors AZD8055 and BEZ235 for 4-hr pre-treatment during cell growth, consistent with the mixing experiment results using cells with 4-hr pre-treatment with rapamycin. These results indicate that the mTORC1 pathway has distinct functions in growth and later development, while mTORC2 might also be affected in chronic rapamycin treatment as reported in mammalian systems. It is also possible that mTORC1 pathway-regulated protein synthesis prior to development is required for cells to prepare for starvation or to choose the spore cell lineage, while in mid-development stages protein synthesis is also required to prepare cells to differentiate into stalk cells e.g. through vacuolation originated from acidic vesicles like autophagosomes (Uchikawa et al., 2011). Another example investigating drug treatment in growth and development is studying cell fates in the presence of the weak base imidazole. Weak base treatment was reported to target subcellular acidic compartments and promote spore cell differentiation (Davies et al., 1993; Gross et al., 1983), and this was confirmed by my results as long treatment of imidazole led to an obvious spore cell fate tendency. Also, 4-hr pre-treatment with imidazole can restore the stalk-biased *tpc2*$^{-}$ cells to show no bias in mixing experiments, while imidazole pre-treatment showed a smaller trend of spore cell fate bias in monolayer assays. However, it is difficult to distinguish whether

effects on cell fate are during growth or development when using genetic mutants as the mutations are present throughout. When studying the effect of mTORC1 pathway activity on cell fate decisions, cell fate experiments only overexpressing Rheb_FLAG during development were performed by inducing with doxycycline, but the suspicious leaking expression in growth due to the strong promoter used in the Dox-on system is an explanation for the opposite stalk cell fate, or perhaps the importance of Rheb in *Dictyostelium* mTORC1 pathway is minimal. Use of developmentally regulated promoters can be an option to try and obtain tighter control of Rheb expression system to drive the increase of mTORC1 activity in development only.

(6) The *rrgA/rigA* expression ratio in growing cells has been reported to be predictive of cell fate bias (Gruenheit et al., 2018). Consistent with the results reported in Gruenheit et al. (2018), our data showed that stalk cell fate tendency is correlated with high *rrgA/rigA* ratio, while a low *rrgA/rigA* ratio is detected in growing cells with a spore cell fate tendency. For altered conditions during growth, the length of treatment was important for the cell fate prediction using the *rrgA/rigA* expression ratio, as 4-hr pre-treatment with rapamycin and increased pH or reduced vesicle acidity by imidazole were not enough to change the ratio whereas 24 hours was. This likely reflects the time taken for existing mRNA to be lost or accumulate in the cytosol following a change in transcription. This is in agreement with Gruenheit et al. (2018) that GefE-RasD regulatory network functions as a buffering mechanism and the expression changes in genes involved in this network is a consequence of signalling perturbation by changes of cell fate determinants. However, both *iplA*$^{-}$ and *fbxA*$^{-}$ cells showed higher *rrgA/rigA* ratio, which did not reflect the final fate bias in mixing experiments where they both formed more spores in chimeric mixing experiments when developing with wildtype cells. Since *fbxA*$^{-}$ did reflect the alternative pre-stalk bias seen in monolayer assays, *rrgA/rigA* expression ratios in terms of cell fate prediction match with monolayer assays better than mixing experiments where the two differ. Therefore, this approach might be useful in unravelling the molecular components of a bias during growth from changes in bias later in development.

(7) Analysis of *set1*$^{-}$ cells demonstrated that methylation of histone H3 on lysine 4, a modification found enriched at promoters, plays a role in setting a high *rrgA/rigA*

ratio, high mTORC1 pathway activity and a stalk cell fate-bias, verified in both cell fate assays, dependent on the catalytic activity of Set1. The H3bK4A strain also had a stalk cell fate tendency, indicating that the depletion of H3K4me is enough to alter cell fate decisions. I also provide evidence that this methylation mark is working through recruitment of Gcn5 via Sgf29, which leads to acetylation of histones containing the H3K4me3. This reveals a possible mechanism for upregulation of genes such as *rrgA* and downregulation of others such as *rigA*. It would be of interest to analyse the levels of chromatin modification on these genes in cells with different cell fate bias. However, experiments using the HDAC inhibitor TSA which increases histone acetylation levels in growing cells and early development (Hsu et al., 2012; Huang et al., 2021) also predisposed cells a stalk cell fate bias in mixing experiments, though not in the monolayer assay. The 4-hr pre-treatment time in growth might not be sufficient to induce DIF-1 mediated stalk cell fates or histone acetylation plays a different role in cell fate at later stages of development, and assessments of *rrgA/rigA* expression ratio or mTORC1 pathway activity could be helpful to distinguish effects on growth or development. Blocking both addition and loss of acetylation gave a stalk fate bias, it could also be that it is turnover of acetylation is important rather than the absolute level.

(8) I have also conducted a side project investigating the effect of iron in *Dictyostelium* development and cell fate decisions in collaboration with Drakesmith lab. Iron is a trace element involved in many processes including incorporation in Fe-S clusters as a co-factor for many enzymes and is an essential nutrient source, but its role in *Dictyostelium* cell fate is not documented. Aggregation of cells was found to be inhibited when overloaded with iron ($FeCl_3$), while cells grown without iron for 24 hrs in growth tend to aggregate in the absence of starvation. Iron deficiency in growth leads cells to choose a stalk cell fate bias in mixing experiment and have high mTORC1 activity during the first hour development, and an expression ratio predictive of a stalk bias during growth. The link between iron depletion and these processes is not known, although it is possible that loss of Fe-S clusters in proteins involved in mitochondrial respiration will play a role in this.

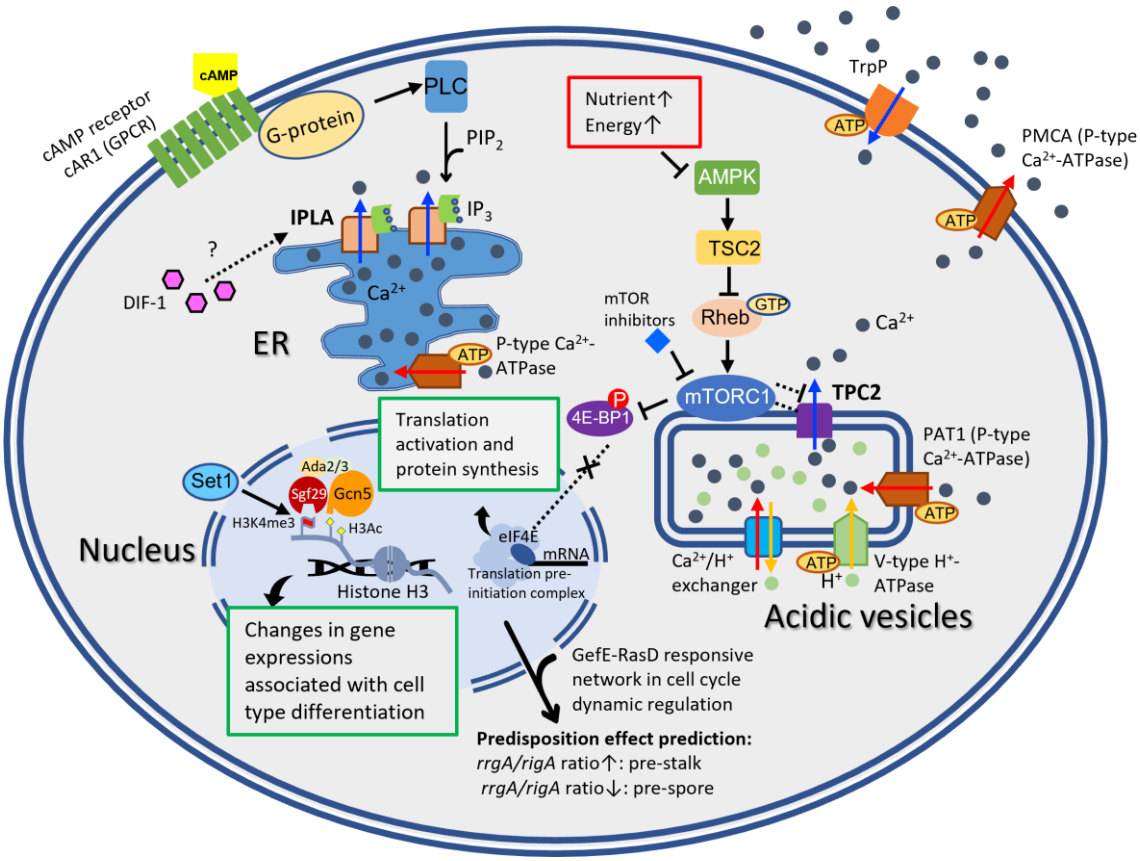


Figure 7.1. Summary of potential mechanisms of *Dictyostelium* cell fate decision. (1) Ca^{2+} channels and cell fate decisions: TPC2 has roles in regulating lysosomal Ca^{2+} release and vesicle pH in acidic Ca^{2+} stores, while IPLA, localized on neutral Ca^{2+} store ER, is the key player in controlling cytosolic Ca^{2+} levels. Loss of TPC2 or IPLA can lead to lowered cytosolic Ca^{2+} levels, and yet they have opposite cell fate tendencies. The increase of vesicle pH by weak base imidazole in *tpc2* null cells can override the intrinsic stalk cell fate bias. Aberrant DIF-1 mediated Ca^{2+} responses in *iplA*$^{-}$ cells have also been reported. (2) mTORC1 activity correlates with cell fate decisions and is regulated, perhaps via vesicle pH, by TPC2: In mammalian cells when intracellular nutrients and energy are sufficient, mTORC1 is activated and it interacts with TPC2 to negatively regulate TPC2-mediated Ca^{2+} signalling. The activity of the mTORC1 pathway leads to protein synthesis by activation of translation via phosphorylation of 4E-BP1 released from eIF4E within the translation pre-initiation complex. This has not been shown in *Dictyostelium*. AMPK is an energy sensor antagonizing mTORC1. Loss of AMPK in cells leads to an increased phospho-4E-BP1 level and correlates to stalk cell fate, while *rheb*$^{-}$ cells have low mTORC1 activity and prefer the spore cell fate. Conversely, overexpression of Rheb has high mTORC1 level and a stalk cell fate bias. Short term treatment with mTOR inhibitors including rapamycin, AZD8055 and BEZ235 lead to consistent results by favouring spore cell differentiation. Treatment with rapamycin throughout development indicates that the predisposition and later developmental effects of mTORC1 pathway activity might differ. (3) Cell cycle perturbation buffering system and cell fate prediction via assessing gene expression ratio in GefE-RasD regulatory network: Perturbation of cell cycle dynamics during cell growth has a solution by establishing a buffering mechanism to alter gene expression involved in GefE-

RasD, where *rrgA* and *rigA* genes are two examples that give reciprocal expression in response to cell fate-biased conditions. This *rrgA/rigA* expression ratio in growing cells works as a biomarker for predicting cell fate upon different predisposition factors. (4) Histone modification regulating gene expression regulation correlating to alteration of cell fate bias: Set1-Sgf29-Gcn5 axis is a potential signalling pathway that alters gene expression by modifying histone H3 tails. Set1 deposits H3K4me marks via HMT activity, and Sgf29 recognizes H3K4me3 enriched in gene promoter regions and recruits the HAT module of SAGA complex for H3Ac mediated by the Gcn5 subunit. This promotes the expression of genes involved in cell type bias. Dotted arrow and inhibitory symbol showed possible activities and the dashed line shows the interactions between proteins. Red arrows show the mobilizations of Ca^{2+} to reduce cytosolic Ca^{2+} level and blue arrows show the Ca^{2+} movements that increase of cytosolic Ca^{2+} level, while yellow arrows indicate the movement of proton at acidic compartments.

7.2 Future experiments:

(1) Ca^{2+} imaging of the putative Ca^{2+} channel disrupted mutant *dmpA*$^{-}$ to verify its basal cytosolic Ca^{2+} and the DIF-1 induced Ca^{2+} responses in other Ca^{2+} channel mutants, using cells expressing the YC-Nano15 ultrasensitive Ca^{2+} indicator.

(2) Weak acids such as acetic acid can be used to study whether reduced pH in acidic vesicles can affect cells fate decisions including in spore cell fate-biased strains such as *iplA*$^{-}$.

(3) To alter endogenous mTORC1 activity via gene modulation other mutant strains could be generated and tested, such as the Rheb^{Q64L} strain expressing a constitutively active GTP-bound version of Rheb by introducing mutation Q64L (Rosel et al., 2012) to increase mTORC1 activity and a CRIPSR/Cas9 disrupted *tor* cell line (Dr T. Muramoto, pers. comm.) to reduce mTORC1 activity can be used, although this would disrupt mTORC2 activity as well.

(4) Mutant strains with altered mTORC2 activity such as *pia*$^{-}$ cells with disrupted Rictor and *rip3*$^{-}$ with disrupted Sin1 (Rosel et al., 2012) can also be used for investigating the role of mTORC2 in cell fate decision regulation.

(5) Developmental promoter regulated constructs such as pre-stalk *ecmB* and pre-spore *pspA* promoters can be used to express mTORC1 regulators at later stages in development, in order to separate the effect of predisposition during growth and events later during development on influencing cell fate biases.

(6) Pharmacological alteration of histone modifications with longer pre-treatment of drugs such as HDAC inhibitor TSA can be used to verify the proposed pathway of H3K4me3-primed histone acetylation is correlated to cell fate bias, and other

inhibitors targeting other modification such as H3K4-specific methylation (Yang et al., 2021) can also be investigated.

(7) To further study the effect of iron in cell type differentiation, *nfs-1* silenced cells lacking a key enzyme NFS1 involved in Fe-S synthesis (Kelly et al., 2021) can be used to study whether iron affects cell fate decision via Fe-S cluster-mediated pathway.

References

Abbaspour, N., Hurrell, R., Kelishadi, R., 2014. Review on iron and its importance for human health. J Res Med Sci 19, 164-174.

Abe, T., Maeda, Y., 1989. The Prestalk Prespore Differentiation and Polarized Cell-Movement in Dictyostelium-Discoideum Slugs - a Possible Involvement of the Intracellular Ca-2+-Concentration. Protoplasma 151, 175-178.

Abe, T., Maeda, Y., Iijima, T., 1988. Transient increase of the intracellular Ca2+ concentration during chemotactic signal transduction in Dictyostelium discoideum cells. Differentiation 39, 90-96.

Adiba, S., Nizak, C., Van Baalen, M., Denamur, E., Depaulis, F., 2010. From Grazing Resistance to Pathogenesis: The Coincidental Evolution of Virulence Factors. PLoS ONE 5, e11882.

Aerts, R.J., 1988. Changes in cytoplasmic pH are involved in the cell type regulation of Dictyostelium. Cell Differ 23, 125-131.

Aerts, R.J., Durston, A.J., Konijn, T.M., 1987. Cytoplasmic pH at the onset of development in Dictyostelium. J Cell Sci 87 (Pt 3), 423-430.

Aerts, R.J., Durston, A.J., Moolenaar, W.H., 1985. Cytoplasmic pH and the regulation of the Dictyostelium cell cycle. Cell 43, 653-657.

Ahmad, K., Henikoff, S., 2002. The histone variant H3.3 marks active chromatin by replication-independent nucleosome assembly. Mol Cell 9, 1191-1200.

Aissat, N., Le Tourneau, C., Ghoul, A., Serova, M., Bieche, I., Lokiec, F., Raymond, E., Faivre, S., 2008. Antiproliferative effects of rapamycin as a single agent and in combination with carboplatin and paclitaxel in head and neck cancer cell lines. Cancer Chemotherapy and Pharmacology 62, 305-313.

Alberts, B., 2002. Molecular biology of the cell, 4th ed. Garland Science, New York.

Allan, J., Hartman, P.G., Crane-Robinson, C., Aviles, F.X., 1980. The structure of histone H1 and its location in chromatin. Nature 288, 675-679.

Alqurashi, N., Hashimi, S.M., Alowaidi, F., Ivanovski, S., Wei, M.Q., 2018. Dual mTOR/PI3K inhibitor NVPBEZ235 arrests colorectal cancer cell growth and displays differential inhibition of 4EBP1. Oncol Rep 40, 1083-1092.

Alvarez, S.W., Sviderskiy, V.O., Terzi, E.M., Papagiannakopoulos, T., Moreira, A.L., Adams, S., Sabatini, D.M., Birsoy, K., Possemato, R., 2017. NFS1 undergoes positive selection in lung tumours and protects cells from ferroptosis. Nature 551, 639-643.

Ambros, V., 1999. Cell cycle-dependent sequencing of cell fate decisions in Caenorhabditis elegans vulva precursor cells. Development 126, 1947-1956.

Andrade, M.A., Bork, P., 1995. HEAT repeats in the Huntington's disease protein. Nature Genetics 11.

Andreini, C., Putignano, V., Rosato, A., Banci, L., 2018. The human iron-proteome. Metallomics 10, 1223-1231.

Annesley, S.J., Fisher, P.R., 2009. Dictyostelium discoideum-a model for many reasons. Mol Cell Biochem 329, 73-91.

Araki, K., Youngblood, B., Ahmed, R., 2010. The role of mTOR in memory CD8+ T-cell differentiation. Immunological Reviews 235, 234-243.

Araki, T., Gamper, M., Early, A., Fukuzawa, M., Abe, T., Kawata, T., Kim, E., Firtel, R.A., Williams, J.G., 1998. Developmentally and spatially regulated activation of a Dictyostelium STAT protein by a serpentine receptor. The EMBO Journal 17, 4018-4028.

Araki, T., Nakao, H., Takeuchi, I., Maeda, Y., 1994. Cell-cycle-dependent sorting in the development of Dictyostelium cells. Dev Biol 162, 221-228.

Ardestani, A., Lupse, B., Kido, Y., Leibowitz, G., Maedler, K., 2018. mTORC1 Signaling: A Double-Edged Sword in Diabetic beta Cells. Cell Metab 27, 314-331.
Ashworth, J.M., Watts, D.J., 1970. Metabolism of the Cellular Slime Mould Dictyostelium discoideum Grown in Axenic Culture. Biochemical Journal 119, 175-182.
Aspuria, P.J., Sato, T., Tamanoi, F., 2007. The TSC/Rheb/TOR signaling pathway in fission yeast and mammalian cells: temperature sensitive and constitutive active mutants of TOR. Cell Cycle 6, 1692-1695.
Aspuria, P.J., Tamanoi, F., 2004. The Rheb family of GTP-binding proteins. Cell Signal 16, 1105-1112.
Aubry, L., Klein, G., Martiel, J.L., Satre, M., 1993. Kinetics of endosomal pH evolution in Dictyostelium discoideum amoebae. Study by fluorescence spectroscopy. J Cell Sci 105 (Pt 3), 861-866.
Austin, M.B., Saito, T., Bowman, M.E., Haydock, S., Kato, A., Moore, B.S., Kay, R.R., Noel, J.P., 2006. Biosynthesis of Dictyostelium discoideum differentiation-inducing factor by a hybrid type I fatty acid-type III polyketide synthase. Nat Chem Biol 2, 494-502.
Azhar, M., Kennady, P.K., Pande, G., Espiritu, M., Holloman, W., Brazill, D., Gomer, R.H., Nanjundiah, V., 2001. Cell cycle phase, cellular Ca2+ and development in Dictyostelium discoideum. Int J Dev Biol 45, 405-414.
Azhar, M., Kennady, P.K., Pande, G., Nanjundiah, V., 1997. Stimulation by DIF causes an increase of intracellular Ca2+ in Dictyostelium discoideum. Exp Cell Res 230, 403-406.
Azhar, M., Manogaran, P.S., Kennady, P.K., Pande, G., Nanjundiah, V., 1996. A Ca(2+)-dependent early functional heterogeneity in amoebae of Dictyostelium discoideum, revealed by flow cytometry. Exp Cell Res 227, 344-351.
Bagur, R., Hajnoczky, G., 2017. Intracellular Ca2+ Sensing: Its Role in Calcium Homeostasis and Signaling. Molecular Cell 66, 780-788.
Bai, X., Ma, D., Liu, A., Shen, X., Wang, Q.J., Liu, Y., Jiang, Y., 2007. Rheb activates mTOR by antagonizing its endogenous inhibitor, FKBP38. Science 318, 977-980.
Baines, A., Parkinson, K., Sim, J.A., Bragg, L., Thompson, C.R.L., North, R.A., 2013. Functional properties of five Dictyostelium discoideum P2X receptors. J Biol Chem 288, 20992-21000.
Bannister, A.J., Kouzarides, T., 2011. Regulation of chromatin by histone modifications. Cell Research 21, 381-395.
Bar-Peled, L., Chantranupong, L., Cherniack, A.D., Chen, W.W., Ottina, K.A., Grabiner, B.C., Spear, E.D., Carter, S.L., Meyerson, M., Sabatini, D.M., 2013. A Tumor Suppressor Complex with GAP Activity for the Rag GTPases That Signal Amino Acid Sufficiency to mTORC1. Science 340, 1100-1106.
Bar-Peled, L., Schweitzer, L.D., Zoncu, R., Sabatini, D.M., 2012. Ragulator is a GEF for the rag GTPases that signal amino acid levels to mTORC1. Cell 150, 1196-1208.
Barry, E.R., Krueger, W., Jakuba, C.M., Veilleux, E., Ambrosi, D.J., Nelson, C.E., Rasmussen, T.P., 2009. ES cell cycle progression and differentiation require the action of the histone methyltransferase Dot1L. Stem Cells 27, 1538-1547.
Baskar, R., Chhabra, P., Mascarenhas, P., Nanjundiah, V., 2000. A cell type-specific effect of calcium on pattern formation and differentiation in dictyostelium discoideum. Int J Dev Biol 44, 491-498.
Bayeva, M., Khechaduri, A., Puig, S., Chang, H.-C., Patial, S., Perry, Ardehali, H., 2012. mTOR Regulates Cellular Iron Homeostasis through Tristetraprolin. Cell Metabolism 16, 645-657.
Becker, J.S., Nicetto, D., Zaret, K.S., 2016. H3K9me3-Dependent Heterochromatin: Barrier to Cell Fate Changes. Trends Genet 32, 29-41.

Benabentos, R., Hirose, S., Sucgang, R., Curk, T., Katoh, M., Ostrowski, E.A., Strassmann, J.E., Queller, D.C., Zupan, B., Shaulsky, G., Kuspa, A., 2009. Polymorphic members of the lag gene family mediate kin discrimination in Dictyostelium. Curr Biol 19, 567-572.
Berks, M., Kay, R.R., 1988. Cyclic-Amp Is an Inhibitor of Stalk Cell-Differentiation in Dictyostelium-Discoideum. Developmental Biology 126, 108-114.
Bernhofer, M., Kloppmann, E., Reeb, J., Rost, B., 2016. TMSEG: Novel prediction of transmembrane helices. Proteins 84, 1706-1716.
Bernstein, B.E., Humphrey, E.L., Erlich, R.L., Schneider, R., Bouman, P., Liu, J.S., Kouzarides, T., Schreiber, S.L., 2002. Methylation of histone H3 Lys 4 in coding regions of active genes. Proceedings of the National Academy of Sciences 99, 8695-8700.
Berridge, M.J., 1998. Neuronal calcium signaling. Neuron 21, 13-26.
Berridge, M.J., 2014. Calcium regulation of neural rhythms, memory and Alzheimer's disease. J Physiol 592, 281-293.
Berridge, M.J., Bootman, M.D., Roderick, H.L., 2003. Calcium signalling: dynamics, homeostasis and remodelling. Nat Rev Mol Cell Biol 4, 517-529.
Berridge, M.J., Lipp, P., Bootman, M.D., 2000. The versatility and universality of calcium signalling. Nat Rev Mol Cell Biol 1, 11-21.
Bian, C., Xu, C., Ruan, J., Lee, K.K., Burke, T.L., Tempel, W., Barsyte, D., Li, J., Wu, M., Zhou, B.O., Fleharty, B.E., Paulson, A., Allali-Hassani, A., Zhou, J.Q., Mer, G., Grant, P.A., Workman, J.L., Zang, J., Min, J., 2011. Sgf29 binds histone H3K4me2/3 and is required for SAGA complex recruitment and histone H3 acetylation. EMBO J 30, 2829-2842.
Biederbick, A., Stehling, O., Rosser, R., Niggemeyer, B., Nakai, Y., Elsasser, H.P., Lill, R., 2006. Role of human mitochondrial Nfs1 in cytosolic iron-sulfur protein biogenesis and iron regulation. Molecular and Cellular Biology 26, 5675-5687.
Bird, A.W., Yu, D.Y., Pray-Grant, M.G., Qiu, Q.F., Harmon, K.E., Megee, P.C., Grant, P.A., Smith, M.M., Christman, M.F., 2002. Acetylation of histone H4 by Esa1 is required for DNA double-strand break repair. Nature 419, 411-415.
Bissler, J.J., McCormack, F.X., Young, L.R., Elwing, J.M., Chuck, G., Leonard, J.M., Schmithorst, V.J., Laor, T., Brody, A.S., Bean, J., Salisbury, S., Franz, D.N., 2008. Sirolimus for angiomyolipoma in tuberous sclerosis complex or lymphangioleiomyomatosis. The New England journal of medicine 358, 140-151.
Blaauw, M., Linskens, M.H., van Haastert, P.J., 2000. Efficient control of gene expression by a tetracycline-dependent transactivator in single Dictyostelium discoideum cells. Gene 252, 71-82.
Black, B.E., Foltz, D.R., Chakravarthy, S., Luger, K., Woods, V.L., Jr., Cleveland, D.W., 2004. Structural determinants for generating centromeric chromatin. Nature 430, 578-582.
Blackwell, T.K., Sewell, A.K., Wu, Z., Han, M., 2019. TOR Signaling in Caenorhabditis elegans Development, Metabolism, and Aging. Genetics 213, 329-360.
Blagih, J., Coulombe, F., Vincent, E.E., Dupuy, F., Galicia-Vázquez, G., Yurchenko, E., Raissi, T.C., van der Windt, G.J., Viollet, B., Pearce, E.L., Pelletier, J., Piccirillo, C.A., Krawczyk, C.M., Divangahi, M., Jones, R.G., 2015. The energy sensor AMPK regulates T cell metabolic adaptation and effector responses in vivo. Immunity 42, 41-54.
Blaschke, A., Weijer, C., Macwilliams, H., 1986. Dictyostelium discoideum: Cell-type proportioning, cell-differentiation preference, cell fate, and the behavior of anterior-like cells in Hs1/Hs2 and G+/G− mixtures. Differentiation 32, 1-9.
Bloomfield, G., Pears, C., 2003. Superoxide signalling required for multicellular development of Dictyostelium. J Cell Sci 116, 3387-3397.
Bloomfield, G., Traynor, D., Sander, S.P., Veltman, D.M., Pachebat, J.A., Kay, R.R., 2015. Neurofibromin controls macropinocytosis and phagocytosis in Dictyostelium. eLife 4, e04940.

Bok, J.W., Sone, T., Silverman-Gavrila, L.B., Lew, R.R., Bowring, F.J., Catcheside, D.E., Griffiths, A.J., 2001. Structure and function analysis of the calcium-related gene spray in Neurospora crassa. Fungal genetics and biology : FG & B 32, 145-158.
Boldt, D.H., 1999. New perspectives on iron: an introduction. Am J Med Sci 318, 207-212.
Bolourani, P., Spiegelman, G.B., Weeks, G., 2006. Delineation of the roles played by RasG and RasC in cAMP-dependent signal transduction during the early development of Dictyostelium discoideum. Mol Biol Cell 17, 4543-4550.
Bonner, J.T., 1947. Evidence for the formation of cell aggregates by chemotaxis in the development of the slime mold Dictyostelium discoideum. J Exp Zool 106, 1-26.
Bonner, J.T., 1967. The cellular slime molds, 2nd ed. Princeton University Press, Princeton.
Bonner, J.T., 1970. Induction of stalk cell differentiation by cyclic AMP in the cellular slime mold Dictyostelium discoideum. Proc Natl Acad Sci U S A 65, 110-113.
Bozzaro, S., Buracco, S., Peracino, B., 2013. Iron metabolism and resistance to infection by invasive bacteria in the social amoeba Dictyostelium discoideum. Front Cell Infect Microbiol 3, 50.
Bozzaro, S., Eichinger, L., 2011. The Professional Phagocyte Dictyostelium discoideum as a Model Host for Bacterial Pathogens. Curr Drug Targets 12, 942-954.
Brazil, D.P., Hemmings, B.A., 2001. Ten years of protein kinase B signalling: a hard Akt to follow. Trends Biochem Sci 26, 657-664.
Brazill, D.T., Caprette, D.R., Myler, H.A., Hatton, R.D., Ammann, R.R., Lindsey, D.F., Brock, D.A., Gomer, R.H., 2000. A Protein Containing a Serine-rich Domain with Vesicle Fusing Properties Mediates Cell Cycle-dependent Cytosolic pH Regulation*. Journal of Biological Chemistry 275, 19231-19240.
Briggs, S.D., Bryk, M., Strahl, B.D., Cheung, W.L., Davie, J.K., Dent, S.Y., Winston, F., Allis, C.D., 2001. Histone H3 lysine 4 methylation is mediated by Set1 and required for cell growth and rDNA silencing in Saccharomyces cerevisiae. Genes Dev 15, 3286-3295.
Brodskiy, P.A., Wu, Q., Soundarrajan, D.K., Huizar, F.J., Chen, J., Liang, P., Narciso, C., Levis, M.K., Arredondo-Walsh, N., Chen, D.Z., Zartman, J.J., 2019. Decoding Calcium Signaling Dynamics during Drosophila Wing Disc Development. Biophys J 116, 725-740.
Brown, D.T., Wellman, S.E., Sittman, D.B., 1985. Changes in the levels of three different classes of histone mRNA during murine erythroleukemia cell differentiation. Mol Cell Biol 5, 2879-2886.
Brown, E.J., Albers, M.W., Shin, T.B., Ichikawa, K., Keith, C.T., Lane, W.S., Schreibert, S.L., 1994. A mammalian protein targeted by G1-arresting rapamycin receptor complex. Nature 369.
Bundscherer, A., Hafner, C., Maisch, T., Becker, B., Landthaler, M., Vogt, T., 2008. Antiproliferative and proapoptotic effects of rapamycin and celecoxib in malignant melanoma cell lines. Oncol Rep 19, 547-553.
Buracco, S., Peracino, B., Andreini, C., Bracco, E., Bozzaro, S., 2017. Differential Effects of Iron, Zinc, and Copper on Dictyostelium discoideum Cell Growth and Resistance to Legionella pneumophila. Front Cell Infect Microbiol 7, 536.
Burnett, P.E., Barrow, R.K., Cohen, N.A., Snyder, S.H., Sabatini, D.M., 1998. RAFT1 phosphorylation of the translational regulators p70 S6 kinase and 4E-BP1. Proc Natl Acad Sci U S A 95, 1432-1437.
Cabrera, C.V., 1990. Lateral Inhibition and Cell Fate during Neurogenesis in Drosophila - the Interactions between Scute, Notch and Delta. Development 110, 733-742.
Calcraft, P.J., Ruas, M., Pan, Z., Cheng, X.T., Arredouani, A., Hao, X.M., Tang, J.S., Rietdorf, K., Teboul, L., Chuang, K.T., Lin, P.H., Xiao, R., Wang, C.B., Zhu, Y.M., Lin, Y.K., Wyatt, C.N., Parrington, J., Ma, J.J., Evans, A.M., Galione, A., Zhu, M.X., 2009.

NAADP mobilizes calcium from acidic organelles through two-pore channels. Nature 459, 596-U130.
Calvo-Garrido, J., Carilla-Latorre, S., Kubohara, Y., Santos-Rodrigo, N., Mesquita, A., Soldati, T., Golstein, P., Escalante, R., 2010. Autophagy in Dictyostelium: genes and pathways, cell death and infection. Autophagy 6, 686-701.
Calvo-Garrido, J., Carilla-Latorre, S., Lazaro-Dieguez, F., Egea, G., Escalante, R., 2008. Vacuole membrane protein 1 is an endoplasmic reticulum protein required for organelle biogenesis, protein secretion, and development. Molecular Biology of the Cell 19, 3442-3453.
Cang, C., Zhou, Y., Navarro, B., Seo, Y.J., Aranda, K., Shi, L., Battaglia-Hsu, S., Nissim, I., Clapham, D.E., Ren, D., 2013. mTOR regulates lysosomal ATP-sensitive two-pore Na(+) channels to adapt to metabolic state. Cell 152, 778-790.
Cardenal-Munoz, E., Arafah, S., Lopez-Jimenez, A.T., Kicka, S., Falaise, A., Bach, F., Schaad, O., King, J.S., Hagedorn, M., Soldati, T., 2017. Mycobacterium marinum antagonistically induces an autophagic response while repressing the autophagic flux in a TORC1-and ESX-1-dependent manner. Plos Pathog 13.
Cardenal-Muñoz, E., Arafah, S., López-Jiménez, A.T., Kicka, S., Falaise, A., Bach, F., Schaad, O., King, J.S., Hagedorn, M., Soldati, T., 2017. Mycobacterium marinum antagonistically induces an autophagic response while repressing the autophagic flux in a TORC1- and ESX-1-dependent manner. Plos Pathog 13, e1006344.
Carroll, S.B., 2001. Chance and necessity: the evolution of morphological complexity and diversity. Nature 409, 1102-1109.
Casey, B.H., Kollipara, R.K., Pozo, K., Johnson, J.E., 2018. Intrinsic DNA binding properties demonstrated for lineage-specifying basic helix-loop-helix transcription factors. Genome Res 28, 484-496.
Chang, F.-S., 2016. Analysis of two pore channel proteins in Dictyostelium development, in: Chang, F.-S., Pears, C., Galione, A., Churchill, G., Williams, R. (Eds.), Department of Biochemistry. University of Oxford.
Chang, F.S., Wang, Y., Dmitriev, P., Gross, J., Galione, A., Pears, C., 2020. A two-pore channel protein required for regulating mTORC1 activity on starvation. BMC Biol 18, 8.
Charlie, N.K., Thomure, A.M., Schade, M.A., Miller, K.G., 2006. The Dunce cAMP phosphodiesterase PDE-4 negatively regulates G alpha(s)-dependent and G alpha(s)-independent cAMP pools in the Caenorhabditis elegans synaptic signaling network. Genetics 173, 111-130.
Charruyer, A., Ghadially, R., 2018. Influence of pH on Skin Stem Cells and Their Differentiation. Curr Probl Dermatol 54, 71-78.
Chattwood, A., Nagayama, K., Bolourani, P., Harkin, L., Kamjoo, M., Weeks, G., Thompson, C.R., 2013. Developmental lineage priming in Dictyostelium by heterogeneous Ras activation. Elife 2, e01067.
Chattwood, A., Thompson, C.R., 2011. Non-genetic heterogeneity and cell fate choice in Dictyostelium discoideum. Dev Growth Differ 53, 558-566.
Chen, G., Kuspa, A., 2005. Prespore cell fate bias in G1 phase of the cell cycle in Dictyostelium discoideum. Eukaryot Cell 4, 1755-1764.
Chen, J., Zheng, X.-F., Brown, E.J., SCHREIBER, S.L., 1995. Identification of an 11-kDa FKBP12-rapamycin-binding domain within the 289-kDa FKBP12-rapamycin-associated protein and characterization of a critical serine residue. Biochemistry 92, 4947-4951.
Chen, L.Y., Jin, T.F., Zhu, K., Piao, Y.S., Quan, T.H., Quan, C.J., Lin, Z.H., 2017. PI3K/mTOR dual inhibitor BEZ235 and histone deacetylase inhibitor Trichostatin A synergistically exert anti-tumor activity in breast cancer. Oncotarget 8, 11937-11949.

Chen, Q., Shi, J., Tao, Y., Zernicka-Goetz, M., 2018. Tracing the origin of heterogeneity and symmetry breaking in the early mammalian embryo. Nature Communications 9.
Chen, T., Shen, L., Yu, J., Wan, H., Guo, A., Chen, J., Long, Y., Zhao, J., Pei, G., 2011. Rapamycin and other longevity-promoting compounds enhance the generation of mouse induced pluripotent stem cells. Aging Cell 10, 908-911.
Cheng, Y., He, C., Wang, M., Ma, X., Mo, F., Yang, S., Han, J., Wei, X., 2019. Targeting epigenetic regulators for cancer therapy: mechanisms and advances in clinical trials. Signal Transduction and Targeted Therapy 4, 62.
Chi, H., 2012. Regulation and function of mTOR signalling in T cell fate decisions. Nat Rev Immunol 12, 325-338.
Chiarini, F., Grimaldi, C., Ricci, F., Tazzari, P.L., Evangelisti, C., Ognibene, A., Battistelli, M., Falcieri, E., Melchionda, F., Pession, A., Pagliaro, P., McCubrey, J.A., Martelli, A.M., 2010. Activity of the Novel Dual Phosphatidylinositol 3-Kinase/Mammalian Target of Rapamycin Inhibitor NVP-BEZ235 against T-Cell Acute Lymphoblastic Leukemia. Cancer Research 70, 8097-8107.
Chisolm, D.A., Weinmann, A.S., 2018. Connections Between Metabolism and Epigenetics in Programming Cellular Differentiation. Annu Rev Immunol 36, 221-246.
Chiu, M.I., Katz, H., Berlin, V., 1994. RAPT1, a mammalian homolog of yeast Tor, interacts with the FKBP12/rapamycin complex. Proc Natl Acad Sci U S A 91, 12574-12578.
Choo, A.Y., Blenis, J., 2009. Not all substrates are treated equally: implications for mTOR, rapamycin-resistance and cancer therapy. Cell Cycle 8, 567-572.
Chresta, C.M., Davies, B.R., Hickson, I., Harding, T., Cosulich, S., Critchlow, S.E., Vincent, J.P., Ellston, R., Jones, D., Sini, P., James, D., Howard, Z., Dudley, P., Hughes, G., Smith, L., Maguire, S., Hummersone, M., Malagu, K., Menear, K., Jenkins, R., Jacobsen, M., Smith, G.C.M., Guichard, S., Pass, M., 2010. AZD8055 Is a Potent, Selective, and Orally Bioavailable ATP-Competitive Mammalian Target of Rapamycin Kinase Inhibitor with In vitro and In vivo Antitumor Activity. Cancer Research 70, 288-298.
Chuang, C.Y., Degendorfer, G., Davies, M.J., 2014. Oxidation and modification of extracellular matrix and its role in disease. Free Radic Res 48, 970-989.
Chubb, J.R., Bloomfield, G., Xu, Q., Kaller, M., Ivens, A., Skelton, J., Turner, B.M., Nellen, W., Shaulsky, G., Kay, R.R., Bickmore, W.A., Singer, R.H., 2006a. Developmental timing in Dictyostelium is regulated by the Set1 histone methyltransferase. Dev Biol 292, 519-532.
Chubb, J.R., Trcek, T., Shenoy, S.M., Singer, R.H., 2006b. Transcriptional Pulsing of a Developmental Gene. Current Biology 16, 1018-1025.
Chung, J., Grammer, T.C., Lemon, K.P., Kazlauskas, A., Blenis, J., 1994. PDGF- and insulin-dependent pp70S6k activation mediated by phosphatidylinositol-3-OH kinase. Nature 370, 71-75.
Chung, J., Kuo, C.J., Crabtree, G.R., Blenis, J., 1992. Rapamycin-FKBP Specifically Blocks Growth-Dependent Activation of and Signaling by the 70 kd S6 Protein Kinases. Cell 69, 1227-1236.
Cieniewicz, A.M., Moreland, L., Ringel, A.E., Mackintosh, S.G., Raman, A., Gilbert, T.M., Wolberger, C., Tackett, A.J., Taverna, S.D., 2014. The Bromodomain of Gcn5 Regulates Site Specificity of Lysine Acetylation on Histone H3. Mol Cell Proteomics 13, 2896-2910.
Ciofi-Baffoni, S., Nasta, V., Banci, L., 2018. Protein networks in the maturation of human iron-sulfur proteins. Metallomics 10, 49-72.
Clapham, D.E., 2007. Calcium signaling. Cell 131, 1047-1058.
Clarke, M., Kohler, J., Arana, Q., Liu, T., Heuser, J., Gerisch, G., 2002. Dynamics of the vacuolar H(+)-ATPase in the contractile vacuole complex and the endosomal pathway of Dictyostelium cells. J Cell Sci 115, 2893-2905.

Cohen, M., Georgiou, M., Stevenson, N.L., Miodownik, M., Baum, B., 2010. Dynamic filopodia transmit intermittent Delta-Notch signaling to drive pattern refinement during lateral inhibition. Dev Cell 19, 78-89.
Coleman, M.L., Marshall, C.J., Olson, M.F., 2004. RAS and RHO GTPases in G1-phase cell-cycle regulation. Nat Rev Mol Cell Biol 5, 355-366.
Concordet, J.P., Haeussler, M., 2018. CRISPOR: intuitive guide selection for CRISPR/Cas9 genome editing experiments and screens. Nucleic Acids Res 46, W242-W245.
Consalvo, K.M., Rijal, R., Tang, Y., Kirolos, S.A., Smith, M.R., Gomer, R.H., 2019. Extracellular signaling in Dictyostelium. Int J Dev Biol 63, 395-405.
Cooper, G.M., 2000. The cell : a molecular approach, 2nd ed. ASM Press ;

Sinauer Associates, Washington, D.C.

Sunderland, Mass.
Cornu, M., Albert, V., Hall, M.N., 2013. mTOR in aging, metabolism, and cancer. Curr Opin Genet Dev 23, 53-62.
Crespo, P., Leon, J., 2000. Ras proteins in the control of the cell cycle and cell differentiation. Cell Mol Life Sci 57, 1613-1636.
Crump, N.T., Hazzalin, C.A., Bowers, E.M., Alani, R.M., Cole, P.A., Mahadevan, L.C., 2011. Dynamic acetylation of all lysine-4 trimethylated histone H3 is evolutionarily conserved and mediated by p300/CBP. P Natl Acad Sci USA 108, 7814-7819.
Cunniff, B., McKenzie, A.J., Heintz, N.H., Howe, A.K., 2016. AMPK activity regulates trafficking of mitochondria to the leading edge during cell migration and matrix invasion. Mol Biol Cell 27, 2662-2674.
Cutler, N.S., Pan, X.W., Heitman, J., Cardenas, M.E., 2001. The TOR signal transduction cascade controls cellular differentiation in response to nutrients. Molecular Biology of the Cell 12, 4103-4113.
Darmon, M., Klein, C., 1978. Effects of amino acids and glucose on adenylate cyclase and cell differentiation of Dictyostelium discoideum. Developmental Biology 63, 377-389.
Davidson, A.J., King, J.S., Insall, R.H., 2013. The use of streptavidin conjugates as immunoblot loading controls and mitochondrial markers for use with Dictyostelium discoideum. Biotechniques 55, 39-41.
Davies, L., Farrar, N.A., Satre, M., Dottin, R.P., Gross, J.D., 1996. Vacuolar H(+)-ATPase and weak base action in Dictyostelium. Mol Microbiol 22, 119-126.
Davies, L., Satre, M., Martin, J.B., Gross, J.D., 1993. The target of ammonia action in dictyostelium. Cell 75, 321-327.
Davies, O.R., Lin, C.Y., Radzisheuskaya, A., Zhou, X., Taube, J., Blin, G., Waterhouse, A., Smith, A.J., Lowell, S., 2013. Tcf15 primes pluripotent cells for differentiation. Cell Rep 3, 472-484.
De Poi, S.P., Xie, J., Smales, C.M., Proud, C.G., 2021. Constitutively active Rheb mutants [T23M] and [E40K] drive increased production and secretion of recombinant protein in Chinese hamster ovary cells. Biotechnol Bioeng 118, 2422-2434.
Del Rizzo, P.A., Trievel, R.C., 2011. Substrate and product specificities of SET domain methyltransferases. Epigenetics 6, 1059-1067.
Dominguez-Martin, E., Cardenal-Munoz, E., King, J.S., Soldati, T., Coria, R., Escalante, R., 2017. Methods to Monitor and Quantify Autophagy in the Social Amoeba Dictyostelium discoideum. Cells 6.
Dominguez, D.C., Guragain, M., Patrauchan, M., 2015. Calcium binding proteins and calcium signaling in prokaryotes. Cell Calcium 57, 151-165.

Dominov, J.A., Town, C.D., 1986. Regulation of stalk and spore antigen expression in monolayer cultures of Dictyostelium discoideum by pH. J Embryol Exp Morphol 96, 131-150.
Donfrancesco, A., Deb, G., Dominici, C., Pileggi, D., Castello, M.A., Helson, L., 1990. Effects of a single course of deferoxamine in neuroblastoma patients. Cancer Res 50, 4929-4930.
Dong, P., Xiong, F.J., Que, Y.M., Wang, K., Yu, L.H., Li, Z.G., Ren, M.Z., 2015. Expression profiling and functional analysis reveals that TOR is a key player in regulating photosynthesis and phytohormone signaling pathways in Arabidopsis. Front Plant Sci 6.
Dubin, M., Fuchs, J., Gräf, R., Schubert, I., Nellen, W., 2010. Dynamics of a novel centromeric histone variant CenH3 reveals the evolutionary ancestral timing of centromere biogenesis. Nucleic Acids Research 38, 7526-7537.
Dumont, F.J., Su, Q., 1995. Mechanism of action of the immunosuppressant rapamycin. Life Sciences 58, 373-395.
Early, A., Abe, T., Williams, J., 1995. Evidence for positional differentiation of prestalk cells and for a morphogenetic gradient in Dictyostelium. Cell 83, 91-99.
Early, A.E., Gaskell, M.J., Traynor, D., Williams, J.G., 1993. Two distinct populations of prestalk cells within the tip of the migratory Dictyostelium slug with differing fates at culmination. Development 118, 353-362.
Early, A.E., Williams, J.G., 1988. A Dictyostelium prespore-specific gene is transcriptionally repressed by DIF in vitro. Development 103, 519-524.
Eble, J.A., de Rezende, F.F., 2014. Redox-relevant aspects of the extracellular matrix and its cellular contacts via integrins. Antioxid Redox Signal 20, 1977-1993.
Efeyan, A., Zoncu, R., Chang, S., Gumper, I., Snitkin, H., Wolfson, R.L., Kirak, O., Sabatini, D.D., Sabatini, D.M., 2013. Regulation of mTORC1 by the Rag GTPases is necessary for neonatal autophagy and survival. Nature 493, 679-683.
Ehninger, D., Neff, F., Xie, K., 2014. Longevity, aging and rapamycin. Cell Mol Life Sci 71, 4325-4346.
Eichinger, L., Pachebat, J.A., Glockner, G., Rajandream, M.A., Sucgang, R., Berriman, M., Song, J., Olsen, R., Szafranski, K., Xu, Q., Tunggal, B., Kummerfeld, S., Madera, M., Konfortov, B.A., Rivero, F., Bankier, A.T., Lehmann, R., Hamlin, N., Davies, R., Gaudet, P., Fey, P., Pilcher, K., Chen, G., Saunders, D., Sodergren, E., Davis, P., Kerhornou, A., Nie, X., Hall, N., Anjard, C., Hemphill, L., Bason, N., Farbrother, P., Desany, B., Just, E., Morio, T., Rost, R., Churcher, C., Cooper, J., Haydock, S., van Driessche, N., Cronin, A., Goodhead, I., Muzny, D., Mourier, T., Pain, A., Lu, M., Harper, D., Lindsay, R., Hauser, H., James, K., Quiles, M., Babu, M.M., Saito, T., Buchrieser, C., Wardroper, A., Felder, M., Thangavelu, M., Johnson, D., Knights, A., Loulseged, H., Mungall, K., Oliver, K., Price, C., Quail, M.A., Urushihara, H., Hernandez, J., Rabbinowitsch, E., Steffen, D., Sanders, M., Ma, J., Kohara, Y., Sharp, S., Simmonds, M., Spiegler, S., Tivey, A., Sugano, S., White, B., Walker, D., Woodward, J., Winckler, T., Tanaka, Y., Shaulsky, G., Schleicher, M., Weinstock, G., Rosenthal, A., Cox, E.C., Chisholm, R.L., Gibbs, R., Loomis, W.F., Platzer, M., Kay, R.R., Williams, J., Dear, P.H., Noegel, A.A., Barrell, B., Kuspa, A., 2005. The genome of the social amoeba Dictyostelium discoideum. Nature 435, 43-57.
Elsaesser, S.J., Goldberg, A.D., Allis, C.D., 2010. New functions for an old variant: no substitute for histone H3.3. Curr Opin Genet Dev 20, 110-117.
Ennis, H.L., Dao, D.N., Wu, M.Y., Kessin, R.H., 2003. Mutation of the Dictyostelium fbxA gene affects cell-fate decisions and spatial patterning. Protist 154, 419-429.
Ennis, H.L.D., Dee N., Pukatzki, S.U., Kessin, R.H., 2000. Dictyostelium amoebae lacking an F-box protein form spores rather than stalk in chimeras with wild type. PNAS 97, 3292-3297.

Europe-Finner, G.N., Newell, P.C., 1986. Inositol 1,4,5-triphosphate induces calcium release from a non- mitochondrial pool in amoebae of Dictyostelium. Biochim Biophys Acta 887, 335-340.
Faix, J., Kreppel, L., Shaulsky, G., Schleicher, M., Kimmel, A.R., 2004. A rapid and efficient method to generate multiple gene disruptions in Dictyostelium discoideum using a single selectable marker and the Cre-loxP system. Nucleic Acids Research 32.
Fenton, T.R., Gout, I.T., 2011. Functions and regulation of the 70kDa ribosomal S6 kinases. Int J Biochem Cell Biol 43, 47-59.
Fernández-Medarde, A., Santos, E., 2011. Ras in cancer and developmental diseases. Genes & cancer 2, 344-358.
Fey, P., Kowal, A.S., Gaudet, P., Pilcher, K.E., Chisholm, R.L., 2007. Protocols for growth and development of Dictyostelium discoideum. Nat Protoc 2, 1307-1316.
Fiegna, F., Yu, Y.-T.N., Kadam, S.V., Velicer, G.J., 2006. Evolution of an obligate social cheater to a superior cooperator. Nature 441, 310-314.
Finlay, D.K., Rosenzweig, E., Sinclair, L.V., Feijoo-Carnero, C., Hukelmann, J.L., Rolf, J., Panteleyev, A.A., Okkenhaug, K., Cantrell, D.A., 2012. PDK1 regulation of mTOR and hypoxia-inducible factor 1 integrate metabolism and migration of CD8+ T cells. Journal of Experimental Medicine 209, 2441-2453.
Finnin, M.S., Donigian, J.R., Cohen, A., Richon, V.M., Rifkind, R.A., Marks, P.A., Breslow, R., Pavletich, N.P., 1999. Structures of a histone deacetylase homologue bound to the TSA and SAHA inhibitors. Nature 401, 188-193.
Flaadt, H., Jaworski, E., Malchow, D., 1993a. Evidence for two intracellular calcium pools in Dictyostelium: the cAMP-induced calcium influx is directed into a NBD-Cl- and 2,5-di-(tert-butyl)1,4-hydroquinone-sensitive pool. J Cell Sci 105 (Pt 4), 1131-1135.
Flaadt, H., Jaworski, E., Schlatterer, C., Malchow, D., 1993b. Cyclic AMP- and Ins(1,4,5)P3-induced Ca2+ fluxes in permeabilised cells of Dictyostelium discoideum: cGMP regulates Ca2+ entry across the plasma membrane. J Cell Sci 105 (Pt 1), 255-261.
Flinck, M., Kramer, S.H., Pedersen, S.F., 2018. Roles of pH in control of cell proliferation. Acta physiologica (Oxford, England) 223, e13068.
Forte, M., Adelsberger-Mangan, D., Colombini, M., 1987. Purification and characterization of the voltage-dependent anion channel from the outer mitochondrial membrane of yeast. J Membr Biol 99, 65-72.
Fosnaugh, K.L., Loomis, W.F., 1991. Coordinate regulation of the spore coat genes in Dictyostelium discoideum. Dev Genet 12, 123-132.
Fountain, S.J., Parkinson, K., Young, M.T., Cao, L.S., Thompson, C.R.L., North, R.A., 2007. An intracellular P2X receptor required for osmoregulation in Dictyostelium discoideum. Nature 448, 200-203.
Franke, J., Kessin, R., 1977. A defined minimal medium for axenic strains of Dictyostelium discoideum. Proc Natl Acad Sci U S A 74, 2157-2161.
Franke, J., Kessin, R.H., 1992. The cyclic nucleotide phosphodiesterases of Dictyostelium discoideum: molecular genetics and biochemistry. Cell Signal 4, 471-478.
Frias, M.A., Thoreen, C.C., Jaffe, J.D., Schroder, W., Sculley, T., Carr, S.A., Sabatini, D.M., 2006. mSin1 is necessary for Akt/PKB phosphorylation, and its isoforms define three distinct mTORC2s. Current Biology 16, 1865-1870.
Friedberg, F., Rivero, F., 2010. Single and multiple CH (calponin homology) domain containing multidomain proteins in Dictyostelium discoideum: an inventory. Molecular Biology Reports 37, 2853-2862.
Frost, J.N., Tan, T.K., Abbas, M., Wideman, S.K., Bonadonna, M., Stoffel, N.U., Wray, K., Kronsteiner, B., Smits, G., Campagna, D.R., Duarte, T.L., Lopes, J.M., Shah, A., Armitage, A.E., Arezes, J., Lim, P.J., Preston, A.E., Ahern, D., Teh, M., Naylor, C., Salio, M., Gileadi,

U., Andrews, S.C., Dunachie, S.J., Zimmermann, M.B., van der Klis, F.R.M., Cerundolo, V., Bannard, O., Draper, S.J., Townsend, A.R.M., Galy, B., Fleming, M.D., Lewis, M.C., Drakesmith, H., 2021. Hepcidin-Mediated Hypoferremia Disrupts Immune Responses to Vaccination and Infection. Med (N Y) 2, 164-179 e112.
Fukuzawa, M., 2011. Control of prestalk-cell differentiation by transcription factors. Development, Growth & Differentiation 53, 538-547.
Fukuzawa, M., Araki, T., Adrian, I., Williams, J.G., 2001. Tyrosine Phosphorylation-Independent Nuclear Translocation of a Dictyostelium STAT in Response to DIF Signaling. Molecular Cell 7, 779-788.
Furuichi, T., Cunningham, K.W., Muto, S., 2001. A putative two pore channel AtTPC1 mediates Ca(2+) flux in Arabidopsis leaf cells. Plant Cell Physiol 42, 900-905.
Furumai, R., Komatsu, Y., Nishino, N., Khochbin, S., Yoshida, M., Horinouchi, S., 2001. Potent histone deacetylase inhibitors built from trichostatin A and cyclic tetrapeptide antibiotics including trapoxin. Proc Natl Acad Sci U S A 98, 87-92.
Galaris, D., Barbouti, A., Pantopoulos, K., 2019. Iron homeostasis and oxidative stress: An intimate relationship. Biochim Biophys Acta Mol Cell Res 1866, 118535.
Galione, A., 2019. NAADP Receptors. Cold Spring Harb Perspect Biol 11.
Galvin-Burgess, K.E., Travis, E.D., Pierson, K.E., Vivian, J.L., 2013. TGF-beta-superfamily signaling regulates embryonic stem cell heterogeneity: self-renewal as a dynamic and regulated equilibrium. Stem Cells 31, 48-58.
Garcia-Martinez, J.M., Alessi, D.R., 2008. mTOR complex 2 (mTORC2) controls hydrophobic motif phosphorylation and activation of serum- and glucocorticoid-induced protein kinase 1 (SGK1). Biochem J 416, 375-385.
Garcia-Martinez, J.M., Wullschleger, S., Preston, G., Guichard, S., Fleming, S., Alessi, D.R., Duce, S.L., 2011. Effect of PI3K- and mTOR-specific inhibitors on spontaneous B-cell follicular lymphomas in PTEN/LKB1-deficient mice. Br J Cancer 104, 1116-1125.
Garcia, M., Ray, S., Brown, I., Irom, J., Brazill, D., 2014. PakD, a Putative p21-Activated Protein Kinase in Dictyostelium discoideum, Regulates Actin. Eukaryotic Cell 13, 119-126.
Gaskell, M.J., Jermyn, K.A., Watts, D.J., Treffry, T., Williams, J.G., 1992. Immuno-localization and separation of multiple prestalk cell types in Dictyostelium. Differentiation 51, 171-176.
Gilbert, O.M., Foster, K.R., Mehdiabadi, N.J., Strassmann, J.E., Queller, D.C., 2007. High relatedness maintains multicellular cooperation in a social amoeba by controlling cheater mutants. Proc Natl Acad Sci U S A 104, 8913-8917.
Goldberg, J.M., Manning, G., Liu, A., Fey, P., Pilcher, K.E., Xu, Y., Smith, J.L., 2006. The dictyostelium kinome--analysis of the protein kinases from a simple model organism. PLoS Genet 2, e38.
Goldberg, T., Hecht, M., Hamp, T., Karl, T., Yachdav, G., Ahmed, N., Altermann, U., Angerer, P., Ansorge, S., Balasz, K., Bernhofer, M., Betz, A., Cizmadija, L., Do, K.T., Gerke, J., Greil, R., Joerdens, V., Hastreiter, M., Hembach, K., Herzog, M., Kalemanov, M., Kluge, M., Meier, A., Nasir, H., Neumaier, U., Prade, V., Reeb, J., Sorokoumov, A., Troshani, I., Vorberg, S., Waldraff, S., Zierer, J., Nielsen, H., Rost, B., 2014. LocTree3 prediction of localization. Nucleic Acids Res 42, W350-355.
Gomer, R.H., Ammann, R.R., 1996. A cell-cycle phase-associated cell-type choice mechanism monitors the cell cycle rather than using an independent timer. Developmental Biology 174, 82-91.
Gomer, R.H., Datta, S., Firtel, R.A., 1986. Cellular and subcellular distribution of a cAMP-regulated prestalk protein and prespore protein in Dictyostelium discoideum: a study on the ontogeny of prestalk and prespore cells. J Cell Biol 103, 1999-2015.

Gomer, R.H., Firtel, R.A., 1987. Cell-Autonomous Determination of Cell-Type Choice in Dictyostelium Development by Cell-Cycle Phase. Science 237 758-762.
Göttlicher, M., Minucci, S., Zhu, P., Krämer, O.H., Schimpf, A., Giavara, S., Sleeman, J.P., Lo Coco, F., Nervi, C., Pelicci, P.G., Heinzel, T., 2001. Valproic acid defines a novel class of HDAC inhibitors inducing differentiation of transformed cells. The EMBO Journal 20, 6969-6978.
Grabarek, J.B., Zyzyńska, K., Saiz, N., Piliszek, A., Frankenberg, S., Nichols, J., Hadjantonakis, A.K., Plusa, B., 2012. Differential plasticity of epiblast and primitive endoderm precursors within the ICM of the early mouse embryo. Development 139, 129-139.
Grant, P.A., 2001. A tale of histone modifications. Genome Biol 2, REVIEWS0003.
Grewe, M., Gansauge, F., Schmid, R.M., Adler, G., Seufferlein, T., 1999. Regulation of cell growth and cyclin D1 expression by the constitutively active FRAP-p70s6K pathway in human pancreatic cancer cells. Cancer Res 59, 3581-3587.
Gross, J.D., 2009. Acidic Ca2+ stores, excitability, and cell patterning in Dictyostelium discoideum. Eukaryot Cell 8, 696-702.
Gross, J.D., Bradbury, J., Kay, R.R., Peacey, M.J., 1983. Intracellular pH and the control of cell differentiation in Dictyostelium discoideum. Nature 303, 244-245.
Gross, J.D., Peacey, M.J., von Strandmann, R.P., 1988. Plasma membrane proton pump inhibition and stalk cell differentiation in Dictyostelium discoideum. Differentiation 38, 91-98.
Gross, J.D., Town, C.D., Brookman, J.J., Jermyn, K.A., Peacey, M.J., Kay, R.R., 1981. Cell patterning in Dictyostelium. Philos Trans R Soc Lond B Biol Sci 295, 497-508.
Gruenheit, N., Baldwin, A., Stewart, B., Jaques, S., Keller, T., Parkinson, K., Salvidge, W., Baines, R., Brimson, C., Wolf, J.B., Chisholm, R., Harwood, A.J., Thompson, C.R.L., 2021. Mutant resources for functional genomics in Dictyostelium discoideum using REMI-seq technology. BMC Biology 19.
Gruenheit, N., Parkinson, K., Brimson, C.A., Kuwana, S., Johnson, E.J., Nagayama, K., Llewellyn, J., Salvidge, W.M., Stewart, B., Keller, T., van Zon, W., Cotter, S.L., Thompson, C.R.L., 2018. Cell Cycle Heterogeneity Can Generate Robust Cell Type Proportioning. Dev Cell 47, 494-508 e494.
Guertin, D.A., Sabatini, D.M., 2005. An expanding role for mTOR in cancer. Trends Mol Med 11, 353-361.
Guertin, D.A., Sabatini, D.M., 2007. Defining the role of mTOR in cancer. Cancer Cell 12, 9-22.
Guo, Q., Li, L., Hou, S., Yuan, Z., Li, C., Zhang, W., Zheng, L., Li, X., 2021. The Role of Iron in Cancer Progression. Front Oncol 11, 778492.
Hadjivasiliou, Z., Hunter, G.L., Baum, B., 2016. A new mechanism for spatial pattern formation via lateral and protrusion-mediated lateral signalling. J R Soc Interface 13.
Hake, S.B., Allis, C.D., 2006. Histone H3 variants and their potential role in indexing mammalian genomes: The “H3 barcode hypothesis”. Proceedings of the National Academy of Sciences 103, 6428-6435.
Hamilton, W.D., 1964a. The genetical evolution of social behaviour. I. J Theor Biol 7, 1-16.
Hamilton, W.D., 1964b. The genetical evolution of social behaviour. II. J Theor Biol 7, 17-52.
Hardie, D.G., Ross, F.A., Hawley, S.A., 2012. AMPK: a nutrient and energy sensor that maintains energy homeostasis. Nat Rev Mol Cell Bio 13, 251-262.
Hashimura, H., Morimoto, Y.V., Hirayama, Y., Ueda, M., 2022. Calcium responses to external mechanical stimuli in the multicellular stage of Dictyostelium discoideum. Sci Rep 12, 12428.

Hay, N., Sonenberg, N., 2004. Upstream and downstream of mTOR. Genes Dev 18, 1926-1945.
Hazzalin, C.A., Mahadevan, L.C., 2005. Dynamic acetylation of all lysine 4-methylated histone H3 in the mouse nucleus: Analysis at c-fos and c-jun. Plos Biology 3, 2111-2126.
Heidorn-Czarna, M., Heidorn, H.M., Fernando, S., Sanislav, O., Jarmuszkiewicz, W., Mutzel, R., Fisher, P.R., 2021. Chronic Activation of AMPK Induces Mitochondrial Biogenesis through Differential Phosphorylation and Abundance of Mitochondrial Proteins in Dictyostelium discoideum. International Journal of Molecular Sciences 22.
Heitman, J., Movva, N.R., Hall, M.N., 1991. Targets for Cell Cycle Arrest by the Immunosuppressant Rapamycin in Yeast. Science 253, 905-909.
Hentze, M.W., Muckenthaler, M.U., Galy, B., Camaschella, C., 2010. Two to Tango: Regulation of Mammalian Iron Metabolism. Cell 142, 24-38.
Hill-Eubanks, D.C., Werner, M.E., Heppner, T.J., Nelson, M.T., 2011. Calcium signaling in smooth muscle. Cold Spring Harb Perspect Biol 3, a004549.
Hirose, S., Benabentos, R., Ho, H.-I., Kuspa, A., Shaulsky, G., 2011. Self-Recognition in Social Amoebae Is Mediated by Allelic Pairs of Tiger Genes. Science 333, 467-470.
Hoeller, O., Kay, R.R., 2007. Chemotaxis in the absence of PIP3 gradients. Curr Biol 17, 813-817.
Horikawa, K., Yamada, Y., Matsuda, T., Kobayashi, K., Hashimoto, M., Matsu-Ura, T., Miyawaki, A., Michikawa, T., Mikoshiba, K., Nagai, T., 2010. Spontaneous network activity visualized by ultrasensitive Ca2+ indicators, yellow Cameleon-Nano. Nature Methods 7, 729-732.
Houghton, P.J., Gorlick, R., Kolb, E.A., Lock, R., Carol, H., Morton, C.L., Keir, S.T., Reynolds, C.P., Kang, M.H., Phelps, D., Maris, J.M., Billups, C., Smith, M.A., 2012. Initial testing (stage 1) of the mTOR kinase inhibitor AZD8055 by the pediatric preclinical testing program. Pediatr Blood Cancer 58, 191-199.
Howden, A.J.M., Hukelmann, J.L., Brenes, A., Spinelli, L., Sinclair, L.V., Lamond, A.I., Cantrell, D.A., 2019. Quantitative analysis of T cell proteomes and environmental sensors during T cell differentiation. Nature Immunology 20, 1542-1554.
Hsu, D.W., Chubb, J.R., Muramoto, T., Pears, C.J., Mahadevan, L.C., 2012. Dynamic acetylation of lysine-4-trimethylated histone H3 and H3 variant biology in a simple multicellular eukaryote. Nucleic Acids Res 40, 7247-7256.
Hu, Y., Carraro-Lacroix, L.R., Wang, A., Owen, C., Bajenova, E., Corey, P.N., Brumell, J.H., Voronov, I., 2016. Lysosomal pH Plays a Key Role in Regulation of mTOR Activity in Osteoclasts. J Cell Biochem 117, 413-425.
Huang, E., Blagg, S.L., Keller, T., Katoh, M., Shaulsky, G., Thompson, C.R., 2006. bZIP transcription factor interactions regulate DIF responses in Dictyostelium. Development 133, 449-458.
Huang, J., Berger, S.L., 2008. The emerging field of dynamic lysine methylation of non-histone proteins. Curr Opin Genet Dev 18, 152-158.
Huang, L., 2020. Investigating the role of dynamic histone modification in the mechanism of action of lysine deacetylase inhibitor (KDACi), Department of Biochemistry. University of Oxford.
Huang, L.Y., Hsu, D.W., Pears, C.J., 2021. Methylation-directed acetylation of histone H3 regulates developmental sensitivity to histone deacetylase inhibition. Nucleic Acids Res 49, 3781-3795.
Hukelmann, J.L., Anderson, K.E., Sinclair, L.V., Grzes, K.M., Murillo, A.B., Hawkins, P.T., Stephens, L.R., Lamond, A.I., Cantrell, D.A., 2016. The cytotoxic T cell proteome and its shaping by the kinase mTOR. Nat Immunol 17, 104-112.

Inoki, K., Li, Y., Zhu, T.Q., Wu, J., Guan, K.L., 2002. TSC2 is phosphorylated and inhibited by Akt and suppresses mTOR signalling. Nature Cell Biology 4, 648-657.
Inouye, K., 1989. Regulation of cytoplasmic pH in the differentiating cell types of the cellular slime mould Dictyostelium discoideum. Biochimica Et Biophysica Acta 1012, 64-68.
Inouye, K.E.I., 1988. Differences in Cytoplasmic pH and the Sensitivity to Acid Load Between Prespore Cells and Prestalk Cells of Dictyostelium. Journal of Cell Science 91, 109-115.
Insall, R., Kay, R.R., 1990. A specific DIF binding protein in Dictyostelium. Embo j 9, 3323-3328.
Insall, R., Nayler, O., Kay, R.R., 1992. DIF-1 induces its own breakdown in Dictyostelium. EMBO J 11, 2849-2854.
Ishibashi, K., Suzuki, M., Imai, M., 2000. Molecular cloning of a novel form (two-repeat) protein related to voltage-gated sodium and calcium channels. Biochem Biophys Res Commun 270, 370-376.
Isotani, S., Hara, K., Tokunaga, C., Inoue, H., Avruch, J., Yonezawa, K., 1999. Immunopurified mammalian target of rapamycin phosphorylates and activates p70 S6 kinase alpha in vitro. J Biol Chem 274, 34493-34498.
Ivannikov, M.V., Sugimori, M., Llinas, R.R., 2013. Synaptic vesicle exocytosis in hippocampal synaptosomes correlates directly with total mitochondrial volume. J Mol Neurosci 49, 223-230.
Jacinto, E., Loewith, R., Schmidt, A., Lin, S., Ruegg, M.A., Hall, A., Hall, M.N., 2004. Mammalian TOR complex 2 controls the actin cytoskeleton and is rapamycin insensitive. Nature Cell Biology 6, 1122-U1130.
Jackson, E.K., Dubey, R.K., 2008. CHAPTER 16 - Adenosine in the Kidney: PHYSIOLOGICAL ROLES AND MECHANISMS OF BIOSYNTHESIS, in: Alpern, R.J., Hebert, S.C. (Eds.), Seldin and Giebisch's The Kidney (Fourth Edition). Academic Press, San Diego, pp. 413-423.
Jacob, Y., Bergamin, E., Donoghue, M.T.A., Mongeon, V., LeBlanc, C., Voigt, P., Underwood, C.J., Brunzelle, J.S., Michaels, S.D., Reinberg, D., Couture, J.-F., Martienssen, R.A., 2014. Selective Methylation of Histone H3 Variant H3.1 Regulates Heterochromatin Replication. Science 343, 1249-1253.
Jaffer, Z.M., Khosla, M., Spiegelman, G.B., Weeks, G., 2001. Expression of activated Ras during Dictyostelium development alters cell localization and changes cell fate. Development 128, 907-916.
Jaiswal, P., Kimmel, A.R., 2019. mTORC1/AMPK responses define a core gene set for developmental cell fate switching. BMC Biol 17, 58.
Jaiswal, P., Majithia, A.R., Rosel, D., Liao, X.H., Khurana, T., Kimmel, A.R., 2019. Integrated actions of mTOR complexes 1 and 2 for growth and development of Dictyostelium. Int J Dev Biol 63, 521-527.
Jang, W., Gomer, R.H., 2011. Initial cell type choice in Dictyostelium. Eukaryot Cell 10, 150-155.
Jastrzebski, K., Hannan, K.M., Tchoubrieva, E.B., Hannan, R.D., Pearson, R.B., 2007. Coordinate regulation of ribosome biogenesis and function by the ribosomal protein S6 kinase, a key mediator of mTOR function. Growth Factors 25, 209-226.
Jeon, H.Y., Choi, J., Kraaier, L., Kim, Y.H., Eisenbarth, D., Yi, K., Kang, J.G., Kim, J.W., Shim, H.S., Lee, J.H., Lim, D.S., 2022. Airway secretory cell fate conversion via YAP-mTORC1-dependent essential amino acid metabolism. EMBO J 41, e109365.
Jermyn, K.A., Berks, M., Kay, R.R., Williams, J.G., 1987. Two distinct classes of prestalk-enriched mRNA sequences in Dictyostelium discoideum. Development 100, 745-755.

Jermyn, K.A., Duffy, K.T., Williams, J.G., 1989. A new anatomy of the prestalk zone in Dictyostelium. Nature 340, 144-146.
Jermyn, K.A., Williams, J.G., 1991. An Analysis of Culmination in Dictyostelium Using Prestalk and Stalk-Specific Cell Autonomous Markers. Development 111, 779-787.
Jiang, L., Smith, J.N., Anderson, S.L., Ma, P., Mizzen, C.A., Kelleher, N.L., 2007. Global Assessment of Combinatorial Post-translational Modification of Core Histones in Yeast Using Contemporary Mass Spectrometry. Journal of Biological Chemistry 282, 27923-27934.
Jin, T., Xu, X., Hereld, D., 2008. Chemotaxis, chemokine receptors and human disease. Cytokine 44, 1-8.
Jin, X., Zhang, Y., Alharbi, A., Hanbashi, A., Alhoshani, A., Parrington, J., 2020. Targeting Two-Pore Channels: Current Progress and Future Challenges. Trends Pharmacol Sci 41, 582-594.
Jones, A.L., Hulett, M.D., Parish, C.R., 2005. Histidine-rich glycoprotein: A novel adaptor protein in plasma that modulates the immune, vascular and coagulation systems. Immunology & Cell Biology 83, 106-118.
Journet, A., Klein, G., Brugiere, S., Vandenbrouck, Y., Chapel, A., Kieffer, S., Bruley, C., Masselon, C., Aubry, L., 2012. Investigating the macropinocytic proteome of Dictyostelium amoebae by high-resolution mass spectrometry. Proteomics 12, 241-245.
Jung, J., Genau, H.M., Behrends, C., 2015. Amino Acid-Dependent mTORC1 Regulation by the Lysosomal Membrane Protein SLC38A9. Mol Cell Biol 35, 2479-2494.
Kaller, M., Nellen, W., Chubb, J.R., 2006. Epigenetics in Dictyostelium. Methods Mol Biol 346, 491-505.
Kamimura, Y., Devreotes, P.N., 2010. Phosphoinositide-dependent protein kinase (PDK) activity regulates phosphatidylinositol 3,4,5-trisphosphate-dependent and -independent protein kinase B activation and chemotaxis. J Biol Chem 285, 7938-7946.
Kandel, E.S., Hay, N., 1999. The regulation and activities of the multifunctional serine/threonine kinase Akt/PKB. Exp Cell Res 253, 210-229.
Kaplan, B., Qazi, Y., Wellen, J.R., 2014. Strategies for the management of adverse events associated with mTOR inhibitors. Transplant Rev-Orlan 28, 126-133.
Karbowniczek, M., Cash, T., Cheung, M., Robertson, G.P., Astrinidis, A., Henske, E.P., 2004. Regulation of B-Raf kinase activity by tuberin and Rheb is mammalian target of rapamycin (mTOR)-independent. J Biol Chem 279, 29930-29937.
Karimi, M.M., Guo, Y., Cui, X., Pallikonda, H.A., Horková, V., Wang, Y.-F., Gil, S.R., Rodriguez-Esteban, G., Robles-Rebollo, I., Bruno, L., Georgieva, R., Patel, B., Elliott, J., Dore, M.H., Dauphars, D., Krangel, M.S., Lenhard, B., Heyn, H., Fisher, A.G., Štěpánek, O., Merkenschlager, M., 2021. The order and logic of CD4 versus CD8 lineage choice and differentiation in mouse thymus. Nature Communications 12.
Karmakar, R., Tyree, T., Gomer, R.H., Rappel, W.J., 2021. Cell dispersal by localized degradation of a chemoattractant. P Natl Acad Sci USA 118.
Kawata, T., Shevchenko, A., Fukuzawa, M., Jermyn, K.A., Totty, N.F., Zhukovskaya, N.V., Sterling, A.E., Mann, M., Williams, J.G., 1997. SH2 signaling in a lower eukaryote: A STAT protein that regulates stalk cell differentiation in Dictyostelium. Cell 89, 909-916.
Kay, R.R., 1982. cAMP and spore differentiation in Dictyostelium discoideum. Proc Natl Acad Sci U S A 79, 3228-3231.
Kay, R.R., 1987. Cell differentiation in monolayers and the investigation of slime mold morphogens. Methods Cell Biol 28, 433-448.
Kay, R.R., 1998. The biosynthesis of differentiation-inducing factor, a chlorinated signal molecule regulating Dictyostelium development. J Biol Chem 273, 2669-2675.
Kay, R.R., Flatman, P., Thompson, C.R., 1999. DIF signalling and cell fate. Semin Cell Dev Biol 10, 577-585.

Kay, R.R., Gadian, D.G., Williams, S.R., 1986. Intracellular pH in Dictyostelium: a 31P nuclear magnetic resonance study of its regulation and possible role in controlling cell differentiation. J Cell Sci 83, 165-179.
Kay, R.R., Jermyn, K.A., 1983. A possible morphogen controlling differentiation in Dictyostelium. Nature 303, 242-244.
Kay, R.R., Thompson, C.R., 2009. Forming patterns in development without morphogen gradients: scattered differentiation and sorting out. Cold Spring Harb Perspect Biol 1, a001503.
Kay, R.R., Williams, T.D., Manton, J.D., Traynor, D., Paschke, P., 2019. Living on soup: macropinocytic feeding in amoebae. Int J Dev Biol 63, 473-483.
Kelly, B., Carrizo, G.E., Edwards-Hicks, J., Sanin, D.E., Stanczak, M.A., Priesnitz, C., Flachsmann, L.J., Curtis, J.D., Mittler, G., Musa, Y., Becker, T., Buescher, J.M., Pearce, E.L., 2021. Sulfur sequestration promotes multicellularity during nutrient limitation. Nature 591, 471-476.
Khare, A., Shaulsky, G., 2010. Cheating by exploitation of developmental prestalk patterning in Dictyostelium discoideum. PLoS Genet 6, e1000854.
Khosla, M., Kriebel, P., Parent, C.A., Spiegelman, G.B., Weeks, G., 2006. A secondary disruption of the dmpA gene encoding a large membrane protein allows aggregation defective Dictyostelium rasC- cells to form multicellular structures. Dev Biol 292, 68-78.
Khosla, M., Spiegelman, G.B., Insall, R., Weeks, G., 2000. Functional overlap of the dictyostelium RasG, RasD and RasB proteins. J Cell Sci 113 (Pt 8), 1427-1434.
Kim, E., Goraksha-Hicks, P., Li, L., Neufeld, T.P., Guan, K.L., 2008. Regulation of TORC1 by Rag GTPases in nutrient response. Nat Cell Biol 10, 935-945.
Kim, J., Guan, K.L., 2019. mTOR as a central hub of nutrient signalling and cell growth. Nat Cell Biol 21, 63-71.
Kim, J., Kundu, M., Viollet, B., Guan, K.L., 2011. AMPK and mTOR regulate autophagy through direct phosphorylation of Ulk1. Nature Cell Biology 13, 132-U171.
Kim, J.S., Ro, S.H., Kim, M., Park, H.W., Semple, I.A., Park, H., Cho, U.S., Wang, W., Guan, K.L., Karin, M., Lee, J.H., 2015. Sestrin2 inhibits mTORC1 through modulation of GATOR complexes. Scientific Reports 5.
Kim, Sung J., DeStefano, Michael A., Oh, Won J., Wu, C.-c., Vega-Cotto, Nicole M., Finlan, M., Liu, D., Su, B., Jacinto, E., 2012. mTOR Complex 2 Regulates Proper Turnover of Insulin Receptor Substrate-1 via the Ubiquitin Ligase Subunit Fbw8. Molecular Cell 48, 875-887.
King, J.S., Insall, R.H., 2009. Chemotaxis: finding the way forward with Dictyostelium. Trends Cell Biol 19, 523-530.
King, J.S., Veltman, D.M., Insall, R.H., 2011. The induction of autophagy by mechanical stress. Autophagy 7, 1490-1499.
Klein, P.S., Sun, T.J., Saxe, C.L., 3rd, Kimmel, A.R., Johnson, R.L., Devreotes, P.N., 1988a. A chemoattractant receptor controls development in Dictyostelium discoideum. Science 241, 1467-1472.
Klein, P.S., Sun, T.J., Saxe, C.L., Kimmel, A.R., Johnson, R.L., Devreotes, P.N., 1988b. A Chemoattractant Receptor Controls Development in Dictyostelium-Discoideum. Science 241, 1467-1472.
Koch, L., 2015. GENOMICS Adding another dimension to gene regulation. Nature Reviews Genetics 16, 563-563.
Kolsch, V., Charest, P.G., Firtel, R.A., 2008. The regulation of cell motility and chemotaxis by phospholipid signaling. Journal of Cell Science 121, 551-559.
Kondo, S., Miura, T., 2010. Reaction-Diffusion Model as a Framework for Understanding Biological Pattern Formation. Science 329, 1616-1620.

Konijn, T.M., Van De Meene, J.G., Bonner, J.T., Barkley, D.S., 1967. The acrasin activity of adenosine-3',5'-cyclic phosphate. Proc Natl Acad Sci U S A 58, 1152-1154.
Kopachik, W., Oohata, A., Dhokia, B., Brookman, J.J., Kay, R.R., 1983. Dictyostelium Mutants Lacking Dif, a Putative Morphogen. Cell 33, 397-403.
Kortholt, A., Kataria, R., Keizer-Gunnink, I., Van Egmond, W.N., Khanna, A., Van Haastert, P.J., 2011. Dictyostelium chemotaxis: essential Ras activation and accessory signalling pathways for amplification. EMBO Rep 12, 1273-1279.
Koutelou, E., Hirsch, C.L., Dent, S.Y., 2010. Multiple faces of the SAGA complex. Curr Opin Cell Biol 22, 374-382.
Kouzarides, T., 2007. Chromatin modifications and their function. Cell 128, 693-705.
Kubohara, Y., Arai, A., Gokan, N., Hosaka, K., 2007. Pharmacological evidence that stalk cell differentiation involves increases in the intracellular Ca2+ and H+ concentrations in Dictyostelium discoideum. Development, Growth & Differentiation 49, 253-264.
Kubohara, Y., Kikuchi, H., Nguyen, V.H., Kuwayama, H., Oshima, Y., 2017. Evidence that differentiation-inducing factor-1 controls chemotaxis and cell differentiation, at least in part, via mitochondria in D-discoideum. Biol Open 6, 741-751.
Kubohara, Y., Okamoto, K., 1994. Cytoplasmic Ca2+ and H+ concentrations determine cell fate in Dictyostelium discoideum. FASEB J 8, 869-874.
Kupsa, A., Loomis, W.F., 1992. Tagging developmental genes in Dictyostelium by restriction enzyme-mediated integration of plasmid DNA. Genetics 89, 8803-8807.
Lam, D., Kosta, A., Luciani, M.F., Golstein, P., 2008. The inositol 1,4,5-trisphosphate receptor is required to signal autophagic cell death. Molecular Biology of the Cell 19, 691-700.
Lang, F., Wunderle, L., Badura, S., Schleyer, E., Bruggemann, M., Serve, H., Schnittger, S., Gokbuget, N., Pfeifer, H., Wagner, S., Ashelford, K., Bug, G., Ottmann, O.G., 2020. A phase I study of a dual PI3-kinase/mTOR inhibitor BEZ235 in adult patients with relapsed or refractory acute leukemia. BMC Pharmacol Toxicol 21, 70.
Laplante, M., Sabatini, D.M., 2009. mTOR signaling at a glance. J Cell Sci 122, 3589-3594.
Laplante, M., Sabatini, D.M., 2012. mTOR signaling in growth control and disease. Cell 149, 274-293.
Laude, A.J., Simpson, A.W.M., 2009. Compartmentalized signalling: Ca2+ compartments, microdomains and the many facets of Ca2+ signalling. Febs J 276, 1800-1816.
Law, B.K., 2005. Rapamycin: an anti-cancer immunosuppressant? Crit Rev Oncol Hematol 56, 47-60.
Lawrence, M., Daujat, S., Schneider, R., 2016. Lateral Thinking: How Histone Modifications Regulate Gene Expression. Trends Genet 32, 42-56.
Le, N.T., Richardson, D.R., 2002. The role of iron in cell cycle progression and the proliferation of neoplastic cells. Biochim Biophys Acta 1603, 31-46.
Leach, C.K., Ashworth, J.M., Garrod, D.R., 1973. Cell sorting out during the differentiation of mixtures of metabolically distinct populations of Dictyostelium discoideum. J Embryol Exp Morphol 29, 647-661.
Lee, S., Comer, F.I., Sasaki, A., McLeod, I.X., Duong, Y., Okumura, K., Yates, J.R., 3rd, Parent, C.A., Firtel, R.A., 2005. TOR complex 2 integrates cell movement during chemotaxis and signal relay in Dictyostelium. Mol Biol Cell 16, 4572-4583.
Leimberg, M.J., Prus, E., Konijn, A.M., Fibach, E., 2008. Macrophages function as a ferritin iron source for cultured human erythroid precursors. Journal of Cellular Biochemistry 103, 1211-1218.

Levraud, J.-P., Adam, M., Luciani, M.-F.o., de Chastellier, C., Blanton, R.L., Golstein, P., 2003. Dictyostelium cell death : early emergence and demise of highly polarized paddle cells. J Cell Biol 160, 1105-1114.
Li, H., Lin, J., Wang, X., Yao, G., Wang, L., Zheng, H., Yang, C., Jia, C., Liu, A., Bai, X., 2012. Targeting of mTORC2 prevents cell migration and promotes apoptosis in breast cancer. Breast Cancer Res Treat 134, 1057-1066.
Li, J., Kim, S.G., Blenis, J., 2014. Rapamycin: one drug, many effects. Cell Metab 19, 373-379.
Li, J., Xue, X., Ruan, J., Wu, M., Zhu, Z., Zang, J., 2010. Cloning, purification, crystallization and preliminary crystallographic analysis of the tandem tudor domain of Sgf29 from Saccharomyces cerevisiae. Acta Crystallogr Sect F Struct Biol Cryst Commun 66, 902-904.
Li, S.I., Purugganan, M.D., 2011. The cooperative amoeba: Dictyostelium as a model for social evolution. Trends Genet 27, 48-54.
Liao, X.H., Buggey, J., Kimmel, A.R., 2010. Chemotactic activation of Dictyostelium AGC-family kinases AKT and PKBR1 requires separate but coordinated functions of PDK1 and TORC2. J Cell Sci 123, 983-992.
Libby, A.R.G., Briers, D., Haghighi, I., Joy, D.A., Conklin, B.R., Belta, C., McDevitt, T.C., 2019. Automated Design of Pluripotent Stem Cell Self-Organization. Cell Systems 9, 483-495.e410.
Lim, C.J., Spiegelman, G.B., Weeks, G., 2001. RasC is required for optimal activation of adenylyl cyclase and Akt/PKB during aggregation. EMBO J 20, 4490-4499.
Lima, W.C., Leuba, F., Soldati, T., Cosson, P., 2012. Mucolipin controls lysosome exocytosis in Dictyostelium. J Cell Sci 125, 2315-2322.
Lima, W.C., Vinet, A., Pieters, J., Cosson, P., 2014. Role of PKD2 in rheotaxis in Dictyostelium. PLoS One 9, e88682.
Lin, P.H., Duann, P., Komazaki, S., Park, K.H., Li, H., Sun, M., Sermersheim, M., Gumpper, K., Parrington, J., Galione, A., Evans, A.M., Zhu, M.X., Ma, J., 2015. Lysosomal two-pore channel subtype 2 (TPC2) regulates skeletal muscle autophagic signaling. J Biol Chem 290, 3377-3389.
Lin, X., Han, L., Weng, J., Wang, K., Chen, T., 2018. Rapamycin inhibits proliferation and induces autophagy in human neuroblastoma cells. Bioscience reports 38.
Littmann, M., Heinzinger, M., Dallago, C., Olenyi, T., Rost, B., 2021. Embeddings from deep learning transfer GO annotations beyond homology. Sci Rep 11, 1160.
Liu, X., Vorontchikhina, M., Wang, Y.L., Faiola, F., Martinez, E., 2008. STAGA recruits Mediator to the MYC oncoprotein to stimulate transcription and cell proliferation. Mol Cell Biol 28, 108-121.
Liu, Y., White, K.A., Barber, D.L., 2020. Intracellular pH Regulates Cancer and Stem Cell Behaviors: A Protein Dynamics Perspective. Front Oncol 10, 1401.
Loewith, R., Hall, M.N., 2011. Target of rapamycin (TOR) in nutrient signaling and growth control. Genetics 189, 1177-1201.
Long, X., Lin, Y., Ortiz-Vega, S., Yonezawa, K., Avruch, J., 2005. Rheb binds and regulates the mTOR kinase. Current Biology 15, 702-713.
Long, Y.C., Zierath, J.R., 2006. AMP-activated protein kinase signaling in metabolic regulation. J Clin Invest 116, 1776-1783.
Loomis, W.F., 2014. Cell signaling during development of Dictyostelium. Dev Biol 391, 1-16.
Louis, S.A., Spiegelman, G.B., Weeks, G., 1997. Expression of an activated rasD gene changes cell fate decisions during Dictyostelium development. Mol Biol Cell 8, 303-312.

Lu, M., Wang, J., Jones, K.T., Ives, H.E., Feldman, M.E., Yao, L.J., Shokat, K.M., Ashrafi, K., Pearce, D., 2010. mTOR complex-2 activates ENaC by phosphorylating SGK1. J Am Soc Nephrol 21, 811-818.
Lu, Y.Y., Chen, Y.C., Kao, Y.H., Lin, Y.K., Yeh, Y.H., Chen, S.A., Chen, Y.J., 2016. Colchicine modulates calcium homeostasis and electrical property of HL-1 cells. J Cell Mol Med 20, 1182-1190.
Luan, F.L., Hojo, M., Maluccio, M., Yamaji, K., Suthanthiran, M., 2002. Rapamycin blocks tumor progression: unlinking immunosuppression from antitumor efficacy. Transplantation 73, 1565-1572.
Luciano, P., Jeon, J., El-Kaoutari, A., Challal, D., Bonnet, A., Barucco, M., Candelli, T., Jourquin, F., Lesage, P., Kim, J., Libri, D., Géli, V., 2017. Binding to RNA regulates Set1 function. Cell discovery 3, 17040.
Ludlow, M.J., Durai, L., Ennion, S.J., 2009. Functional Characterization of Intracellular Dictyostelium discoideum P2X Receptors. Journal of Biological Chemistry 284, 35227-35239.
Ludlow, M.J., Traynor, D., Fisher, P.R., Ennion, S.J., 2008. Purinergic-mediated Ca2+ influx in Dictyostelium discoideum. Cell Calcium 44, 567-579.
Luger, K., Mäder, A.W., Richmond, R.K., Sargent, D.F., Richmond, T.J., 1997. Crystal structure of the nucleosome core particle at 2.8 Å resolution. Nature 389, 251-260.
Lusche, D.F., Wessels, D., Scherer, A., Daniels, K., Kuhl, S., Soll, D.R., 2012. The IplA Ca2+ channel of Dictyostelium discoideum is necessary for chemotaxis mediated through Ca2+, but not through cAMP, and has a fundamental role in natural aggregation. Journal of Cell Science 125, 1770-1783.
Lyons, N.A., Kolter, R., 2015. On the evolution of bacterial multicellularity. Current Opinion in Microbiology 24, 21-28.
Ma, L., Chen, Z., Erdjument-Bromage, H., Tempst, P., Pandolfi, P.P., 2005. Phosphorylation and functional inactivation of TSC2 by Erk implications for tuberous sclerosis and cancer pathogenesis. Cell 121, 179-193.
Ma, X.M., Blenis, J., 2009. Molecular mechanisms of mTOR-mediated translational control. Nat Rev Mol Cell Biol 10, 307-318.
Machaca, K., 2010. Ca2+ signaling, genes and the cell cycle. Cell Calcium 48, 243-250.
Maeda, Y., 1970. Influence of ionic conditions on cell differentiation and morphogenesis of the cellular slime molds. Dev Growth Differ 12, 217-227.
Maeda, Y., 1986. A New Method for Inducing Synchronous Growth of Dictyostelium-Discoideum Cells Using Temperature Shifts. J Gen Microbiol 132, 1189-1196.
Magnuson, B., Ekim, B., Fingar, D.C., 2012. Regulation and function of ribosomal protein S6 kinase (S6K) within mTOR signalling networks. Biochemical Journal 441, 1-21.
Mahesh, A., Khan, M.I.K., Govindaraju, G., Verma, M., Awasthi, S., Chavali, P.L., Chavali, S., Rajavelu, A., Dhayalan, A., 2020. SET7/9 interacts and methylates the ribosomal protein, eL42 and regulates protein synthesis. Biochim Biophys Acta Mol Cell Res 1867, 118611.
Maira, S.M., Stauffer, F., Brueggen, J., Furet, P., Schnell, C., Fritsch, C., Brachmann, S., Chene, P., De Pover, A., Schoemaker, K., Fabbro, D., Gabriel, D., Simonen, M., Murphy, L., Finan, P., Sellers, W., Garcia-Echeverria, C., 2008. Identification and characterization of NVP-BEZ235, a new orally available dual phosphatidylinositol 3-kinase/mammalian target of rapamycin inhibitor with potent in vivo antitumor activity. Mol Cancer Ther 7, 1851-1863.
Malchow, D., Lusche, D.F., De Lozanne, A., Schlatterer, C., 2008. A fast Ca2+-induced Ca2+-release mechanism in Dictyostelium discoideum. Cell Calcium 43, 521-530.
Manahan, C.L., Iglesias, P.A., Long, Y., Devreotes, P.N., 2004. Chemoattractant signaling in Dictyostelium discoideum. Annu Rev Cell Dev Bi 20, 223-253.

Mann, S.K.O., Firtel, R.A., 1987. Cyclic-Amp Regulation of Early Gene-Expression in Dictyostelium-Discoideum - Mediation Via the Cell-Surface Cyclic-Amp Receptor. Molecular and Cellular Biology 7, 458-469.
Marcinkowska, M., Fajkis-Zajączkowska, N., Szafrańska, K., Jończyk, J., Siwek, A., Mordyl, B., Karcz, T., Latacz, G., Kolaczkowski, M., 2023. 2-(4-Fluorophenyl)-1H-benzo[d]imidazole as a Promising Template for the Development of Metabolically Robust, α1β2γ2GABA-A Receptor-Positive Allosteric Modulators. ACS Chemical Neuroscience 14, 1166-1180.
Marin, F.T., 1976. Regulation of development in Dictyostelium discoideum: I. Initiation of the growth to development transition by amino acid starvation. Developmental Biology 48, 110-117.
Marsh, D.J., Trahair, T.N., Martin, J.L., Chee, W.Y., Walker, J., Kirk, E.P., Baxter, R.C., Marshall, G.M., 2008. Rapamycin treatment for a child with germline PTEN mutation. Nat Clin Pract Oncol 5, 357-361.
Masaki, N., Fujimoto, K., Honda-Kitahara, M., Hada, E., Sawai, S., 2013. Robustness of self-organizing chemoattractant field arising from precise pulse induction of its breakdown enzyme: a single-cell level analysis of PDE expression in Dictyostelium. Biophys J 104, 1191-1202.
Masento, M.S., Morris, H.R., Taylor, G.W., Johnson, S.J., Skapski, A.C., Kay, R.R., 1988. Differentiation-inducing factor from the slime mould Dictyostelium discoideum and its analogues. Synthesis, structure and biological activity. Biochem J 256, 23-28.
Maurya, R., Kumar, R., Saran, S., 2017. Dictyostelium AMPK alpha regulates aggregate size and cell-type patterning. Open Biology 7.
Maurya, R., Kumar, R., Saran, S., 2020. AMPKα promotes basal autophagy induction in Dictyostelium discoideum. Journal of cellular physiology 235, 4941-4953.
McDonald, S.A., Durston, A.J., 1984. The cell cycle and sorting behaviour in Dictyostelium discoideum. J Cell Sci 66, 195-204.
McMillin, D.W., Ooi, M., Delmore, J., Negri, J., Hayden, P., Mitsiades, N., Jakubikova, J., Maira, S.M., Garcia-Echeverria, C., Schlossman, R., Munshi, N.C., Richardson, P.G., Anderson, K.C., Mitsiades, C.S., 2009. Antimyeloma Activity of the Orally Bioavailable Dual Phosphatidylinositol 3-Kinase/Mammalian Target of Rapamycin Inhibitor NVP-BEZ235. Cancer Research 69, 5835-5842.
Meili, R., Ellsworth, C., Firtel, R.A., 2000. A novel Akt/PKB-related kinase is essential for morphogenesis in Dictyostelium. Curr Biol 10, 708-717.
Meili, R., Ellsworth, C., Lee, S., Reddy, T.B., Ma, H., Firtel, R.A., 1999a. Chemoattractant-mediated transient activation and membrane localization of Akt/PKB is required for efficient chemotaxis to cAMP in Dictyostelium. Embo j 18, 2092-2105.
Meili, R., Ellsworth, C., Lee, S., Reddy, T.B.K., Ma, H., Firtel, R.A., 1999b. Chemoattractant-mediated transient activation and membrane localization of Akt/PKB is required for efficient chemotaxis to cAMP in Dictyostelium. Embo Journal 18, 2092-2105.
Mendez, R., Myers, M.G., White, M.F., Rhoads, R.E., 1996. Stimulation of protein synthesis, eukaryotic translation initiation factor 4E phosphorylation, and PHAS-I phosphorylation by insulin requires insulin receptor substrate 1 and phosphatidylinositol 3-kinase. Molecular and Cellular Biology 16, 2857-2864.
Mesquita, A., Cardenal-Muñoz, E., Dominguez, E., Muñoz-Braceras, S., Nuñez-Corcuera, B., Phillips, B.A., Tábara, L.C., Xiong, Q., Coria, R., Eichinger, L., Golstein, P., King, J.S., Soldati, T., Vincent, O., Escalante, R., 2017. Autophagy in Dictyostelium: Mechanisms, regulation and disease in a simple biomedical model. Autophagy 13, 24-40.
Miao, Y.L., Williams, C.J., 2012. Calcium signaling in mammalian egg activation and embryo development: the influence of subcellular localization. Mol Reprod Dev 79, 742-756.

Michod, R.E., 1999. Darwinian Dynamics: Evolutionary Transitions in Fitness and Individuality. Princeton University Press.
Michod, R.E., 2007. Evolution of individuality during the transition from unicellular to multicellular life. Proc Natl Acad Sci U S A 104 Suppl 1, 8613-8618.
Michod, R.E., Nedelcu, A.M., 2003. On the reorganization of fitness during evolutionary transitions in individuality. Integr Comp Biol 43, 64-73.
Mihajlovic, A.I., Bruce, A.W., 2017. The first cell-fate decision of mouse preimplantation embryo development: integrating cell position and polarity. Open Biol 7.
Milkereit, R., Persaud, A., Vanoaica, L., Guetg, A., Verrey, F., Rotin, D., 2015. LAPTM4b recruits the LAT1-4F2hc Leu transporter to lysosomes and promotes mTORC1 activation. Nat Commun 6, 7250.
Miller, R.A., Harrison, D.E., Astle, C.M., Fernandez, E., Flurkey, K., Han, M., Javors, M.A., Li, X., Nadon, N.L., Nelson, J.F., Pletcher, S., Salmon, A.B., Sharp, Z.D., Van Roekel, S., Winkleman, L., Strong, R., 2014. Rapamycin-mediated lifespan increase in mice is dose and sex dependent and metabolically distinct from dietary restriction. Aging Cell 13, 468-477.
Milne, J.L., Coukell, M.B., 1989. Identification of a high-affinity Ca2+ pump associated with endocytotic vesicles in Dictyostelium discoideum. Exp Cell Res 185, 21-32.
Mischerikow, N., Spedale, G., Altelaar, A.F., Timmers, H.T., Pijnappel, W.W., Heck, A.J., 2009. In-depth profiling of post-translational modifications on the related transcription factor complexes TFIID and SAGA. J Proteome Res 8, 5020-5030.
Moniakis, J., Coukell, M.B., Forer, A., 1995. Molecular-Cloning of an Intracellular P-Type Atpase from Dictyostelium That Is up-Regulated in Calcium-Adapted Cells. Journal of Biological Chemistry 270, 28276-28281.
Moniakis, J., Coukell, M.B., Janiec, A., 1999. Involvement of the Ca2+-ATPase PAT1 and the contractile vacuole in calcium regulation in Dictyostelium discoideum. J Cell Sci 112 (Pt 3), 405-414.
Morales, V., Giamarchi, C., Chailleux, C., Moro, F., Marsaud, V., Le Ricousse, S., Richard-Foy, H., 2001. Chromatin structure and dynamics: functional implications. Biochimie 83, 1029-1039.
Morgan, A.J., Davis, L.C., Ruas, M., Galione, A., 2015. TPC: the NAADP discovery channel? Biochem Soc Trans 43, 384-389.
Morgan, A.J., Davis, L.C., Wagner, S.K.T.Y., Lewis, A.M., Parrington, J., Churchill, G.C., Galione, A., 2013. Bidirectional Ca2+ signaling occurs between the endoplasmic reticulum and acidic organelles. J Cell Biol 200, 789-805.
Morio, T., Yasukawa, H., Urushihara, H., Saito, T., Ochiai, H., Takeuchi, I., Maeda, M., Tanaka, Y., 2001. FebA: a gene for eukaryotic translation initiation factor 4E-binding protein (4E-BP) in Dictyostelium discoideum. Biochim Biophys Acta 1519, 65-69.
Morris, S.A., 2016. Direct lineage reprogramming via pioneer factors; a detour through developmental gene regulatory networks. Development 143, 2696-2705.
Morris, S.A., Teo, R.T.Y., Li, H., Robson, P., Glover, D.M., Zernicka-Goetz, M., 2010. Origin and formation of the first two distinct cell types of the inner cell mass in the mouse embryo. Proceedings of the National Academy of Sciences 107, 6364-6369.
Morrison, A., Blanton, R.L., Grimson, M., Fuchs, M., Williams, K., Williams, J., 1994. Disruption of the gene encoding the EcmA, extracellular matrix protein of Dictyostelium alters slug morphology. Dev Biol 163, 457-466.
Muller-Taubenberger, A., Bonisch, C., Furbringer, M., Wittek, F., Hake, S.B., 2011. The histone methyltransferase Dot1 is required for DNA damage repair and proper development in Dictyostelium. Biochem Bioph Res Co 404, 1016-1022.
Muñoz-Braceras, S., Mesquita, A., Escalante, R., 2013. Dictyosteliumdiscoideum as a Model in Biomedical Research, in: Romeralo, M., Baldauf, S., Escalante, R. (Eds.), Dictyostelids:

Evolution, Genomics and Cell Biology. Springer Berlin Heidelberg, Berlin, Heidelberg, pp. 1-34.
Muramoto, T., Chubb, J.R., 2008. Live imaging of the Dictyostelium cell cycle reveals widespread S phase during development, a G2 bias in spore differentiation and a premitotic checkpoint. Development 135, 1647-1657.
Muramoto, T., Iriki, H., Watanabe, J., Kawata, T., 2019. Recent Advances in CRISPR/Cas9-Mediated Genome Editing in Dictyostelium. Cells 8.
Muramoto, T., Müller, I., Thomas, G., Melvin, A., Chubb, J.R., 2010. Methylation of H3K4 Is Required for Inheritance of Active Transcriptional States. Current Biology 20, 397-406.
Nakano, A., Kato, H., Watanabe, T., Min, K.D., Yamazaki, S., Asano, Y., Seguchi, O., Higo, S., Shintani, Y., Asanuma, H., Asakura, M., Minamino, T., Kaibuchi, K., Mochizuki, N., Kitakaze, M., Takashima, S., 2010. AMPK controls the speed of microtubule polymerization and directional cell migration through CLIP-170 phosphorylation. Nat Cell Biol 12, 583-590.
Narita, T.B., Koide, K., Morita, N., Saito, T., 2011. Dictyostelium hybrid polyketide synthase, SteelyA, produces 4-methyl-5-pentylbenzene-1,3-diol and induces spore maturation. FEMS Microbiology Letters 319, 82-87.
Nazarieh, M., Hoeppner, M., Helms, V., 2021. Identification of Biomarkers Controlling Cell Fate In Blood Cell Development. Frontiers in Bioinformatics 1.
Neave, N., Sobolewski, A., Weeks, G., 1983. The effect of ammonia on stalk cell formation in submerged monolayers of Dictyostelium discoideum. Cell Differ 13, 301-307.
Neff, F., Flores-Dominguez, D., Ryan, D.P., Horsch, M., Schröder, S., Adler, T., Afonso, L.C., Aguilar-Pimentel, J.A., Becker, L., Garrett, L., Hans, W., Hettich, M.M., Holtmeier, R., Hölter, S.M., Moreth, K., Prehn, C., Puk, O., Rácz, I., Rathkolb, B., Rozman, J., Naton, B., Ordemann, R., Adamski, J., Beckers, J., Bekeredjian, R., Busch, D.H., Ehninger, G., Graw, J., Höfler, H., Klingenspor, M., Klopstock, T., Ollert, M., Stypmann, J., Wolf, E., Wurst, W., Zimmer, A., Fuchs, H., Gailus-Durner, V., Hrabe de Angelis, M., Ehninger, D., 2013. Rapamycin extends murine lifespan but has limited effects on aging. J Clin Invest 123, 3272-3291.
Nelson, M.K., Clark, A., Abe, T., Nomura, A., Yadava, N., Funair, C.J., Jermyn, K.A., Mohanty, S., Firtel, R.A., Williams, J.G., 2000. An F-Box/WD40 repeat-containing protein important for Dictyostelium cell-type proportioning, slug behaviour, and culmination. Developmental Biology 224, 42-59.
Neumann, C.S., Walsh, C.T., Kay, R.R., 2010. A flavin-dependent halogenase catalyzes the chlorination step in the biosynthesis of Dictyostelium differentiation-inducing factor 1. Proc Natl Acad Sci U S A 107, 5798-5803.
Ng, H.H., Robert, F., Young, R.A., Struhl, K., 2003. Targeted recruitment of Set1 histone methylase by elongating Pol II provides a localized mark and memory of recent transcriptional activity. Mol Cell 11, 709-719.
Nguyen, V.N., Abagyan, R., Tsunoda, S., 2019. mTOR Inhibitors Associated with Higher Cardiovascular Adverse Events -A Large Population Database Analysis. Am J Transplant 19, 1108-1108.
Nicetto, D., Donahue, G., Jain, T., Peng, T., Sidoli, S., Sheng, L., Montavon, T., Becker, J.S., Grindheim, J.M., Blahnik, K., Garcia, B.A., Tan, K., Bonasio, R., Jenuwein, T., Zaret, K.S., 2019. H3K9me3-heterochromatin loss at protein-coding genes enables developmental lineage specification. Science 363, 294-297.
Nicholas Europe-Finner, G., Newell, P.C., 1985. Inositol 1,4,5-trisphosphate induces cyclic GMP formation in Dictyostelium discoideum. Biochem Bioph Res Co 130, 1115-1122.
Nicklin, P., Bergman, P., Zhang, B., Triantafellow, E., Wang, H., Nyfeler, B., Yang, H., Hild, M., Kung, C., Wilson, C., Myer, V.E., MacKeigan, J.P., Porter, J.A., Wang, Y.K., Cantley,

L.C., Finan, P.M., Murphy, L.O., 2009. Bidirectional transport of amino acids regulates mTOR and autophagy. Cell 136, 521-534.
Nislow, C., Ray, E., Pillus, L., 1997. SET1, a yeast member of the trithorax family, functions in transcriptional silencing and diverse cellular processes. Mol Biol Cell 8, 2421-2436.
Nobukuni, T., Joaquin, M., Roccio, M., Dann, S.G., Kim, S.Y., Gulati, P., Byfield, M.P., Backer, J.M., Natt, F., Bos, J.L., Zwartkruis, F.J., Thomas, G., 2005. Amino acids mediate mTOR/raptor signaling through activation of class 3 phosphatidylinositol 3OH-kinase. Proc Natl Acad Sci U S A 102, 14238-14243.
Nojima, H., Tokunaga, C., Eguchi, S., Oshiro, N., Hidayat, S., Yoshino, K., Hara, K., Tanaka, N., Avruch, J., Yonezawa, K., 2003. The mammalian target of rapamycin (mTOR) partner, raptor, binds the mTOR substrates p70 S6 kinase and 4E-BP1 through their TOR signaling (TOS) motif. Journal of Biological Chemistry 278, 15461-15464.
Noma, K., Allis, C.D., Grewal, S.I.S., 2001. Transitions in distinct histone H3 methylation patterns at the heterochromatin domain boundaries. Science 293, 1150-1155.
Oexle, H., Gnaiger, E., Weiss, G., 1999. Iron-dependent changes in cellular energy metabolism: influence on citric acid cycle and oxidative phosphorylation. Biochim Biophys Acta 1413, 99-107.
Ogasawara, T., Watanabe, J., Adachi, R., Ono, Y., Kamimura, Y., Muramoto, T., 2022. CRISPR/Cas9-based genome-wide screening of Dictyostelium. Sci Rep 12, 11215.
Ogunbayo, O.A., Duan, J., Xiong, J., Wang, Q., Feng, X., Ma, J., Zhu, M.X., Evans, A.M., 2018. mTORC1 controls lysosomal Ca2+ release through the two-pore channel TPC2. Science Signaling 11, 1-10.
Oh, W.J., Jacinto, E., 2011. mTOR complex 2 signaling and functions. Cell Cycle 10, 2305-2316.
Ooga, M., Inoue, A., Kageyama, S.I., Akiyama, T., Nagata, M., Aoki, F., 2008. Changes in H3K79 methylation during preimplantation development in mice. Biol Reprod 78, 413-424.
Ostrowski, E.A., Katoh, M., Shaulsky, G., Queller, D.C., Strassmann, J.E., 2008. Kin Discrimination Increases with Genetic Distance in a Social Amoeba. PLoS Biology 6, e287.
Otsubo, Y., Yamamato, M., 2008. TOR signaling in fission yeast. Crit Rev Biochem Mol Biol 43, 277-283.
Oudet, P., Grossbellard, M., Chambon, P., 1975. Electron-Microscopic and Biochemical Evidence That Chromatin Structure Is a Repeating Unit. Cell 4, 281-300.
Outten, F.W., Theil, E.C., 2009. Iron-Based Redox Switches in Biology. Antioxidants & Redox Signaling 11, 1029-1046.
Padh, H., Ha, J., Lavasa, M., Steck, T.L., 1993. A post-lysosomal compartment in Dictyostelium discoideum. J Biol Chem 268, 6742-6747.
Pallet, N., Legendre, C., 2013. Adverse events associated with mTOR inhibitors. Expert Opin Drug Saf 12, 177-186.
Pan, M., Xu, X.H., Chen, Y., Jin, T., 2016. Identification of a Chemoattractant G-Protein-Coupled Receptor for Folic Acid that Controls Both Chemotaxis and Phagocytosis. Developmental Cell 36, 428-439.
Parikh, A., Miranda, E.R., Katoh-Kurasawa, M., Fuller, D., Rot, G., Zagar, L., Curk, T., Sucgang, R., Chen, R., Zupan, B., Loomis, W.F., Kuspa, A., Shaulsky, G., 2010. Conserved developmental transcriptomes in evolutionarily divergent species. Genome Biol 11, R35.
Parmar, N., Tamanoi, F., 2010. Rheb G-Proteins and the Activation of mTORC1. Enzymes 27, 39-56.
Patel, C.H., Powell, J.D., 2017. Targeting T cell metabolism to regulate T cell activation, differentiation and function in disease. Curr Opin Immunol 46, 82-88.
Paul, S., Knott, J.G., 2014. Epigenetic control of cell fate in mouse blastocysts: the role of covalent histone modifications and chromatin remodeling. Mol Reprod Dev 81, 171-182.

Peracino, B., Buracco, S., Bozzaro, S., 2013. The Nramp (Slc11) proteins regulate development, resistance to pathogenic bacteria and iron homeostasis in Dictyostelium discoideum. J Cell Sci 126, 301-311.
Peracino, B., Wagner, C., Balest, A., Balbo, A., Pergolizzi, B., Noegel, A.A., Steinert, M., Bozzaro, S., 2006. Function and Mechanism of Action of Dictyostelium Nramp1 (Slc11a1) in Bacterial Infection. Traffic 7, 22-38.
Pergolizzi, B., Panuzzo, C., Ali, M.S., Lo Iacono, M., Levra Levron, C., Ponzone, L., Prelli, M., Cilloni, D., Calautti, E., Bozzaro, S., Bracco, E., 2019. Two conserved glycine residues in mammalian and Dictyostelium Rictor are required for mTORC2 activity and integrity. Journal of Cell Science 132, jcs236505.
Petit, C.S., Roczniak-Ferguson, A., Ferguson, S.M., 2013. Recruitment of folliculin to lysosomes supports the amino acid-dependent activation of Rag GTPases. J Cell Biol 202, 1107-1122.
Pfeifhofer-Obermair, C., Tymoszuk, P., Nairz, M., Schroll, A., Klais, G., Demetz, E., Engl, S., Brigo, N., Weiss, G., 2021. Regulation of Th1 T Cell Differentiation by Iron via Upregulation of T Cell Immunoglobulin and Mucin Containing Protein-3 (TIM-3). Front Immunol 12, 637809.
Pitt, S.J., Funnell, T.M., Sitsapesan, M., Venturi, E., Rietdorf, K., Ruas, M., Ganesan, A., Gosain, R., Churchill, G.C., Zhu, M.X., Parrington, J., Galione, A., Sitsapesan, R., 2010. TPC2 Is a Novel NAADP-sensitive Ca2+ Release Channel, Operating as a Dual Sensor of Luminal pH and Ca2+. Journal of Biological Chemistry 285, 35039-35046.
Plattner, H., Verkhratsky, A., 2013. Ca2+ signalling early in evolution--all but primitive. J Cell Sci 126, 2141-2150.
Pongas, G., Fojo, T., 2016. BEZ235: When Promising Science Meets Clinical Reality. Oncologist 21, 1033-1034.
Ponsford, A.H., Ryan, T.A., Raimondi, A., Cocucci, E., Wycislo, S.A., Frohlich, F., Swan, L.E., Stagi, M., 2021. Live imaging of intra-lysosome pH in cell lines and primary neuronal culture using a novel genetically encoded biosensor. Autophagy 17, 1500-1518.
Ponting, C., Schultz, J., Bork, P., 1997. SPRY domains in ryanodine receptors (Ca2+-release channels). Trends in Biochemical Sciences 22, 193-194.
Price, D.J., Grove, J.R., Calvo, V., Avruch, J., Bierer, B.E., 1992. Rapamycin-Induced Inhibition of the 70-Kilodalton S6 Protein Kinase. Science 257, 973-977.
Pruitt, K., Der, C.J., 2001. Ras and Rho regulation of the cell cycle and oncogenesis. Cancer Lett 171, 1-10.
Rafia, S., Saran, S., 2019. Sestrin-like protein from Dictyostelium discoideum is involved in autophagy under starvation stress. Microbiological Research 220, 61-71.
Raper, K.B., 1940. PSEUDOPLASMODIUM FORMATION AND ORGANIZATION IN DICTYOSTELIUM DISCOIDEUM. Journal of the Elisha Mitchell Scientific Society 56, 241-282.
Ratner, D.I., 1986. Equivalence of Intracellular Ph of Differentiating Dictyostelium Cell-Types. Nature 321, 180-182.
Ravnskjaer, K., Madiraju, A., Montminy, M., 2016. Role of the cAMP Pathway in Glucose and Lipid Metabolism. Handb Exp Pharmacol 233, 29-49.
Real, E., Howick, V.M., Dahalan, F.A., Witmer, K., Cudini, J., Andradi-Brown, C., Blight, J., Davidson, M.S., Dogga, S.K., Reid, A.J., Baum, J., Lawniczak, M.K.N., 2021. A single-cell atlas of Plasmodium falciparum transmission through the mosquito. Nature Communications 12.
Rebsamen, M., Pochini, L., Stasyk, T., de Araújo, M.E., Galluccio, M., Kandasamy, R.K., Snijder, B., Fauster, A., Rudashevskaya, E.L., Bruckner, M., Scorzoni, S., Filipek, P.A., Huber, K.V., Bigenzahn, J.W., Heinz, L.X., Kraft, C., Bennett, K.L., Indiveri, C., Huber,

L.A., Superti-Furga, G., 2015. SLC38A9 is a component of the lysosomal amino acid sensing machinery that controls mTORC1. Nature 519, 477-481.
Reinders, Y., Schulz, I., Gräf, R., Sickmann, A., 2006. Identification of Novel Centrosomal Proteins in Dictyostelium discoideum by Comparative Proteomic Approaches. Journal of Proteome Research 5, 589-598.
Remenyi, A., Scholer, H.R., Wilmanns, M., 2004. Combinatorial control of gene expression. Nat Struct Mol Biol 11, 812-815.
Reymond, C.D., Gomer, R.H., Mehdy, M.C., Firtel, R.A., 1984. Developmental regulation of a Dictyostelium gene encoding a protein homologous to mammalian ras protein. Cell 39, 141-148.
Reymond, C.D., Gomer, R.H., Nellen, W., Theibert, A., Devreotes, P., Firtel, R.A., 1986. Phenotypic Changes Induced by a Mutated Ras Gene during the Development of Dictyostelium Transformants. Nature 323, 340-343.
Ringel, A.E., Cieniewicz, A.M., Taverna, S.D., Wolberger, C., 2015. Nucleosome competition reveals processive acetylation by the SAGA HAT module. Proc Natl Acad Sci U S A 112, E5461-5470.
Robbins, S.M., Williams, J.G., Jermyn, K.A., Spiegelman, G.B., Weeks, G., 1989. Growing and developing Dictyostelium cells express different ras genes. Proc Natl Acad Sci U S A 86, 938-942.
Rodgers, J.T., King, K.Y., Brett, J.O., Cromie, M.J., Charville, G.W., Maguire, K.K., Brunson, C., Mastey, N., Liu, L., Tsai, C.R., Goodell, M.A., Rando, T.A., 2014. mTORC1 controls the adaptive transition of quiescent stem cells from G0 to G(Alert). Nature 510, 393-396.
Roesler, W.J., Vandenbark, G.R., Hanson, R.W., 1988. Cyclic AMP and the induction of eukaryotic gene transcription. J Biol Chem 263, 9063-9066.
Roguev, A., Schaft, D., Shevchenko, A., Pijnappel, W.W., Wilm, M., Aasland, R., Stewart, A.F., 2001. The Saccharomyces cerevisiae Set1 complex includes an Ash2 homologue and methylates histone 3 lysine 4. Embo j 20, 7137-7148.
Romeralo, M., Baldauf, S., Escalante, R., 2013. Dictyostelids : evolution, genomics and cell biology. Springer, Berlin

New York.
Rooney, E.K., Gross, J.D., 1992a. ATP-driven Ca2+/H+ antiport in acid vesicles from Dictyostelium. Proceedings of the National Academy of Sciences 89, 8025-8029.
Rooney, E.K., Gross, J.D., 1992b. ATP-driven Ca2+/H+ antiport in acid vesicles from Dictyostelium. Proc Natl Acad Sci U S A 89, 8025-8029.
Roper, J., Richardson, M.P., Wang, W.V., Richard, L.G., Chen, W., Coffee, E.M., Sinnamon, M.J., Lee, L., Chen, P.C., Bronson, R.T., Martin, E.S., Hung, K.E., 2011. The Dual PI3K/mTOR Inhibitor NVP-BEZ235 Induces Tumor Regression in a Genetically Engineered Mouse Model of PIK3CA Wild-Type Colorectal Cancer. Plos One 6.
Ropolo, A., Grasso, D., Pardo, R., Sacchetti, M.L., Archange, C., Lo Re, A., Seux, M., Nowak, J., Gonzalez, C.D., Iovanna, J.L., Vaccaro, M.I., 2007. The pancreatitis-induced vacuole membrane protein 1 triggers autophagy in mammalian cells. Journal of Biological Chemistry 282, 37124-37133.
Rosel, D., Khurana, T., Majithia, A., Huang, X., Bhandari, R., Kimmel, A.R., 2012. TOR complex 2 (TORC2) in Dictyostelium suppresses phagocytic nutrient capture independently of TORC1-mediated nutrient sensing. Journal of Cell Science 125, 37-48.
Rosenfeld, J.A., Wang, Z., Schones, D.E., Zhao, K., DeSalle, R., Zhang, M.Q., 2009. Determination of enriched histone modifications in non-genic portions of the human genome. BMC Genomics 10, 143.

Rosengarten, R.D., Santhanam, B., Fuller, D., Katoh-Kurasawa, M., Loomis, W.F., Zupan, B., Shaulsky, G., 2015. Leaps and lulls in the developmental transcriptome of Dictyostelium discoideum. BMC Genomics 16, 294.
Rouault, T.A., 2006. The role of iron regulatory proteins in mammalian iron homeostasis and disease. Nature Chemical Biology 2, 406-414.
Rugg-Gunn, P.J., Cox, B.J., Ralston, A., Rossant, J., 2010. Distinct histone modifications in stem cell lines and tissue lineages from the early mouse embryo. Proc Natl Acad Sci U S A 107, 10783-10790.
Ryall, J.G., Cliff, T., Dalton, S., Sartorelli, V., 2015. Metabolic Reprogramming of Stem Cell Epigenetics. Cell Stem Cell 17, 651-662.
Sabatini, D.M., 2006. mTOR and cancer: insights into a complex relationship. Nature Reviews Cancer 6, 729-734.
Sabatini, D.M., 2017. Twenty-five years of mTOR: Uncovering the link from nutrients to growth. Proc Natl Acad Sci U S A 114, 11818-11825.
Sabatini, D.M., Erdjumentbromage, H., Lui, M., Tempst, P., Snyder, S.H., 1994. RAFT1: A mammalian protein that binds to FKBP12 in a rapamycin-dependent fashion and is homologous to yeast TORs. Cell 78, 35-43.
Sabers, C.J., Martin, M.M., Brunn, G.J., Williams, J.M., Dumont, F.J., Wiederrecht, G., Abraham, R.T., 1995. Isolation of a Protein Target of the FKBP12-Rapamycin Complex in Mammalian Cells. The Journal of Biological Chemistry 270.
Sagner, A., Briscoe, J., 2017. Morphogen interpretation: concentration, time, competence, and signaling dynamics. WIREs Developmental Biology 6, e271.
Saito, T., Kato, A., Kay, R.R., 2008. DIF-1 induces the basal disc of the Dictyostelium fruiting body. Dev Biol 317, 444-453.
Sambrook, J., Fritsch, E.F., Maniatis, T., 1989. Molecular cloning : a laboratory manual, 2nd ed. Cold Spring Harbor Laboratory Press, Cold Spring Harbor.
Sancak, Y., Bar-Peled, L., Zoncu, R., Markhard, A.L., Nada, S., Sabatini, D.M., 2010. Ragulator-Rag Complex Targets mTORC1 to the Lysosomal Surface and Is Necessary for Its Activation by Amino Acids. Cell 141, 290-303.
Sancak, Y., Peterson, T.R., Shaul, Y.D., Lindquist, R.A., Thoreen, C.C., Bar-Peled, L., Sabatini, D.M., 2008. The Rag GTPases bind raptor and mediate amino acid signaling to mTORC1. Science 320, 1496-1501.
Sanders, S.L., Jennings, J., Canutescu, A., Link, A.J., Weil, P.A., 2002. Proteomics of the eukaryotic transcription machinery: identification of proteins associated with components of yeast TFIID by multidimensional mass spectrometry. Mol Cell Biol 22, 4723-4738.
Santorelli, L.A., Kuspa, A., Shaulsky, G., Queller, D.C., Strassmann, J.E., 2013. A new social gene in Dictyostelium discoideum, chtB. BMC Evolutionary Biology 13.
Santorelli, L.A., Thompson, C.R., Villegas, E., Svetz, J., Dinh, C., Parikh, A., Sucgang, R., Kuspa, A., Strassmann, J.E., Queller, D.C., Shaulsky, G., 2008. Facultative cheater mutants reveal the genetic complexity of cooperation in social amoebae. Nature 451, 1107-1110.
Santos-Rosa, H., Schneider, R., Bannister, A.J., Sherriff, J., Bernstein, B.E., Emre, N.C.T., Schreiber, S.L., Mellor, J., Kouzarides, T., 2002. Active genes are tri-methylated at K4 of histone H3. Nature 419, 407-411.
Saran, S., Azhar, M., Manogaran, P.S., Pande, G., Nanjundiah, V., 1994. The level of sequestered calcium in vegetative amoebae of Dictyostelium discoideum can predict post-aggregative cell fate. Differentiation 57, 163-169.
Sarbassov, D.D., Ali, S.M., Sengupta, S., Sheen, J.H., Hsu, P.P., Bagley, A.F., Markhard, A.L., Sabatini, D.M., 2006. Prolonged rapamycin treatment inhibits mTORC2 assembly and Akt/PKB. Mol Cell 22, 159-168.

Sarbassov, D.D., Guertin, D.A., Ali, S.M., Sabatini, D.M., 2005. Phosphorylation and regulation of Akt/PKB by the rictor-mTOR complex. Science 307, 1098-1101.
Sardet, C., Roegiers, F., Dumollard, R., Rouviere, C., McDougall, A., 1998. Calcium waves and oscillations in eggs. Biophys Chem 72, 131-140.
Saunders, R.N., Metcalfe, M.S., Nicholson, M.L., 2001. Rapamycin in transplantation: a review of the evidence. Kidney International 59, 3-16.
Saxe, C.L., 3rd, Klein, P., Sun, T.J., Kimmel, A.R., Devreotes, P.N., 1988. Structure and expression of the cAMP cell-surface receptor. Dev Genet 9, 227-235.
Saxton, R.A., Sabatini, D.M., 2017. mTOR Signaling in Growth, Metabolism, and Disease. Cell 168, 960-976.
Scalise, M., Galluccio, M., Console, L., Pochini, L., Indiveri, C., 2018. The Human SLC7A5 (LAT1): The Intriguing Histidine/Large Neutral Amino Acid Transporter and Its Relevance to Human Health. Frontiers in chemistry 6, 243.
Schaap, P., 2007. Evolution of size and pattern in the social amoebas. Bioessays 29, 635-644.
Schaap, P., 2011. Evolution of developmental cyclic adenosine monophosphate signaling in the Dictyostelia from an amoebozoan stress response. Dev Growth Differ 53, 452-462.
Schaap, P., Nebl, T., Fisher, P.R., 1996. A slow sustained increase in cytosolic Ca2+ levels mediates stalk gene induction by differentiation inducing factor in Dictyostelium. EMBO J 15, 5177-5183.
Schalm, S.S., Fingar, D.C., Sabatini, D.M., Blenis, J., 2003. TOS motif-mediated raptor binding regulates 4E-BP1 multisite phosphorylation and function. Curr Biol 13, 797-806.
Schaloske, R.H., Lusche, D.F., Bezares-Roder, K., Happle, K., Malchow, D., Schlatterer, C., 2005. Ca2+ regulation in the absence of the iplA gene product in Dictyostelium discoideum. Bmc Cell Biol 6.
Scheid, M.P., Woodgett, J.R., 2001. PKB/AKT: functional insights from genetic models. Nat Rev Mol Cell Biol 2, 760-768.
Schindler, J., Sussman, M., 1979. Inhibition by ammonia of intracellular cAMP accumulation in dictyostelium discoideum: Its significance for the regulation of morphogenesis. Dev Genet 1, 13-20.
Schlatterer, C., Walther, P., Muller, M., Mendgen, K., Zierold, K., Knoll, G., 2001. Calcium stores in differentiated Dictyostelium discoideum: prespore cells sequester calcium more efficiently than prestalk cells. Cell Calcium 29, 171-182.
Schmittgen, T.D., Livak, K.J., 2008. Analyzing real-time PCR data by the comparative CT method. Nature Protocols 3, 1101-1108.
Schreiber, S., 1991. Chemistry and biology of the immunophilins and their immunosuppressive ligands. Science 251, 283-287.
Schrode, N., Xenopoulos, P., Piliszek, A., Frankenberg, S., Plusa, B., Hadjantonakis, A.K., 2013. Anatomy of a blastocyst: cell behaviors driving cell fate choice and morphogenesis in the early mouse embryo. Genesis (New York, N.Y. : 2000) 51, 219-233.
Schubbert, S., Shannon, K., Bollag, G., 2007. Hyperactive Ras in developmental disorders and cancer. Nat Rev Cancer 7, 295-308.
Schürmann, A., Brauers, A., Massmann, S., Becker, W., Joost, H.G., 1995. Cloning of a novel family of mammalian GTP-binding proteins (RagA, RagBs, RagB1) with remote similarity to the Ras-related GTPases. J Biol Chem 270, 28982-28988.
Sehgal, S.N., 1998. Rapamune (R) (RAPA, rapamycin, sirolimus): Mechanism of action immunosuppressive effect results from blockade of signal transduction and inhibition of cell cycle progression. Clin Biochem 31, 335-340.
Sekiguchi, T., Hirose, E., Nakashima, N., Ii, M., Nishimoto, T., 2001. Novel G proteins, Rag C and Rag D, interact with GTP-binding proteins, Rag A and Rag B. J Biol Chem 276, 7246-7257.

Sekine, R., Kawata, T., Muramoto, T., 2018. CRISPR/Cas9 mediated targeting of multiple genes in Dictyostelium. Sci Rep 8, 8471.
Sempou, E., Kostiuk, V., Zhu, J., Cecilia Guerra, M., Tyan, L., Hwang, W., Camacho-Aguilar, E., Caplan, M.J., Zenisek, D., Warmflash, A., Owens, N.D.L., Khokha, M.K., 2022. Membrane potential drives the exit from pluripotency and cell fate commitment via calcium and mTOR. Nature Communications 13, 6681.
Senoo, H., Kamimura, Y., Kimura, R., Nakajima, A., Sawai, S., Sesaki, H., Iijima, M., 2019. Phosphorylated Rho-GDP directly activates mTORC2 kinase towards AKT through dimerization with Ras-GTP to regulate cell migration. Nat Cell Biol 21, 867-878.
Serafimidis, I., Kay, R.R., 2005. New prestalk and prespore inducing signals in Dictyostelium. Developmental Biology 282, 432-441.
Serfontein, J., Nisbet, R.E., Howe, C.J., de Vries, P.J., 2011. Conservation of structural and functional elements of TSC1 and TSC2: a bioinformatic comparison across animal models. Behavior genetics 41, 349-356.
Shang, C., Zhou, H., Liu, W., Shen, T., Luo, Y., Huang, S., 2020. Iron chelation inhibits mTORC1 signaling involving activation of AMPK and REDD1/Bnip3 pathways. Oncogene 39, 5201-5213.
Shanley, L.J., Walczysko, P., Bain, M., MacEwan, D.J., Zhao, M., 2006. Influx of extracellular Ca2+ is necessary for electrotaxis in Dictyostelium. Journal of Cell Science 119, 4741-4748.
Shemarova, I.V., Nesterov, V.P., 2005. Evolution of mechanisms of Ca2+-signaling: Role of calcium ions in signal transduction in prokaryotes. J Evol Biochem Phys+ 41, 12-19.
Shigaki, T., Rees, I., Nakhleh, L., Hirschi, K.D., 2006. Identification of three distinct phylogenetic groups of CAX cation/proton antiporters. J Mol Evol 63, 815-825.
Shimobayashi, M., Hall, M.N., 2016. Multiple amino acid sensing inputs to mTORC1. Cell Research 26, 7-20.
Shogren-Knaak, M., Ishii, H., Sun, J.M., Pazin, M.J., Davie, J.R., Peterson, C.L., 2006. Histone H4-K16 acetylation controls chromatin structure and protein interactions. Science 311, 844-847.
Siegert, F., Weijer, C.J., 1995. Spiral and concentric waves organize multicellular Dictyostelium mounds. Current Biology 5, 937-943.
Sigel, A., Sigel, H., 1998. Metal ions in biological systems, volume 35: iron transport and storage microorganisms, plants, and animals. Met Based Drugs 5, 262.
Sillo, A., Bloomfield, G., Balest, A., Balbo, A., Pergolizzi, B., Peracino, B., Skelton, J., Ivens, A., Bozzaro, S., 2008. Genome-wide transcriptional changes induced by phagocytosis or growth on bacteria in Dictyostelium. BMC Genomics 9, 291.
Singh, D., Nishi, K., Khambata, K., Balasinor, N.H., 2020. Introduction to epigenetics: basic concepts and advancements in the field, in: Tollefsbol, T. (Ed.), Epigenetics and Reproductive Health. Academic Press, pp. xxv-xliv.
Singh, M., Mugler, K., Hailoo, D.W., Burke, S., Nemesure, B., Torkko, K., Shroyer, K.R., 2011. Differential expression of transferrin receptor (TfR) in a spectrum of normal to malignant breast tissues: implications for in situ and invasive carcinoma. Appl Immunohistochem Mol Morphol 19, 417-423.
Smith, F.A., Whittington, J., 1988. Uptake of Imidazole and its Effects on the Intracellular pH and Ionic Relations of Chara corallina. Journal of Experimental Botany 39, 1549-1560.
Smith, P.K., Sen, M.G., Fisher, P.R., Annesley, S.J., 2019. Modelling of Neuronal Ceroid Lipofuscinosis Type 2 in Dictyostelium discoideum Suggests That Cytopathological Outcomes Result from Altered TOR Signalling. Cells 8.
Soffers, J.H.M., Workman, J.L., 2020. The SAGA chromatin-modifying complex: the sum of its parts is greater than the whole. Genes & Development 34, 1287-1303.

Song, L.S., Guatimosim, S., Gomez-Viquez, L., Sobie, E.A., Ziman, A., Hartmann, H., Lederer, W.J., 2005. Calcium biology of the transverse tubules in heart. Ann N Y Acad Sci 1047, 99-111.
Srivastava, N., Traynor, D., Piel, M., Kabla, A.J., Kay, R.R., 2020. Pressure sensing through Piezo channels controls whether cells migrate with blebs or pseudopods. P Natl Acad Sci USA 117, 2506-2512.
Stajdohar, M., Rosengarten, R.D., Kokosar, J., Jeran, L., Blenkus, D., Shaulsky, G., Zupan, B., 2017. dictyExpress: a web-based platform for sequence data management and analytics in Dictyostelium and beyond. Bmc Bioinformatics 18.
Sternfeld, J., 1992. A study of PstB cells during Dictyostelium migration and culmination reveals a unidirectional cell type conversion process. Roux's Archives of Developmental Biology 201, 354-363.
Sternfeld, J., David, C.N., 1979. Ammonia Plus Another Factor Are Necessary for Differentiation in Submerged Clumps of Dictyostelium. Journal of Cell Science 38, 181-191.
Steuer Costa, W., Yu, S.C., Liewald, J.F., Gottschalk, A., 2017. Fast cAMP Modulation of Neurotransmission via Neuropeptide Signals and Vesicle Loading. Curr Biol 27, 495-507.
Stevense, M., Chubb, J.R., Muramoto, T., 2011. Nuclear organization and transcriptional dynamics in Dictyostelium. Dev Growth Differ 53, 576-586.
Stewart, T.A., Davis, F.M., 2019. An element for development: Calcium signaling in mammalian reproduction and development. Biochim Biophys Acta Mol Cell Res 1866, 1230-1238.
Strahl, B.D., Allis, C.D., 2000. The language of covalent histone modifications. Nature 403, 41-45.
Strahl, B.D., Ohba, R., Cook, R.G., Allis, C.D., 1999. Methylation of histone H3 at lysine 4 is highly conserved and correlates with transcriptionally active nuclei in Tetrahymena. P Natl Acad Sci USA 96, 14967-14972.
Strassmann, J.E., Zhu, Y., Queller, D.C., 2000. Altruism and social cheating in the social amoeba Dictyostelium discoideum. Nature 408, 965-967.
Strimpakos, A.S., Karapanagiotou, E.M., Saif, M.W., Syrigos, K.N., 2009. The role of mTOR in the management of solid tumors: an overview. Cancer Treat Rev 35, 148-159.
Strmecki, L., Bloomfield, G., Araki, T., Dalton, E., Skelton, J., Schilde, C., Harwood, A., Williams, J.G., Ivens, A., Pears, C., 2007. Proteomic and microarray analyses of the Dictyostelium Zak1-GSK-3 signaling pathway reveal a role in early development. Eukaryot Cell 6, 245-252.
Strober, W., 2015. Trypan Blue Exclusion Test of Cell Viability. Current Protocols in Immunology 111.
Sugeedha, J., Gautam, J., Tyagi, S., 2021. SET1/MLL family of proteins: functions beyond histone methylation. Epigenetics 16, 469-487.
Suka, N., Luo, K., Grunstein, M., 2002. Sir2p and Sas2p opposingly regulate acetylation of yeast histone H4 lysine16 and spreading of heterochromatin. Nat Genet 32, 378-383.
Suka, N., Suka, Y., Carmen, A.A., Wu, J., Grunstein, M., 2001. Highly specific antibodies determine histone acetylation site usage in yeast heterochromatin and euchromatin. Mol Cell 8, 473-479.
Sun, G.C., Chen, H.H., Liang, W.Z., Jan, C.R., 2019. Exploration of the effect of the alkaloid colchicine on Ca(2+) handling and its related physiology in human oral cancer cells. Arch Oral Biol 102, 179-185.
Sussman, R., Sussman, M., 1967. Cultivation of Dictyostelium discoideum in axenic medium. Biochem Biophys Res Commun 29, 53-55.

Swer, P.B., Bhadoriya, P., Saran, S., 2014. Analysis of Rheb in the cellular slime mold Dictyostelium discoideum: cellular localization, spatial expression and overexpression. J Biosci 39, 75-84.
Swer, P.B., Mishra, H., Lohia, R., Saran, S., 2016. Overexpression of TOR (target of rapamycin) inhibits cell proliferation in Dictyostelium discoideum. J Basic Microbiol 56, 510-519.
Tae, H., Casarotto, M.G., Dulhunty, A.F., 2009. Ubiquitous SPRY domains and their role in the skeletal type ryanodine receptor. European Biophysics Journal 39, 51-59.
Tagami, H., Ray-Gallet, D., Almouzni, G., Nakatani, Y., 2004. Histone H3.1 and H3.3 complexes mediate nucleosome assembly pathways dependent or independent of DNA synthesis. Cell 116, 51-61.
Takahara, T., Amemiya, Y., Sugiyama, R., Maki, M., Shibata, H., 2020. Amino acid-dependent control of mTORC1 signaling: a variety of regulatory modes. J Biomed Sci 27, 87.
Tanaka, K., Adachi, H., Konishi, H., Iwamatsu, A., Ohkawa, K., Shirai, T., Nagata, S., Kikkawa, U., Fukui, Y., 1999. Identification of protein kinase B (PKB) as a phosphatidylinositol 3,4,5-trisphosphate binding protein in Dictyostelium discoideum. Bioscience, biotechnology, and biochemistry 63, 368-372.
Tanimoto, Y., Yamazoe-Umemoto, A., Fujita, K., Kawazoe, Y., Miyanishi, Y., Yamazaki, S.J., Fei, X., Busch, K.E., Gengyo-Ando, K., Nakai, J., Iino, Y., Iwasaki, Y., Hashimoto, K., Kimura, K.D., 2017. Calcium dynamics regulating the timing of decision-making in C. elegans. Elife 6.
Taverna, S.D., Ilin, S., Rogers, R.S., Tanny, J.C., Lavender, H., Li, H.T., Baker, L., Boyle, J., Blair, L.P., Chait, B.T., Patel, D.J., Aitchison, J.D., Tackett, A.J., Allis, C.D., 2006. Yng1 PHD finger binding to H3 trimethylated at K4 promotes NuA3 HAT activity at K14 of H3 and transcription at a subset of targeted ORFs. Molecular Cell 24, 785-796.
Teh, M.R., Frost, J.N., Armitage, A.E., Drakesmith, H., 2021. Analysis of Iron and Iron-Interacting Protein Dynamics During T-Cell Activation. Front Immunol 12, 714613.
Thompson, C.R., Fu, Q., Buhay, C., Kay, R.R., Shaulsky, G., 2004. A bZIP/bRLZ transcription factor required for DIF signaling in Dictyostelium. Development 131, 513-523.
Thompson, C.R., Kay, R.R., 2000a. Cell-fate choice in Dictyostelium: intrinsic biases modulate sensitivity to DIF signaling. Dev Biol 227, 56-64.
Thompson, C.R., Kay, R.R., 2000b. The role of DIF-1 signaling in Dictyostelium development. Mol Cell 6, 1509-1514.
Thompson, J., Fernandez-Reyes, D., Sharling, L., Moore, S.G., Eling, W.M., Kyes, S.A., Newbold, C.I., Kafatos, F.C., Janse, C.J., Waters, A.P., 2007. Plasmodium cysteine repeat modular proteins 1-4: complex proteins with roles throughout the malaria parasite life cycle. Cell Microbiol 9, 1466-1480.
Tomancak, P., Berman, B.P., Beaton, A., Weiszmann, R., Kwan, E., Hartenstein, V., Celniker, S.E., Rubin, G.M., 2007. Global analysis of patterns of gene expression during Drosophilaembryogenesis. Genome Biol 8, R145.
Torija, P., Robles, A., Escalante, R., 2006a. Optimization of a large-scale gene disruption protocol in Dictyostelium and analysis of conserved genes of unknown function. Bmc Microbiol 6.
Torija, P., Vicente, J.J., Rodrigues, T.B., Robles, A., Cerdán, S.n., Sastre, L., Calvo, R.M., Escalante, R., 2006b. Functional genomics in Dictyostelium: MidA, a new conserved protein, is required for mitochondrial function and development. Journal of Cell Science 119, 1154-1164.
Torrence, M.E., MacArthur, M.R., Hosios, A.M., Valvezan, A.J., Asara, J.M., Mitchell, J.R., Manning, B.D., 2021. The mTORC1-mediated activation of ATF4 promotes protein and glutathione synthesis downstream of growth signals. Elife 10.

Torti, S.V., Manz, D.H., Paul, B.T., Blanchette-Farra, N., Torti, F.M., 2018. Iron and Cancer. Annual Review of Nutrition 38, 97-125.
Town, C.D., Gross, J.D., Kay, R.R., 1976. Cell-Differentiation without Morphogenesis in Dictyostelium-Discoideum. Nature 262, 717-719.
Traynor, D., Kay, R.R., 1991. The DIF-1 signaling system in Dictyostelium. Metabolism of the signal. J Biol Chem 266, 5291-5297.
Traynor, D., Kay, R.R., 2017. A polycystin-type transient receptor potential (Trp) channel that is activated by ATP. Biol Open 6, 200-209.
Traynor, D., Milne, J.L., Insall, R.H., Kay, R.R., 2000. Ca(2+) signalling is not required for chemotaxis in Dictyostelium. EMBO J 19, 4846-4854.
Tsun, Z.Y., Bar-Peled, L., Chantranupong, L., Zoncu, R., Wang, T., Kim, C., Spooner, E., Sabatini, D.M., 2013. The folliculin tumor suppressor is a GAP for the RagC/D GTPases that signal amino acid levels to mTORC1. Mol Cell 52, 495-505.
Tu, C.L., Bikle, D.D., 2013. Role of the calcium-sensing receptor in calcium regulation of epidermal differentiation and function. Best Pract Res Clin Endocrinol Metab 27, 415-427.
Turing, A.M., 1990. The chemical basis of morphogenesis. 1953. Bull Math Biol 52, 153-197; discussion 119-152.
Uchikawa, T., Yamamoto, A., Inouye, K., 2011. Origin and function of the stalk-cell vacuole in Dictyostelium. Developmental Biology 352, 48-57.
Ueda, H.R., 2007. Systems biology of mammalian circadian clocks. Cold Spring Harb Symp Quant Biol 72, 365-380.
Ulmschneider, B., Grillo-Hill, B.K., Benitez, M., Azimova, D.R., Barber, D.L., Nystul, T.G., 2016. Increased intracellular pH is necessary for adult epithelial and embryonic stem cell differentiation. J Cell Biol 215, 345-355.
Vaccaro, M.I., Ropolo, A., Grasso, D., Iovanna, J.L., 2008. A novel mammalian trans-membrane protein reveals an alternative initiation pathway for autophagy. Autophagy 4, 388-390.
van de Waterbeemd, B., Zomer, G., van den Ijssel, J., van Keulen, L., Eppink, M.H., van der Ley, P., van der Pol, L.A., 2013. Cysteine depletion causes oxidative stress and triggers outer membrane vesicle release by Neisseria meningitidis; implications for vaccine development. PLoS One 8, e54314.
Van Dijken, P., de Haas, J.-R., Craxton, A., Erneux, C., Shears, S.B., Van Haastert, P.J.M., 1995. A Novel, Phospholipase C-independent Pathway of Inositol 1,4,5-Trisphosphate Formation in Dictyostelium and Rat Liver(∗). Journal of Biological Chemistry 270, 29724-29731.
van Es, S., Hodgkinson, S., Schaap, P., Kay, R.R., 1994. Metabolic pathways for differentiation-inducing factor-1 and their regulation are conserved between closely related Dictyostelium species, but not between distant members of the family. Differentiation 58, 95-100.
Van Haastert, P.J., Devreotes, P.N., 2004. Chemotaxis: signalling the way forward. Nat Rev Mol Cell Biol 5, 626-634.
van Haastert, P.J., Keizer-Gunnink, I., Kortholt, A., 2007. Essential role of PI3-kinase and phospholipase A2 in Dictyostelium discoideum chemotaxis. J Cell Biol 177, 809-816.
Velazquez, F., Peak-Chew, S.Y., Fernandez, I.S., Neumann, C.S., Kay, R.R., 2011. Identification of a eukaryotic reductive dechlorinase and characterization of its mechanism of action on its natural substrate. Chem Biol 18, 1252-1260.
Velicer, G.J., Kroos, L., Lenski, R.E., 1998. Loss of social behaviors by Myxococcus xanthus during evolution in an unstructured habitat. P Natl Acad Sci USA 95, 12376-12380.
Velicer, G.J., Kroos, L., Lenski, R.E., 2000. Developmental cheating in the social bacterium Myxococcus xanthus. Nature 404, 598-601.

Veltman, D.M., Keizer-Gunnink, I., Haastert, P.J., 2009. An extrachromosomal, inducible expression system for Dictyostelium discoideum. Plasmid 61, 119-125.
Venkataraman, P., Lamb, R.A., Pinto, L.H., 2005. Chemical rescue of histidine selectivity filter mutants of the M2 ion channel of influenza A virus. J Biol Chem 280, 21463-21472.
Verkerke-van Wijk, I., Brandt, R., Bosman, L., Schaap, P., 1998. Two distinct signaling pathways mediate DIF induction of prestalk gene expression in Dictyostelium. Exp Cell Res 245, 179-185.
Vermaak, D., Ahmad, K., Henikoff, S., 2003. Maintenance of chromatin states: an open-and-shut case. Current Opinion in Cell Biology 15, 266-274.
Vermeulen, M., Eberl, H.C., Matarese, F., Marks, H., Denissov, S., Butter, F., Lee, K.K., Olsen, J.V., Hyman, A.A., Stunnenberg, H.G., Mann, M., 2010. Quantitative Interaction Proteomics and Genome-wide Profiling of Epigenetic Histone Marks and Their Readers. Cell 142, 967-980.
Vézina, C., Kudelski, A., Sehgal, S.N., 1975. RAPAMYCIN (AY-22,989), A NEW ANTIFUNGAL ANTIBIOTIC. The Journal of Antibiotics.
Villegas, F., Lehalle, D., Mayer, D., Rittirsch, M., Stadler, M.B., Zinner, M., Olivieri, D., Vabres, P., Duplomb-Jego, L., De Bont, E., Duffourd, Y., Duijkers, F., Avila, M., Genevieve, D., Houcinat, N., Jouan, T., Kuentz, P., Lichtenbelt, K.D., Thauvin-Robinet, C., St-Onge, J., Thevenon, J., van Gassen, K.L.I., van Haelst, M., van Koningsbruggen, S., Hess, D., Smallwood, S.A., Riviere, J.B., Faivre, L., Betschinger, J., 2019. Lysosomal Signaling Licenses Embryonic Stem Cell Differentiation via Inactivation of Tfe3. Cell Stem Cell 24, 257-270 e258.
Vinet, A.F., Fiedler, T., Studer, V., Froquet, R., Dardel, A., Cosson, P., Pieters, J., 2014. Initiation of multicellular differentiation in Dictyostelium discoideum is regulated by coronin A. Molecular Biology of the Cell 25, 688-701.
Waickman, A.T., Powell, J.D., 2012. mTOR, metabolism, and the regulation of T-cell differentiation and function. Immunol Rev 249, 43-58.
Walton, Z.E., Brooks, R.C., Dang, C.V., 2019. mTOR Senses Intracellular pH through Lysosome Dispersion from RHEB. Bioessays 41.
Wander, S.A., Hennessy, B.T., Slingerland, J.M., 2011. Next-generation mTOR inhibitors in clinical oncology: how pathway complexity informs therapeutic strategy. J Clin Invest 121, 1231-1241.
Wang, M., Vanhaastert, P.J.M., Schaap, P., 1986. Multiple Effects of Differentiation-Inducing Factor on Prespore Differentiation and Cyclic-Amp Signal Transduction in Dictyostelium. Differentiation 33, 24-28.
Wang, S., Tsun, Z.-Y., Wolfson, R.L., Shen, K., Wyant, G.A., Plovanich, M.E., Yuan, E.D., Jones, T.D., Chantranupong, L., Comb, W., Wang, T., Bar-Peled, L., Zoncu, R., Straub, C., Kim, C., Park, J., Sabatini, B.L., Sabatini, D.M., 2015. Lysosomal amino acid transporter SLC38A9 signals arginine sufficiency to mTORC1. Science 347, 188-194.
Wang, S.Y., Pollina, E.A., Wang, I.H., Pino, L.K., Bushnell, H.L., Takashima, K., Fritsche, C., Sabin, G., Garcia, B.A., Greer, P.L., Greer, E.L., 2021. Role of epigenetics in unicellular to multicellular transition in Dictyostelium. Genome Biol 22.
Warren, E.C., Dooves, S., Lugara, E., Damstra-Oddy, J., Schaf, J., Heine, V.M., Walker, M.C., Williams, R.S.B., 2020. Decanoic acid inhibits mTORC1 activity independent of glucose and insulin signaling. Proc Natl Acad Sci U S A 117, 23617-23625.
Watts, D.J., Ashworth, J.M., 1970. Growth of myxameobae of the cellular slime mould Dictyostelium discoideum in axenic culture. Biochem J 119, 171-174.
Weeks, G., 1984. The Spore Cell Induction Activity of Conditioned Media and Subcellular-Fractions of Dictyostelium-Discoideum. Experimental Cell Research 153, 81-90.

Weeks, G., Weijer, C.J., 1994. The Dictyostelium cell cycle and its relationship to differentiation. FEMS Microbiol Lett 124, 123-130.
Weijer, C.J., Duschl, G., David, C.N., 1984a. Dependence of cell-type proportioning and sorting on cell cycle phase in Dictyostelium discoideum. J Cell Sci 70, 133-145.
Weijer, C.J., Duschl, G., David, C.N., 1984b. A revision of the Dictyostelium discoideum cell cycle. J Cell Sci 70, 111-131.
Wessels, D., Brincks, R., Kuhl, S., Stepanovic, V., Daniels, K.J., Weeks, G., Lim, C.J., Spiegelman, G., Fuller, D., Iranfar, N., Loomis, W.F., Soll, D.R., 2004. RasC plays a role in transduction of temporal gradient information in the Cyclic-AMP wave of Dictyostelium discoideum. Eukaryotic Cell 3, 646-662.
Wick, U., Malchow, D., Gerisch, G., 1978. Cyclic-AMP stimulated calcium influx into aggregating cells of Dictyostelium discoideum. Cell biology international reports 2, 71-79.
Wiedemann, S.M., Mildner, S.N., Bonisch, C., Israel, L., Maiser, A., Matheisl, S., Straub, T., Merkl, R., Leonhardt, H., Kremmer, E., Schermelleh, L., Hake, S.B., 2010. Identification and characterization of two novel primate-specific histone H3 variants, H3.X and H3.Y. J Cell Biol 190, 777-791.
Wilczynska, Z., Happle, K., Muller-Taubenberger, A., Schlatterer, C., Malchow, D., Fisher, P.R., 2005. Release of Ca2+ from the endoplasmic reticulum contributes to Ca2+ signaling in Dictyostelium discoideum. Eukaryot Cell 4, 1513-1525.
Wilkins, A., Khosla, M., Fraser, D.J., Spiegelman, G.B., Fisher, P.R., Weeks, G., Insall, R.H., 2000. Dictyostelium RasD is required for normal phototaxis, but not differentiation. Genes and Development 14, 1407–1413
Wilkins, A., Szafranski, K., Fraser, D.J., Bakthavatsalam, D., Müller, R., Fisher, P.R., Glöckner, G., Eichinger, L., Noegel, A.A., Insall, R.H., 2005. The Dictyostelium genome encodes numerous RasGEFs with multiple biological roles. Genome Biol 6, R68.
Wilkinson, J.E., Burmeister, L., Brooks, S.V., Chan, C.C., Friedline, S., Harrison, D.E., Hejtmancik, J.F., Nadon, N., Strong, R., Wood, L.K., Woodward, M.A., Miller, R.A., 2012. Rapamycin slows aging in mice. Aging Cell 11, 675-682.
Willems, L., Chapuis, N., Puissant, A., Maciel, T.T., Green, A.S., Jacque, N., Vignon, C., Park, S., Guichard, S., Herault, O., Fricot, A., Hermine, O., Moura, I.C., Auberger, P., Ifrah, N., Dreyfus, F., Bonnet, D., Lacombe, C., Mayeux, P., Bouscary, D., Tamburini, J., 2012. The dual mTORC1 and mTORC2 inhibitor AZD8055 has anti-tumor activity in acute myeloid leukemia. Leukemia 26, 1195-1202.
William, J., Morrison, A., 1994. Prestalk Cell-differentiation and Movement during the Morphogenesis of Dictyostelium discoideum, in: Cohn, W.E., Moldave, K. (Eds.), Progress in Nucleic Acid Research and Molecular Biology. Academic Press, pp. 1-27.
Williams, J.G., Ceccarelli, A., Mcrobbie, S., Mahbubani, H., Kay, R.R., Early, A., Berks, M., Jermyn, K.A., 1987. Direct induction of Dictyostelium prestalk gene expression by DIF provides evidence that DIF is a morphogen. Cell 49, 185-192.
Williams, J.G., Noegel, A.A., Eichinger, L., 2005. Manifestations of multicellularity: Dictyostelium reports in. Trends Genet 21, 392-398.
Williams, T.D., Peak-Chew, S.Y., Paschke, P., Kay, R.R., 2019. Akt and SGK protein kinases are required for efficient feeding by macropinocytosis. J Cell Sci 132.
Winkler, M.M., Grainger, J.L., 1978. Mechanism of action of NH4Cl and other weak bases in the activation of sea urchin eggs. Nature 273, 536-538.
Wolfson, R.L., Sabatini, D.M., 2017. The Dawn of the Age of Amino Acid Sensors for the mTORC1 Pathway. Cell Metab 26, 301-309.
Wood, S.A., Ammann, R.R., Brock, D.A., Li, L., Spann, T., Gomer, R.H., 1996. RtoA links initial cell type choice to the cell cycle in Dictyostelium. Development 122, 3677-3685.

Wu, Y., Li, M., Yang, M., 2021. Post-Translational Modifications in Oocyte Maturation and Embryo Development. Front Cell Dev Biol 9, 645318.
Wu, Y.S., Li, Y., Zhang, H., Huang, Y.H., Zhao, P., Tang, Y.J., Qiu, X.H., Ying, Y., Li, W., Ni, S., Zhang, M., Liu, L.Q., Xu, Y., Zhuang, Q., Luo, Z.W., Benda, C., Song, H., Liu, B.H., Lai, L.X., Liu, X.G., Tse, H.F., Bao, X.C., Chan, W.Y., Esteban, M.A., Qin, B.M., Pei, D.Q., 2015. Autophagy and mTORC1 regulate the stochastic phase of somatic cell reprogramming. Nature Cell Biology 17, 715-+.
Wunsch, A.M., Lough, J., 1987. Modulation of histone H3 variant synthesis during the myoblast-myotube transition of chicken myogenesis. Dev Biol 119, 94-99.
Xie, J., Wang, X., Proud, C.G., 2016a. mTOR inhibitors in cancer therapy. F1000Res 5.
Xie, W., Lorenz, S., Dolder, S., Hofstetter, W., 2016b. Extracellular Iron is a Modulator of the Differentiation of Osteoclast Lineage Cells. Calcified Tissue International 98, 275-283.
Xie, Y., Coukell, M.B., Gombos, Z., 1996. Antisense RNA inhibition of the putative vacuolar H(+)-ATPase proteolipid of Dictyostelium reduces intracellular Ca2+ transport and cell viability. J Cell Sci 109 (Pt 2), 489-497.
Xu, K., Liu, P., Wei, W., 2014. mTOR signaling in tumorigenesis. Biochim Biophys Acta 1846, 638-654.
Xu, X., Müller-Taubenberger, A., Adley, K.E., Pawolleck, N., Lee, V.W., Wiedemann, C., Sihra, T.S., Maniak, M., Jin, T., Williams, R.S., 2007. Attenuation of phospholipid signaling provides a novel mechanism for the action of valproic acid. Eukaryot Cell 6, 899-906.
Yamada, Y., Nunez-Corcuera, B., Williams, J.G., 2011. DIF-1 regulates Dictyostelium basal disc differentiation by inducing the nuclear accumulation of a bZIP transcription factor. Dev Biol 354, 77-86.
Yamada, Y., Sakamoto, H., Ogihara, S., Maeda, M., 2005. Novel patterns of the gene expression regulation in the prestalk region along the antero-posterior axis during multicellular development of Dictyostelium. Gene Expression Patterns 6, 63-68.
Yamamizu, K., Piao, Y., Sharov, A.A., Zsiros, V., Yu, H., Nakazawa, K., Schlessinger, D., Ko, M.S., 2013. Identification of transcription factors for lineage-specific ESC differentiation. Stem Cell Reports 1, 545-559.
Yamanaka, Y., Lanner, F., Rossant, J., 2010. FGF signal-dependent segregation of primitive endoderm and epiblast in the mouse blastocyst. Development 137, 715-724.
Yan, Y., Tsukamoto, O., Nakano, A., Kato, H., Kioka, H., Ito, N., Higo, S., Yamazaki, S., Shintani, Y., Matsuoka, K., Liao, Y., Asanuma, H., Asakura, M., Takafuji, K., Minamino, T., Asano, Y., Kitakaze, M., Takashima, S., 2015. Augmented AMPK activity inhibits cell migration by phosphorylating the novel substrate Pdlim5. Nat Commun 6, 6137.
Yang, H., Jiang, X., Li, B., Yang, H.J., Miller, M., Yang, A., Dhar, A., Pavletich, N.P., 2017. Mechanisms of mTORC1 activation by RHEB and inhibition by PRAS40. Nature 552, 368-373.
Yang, H., Rudge, D.G., Koos, J.D., Vaidialingam, B., Yang, H.J., Pavletich, N.P., 2013. mTOR kinase structure, mechanism and regulation. Nature 497, 217-223.
Yang, L., Jin, M., Jeong, K.W., 2021. Histone H3K4 Methyltransferases as Targets for Drug-Resistant Cancers. Biology 10.
Yao, H., Arunachalam, G., Hwang, J.W., Chung, S., Sundar, I.K., Kinnula, V.L., Crapo, J.D., Rahman, I., 2010. Extracellular superoxide dismutase protects against pulmonary emphysema by attenuating oxidative fragmentation of ECM. Proc Natl Acad Sci U S A 107, 15571-15576.
Yao, T., Asayama, Y., 2017. Animal-cell culture media: History, characteristics, and current issues. Reprod Med Biol 16, 99-117.
Yao, Z., Chen, Y., Cao, W., Shyh-Chang, N., 2020. Chromatin-modifying drugs and metabolites in cell fate control. Cell Prolif 53, e12898.

Yoshida, M., Kijima, M., Akita, M., Beppu, T., 1990. Potent and specific inhibition of mammalian histone deacetylase both in vivo and in vitro by trichostatin A. Journal of Biological Chemistry 265, 17174-17179.
Yu, L., McPhee, C.K., Zheng, L.X., Mardones, G.A., Rong, Y.G., Peng, J.Y., Mi, N., Zhao, Y., Liu, Z.H., Wan, F.Y., Hailey, D.W., Oorschot, V., Klumperman, J., Baehrecke, E.H., Lenardo, M.J., 2010. Termination of autophagy and reformation of lysosomes regulated by mTOR. Nature 465, 942-U911.
Yuan, Y., Cao, C., Wen, M.R., Li, M., Dong, Y., Wu, L.J., Wu, J., Cui, T.X., Li, D.F., Chou, J.J., OuYang, B., 2020. Structural Characterization of the N-Terminal Domain of the Dictyostelium discoideum Mitochondrial Calcium Uniporter. Acs Omega 5, 6452-6460.
Zada-Hames, I.M., Ashworth, J.M., 1978. The cell cycle during the vegetative stage of Dictyostelium discoideum and its response to temperature change. J Cell Sci 32, 1-20.
Zeng, H., Cohen, S., Guy, C., Shrestha, S., Neale, G., Brown, S.A., Cloer, C., Kishton, R.J., Gao, X., Youngblood, B., Do, M., Li, M.O., Locasale, J.W., Rathmell, J.C., Chi, H., 2016. mTORC1 and mTORC2 Kinase Signaling and Glucose Metabolism Drive Follicular Helper T Cell Differentiation. Immunity 45, 540-554.
Zernicka-Goetz, M., Morris, S.A., Bruce, A.W., 2009. Making a firm decision: multifaceted regulation of cell fate in the early mouse embryo. Nat Rev Genet 10, 467-477.
Zhang, C.S., Jiang, B., Li, M., Zhu, M., Peng, Y., Zhang, Y.L., Wu, Y.Q., Li, T.Y., Liang, Y., Lu, Z., Lian, G., Liu, Q., Guo, H., Yin, Z., Ye, Z., Han, J., Wu, J.W., Yin, H., Lin, S.Y., Lin, S.C., 2014. The lysosomal v-ATPase-Ragulator complex is a common activator for AMPK and mTORC1, acting as a switch between catabolism and anabolism. Cell Metab 20, 526-540.
Zhang, J., Gao, Z., Ye, J., 2013a. Phosphorylation and degradation of S6K1 (p70S6K1) in response to persistent JNK1 Activation. Biochim Biophys Acta 1832, 1980-1988.
Zhang, K., Tang, H., Huang, L., Blankenship, J.W., Jones, P.R., Xiang, F., Yau, P.M., Burlingame, A.L., 2002. Identification of acetylation and methylation sites of histone H3 from chicken erythrocytes by high-accuracy matrix-assisted laser desorption ionization-time-of-flight, matrix-assisted laser desorption ionization-postsource decay, and nanoelectrospray ionization tandem mass spectrometry. Anal Biochem 306, 259-269.
Zhang, Y.-L., Guo, H., Zhang, C.-S., Lin, S.-Y., Yin, Z., Peng, Y., Luo, H., Shi, Y., Lian, G., Zhang, C., Li, M., Ye, Z., Ye, J., Han, J., Li, P., Wu, J.-W., Lin, S.-C., 2013b. AMP as a Low-Energy Charge Signal Autonomously Initiates Assembly of AXIN-AMPK-LKB1 Complex for AMPK Activation. Cell Metabolism 18, 546-555.
Zheng, Y., Collins, S.L., Lutz, M.A., Allen, A.N., Kole, T.P., Zarek, P.E., Powell, J.D., 2007. A role for mammalian target of rapamycin in regulating T cell activation versus anergy. The Journal of Immunology 178, 2163-2170.
Zhou, V.W., Goren, A., Bernstein, B.E., 2011. Charting histone modifications and the functional organization of mammalian genomes. Nature Reviews Genetics 12, 7-18.
Zhu, S., Li, W., Zhou, H., Wei, W., Ambasudhan, R., Lin, T., Kim, J., Zhang, K., Ding, S., 2010. Reprogramming of human primary somatic cells by OCT4 and chemical compounds. Cell Stem Cell 7, 651-655.
Zhukovskaya, N.V., Fukuzawa, M., Yamada, Y., Araki, T., Williams, J.G., 2006. The Dictyostelium bZIP transcription factor DimB regulates prestalk-specific gene expression. Development 133, 439-448.
Zoncu, R., Bar-Peled, L., Efeyan, A., Wang, S.Y., Sancak, Y., Sabatini, D.M., 2011. mTORC1 Senses Lysosomal Amino Acids Through an Inside-Out Mechanism That Requires the Vacuolar H+-ATPase. Science 334, 678-683.
Zou, Z.L., Tao, T., Li, H.M., Zhu, X., 2020. mTOR signaling pathway and mTOR inhibitors in cancer: progress and challenges. Cell Biosci 10.